Papers presented to the

TENTH SYMPOSIUM

ON ANTARCTIC METEORITES

25-27 March 1985

NATIONAL INSTITUTE OF POLAR RESEARCH,
TOKYO

国立極地研究所

The Tenth Symposium on Antarctic Meteorites

Programme

25 - 27 March, 1985

National Institute of Polar Research, Tokyo

N O T I C E

The publication of the full papers, which are here presented as abstracts, will be in the Proceecings of the Tenth Symposium on Antarctic Meteorites, a special issue of the Memoirs of the National Institute of Polar Research. For inclusion in this publication the full text and illustrations of a paper must be received by the organizing secretary by June 28, 1985.

Please send manuscripts to:
Dr. K. Yanai
National Institute of Polar Research
9-10 Kaga 1-chome
Itabashi-ku
Tokyo 173
Japan

Monday, March 25, 1985

0830-1200 Registration Auditorium (6th Floor)

* Speaker

0930 - 0935 Tatsuro Matsuda : Opening address

Chairmen: Mineo Kumazawa and Masao Kitamura

1 0935 - 0945 Yanai K.* and Kojima H.
Processing of Antarctic meteorites in the National Institute of Polar Research

2 0945 - 1000 Nishio F.
Measured and computed meteorite concentration and age of ice in the Meteorite Ice field near the Yamato Mountains

3 1000 - 1015 Graham A. L.* Yanai K. and Kojima H.
A review of the Yamato-80, 81 and 82 meteorite collections

4 1015 - 1030 Chang Shuyuan
The research of meteorite in China expediting the development of related fields

5 1030 - 1045 Pesonen L. J.* Kukkonen I. T. and Lehtinen M.
Identification of mineralogical-petrological classes of meteorites -- A petrophysical method

6 1045 - 1100 Dennison J. E. Kaczaral P. W. Lingner D. W. and Lipschutz M. E.*
Ordinary chondrite falls and congeners from Victoria Land, Antarctica: variations in parent spirce regions

7 1100 - 1115 Nagahara H.
Petrology of enstatite chondrites, Y-691 (EH3) and Y-74370 (EH4)

8 1115 - 1130 Wang Daode* Kallemeyn G. W. and Wasson J. T.
Chemical composition of 19 L and LL chondrites and its application to taxonomy

9 1130 - 1145 Watanabe S.* Kitamura M. Morimoto N. and Kawasaki T.
Fine grained lithic fragments in the L3 chondrites

10 1145 - 1200 Momose K. and Nagai H.*
Low temperature remanent magnetization of Fe-Ni alloy

11 1200 - 1215 Splettstoesser J. F.
Ventifaction of meteorites exposed in polar areas

1215 - 1300 Lunch Time

Chairmen: Teruaki Ishii and Mitsuru Ebihara

12 1300 - 1315 Kitamura M.* Watanabe S. and Morimoto N.
Rounding of chondrules by abrasion

13 1315 - 1330 Miyamoto M.* McKay D. S. McKay G. A. and Duke M. B.
Chemical zoning and homogenization of olivines in chondritic breccia Yamato-75028

14 1330 - 1345 Fujii N.* Hasegawa M. Ito K. Miyamoto M. and Funaki M.
Shape analysis of Fe-Ni grains among Antarctic ordinary chondrites (II)

15 1345 - 1400 Inoue Y.
Opaque minerals in Semarkona chondrite

16 1400 - 1415 Kimura M.
Opaque minerals in Y-691 enstatite chondrite

17 1415 - 1430 Matsueda H.* and Sanga T.
Metal-sulfide equilibrium in Yamato-74, -75 chondrites (preliminary report)

18 1430 - 1445 Kurat G.
Geochemistry of chondrules from carbonaceous, ordinary, and E chondrites

19 1445 - 1500 Lang B.* Grodziński A. Zbik M. and Stoch L.
Thermoanalytical study of carbonaceous chondrites: Yamato-74662 - Kainsaz - Allende

1500 - 1530 Tea Time

Chairmen: Noboru Nakamura and Andrew L. Graham

20 1530 - 1545 Kojima H.* Yanai K. and Ikadai S.
Chromium distribution in type 3 ordinary chondrites

21 1545 - 1600 Kallemeyn G. W.
Compositional comparisons of metamorphosed carbonaceous chondrites

22 1600 - 1615 Akai J.* and Kanno J.
Mineralogical study of matrix phyllosilicates and isolated olivines in Yamato-791198 and -793321

23 1615 - 1630 Murae T.* Masuda A. and Takahashi T.
Possibility of classification of carbonaceous chondrite based on carbonaceous matter

24 1630 - 1645 Shimoyama A.* Harada K. and Yanai K.
Indegenous amino acids from the Yamato-771198 carbonaceous chondrite

25 1645 - 1700 Ponnamperuma C.
Genetic bases in carbonaceous chondrites

-- Special Lecture --

26 1700 - 1745 Wasson J. T. (Invited Speaker)
Evidence regarding the origin of chondrules

1800 - 2000 Reception (Lecture Room, 2nd Floor in Research Building)

Tuesday, March 26, 1985

Chairmen: Nobuo Morimoto and Eiichi Takahashi

27 0900 - 0915 Takahashi E.* Matsui Y. and Ito E.
Melting of peridotite and a chondrite under ultrahigh-pressure

28 0915 - 0930 Matsunami S.* Nagahara H. and Kushiro I.
Compositional variations of matrix olivine in experimentally heated ALH-77214 (L3.4) chondrite:

29 0930 - 0945 Kushiro I.* and Nagahara H.
Origin of iron-rich olivine in the matrices of type 3 ordinary chondrites

30 0945 - 1000 Miura Y* Yanai K. and Tanosaki T.
Composition and structural substitution of meteoritic plagioclases (II)

31 1000 - 1015 Okada A.* Keil K. and Taylor G. J.
Norton county enstatite achondrite and its lithic fragments

32 1015 - 1030 Ostertag R.
Shock effects in polymict achondrite breccias Y-7308, Y-74450, Y-75302 and Y-790260

33 1030 - 1045 Takeda H.
Origin and some problems of pyroxene cumulate achondrites

34 1045 - 1100 Mori H.* and Takeda H.
Oriented chromite inclusions in pigeonite crystals of eucrite meteorites

35 1100 - 1115 Toyoda H.* Haga N. Tachikawa O. Takeda H. and Ishii T.
Cation distribution and mineral chemistry of PGA 82506 and related ureilites

36 1115 - 1130 Isobe H.* Kitamura M. and Morimoto N.
Fractional trend of bulk chemistry of chondrules in the Allende meteorite

37 1130 - 1145 Yabuki H.* and El Goresy A.
Phosphate-bearing microspherules in chondrules of unequilibrated ordinary chondrites

38 1145 - 1200 Kinoshita M* Miyamoto M. and Takano Y.
Theoretical approach to determine spectral reflectances of mineral mixtures

1200 - 1300 Lunch Time

- Special session: Lunar meteorite, Yamato-791197 and other specimens -

Chairmen: Ikuo Kushiro and Ichiro Sunagawa

39 1300 - 1315 Yanai K.* and Kojima H.
Lunar meteorites; recovery, curation and distribution

40 1315 - 1335 Warren P. H.* and Kallemeyn G. W.
Geochemistry of lunar meteorites Yamato-971197 and ALHA81005

41 1335 - 1350 Fukuoka T.* Laul J. C. Smith M. R. Hughes S. S. and Schmitt R. A.
Chemistry of Yamato-791197 meteorite: evidence for lunar highland origin

42 1350 - 1405 Ostertag R.* Bischoff A. Palme H. Spettel B. Stöffler D. Weckwerth G. and Wänke H.
Lunar meteorite Y-791197: a lunar highland regolith breccia

43 1405 - 1420 Takeda H.* Tagai T. and Mori H.
Mineralogy of Antarctic lunar meteorites and differentiated product of the lunar crust

44 1420 - 1435 Kaczaral P. W. Dennison J. E. and Lipschutz M. E.*
Yamato 791197: a trace element-rich lunar highlands sample

45 1435 - 1450 Nakamura N.* Unruh D. M. and Tatsumoto M.
REE, Rb-Sr and U-Pb systematics of "lunar" meteorite Yamato-791197

46 1450 - 1505 Takahashi K.* Shimizu H. and Masuda A.
REE abundances in the Yamato-791197, 108

1505 - 1530 Tea Time

Chairmen: Hiroshi Hasegawa and Ken-ichiro Aoki

47 1530 - 1545 Kaneoka I.* and Takaoka N.
40Ar-39Ar analyses of Yamato-791197

48 1545 - Nishiizumi K.* and Elmore D.
Age of Antarctic meteorites and ice

49 Crozaz G. (Nishiizumi K.*)
A search for nuclear particle tracks in lunar meteorite Yamato-791197

50 1615 Sutton S. R. (Nishiizumi K.*)
Thermoluminescence of Antarctic meteorite Yamato-791197 and comparison with ALHA-81005 and lunar fines

51 1615 - 1630 Takaoka N.
Noble gases in Yamato-791197: Evidence for lunar origin

52 1630 - 1645 Nagata T.* and Funaki M.
Magnetic properties of Yamato 791197 meterite in comparison with those of Apollo 15148 lunar breccia

53 1645 - 1700 Lindstrom M. M. Lindstrom D. J. Korotev R. L. and Haskin L. A.
Lunar meteorites Yamato 791197 and ALHA 81005: the same yet differnt

(93) 1700 - 1715 McFadden L. Pieters C. M. Huguenin R. L. King T. V. V. Gaffey M. J. and Hawke B. R.
Yamato 791197- major mineralogical constituents and its relation to remotely sensed regions of the moon from reflectance spectroscopy

54 1715 - 1735 Keil K.
Lunar meteorite Allan Hills A81005: A review

-- Spcial Lecture --

55 1735 - 1820 Keil K. (Invited Speaker)
Meteoritic Breccias

Wednesday, March 27, 1985

Chairmen: Jun-ichi Matsuda and Takaaki Fukuoka

56 0900 - 0915 Amari S.* and Ozima M.
Search for the extra-terrestrial materials in deep-sea sediments

57 0915 - 0930 Tanaka T.* Shimizu H. Shibata K. and Masuda A.
Positive cerium anomaly of lunar 14310 and ALH-765: Examination by 138Ce/142Ce

58 0930 - 0945 Okano J.* Ueda C. and Nishimura H.
Magnesium isotope abundance in ALH-77304 and ALH-77003

59 0945 - 1000 Takahashi K.* Shimizu H. and Masuda A.
REE abundances in several diogenites

60 1000 - 1015 Shimizu H.* and Masuda A.
REE patterns of eucrites and their genetic implications

61 1015 - 1030 Ebihara M.
Distribution of rare earth elements and uranium in ordinary chondrites including Antarctic meteorites

62 1030 - 1045 Misawa K.* and Nakamura N.
Precise determination of REE abundances in individual chondrules from Allende (C3) and Hedjaz (L3) chondrites

63 1045 - 1100 Matsuda J.* Nagao K. Yamada Y. and Chang S.
Noble gases in the Kirin (Jilin) chondrite

64 1100 - 1115 Nagao K.* Matsuda J. and Inoue K.
Primordial rare gases in carbonaceous chondrites

65 1115 - 1130 Takaoka N.* and Sekii S.
Noble gas studies of Antarctic meteorites

66 1130 - 1145 Okano O.* and Nakamura N.
Additional evidence of Rb-Sr systimatics and REE abundances for 1.2 b.y. impact-melting event on LL-chondrite parent body

67 1145 - 1200 Nyquist Jr. L.* Bansal B. M. C. Y. Shih Wiesmann H. Wooden J. L. and Takeda H.
Rb-Sr and Sm-Nd internal isochron ages of a subophitic basalt clast from the Y75011 eucrite

1200 - 1300 Lunch Time

Chairmen: Ichiro Kaneoka and Tsuyoshi Tanaka

68 1300 - 1315 Schultz L.
Terrestrial ages of four Yamato achondrites

69 1315 - 1330 Sugiura N.* Matsui T. and Strangway D. W.
Gas permeability of some Antarctic chondrites

70 1330 - 1345 Komura K.* Tan K. L. and Sakanoue M.
Cosmogenic Al-26 in Yamato meteorites and their terrestrial ages

71 1345 - 1400 Matsuda E.* and Kigoshi K.
Carbon-14 terrestrial ages of Antarctic meteorites

72 1400 - 1415 Miono S.* Kujirai H. Yoshida M. Ninagawa K. and Takaoka N.
Terrestrial age of an Antarctic meteorite by thermoruminescence technique

73 1415 - 1430 Ninagawa K.* Takaoka N. Yamashita Y. Wada T. and Yamamoto I.
Study of terrestrial age of Antarctic meteorites by thermoluminescence technique

74 1430 - 1445 Weinke H. H. Kiesl W. Kluger F. Koeberl C.*
Trace element investigations on a Sikhote-Alin IIB iron meteorite sample

75 1445 - 1500 Honda M.* Nagai H. Kume T. and Maeda K.
Scandium and silver in iron meteorites

1500 - 1530 Tea Time

Chairmen: Naoyuki Fujii and Masatake Honda

76 1530 - 1545 Funaki M.* Nagata T. and Danon J. A.
Magnetic properties of clear taenite in Toluca iron meteorite

77 1545 - 1600 Nagata T.* Funaki M. Dunn J. R. and Danon J. A.
Magnetic properties of tetrataenite-rich stony meteorites (II)

78 1600 - 1615 Tagai T.* Takeda H. Tokonami M. and Danon J. A.
Iron-nickel partial ordering in tetrataenite by synchnotron radiation

79 1615 - 1630 Strangway D. W.* and Sugiura N.
Magnetic fractionation in the early solar system

80 1630 - 1645 Danon J. A.* Funaki M. and Nagata T.
Magnetic properties of the Santa Catharina Ni rich ataxite

-- Special Lecture --

81 1645 - 1730 Clarke Jr. R. S. (Invited Speaker)
Antarctic iron meteorites: A review(tentative)

Waiting List

82 Fujimura A.* Furumoto M. Takagi Y. and Mizutani H.
Fractal dimensions of fracture surfaces of rock fragments

83 Nagahara H.* and Ozawa K.
Petrology of Y-791493, lodranite

84 Weinke, H. H. Kiesl W. Kluger F. and Koeberl C.*
Trace element analyses in Cape York IIIAB iron and troilite

85 Matsunami S.*
Sulfidation of Fe-Ni metals in ALH-764 (LL3) chondrite: An estimation of minimum of cooling time scale in the primordial solar nebula

86 Wang Daode* Lin Wenzhu and Chen Yonghen
Zhaodong, Zaoyang and Ningqiang chondrites --- the recently fallen meteorites

87 Chang Shuyuan* and Meng Yanxi
Mineralogical and Petrological investigation of Shuangyang chondrites

88 Wang Daode* Malvin D. J. and Wasson J. T.
Study of chemical composition of 35 iron meteorites and its pallication to taxonomy

89 Koeberl C.
Chemistry of light and dark layers in Muong-nong type indochinites

90 Pesonen L. J.* and Elo S.
Geophysical characteristics of the lake Lappajärvi meteorite impact site, western Finland

91 Miura Y.*
Mineralogical studies of Nio-3 (Miyano) H3 chondrites

92 Fukuoka T.* Arai F. and Nishio F.
The role of tephra layers in the meteorite icefield as a time marker

Abstract only, no oral presentation

93 McFadden L. Pieters C. M. Huguenin R. L. King T. V. V. Gaffey M. J. and Hawke B. R.
Yamato 791197- major mineralogical constituents and its relation to remotely sensed regions of the moon from reflectance spectoscopy

94 Steele, I. M. Skirius C. M. and Smith J. V.
Olivine in Belgica 7904 and other chondrites; evidence for relic olivine with unique chemical and textural features

Monday, March 25, 1985

0800 - 1200	Registration, 6th Floor
0930 - 0935	Opening address, Auditorium
0935 - 1700	Symposium, Auditorium
1700 - 1745	Special lecture Professor John T. Wasson (University of California, Los Angels)
1800 - 2000	Reception, Lecture Room, 2nd Floor

Processing of Antarctic meteorites in the National Institute of Polar Research

Keizo Yanai and Hideyasu Kojima
National Institute of Polar Research, 9-10, Kaga 1-chome, Itabashi, Tokyo 173

Antarctic Meteorites of Japanese collections have been recovered, curated and distributed since 1969. To date over 5,500 meteoritic specimens have been recovered both in the Yamato Mountains area and Allan Hills area, Victoria Land. All specimens except the Yamato-84 meteorite collection have been processed, and identification and detailed classification studies are being continued. Some results of classification studies are given in Table 1, and all collections held by the NIPR are listed in Table 2.

Table 1. Classification of some Yamato, Mount Baldr and Allan Hills Meteorites

Type	Y-69	Y-73	Y-74	Y-75	MBR	ALH-76	ALH-77
Iron				2		1	6
Pallasite			1				
Mesosiderite							1
Lodranite			1	1			
Ureilite			4				1
Diogenite	1		22	7			1
Shergottite							1
Howardite		1					
Eucrite			3	5		1	1
C. Chondrite	1		4	3			4
E Chondrite	1		2				2
H3 Chondrite			9	4			1
L3 Chondrite			5	1			40
LL3 Chondrite			2	1		1	2
L-LL3 Chondrite				2			2
H4 Chondrite	1	3	52	11			34
L4 Chondrite			9	11			2
LL4 Chondrite			3	1			
H5 Chondrite	3	2	236	10	1		131
L5 Chondrite			7	5			5
LL5 Chondrite			1	3			1
H6 Chondrite	2	2	218	14	1	2	26
L6 Chondrite		3	71	215		4	33
LL6 Chondrite		1	5	5			1
LL7 Chondrite			1				
Shocked Chondrite			2				1
Ungrouped meteorite			5	5			1
Total	9	12	663	306	2	9	297

Table 2. Japanese Collection of Antarctic Meteorites

Meteorite Name	Date of find	Iron	Stony-Iron	Chond-rite	Achond-rite	*	**	Total	Search Party
Yamato—69	1969 Dec.			7	1	1		9	JARE-10
Yamato—73	1973 Dec.			11	1			12	JARE-14
Yamato—74	1974 Nov.-Dec.		2	630	28	3		663	JARE-15
Yamato—75	1975-76	2	1	289	12	3		307	JARE-16
Mt. Baldr	1976 Dec.			2				2	Joint Japan-U.S.A.
Allan Hills—76	1977 Jan.	1		7	1	1		10	
Allan Hills—77	1977-78	6	1	234	4	3		248	
Purgatory Peak	1978 Jan.	1						1	
Derrick Peak—78	1978-79	5						5	
Meteorite Hills—78	1978-79			28				28	
Bates Nunatak—78	1978-79			5				5	
Allan Hills—78	1978-79	2		173	8	1		184	
Reckling Peak—78	1978-79			5				5	
Yamato—79	1979-80	7	1	3,549	79	31	9	3,676	JARE-20
Belgica—79	1979 Dec.			4		1		5	JARE-20
Yamato—80	1980-81		1	11	1			13	JARE-21
Yamato—81	1981-82			123	2	7	1	133	JARE-22
Yamato—82	1982-83			179	21	10	1	211	JARE-23
Yamato—83	1983 Dec.			42				42	JARE-24
Yamato—84	1984 Dec.						58	58	JARE-25
Total		24	6	5,299	158	61	69	5,617	

*: Carbonaceous Chondrite, **: Unidentified, JARE: Japanese Antarctic Research Expedition, (March 1985)

Measured and computed meteorite concentration and age of ice in the Meteorite Ice Field near the Yamato Mountains.

Fumihiko NISHIO
National Institute of Polar Research

In order to estimate meteorite concentration and age of ice in the Meteorite Ice Field near the Yamato Mountains, meteorite mass concentration and age of ice are computed based upon the model of meteorite concentration. Figure 1 shows the distribution of meteorite mass concentration, bedrock and surface topography of the bare ice in the area upstream of Massif A to Motoi Nunatak. In this area more than 1000 specimens were found and collected. Most of meteorite pieces were found on the bare ice surface downstream of the presence of the sub-ice ridge, that is, a steep ice thickness gradient. This situation means that ice arrives at the surface with slow downglacier movement and there is more time for concentration before the meteorites are delivered to the end of the glacier.

(1) meteorite mass concentration

The expected meteorite mass concentration in various parts of the Meteorite Ice Field can be calculated by the Whillans's equation. In the results the meteorite mass concentration computed by the equation of the model are more than 10 times larger than that of the Figure 1. The less meteorite concentration predicted by the equation of the model may be affected by the younger ice and the meteorite infall rate on the earth's surface.

(2) Ages of ice

Based upon the structural laboratory studies of ice collected at the surface near Massif A, the age of the bare ice, approximately 30 ka, are estimated by fabric characteristics and estimated stress condition of ice flow. The estimated ages of ice by ice core study are also about 10 times larger than the age of ice computed by the equation of the model.

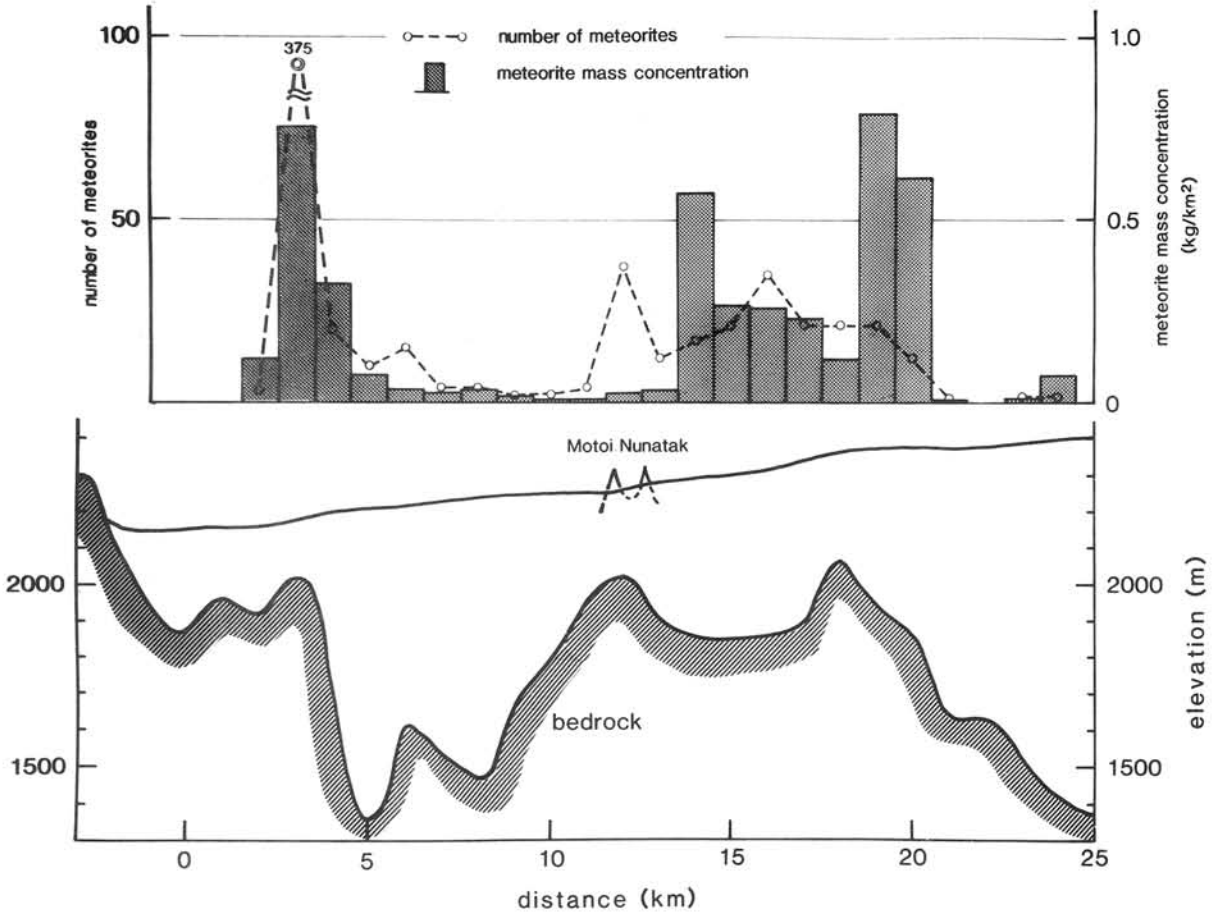

Figure 1. Meteorite mass concentration, ice surface and bedrock elevation from Massif A to Motoi Nunatak in the bare ice area near the Yamato Mountains.

A review of the Yamato-80, 81 and 82 meteorite collections

Graham A. L.,* Yanai K.** and Kojima H.**
*British Museum(Natural History), London
**National Institute of Polar Research, Tokyo

The Japanese Antarctic Research Expeditions for the field seasons 1980-81, 1981-82, 1982-83 and 1983-84 have returned with a total of 396 meteorite specimens. By far the majority of these are fragments of ordinary chondritic material, usually with some fusion crust, and most weigh less than 10 g. For example for the 1983-84 field season, 86% weigh less than 10g. The hand specimens of most of this material have now been described and thin sections made of selected specimens. Worthy of special note are a number of carbonaceous chondrites, both type 2 (CM) and type 3 (CO3), a small individual ureilite and a fragment of a further meteorite which is possibly of lunar origin. In addition a total of 13 basaltic achondrite specimens were recovered during the 1982-83 expedition. One of these is a cumulate eucrite with homogeneous feldspar, An90.5, and pyroxenes in the compositional range Wo4.9 Fs57.6 En37.5 to Wo19.5 Fs45.4 En35.1.

4

The Research of Meteorite in China Expediting The Development of Related Fields

Chang Suyuan
Department of Geology, Peking University, Beijing, China

For a long time Chinese have been paying much attention to the study of meteorite. The earlist information of meteorite might be traced from the myths and legend of ancient China, such as "Nheo (a goddess) repairing the heaven" and "the tear of Change (the goddess of moon)". It is well known that there were a lot of historical meteorites written and recorded in chinese ancient books, such as rain metal, falling stone from the sky and falling star lake (crater),etc..

The event of Jilin meteorite shower in 1976 rapidly expedited the development of the research for meteorite, since then, twenty meteorites with different type and group(iron meteorite-1; stone meteorite-19; C-1, L-4; LL-1, H-3, E-1, undeterminate-9)were discovered, and made headway for reseach in many more aspects. The study of meteorite also pushed foreward the research of the related fields. Since 1979, more material like cosmic dust were discovered at ocean bottom and some strata, especially in precambrian and cenozoic layers, and further work were done with analysis and contrast and evaluation. The abnormality of Iridium was discovered at the bottom of cambrian strata and the bounderies of T-P and E-K. Some people are interested in the relation between the cycle of meteorite and biological extinct. Some scientists are enthusiastic in looking for crater in China mainland. All in all, the research of meteorite are expanding the view of geoscientists giving more attention to the effect of outer earth and are reestablishing of a united view of nature permeated with the heavenly body, the Earth and the biology.

IDENTIFICATION OF MINERALOGICAL-PETROLOGICAL CLASSES OF METEORITES - A PETROPHYSICAL METHOD

Pesonen, L.J.,* Kukkonen, I.T.* and Lehtinen, M.**

* Geological Survey of Finland
SF-02150, Espoo 15, Finland

** Mineralogical Museum
Department of Geology
University of Helsinki
SF-00170, Helsinki 17, Finland

A national program to study the petrophysical systematics of meteorites in Finnish meteorite collections was started by the Geological Survey of Finland (GSF) in 1981 (Kukkonen and Pesonen, 1983). The scope of the program is as follows:

(i) to develop a rapid method to classify meteorites into their main types and groups by measuring the physical properties of the meteorites, such as the low field susceptibility, intensity of the Natural Remanent Magnetization (NRM) and bulk density.

(ii) to calibrate the method by comparing the results with existing petrological-mineralogical classification data

(iii) To use the petrophysical classification scheme to distinguish the genuine meteorites from specimens of rock or other material (false meteorites) which closely resemble meteorites.

(iv) to carry out additional magnetic studies on selected meteorites including magnetic hysteresis measurements as proposed by Nagata (1979) and a.f. and thermal demagnetization studies.

In the first stage of the program we measured the petrophysical properties of 54 meteorite samples in the Laboratory of Petrophysics of the GSF. The specimens included achondrites, chondrites and stony-irons and iron meteorites. The results show distinct relations between susceptibility and NRM and between susceptibility and bulk density. The susceptibility and intensity of NRM increase from achondrites to irons as a function of increasing metallic Ni-Fe content. Moreover, the chemical groups of condrites and stony-irons appear as different groupings in the petrophysical relation diagrams. The susceptibility - density diagram (Fig.1)in particular offers a rapid method for identifying a meteorite group or class. The petrophysical classification method was successfully applied to previously published petrophysical data from the meteorite collections of the U.S.S.R. When meteorites are compared with terrestrial basic igneous rocks, the petrophysical properties of the mafic or ultramafic terrestrial rocks (peridotites, pyroxenites, gabbros, diorites and diabases) are seen to fall outside the area of achondrites in the susceptibility - NRM diagram. Thus it is possible, in principle, to distinguish achondrites from terrestrial rocks by petrohysical measurements. Problems of the method, which will be discussed in this paper, arise from consideration of the effect of shape demagnetization, anisotropy and electrical conductivity on petrophysical measurements.

During the second stage of the current program we have measured nearly 400 meteorite samples of the collection of the Mineralogical Museum of the Helsinki University and of private collections. We have also included tektites, and some "false" meteorites to see how they appear in the petrophysical relation diagrams. Results of these measurements will be presented. Future plans in applying the method in meteorite studies will be discussed.

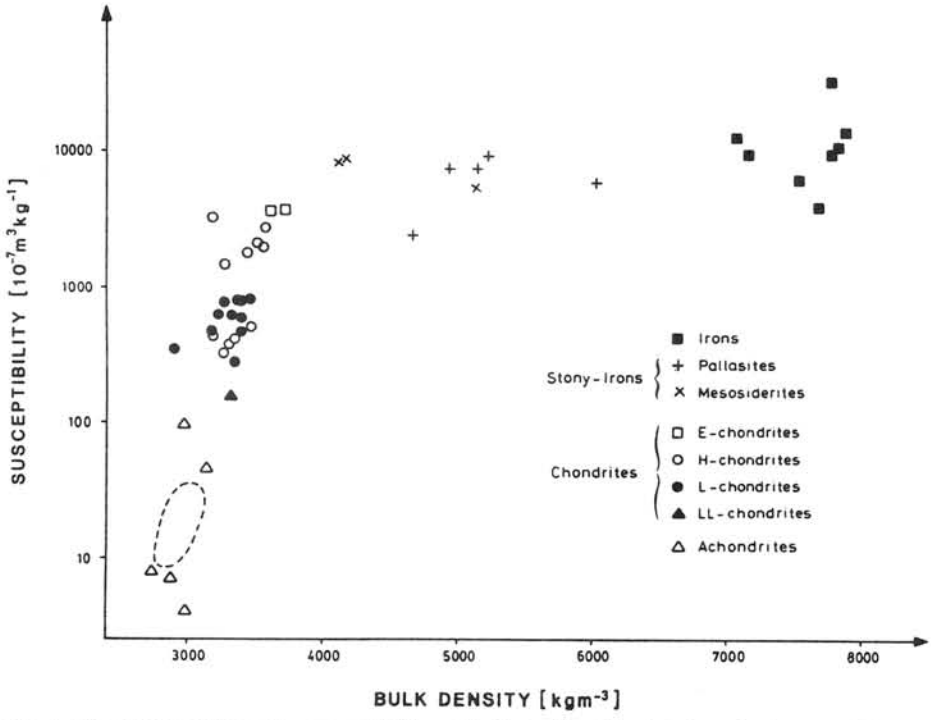

Fig. 5. The relation between the susceptibility and bulk density. Only data (samples from 46 different meteorites) from which the density was measured are included. The closed dashed line gives the area of the most common terrestrial igneous rocks. See text for further details.

Fig.1. From Kukkonen and Pesonen (1983)

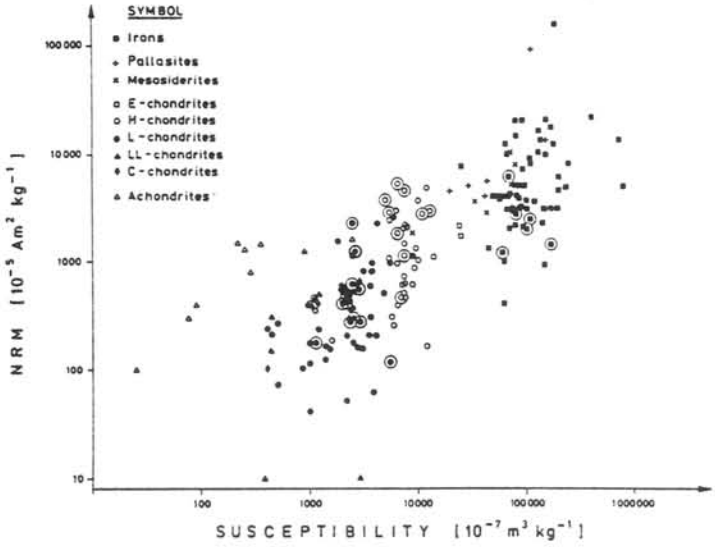

Fig. 3. Test of the petrophysical classification method. NRM is plotted against susceptibility (both per unit mass). The data from the U.S.S.R. meteorite collections are the same as used by Herndon *et al.* (1972) except that they are recalculated into SI units. The results with an extra circle around the symbol are listed in Herndon *et al.* (1972) without chemical classification, which in the present study is taken from Hey (1966) and Hutchison *et al.* (1977). The magnetic classification is in good agreement with the chemical-petrological classification.

Fig.2. From Kukkonen and Pesonen (1983)

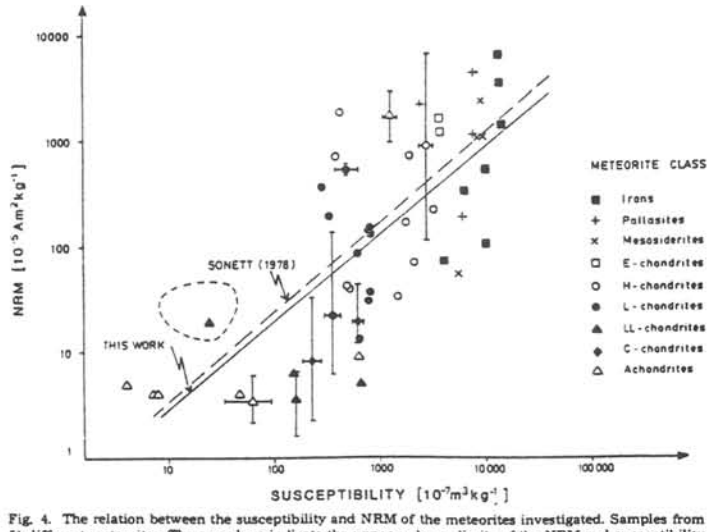

Fig. 4. The relation between the susceptibility and NRM of the meteorites investigated. Samples from 51 different meteorites. The error bars indicate the upper or lower limits of the NRM and susceptibility values for different samples of the same meteorite. The straight line is the best least square fit through all the data points. The broken line is taken from similar work by Sonett (1978). The closed dashed line gives the area of the most common terrestrial igneous rocks. See text for further details.

Fig.3. From Kukkonen and Pesonen (1983)

References

Kukkonen, I.T. and Pesonen, L.J., 1983. Classification of meteorites by petrophysical methods. Bull.Geol.Soc. Finland, 55 (2), 157-177.

Nagata, T., 1979. Meteorite magnetism and Early Solar System Magnetic Field. Phys. Earth Plan. Int., 20, 324-341.

6—1

ORDINARY CHONDRITE FALLS AND CONGENERS FROM VICTORIA LAND, ANTARCTICA: VARIATIONS IN PARENT SOURCE REGIONS

Jane E. Dennison, Patrick W. Kaczaral, David W. Lingner and Michael E. Lipschutz

Dept. of Chemistry, Purdue University, W. Lafayette, IN 47907 U.S.A.

Antarctic meteorite discoveries have created great scientific interest due to the large number of specimens recovered (~7000 so far) and because they include representatives of hitherto rare or unknown types. Some of these are paired: the number of different meteorites represented by the Antarctic collection in unclear therefore. We estimate this as ~1400, a number comparable with the 2613 known non-Antarctic meteorites (1). Antarctic meteorites are so abundant because they have fallen over long periods ($\leq 7 \times 10^5$ years, averaging 3×10^5 years in Victoria Land) and have been preserved, transported and concentrated by the ice sheet (2). Since rare and unique Antarctic and non-Antarctic meteorites differ, we decided to investigate whether more common meteorites also differ. If so, this would have profound implications for planetary studies. Here, we report progress on that study.

We used RNAA to determine 13-15 trace elements (ppm-ppt levels) known from previous studies to yield important genetic information in meteorites. We focused our attention on H5 and L6 chondrites for several reasons. H and L chondrites each constitute 40% of non-Antarctic falls and petrologic types 5 and 6 are, respectively, the overwhelming majority of these chondritic types. We have recently been studying ordinary chondrite genesis and evolution and have therefore generated a great deal of useful data for non-Antarctic falls (**3-6**) useful for comparison with results for unpaired samples from Victoria Land.

We tested means and standard deviations using standard statistical tests for 18 Victoria Land and 20 non-Antarctic H5 chondrites (7) and for 13 and 25 L6 chondrites, respectively. Normal or lognormal distributions were chosen to represent the data. For H5 chondrites, 7 of 13 elements differ at >90% confidence level using a single-sided t-test: for L6 chondrites, 8 of 13 do (Table 1). While elements that differ overlap to some extent, those that do, differ in direction. From this and other data, we can show that differences do not reflect Antarctic weathering or incidental causes (sample selection bias, compositional modeling, analytical bias or chance (7)).

We interpret compositional differences as reflecting derivation of Antarctic meteorites predominantly from parent sources or regions different than those from which contemporary falls derive. Hence, the near-earth meteoroid complex sampled by Victoria Land 3×10^5 years ago differed from that sampled today (7). For example, the Victoria Land L6 chondrite sample population derived from a body or region much more heavily shocked, on average, than the one(s) we now study through contemporary L chondrites (**3-5**). Antarctic meteorites truly constitute a solar system snapshot in time and space.

Acknowledgements - We thank the U.S. National Science Foundation (grant DPP 8111513) and the National Aeronautics and Space Administration (grant NAG 9-48) for partial support of this research and the U.S. Department of Energy for irradiation support (grant DEFG 0280 ER 10725)

REFERENCES: (**1**) A. L. Graham, A. W. R. Bevan and R. Hutchison (1985) The Catalog of Meteorites, 4th Edn. (**2**) C. B. B. Bull and M. E. Lipschutz (1982) Workshop on Antarctic Glaciology and Meteorites, LPI Tech. Rept. 82-03. (**3**) C. W. Neal, R. T. Dodd, E. Jarosewich and M. E. Lipschutz (1981) Geochim. Cosmochim. Acta 45, 891-898. (**4**) T. M. Walsh and M. E. Lipschutz (1982) Geochim. Cosmochim Acta 46, 2491-2500. (**5**) T. J. Huston and M. E. Lipschutz (1984) Geochim. Cosmochim. Acta 48, 1319-1329. (**6**) D. W. Lingner, T. J. Huston and M. E. Lipschutz (1985) in preparation. (**7**) J. E. Dennison, D. W. Lingner and M. E. Lipschutz (1985) in preparation.

Table 1. Comparison of statistically significant (>90% confidence level) differences in H5 and L6 chondrites from Victoria Land, Antarctica with contemporary non-Antarctic falls.

Element	H5 Ant.(18)†	H5 Non(20)†	H5 Sig.†	Element	L6 Ant.(13)†	L6 Non(25)†	L6 Sig.†
Co (ppm)*	810	879	*91*	Co (ppm)*	477	605	97
				Au (ppb)*	145	165	*90*
Se (ppm)*	9.1	8.2	99				
Rb (ppm)	1.91	2.50	98	Rb (ppm)	2.62	2.20	95
				Cs (ppb)	4.02	12.4	99
				Te (ppb)	337	379	*90*
Bi (ppb)	2.6	1.14	95	Bi (ppb)	0.58	2.67	99
				Ag (ppb)	45	71	97
In (ppb)*	0.17	0.49	99				
Zn (ppm)*	41.8	53.1	97				
Cd (ppb)	0.68	3.7	99	Cd (ppb)	1.6	14.2	99

*Arithmetic means: all others are geometric means.

†Column headings: Ant. - Antarctic chondrites from Victoria Land; Non - Non-Antarctic chondrite falls; Sig. - Significance level at which it may be concluded that the respective sample populations do not derive from the same parent population. Numbers in parentheses are number of samples analyzed in that population.

7—1

PETROLOGY OF ENSTATITE CHONDRITES, Y-691(EH3) AND Y-74370(EH4)

Hiroko Nagahara, Geol. Inst., Univ. Tokyo, Hongo, Tokyo 113, Japan

Recent works on primitive chondrites have revealed that they keep informations on the early solar nebula, the interstellar materials, or both. One of the major problems on E chondrites are the time, place, and process of achievement of extremely reducing conditions and anomalous mineral assemblages. In this paper, based on the petrologic study on two antarctic meteorites, Y-691 and Y-74370, the precursor materials and reducing processes in E chondrites are discussed.

Y-691 Constituents of Y-691 are chondrules, metal-sulfide nodules, mineral fragments, and matrix. A characteristic feature is presence of abundant olivine-bearing chondrules; about 50 of 400 chondrules in a thin section studied (about 13%) are ol-bearing. Relic olivine and pyroxene with abundant metal blebs inside the grains showing dusty appearance are abundant in chondrules. Primary composition of those olivine and pyroxene obtained by broad electron beam including metal blebs are Fo85 and En95, respectively [1]. This shows that although most chondrules in EH3 and EH4 chondrites contain scarce or no olivine and they are essentialy free from FeO if any, their precursor materials would have contained both olivine and pyroxene with considerable amounts of FeO. The oxygen fugacity during chondrule formation for E chondrites was variable as shown by various mineral assemblages; such as enstatite-forsterite-metallic iron, enstatite-SiO_2-metallic iron, and niningerite (Mg-sulfide) along with enstatite as a phase of Mg.

Metal-sulfide nodules are similar in size to chondrules and show complex texture and mineral assemblage. They are classified into two types by the presence or absence of silicate inclusions. Nodules without silicate inclusions are more complex than those with silicate inclusions. The texture shows that the nodules could not be chondrules formed through melting of precursor materials. An extreme nodule consists of polycrystalline troilite having lamellae of daubreelite with conjunction angle of 120° in the center indicative of slow cooling, and surrounding kamacite, oldhamite, niningerite, and graphite with small amounts of schreibersite, perryite, caswellsilverite (15.3Na, 36.4Cr, 2.2Fe, 45.3S), and daubreelite (18Fe, 35Cr, 0.5Mn, 2.5Zn, 43S). Polycrystalline lacy kamacite rims the inner part. Rarely djerfisherite (52.4Fe, 1.6Ni, 0.4Na, 7.6K, 4.2Cu, 33.2S)is present. All of these minerals are homogeneous. These nodules do not contain silicates and are essentially free of Si and other major elements except for Fe and Ni in sulfides. This should have been formed under reducing and high f_{S_2} conditions. Those nodules may have been formed by fractionation of Si (possibly as SiC) at high temperatures, aggregation of middle temperature condensates under the condition of C/O~1.5 [2], and subsequent annealing at lower temperatures (lower than several hundreds K). Silicate-bearing nodules always have smooth surface and rounded shape. Most of them are composed mainly of kamacite with or without small amounts of troilite, schreibersite, and niningerite. Silicates are mostly SiO_2 with subordinate albite and enstatite, having oval shape and forming an alignment parallel to the outline of the inclusions. These nodules may be formed through annealing at subsolidus temperatures and under slightly oxidizing condition exsolving Si as SiO_2 from metallic iron with high Si content or precipitation of silicate minerals in the pore space of kamacite at higher temperatures.

Mineral fragments are mainly enstatite, kamacite, troilite, and niningerite. Exceptionally iron-rich pyroxene and olivine are found [1]. They are fairly large, up to 100 μm in size, showing fragmental appearance.

Ferrous pyroxene coexists with SiO_2(Fig. 1) and their composition varies from En85 to En60 from grain to grain (Fig. 2). Besides these pyroxene grains, magnesian pyroxene grains are present. Both ferrous and magnesian pyroxenes do not have compositional gradient between their contacts, indicating that they have not been heated after accretion. Ferrous olivine has numerous lamellae of metal (Fig. 3). The metal free portion of those olivine grains was Fo90-91, whereas primaly olivine including metal lamellae obtained by broad electron beam is Fo88 to Fo75 or less. They are mantled by friable rim and embedded in fine-grained matrix which mainly consists of enstatite (En99-90), SiO_2, albite, kamacite, troilite, and niningerite.

Y-74370 Y-74370 belongs to EH4 [3]. Bulk chemical composition of major elements by wet chemical analysis (Table 1) and that of major and minor elements by INAA and RNAA (Table 2) show that is has a composition wihtin the variation of EH chondrites and that it cannot be distinguished from other EH chondrites. Oxygen isotopic composition, $\delta^{18}O$ +1.35, $\delta^{17}O$ +0.40 (by R. N. Clayton and T. K. Maeda), shows that Y-74370 suffered terrestrial weathering which is also shown in the presence of considerable amount of H_2O by wet chemical analysis. However, it is curious that the composition lies below the terrestrial fractionation line, and further reinvestigation will be required.

Y-74370 characteristically contains chondrules and clasts with anomalous textrure and mineral assemblage [3,4]. Some anomalous chondrules comprise tridymite, niningerite, and troilite with or without albite where Mg and Fe occur as sulfides, and some comprise tridymite and glass of enstatite composition. These chondrules were formed under reducing and high f_{S_2} conditions which were different from those for other chondrules where Mg and Si exist in silicates.

Y-74370 contains scarce olivine and abundant SiO_2 in chondrules and as mineral fragments. Olivine is almost pure forsterite (Fo100-99.5), and pyroxene in chondrules is also magnesian (En99.8-98.0), indicating that Y-74370 is more reduced than Y-691, and that reduction took place after accretion to chondrites and in the parent body.

Conclusion Constituents of E chondrites were formed under various atmospheric conditions; sulfide, phosphide and metallic minerals were formed under highly reducing and high f_{S_2} conditions, which could be achieved under high C/O condition [2] and were different from solar system C/O composition, which might be due to gas-dust fractionation prior to accretion as proposed by [5]. Ferrous pyroxene, ferrous olivine, and chondrule precursor minerals were formed under relatively oxidized conditions which could be similar to ordinary chondrites. Chondrules were reduced during crystallization to have formed metal blebs inside olivine and pyroxene grains. Large olivine grain was reduced before incorporation into chondrites, whereas ferrous pyroxene was not reduced. When those constituents aggregated to have formed a body, their mineral assemblages, forsterite-enstatite-SiO_2-metallic iron-ferrous silicates, was in highly disequilibrium. They suffered further reduction in the parental body to have changed the assemblage into enstatite-SiO_2-metallic iron, due to heating, probably thermal metamorphism.

References [1] H. Nagahara (1985) Lunar Planet. Sci., XVI. in press. [2] J. M. Lattimer et al. (1978) Astrophys. Jour., 219, 230-249. [3]H. Nagahara and A. ElGoresy (1984) Lunar Planet. Sci., XV, 583-584. [4] H. Nagahara (1984) Meteoritics, 19 (in press). [5] J. W. Larimer and H. A. Bartholomay (1983) Lunar Planet. Sci., XIV,423.

Table 1
Bulk chemical composition

	Y-74370
SiO2	34.14
TiO2	0.12
Al2O3	2.51
FeO	3.90
MnO	0.23
MgO	18.20
CaO	1.10
Na2O	0.74
K2O	0.09
H2O(-)	1.05
H2O(+)	5.90
P2O5	0.46
Cr2O3	0.43
Fe	16.60
Ni	1.51
Co	0.05
FeS	12.77
Total	99.8
Fe(tot)	27.74

Analyst: H. Haramura

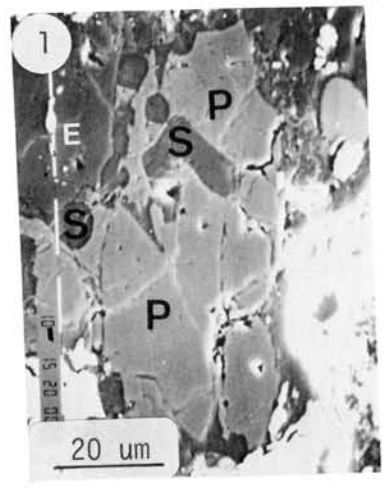

Fig. 1 Fe-rich pyroxene fragment (P) coexisting with SiO_2(S) next to pure enstatite(E) in Y-691.

Fig. 3 Ferrous olivine fragment with lamellae of metallic iron in Y-691.

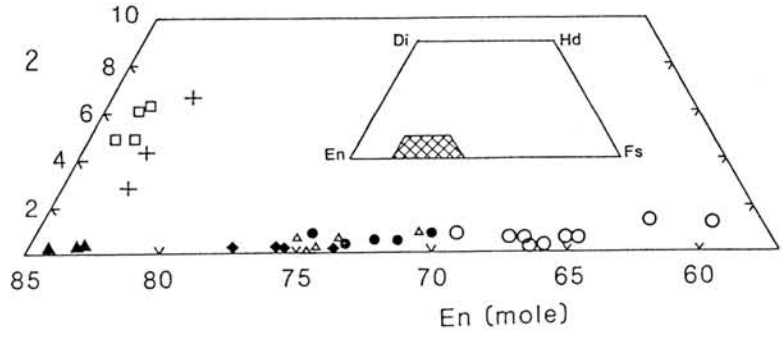

Fig. 2 Composition of ferrous pyroxene in Y-691. One symbole denotes the variation in one grain. After [1].

Table 2 Cemical composition of Y-74370 by INAA and RNAA

Na (mg/g)	Mg (mg/g)	Al (mg/g)	K (ug/g)	Ca (mg/g)	Sc (ug/g)	V (ug/g)	Cr (mg/g)	Mn (mg/g)	Fe (mg/g)
5.78	105	8.11	613	7.78	5.85	51.8	2.92	1.96	260

Co (ug/g)	Ni (mg/g)	Zn (ug/g)	Ga (ug/g)	As (ug/g)	Se (ug/g)	Br (ug/g)	Ru (ng/g)	Sb (ng/g)	Te (ug/g)
804	16.9	159	12.9	2.70	20.6	6.30	1140	135	2.3

La (ng/g)	Sm (ng/g)	Eu (ng/g)	Yb (ng/g)	Lu (ng/g)	Re (ng/g)	Os (ng/g)	Ir (ng/g)	Au (ng/g)
235	127	40	160	23	46	630	555	269

Analysts: G. W. Kallemeyn and J.T.Wasson

CHEMICAL COMPOSITION OF 19 L AND LL CHONDRITES AND ITS APPLICATION TO TAXONOMY

Wang Daode*, G.W.Kallemeyn** and J.T.Wasson**

*Institute of Geochemistry, Academia Sinica, Guiyang, The People's Republic of China

**Institute of Geophysics and Planetary Physics, University of California, Los Angeles, CA 90024, U.S.A.

We determined 25 elements of 19 L and LL chondrites by INAA and analyzed the chemical compositions of olivine in these chondrites. Seven of 19 L and LL chondrites are from China. In order to obtain petrographic controls we sawed single chips weighing 3 grams into several 1-2mm slices with a low-speed saw. Alternating slices were used for thin sections and for neutron activation analysis. Our L and LL chondrite normalized to Mg and to Cl chondrites indicate that for several lithophiles (Al,V,Cr,Mn) the amount of scatter is low, similar to that observed in the carbonaceous chondrites. Our data confirmed the well-known fact that abundance ratios for these refractory and volatile elements are 0.8-0.9. L-group siderophile contents scatter more than that observed in the carbonaceous chondrites, and the LL chondrite siderophiles show still greater variance. Much evidence indicates that L and LL chondrites were formed in separate parent bodies. However, it has been proved difficult to choose the correct group designations for some meteorites. Average LL group siderophile concentrations are lower than those in L-group, but sampling problems are large and siderophile contents of individual chondrites often overlap. To avid sampling problems we suggest that a two-demensional criterion, the atomic ratio of Ir/Au and chemical composition of olivine (Fa %) can be used as a new taxonomic parameter for the classification of ordinary chondrite (H,L and LL). The atomic ratio of Ir/Au for 11 L chondrites range from 2.59-3.35 with an average of 2.84, and for 7 LL chondrites the range is 1.84-2.49 with an average value of 2.2 (Tabl 1). The boundary ratio between the two groups is about 2.50.

Based on the concentration Br and Se in L and LL chondrites we recommend Br concentration and Br/Se atomic ratio as indicators

in discriminating the thermometamorphic degree and petrological type of chondrites. Types 3 and 4 of L and LL chondrites have a relatively high Br concentration ranging from 0.46 to 2.5 (μg/g), with a Br/Se ratio of 0.067-0.26 whereas types 5 and 6 have a somewhat lower Br concentration range of 0.08-0.32 (μg/g), with a Br/Se ratio being 0.008-0.060. Thus Br is shown to be a high volatile element that increases with decreasing petrologic grade. For most chondrites, the Br/Se ratio of type 3 and 4 is greater than 0.05 and that of type 5 and 6, less than 0.05, which is the result of Br loss during thermometamorphism of the parent body.

Table 1. The composition of olivine and Br, Se concentrations and Ir/Au ratio in 19 L and LL chondrites

Chondrites	Type	Fa%	Br (μg/g)	Se (μg/g)	Br/Se (atomic ratio)	Ir/Au (atomic ratio)
Manych	LL3	19.87 32.88 30.26 32.70	1.42	9.2	0.152	2.38
Albareto	LL4	26.61	0.55	10.5	0.052	1.84
Bjurbole	LL4	26.18	0.46	6.4	0.071	2.01
Bo Xian	LL4	28.42	0.79	8.5	0.092	2.28
Barratta	L4	24.08	2.5	9.3	0.265	2.73
Saratov	L4	23.79	0.55	8.1	0.067	2.76
Tennasilm	L4	23.30	1.12	6.9	0.160	2.74
Guidder	LL5	28.63	0.32	5.3	0.060	2.33
Knyahinya	L5	25.10	0.12	8.2	0.014	3.25
Rugao	LL6	27.84	0.21	25.8	0.008	2.20
Dongtai	LL6	26.78	-	10.4	-	2.49
Dhurmsala	LL6	27.50	0.16	10.2	0.016	3.22
Xi Ujigim	L6	26.13	-	11.0	-	2.59
Lishui	L6	25.27	-	10.0	-	2.96
Leedey	L6	25.20	0.08	9.0	0.009	3.05
Jartai	L6	24.64	0.29	7.1	0.040	3.35
Guangrao	L6	25.11	-	8.8	-	2.78
Barwell	L6	25.03	0.26	9.6	0.027	2.78
Alfianell	L6	25.05	0.30	9.3	0.032	2.69

FINE GRAINED LITHIC FRAGMENTS IN THE L3 CHONDRITES

Seiko WATANABE, Masao KITAMURA, Nobuo MORIMOTO
Department of Geology and Mineralogy, Faculty of Science, Kyoto University, Sakyo, Kyoto 606, Japan
and Toshisuke KAWASAKI
Faculty of Education, Kochi University, Kochi 780, Japan

Fine grained lithic fragments (FGF's hereafter) consist mainly of fine grained crystals, about several microns in size (Fig. 1). Kimura (1983) reported that FGF's resemble some chondrules in bulk composition, but fine grained olivines in them are rich in Fe. Refering to dark-zoned chondrules (Dodd and Van Schmus, 1971), he suggested that FGF's have derived from orthodox chondrules through secondary modification by heating and/or shock. On the other hand, Nagahara (1983) pointed out that the texture of FGF's resemble to experimental products heated to temperatures much lower than the liquidus temperature, and suggested that FGF's have derived by lower temperature heating of the same precursor materials as chondrules. In the present study, the texture and chemistry of FGF's have been studied to elucidate their origin.

Seven FGF's in ALH-77015 (L3) and ALH-77214 (L3) were studied by an electron probe microanalyzer.

(a) Four FGF's consist of olivine + Ca-rich pyroxene + opaque minerals + interstitial plagioclase or glass. Fine olivine grains are rich in Fe and homogeneous in each FGF, though the inbeded coaser olivines show the chemical zoning with Fe-poor core. In the most typical case (Figs. 1 and 2), compositions of olivine and pyroxene are Fa_{37-39} and $Fs_{20}Wo_{13}$ - $Fs_{18}Wo_{30}$, respectively.

(b) One FGF consists of olivine + Ca-poor and Ca-rich pyroxenes + opaque minerals + interstitial glass. Olivines are fine grained but heterogeneous in Fa_{19} - Fa_{38}. Pyroxenes are coarse. Ca-poor and Ca-rich pyroxenes are $Fs_{9-11}Wo_{1}$ and $Fs_{7}Wo_{31}$, respectively.

(c) One FGF consists of olivine + Ca-poor pyroxene + opaque minerals + glass. Fine grained olivines are Fa_{45}, and coarse ones Fa_{16-42}. Pyroxenes are coarse and $Fs_{10}Wo_{4}$.

(d) One FGF consists only of olivine (Fa_{42}) + opaque minerals + glass.

The existence of glass suggests the heating event above their solidus temperature. Since the modification of chondrules by heating below their formation temperature must diminish the glass, the precursors should be the minerals in low temperature assemblages.

Preliminary experiments on the origin of the FGF's have been carried out. The starting materials, powders of chondrites, were heated at 1000 - 1300°C. The results show that Fa components of olivines are around Fa_{15}-Fa_{40}, which varies depending on the heating temperature. The compositions of the olivines in the heated charges are almost the same as those of the olivines in the FGF's, indicating that the heating temperature of the FGF's are around 1000 - 1300°C.

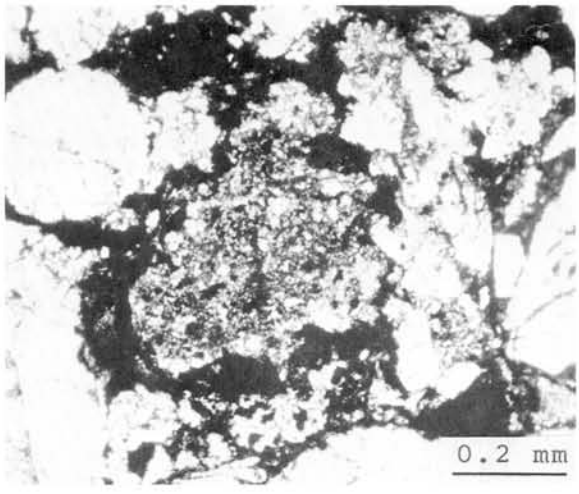

Fig. 1. Optical micrograph of FGF in ALH-77249

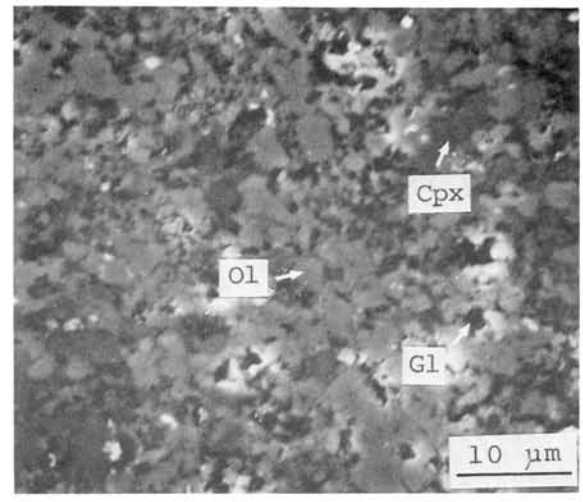

Fig. 2. Scanning electron micrograph of FGF in ALH-77015

[REFERENCES]

Kimura,M. : Mem Natl Inst Polar Res, Spec Issue, **30** 146, 1983
Dodd,R.T.& Van Schmus,W.R. : Chem Erde, **30** 59, 1971
Nagahara,H. : Mem Natl Inst Polar Res, Spec Issue, **30** 61, 1983

LOW TEMPERATURE REMANENT MAGNETIZATION OF Fe-Ni ALLOY

Kan-ichi MOMOSE* and Hiroyuki NAGAI**
(*)Department of Geology and (**)Department of Physics,
Faculty of Science, Shinshu University, Matsumoto 390.

Magnetic properties of synthetic 29at%Ni-Fe alloy were investigated for the purpose of understanding magnetization process of some meteorites. It was found that a stable remanent magnetization is acquired by cooling the alloy at 77K under the influence of geomagnetic field. This RM is a new type RM due to the martensitic transformation from fcc to bcc phase of the alloy. We denote this RM as low temperature RM (LRM). The explanation that the LRM is formed by the martensitic transformation is understood by the following experimental results:

(1) The RM of bcc phase does not change its direction and intensity after cooling in zero magnetic field (less than 40γ).

(2) The LRM of bcc phase acquired by cooling at 77K does not change its direction and intensity of magnetization after repeated cooling at 77K in the geomagnetic field perpendicular to the original LRM.

Therefore, the mechanism to form the RM of bcc phase by cooling and the martensitic transformation differs from the invers TRM (transitional RM) found by Ozima et al. which is acquired by cooling or heating through the isotropic point of Fe_3O_4. Natural remanent magnetization of some meteorites may possibly be of this origin.

Reference

M.Ozima, M.Yama-ai and T.Nagata, Role of crystalline anisotropy energy on the acquisition of stable remanent magnetization, Geofis., Pura Appl., 55, 77-90, 1963.

11

VENTIFACTION OF METEORITES EXPOSED IN POLAR AREAS

Splettstoesser, John F.

Minnesota Geological Survey, University of Minnesota, St. Paul, MN 55114

Ventifacts--stones or pebbles that are shaped, worn, polished, etc., by the abrasive action of wind--are common in polar and other areas where rock materials are exposed for relatively long periods of time to winds of relatively high velocities. Ventifacts are common in Antarctica, and many research studies have been done to explain their origin, such as the cause of specific surface features, the role of salt vs. wind weathering, and the length of time required to produce the features. The length of time is particularly difficult to quantify, even though a number of investigators have conducted both field and laboratory experiments that have been designed to provide estimates of the presumed thousands of years required to produce advanced ventifaction. The time element would be specially useful as an aid in dating glacial retreat in areas where radiocarbon or other chronology is not feasible.

Similarly, it should be possible to estimate age of ventifaction features on meteorites exposed on the ice sheet as a result of glaciological information from investigators who are studying the combined aspects of date of the fall on the ice sheet, englacial transportation mechanism and time of transport, and the approximate length of time of exposure on the surface. Any meteorite (metallic or stony) would be appropriate for analyzing the subtle features of terrestrial (ground-based) wind erosion on meteorites, as distinguished from fusion and related features caused by entry into Earth's upper atmosphere. Meteorite hardness might inhibit erosion by wind, but dust-laden air (free of mineral or ice particles) has been shown to induce ventifact features, and softer materials have been shown to abrade harder materials. Thus, ventifacts are easily formed under a variety of field situations and in a variety of rock lithologies, including meteorites.

ROUNDING OF CHONDRULES BY ABRASION

Masao KITAMURA, Seiko WATANABE and Nobuo MORIMOTO
Department of Geology and Mineralogy, Faculty of Science, Kyoto University, Sakyo, Kyoto 606 Japan

Nowaday, it is widely accepted that the spherical shapes of chondrules are owing to those of the silicate-melt droplets. It has been thought that no meaningful change of the shapes of chondrules occur at the accretion process to the parent body. The change of the shapes between the unequilibrated chondrites (UEC's) and equilibrated chondrites (EC's) had been considered to have resulted from thermal metamorphism after the accretion. However, recent analytical electron microscopic studies [1] suggest that the differences among the petrologic types depend upon that of the cooling rate during or before the accretion. Therefore, the change of the shapes of the chondrules between the UEC's and EC's should be explained by the cooling process.

In the present study, the shape of the chondrules has been compared with each other to elucidate the effect of the cooling rate and the abrasion of chondrules to the rounded shape.

All of the chondrules have the spherical shape as the definition. The surface morphology varies from chondrule to chondrule. Based on the surface morphology, three types of the chondrules were defined : (A) chondrule with rounded and sharp surfaces (Figs. 1 & 2), (B) chondrule with irregular surface (Fig. 3), and (C) chondrule without clear surfaces (Fig. 4). The type C is abundant in the EC's, which had been thought to be modified by the metamorphism in the parent body. The type B is abundant in the UEC's and the petrologic type 4. The type A is not abundant but common in the UEC's.

A typical example of the type A is the pyroxene single crystal with the rounded and clear surface (Fig. 1). Since an euhedral pyroxene crystal has not the rounded morphology, the shape of the chondrule suggests that the surfaces are rounded by abrasion. Barred olivine chondrules with clear surfaces (Fig. 2) are also considered to be rounded by abrasion, becuase most of the barred olivine chondrules belong to the type B and are rimmed not by an intergrowth of olivine and glass (Fig. 2) but only by olivine crystal.

The type B and C chondrules are considered not to have suffered abrasion after the chondrule formation. Some of the irregular surfaces of the type B could be due to the adhesive growth of the chondrule by the fine grains (Fig. 3). The differences between these two types can be considered to be formed by the cooling rate. The surface tension of the melt would not play an important role in retaining the spherical shape when the cooling rate is slow enough to change the shape of the chondrule by the crystal growth (Fig. 4).

Some of the type A chondrules in the UEC's, especially in E3 chondrites, were broken after the abrasion. The abrasion of the chondrules must occur in the condition that the abradant has the energy less than that for the breaking of the chondrule. To keep

this condition, the mass and relative speed of the abradant must be limited to small or slow, respectively. The most probable abradant could be the fine grains consisting of the matrix of the chondrite. The timing of the abrasion should be during the accretion process. The fact that the chondrules rounded by abrasion are common in the UEC's but rare in the EC's suggests that the accretion process is more violent for the UEC's. The higher cooling rate of the chondrules in the UEC's compared with those in the EC's should also be correlated with their degree of the abrasion.

[REFERENCES] [1] Watanabe,S, Kitamura,M & Morimoto,N : EPSL 72 87

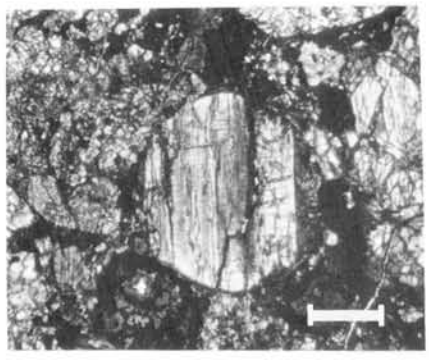

Figure 1. Chondrule of a pyroxene single crystal (L3, ALH-77015). Bar is 0.1mm.

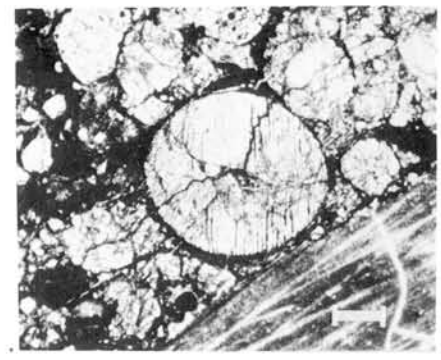

Figure 2. Barred olivine chondrule (L3, ALH-77015) Bar is 0.1mm.

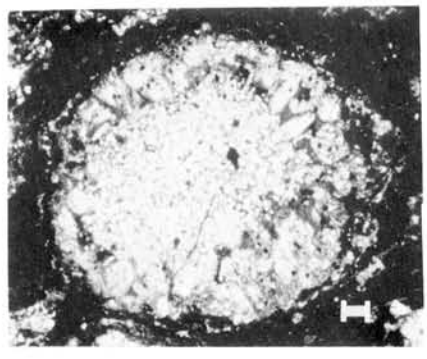

Figure 3. Microporphyritic chondrule(C3, Allende) Bar is 0.1mm.

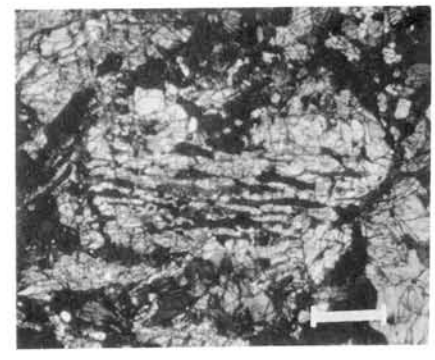

Figure 4. Barred olivine chondrule (L5, Y-790957) Bar is 0.1mm.

CHEMICAL ZONING AND HOMOGENIZATION OF OLIVINES IN CHONDRITIC BRECCIA YAMATO-75028.

M. Miyamoto, Pure & Applied Sci., Coll. of Arts & Sci., Univ. of Tokyo, Komaba, Tokyo 153, D. S. McKay, G. A. McKay, and M. B. Duke, SN4/NASA-JSC, Houston, TX 77058.

We have accurately measured Ca and Mg-Fe zoning profiles of olivines in Yamato-75028, a genomict breccia of H3 and H5 (1,2), by using a Cameca electron microprobe. Some olivines show strong chemical zoning but some olivines show homogenized zoning profiles. We classified several types of Ca-Mg-Fe zoning of olivines in type 3 ordinary chondrites (3). On the basis of Ca-Mg-Fe zoning data, We studied cooling histories during thermal metamorphism.

In order to examine the expected homogenization path of chemical zoning profiles of olivines, we have numerically solved the diffusion equation by finite difference approximation. Diffusion coefficient of Fe in olivine is a function of temperature, concentration, and oxygen fugacity (4). The assumed boundary conditions are that Fa content (=Fe/(Mg+Fe),in atomic %) at the rim of olivine is 18 % for H chondrites and CaO content is 0.02 wt %.

We have calculated cooling rates from 1600-1300 to 1000 ^{o}C during 'initial' cooling after formation of chondrules. If cooling rate is slower than about 15 ^{o}C/hr, Mg-Fe zoning is completely homogenized during initial cooling. If cooling rate is faster than about 7000 ^{o}C/hr, Mg-Fe zoning is not altered. If coolig rate is slower than about 0.1 ^{o}C/hr, CaO zoning is completely homogenized. If cooling rate is faster than about 15 ^{o}C/hr, CaO zoning is not altered. According to dynamic crystallization experiments (e.g. 5), cooling rates to simulate chondrule textures range from 5 to 5000 ^{o}C/hr. Mg-Fe zoning in some olivines may be homogenized during initial cooling, but CaO zoning is kept. Because microporphyritic olivines in type 3 ordinary chondrites often show wide range of chemical zoning, cooling from just below the liquidus at moderately high rates is prefarable to cooling from above the liquidus at low rates in order to make olivine microporphyry (6,7).

We have also studied diffusional homogenization during thermal metamorphism of type 4 ordinary chondrites. If maximum metamorphic temperature of type 4 chondrites is 600-700 ^{o}C (8) and cooling rate is slower than 100 ^{o}C/myr, Mg-Fe zoning in olivine is homogenized. Cooling rates obtained by Fe-Ni data [9] are 1-25 ^{o}C/myr for type 4 chondrites. Olivines in type 4 ordinary chondrites are essentially homogenized (8). Cooling rates needed to homogenize CaO zoning to concentration in type 4 olivines (0.06 wt %; (8)) is 1-1000 ^{o}C/myr. These calculations are consistent with observations. These cooling rates correspond to burial depths of 10^{3}-10^{4} m, assuming a rock-like parent body. If the parent body is regolith-like, they reduce to 10^{2}-10^{3} m.

References: (1)Ohta T. and Takeda H. (1981) In Work Shop on Lunar Breccias and Their Meteoritic Analogs, 102, LPI. (2)Miyamoto M., Takeda H., and Ohta T. (1982) Meteoritics,17, 254. (3) Miyamoto M., McKay D. S., McKay G. A., and Duke M. B. (1984) 47th Meteor. Soc. Meet., K-4, Albuquerque. (4)Buening D. K. and Buseck P. R. (1973) J. Geophys. Res., 78, 6852. (5) Tsuchiyama A., Nagahara, H., Kushiro I. (1980) Earth Planet. Sci. Lett, 48, 155. (6)Nagahara H. (1983) In Chondrules and their Origins, 211, LPI. (7) Hewins R. H. (1983) Ibid., 122, LPI. (8)Dodd R. T. (1981) Meteoritics, Cambridge Univ. Press. (9) Wood J. A. (1979) In Asteroids, 849, Univ. Arizona Press.

14—1

SHAPE ANALYSIS OF Fe-Ni GRAINS AMONG ANTARCTIC ORDINARY CHONDRITES (II)

Naoyuki FUJII, Mitsuru HASEGAWA, Keisuke ITO,
Masamichi MIYAMOTO(#), and Minoru FUNAKI(*)
Department of Earth Sciences, Kobe University, Nada, Kobe 657.
(#)Colledge of General Education, The University of Tokyo, Meguro, Tokyo 113.
(*)National Institute of Polar Research, Itabasi, Tokyo 173.

Lithification, thermal metamorphysm and destruction processes of chondritic parent bodies could produce variety of deformed textures in ordinary chondrites. We have developed several approaches to characterize the irregular shape of Fe-Ni grains with relation to petrologic types, deformation processes, and mechanical properties of chondrites. In this paper, results of the shape analysis of Fe-Ni grains are presented by introducing several appropriate parametors for selected Antarctic ordinary chondrites: ALH-77233(H4), ALH-77115(H6), ALH-77230(L4), ALH-77231(L6), and ALH-77105(L6).

About 40 mm^2 of polished flat surface is surveyed for each chondrite by using the microcomputer-aided picture analyzing system with the optical microscope. Fe-Ni grains with the area larger than 0.001 mm^2 are digitized. In order to distinguish effecs of petrologic types and Fe contents on the shape irregurality of Fe-Ni grains, several parameters are introduced : 1) the axial ratio b/a, 2) the shape parameter $L/\sqrt{S}$, 3) the fractal dimension D (= -log N /log d),and 4) the non-circularity (P) and non-ellipticity (Q) parameters, respectively. a and b are calculated by the principal component analysis. L, S, N, and d are the total perimeter length (with d of 0.01 mm), the area, the number of segments of the perimeter and the divider opening, respectively. P (= $2\cdot\Sigma B_k^2$) and Q (= $P - 2\cdot\Sigma B_2^2$) are obtained from the Fourier Descriptors, B_k in which a radial distance R_j from the center of gravity of a grain is expanded in a finite Fourier series as a function of the perimeter length (Fig. 1).

The mean axial ratio (arrows in Fig. 2) of H4 appears to be smaller than that of H6, which may suggest that higher grade metamorphism could make Fe-Ni grains circular, though the difference is not so significant. The shape parameter, $L/\sqrt{S}$, which indicates roughness of the perimeter relative to the area, tends to distribute more widely in petrologic type 4 than in type 6, though data scattered significantly. The average value of $L/\sqrt{S}$ weighted by S (arrows inFig. 3) appears to be smaller in type 6 than in type 4 both for H- and L-chondrites, which would suggest that the perimeter roughness and/or grain sizes decrease with increasing metamorphic grade.

In contrast, the distribution of the fractal dimenson (Fig. 4) and P and Q (Fig. 5) clearly distinguishes diferences between types 4 and 6. Although the log N *vs* log d diagram shows the break of self-similarity for the divider opening of larger than a few tenths of millimeter, the fractal dimention D, which is another indicator of the perimeter roughness and indipendent on grain sizes, mostly ranges between 1.04 and 1.14 (Fig. 4). D is large and distributes widely in type 4 chondrites relative to that in type 6 (arrows in Fig. 4 indicate mean values). Two-dimensional shape irregularity of grains is comprehensively represented by the Fourier Descriptors and the distribution of P and Q indicates that higher values and wider distributions in type 4 than in type 6 are significant especially for H-chondrites.

All parameters introduced here suggest that the shape irregularity of Fe-Ni grains is likely to be reduced with increasing metamorphic grade and/or deformation of parent bodies. This may be due to thermal effects on ductile properties of metallic grains compared with rock-forming minerals.

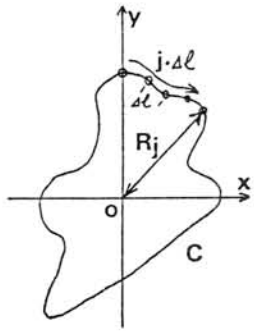

Fig. 1.

$$R_j/R_0 = 1 + 2\cdot\sum_{k=1}^{\frac{N-1}{2}} B_k \cos\left(k\frac{j}{N} - D_k\right)$$

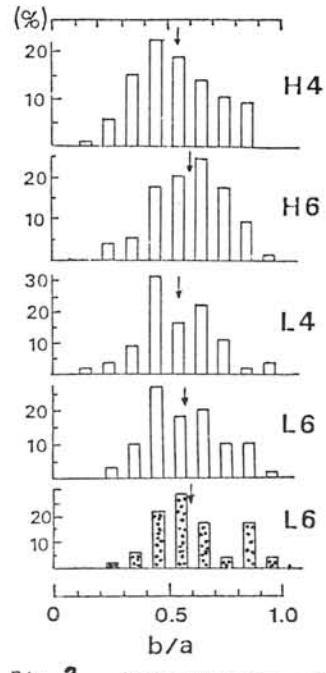

Fig.2. Distribution of the axial ratio.

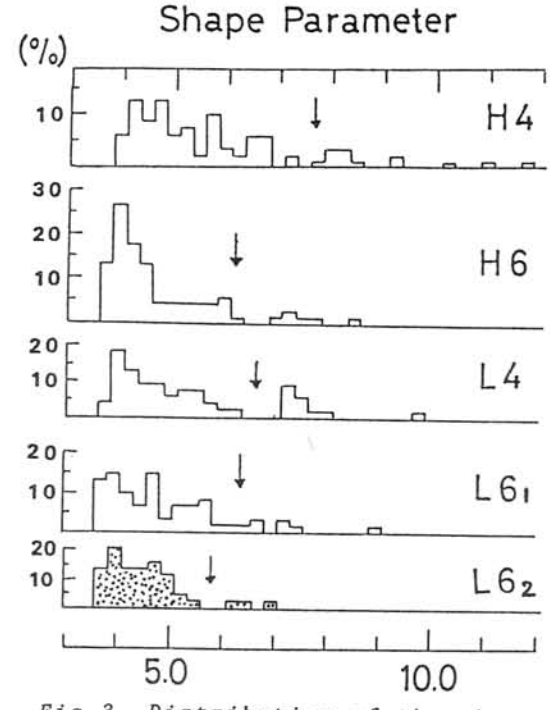

Fig.3. Distribution of the shape parameter.

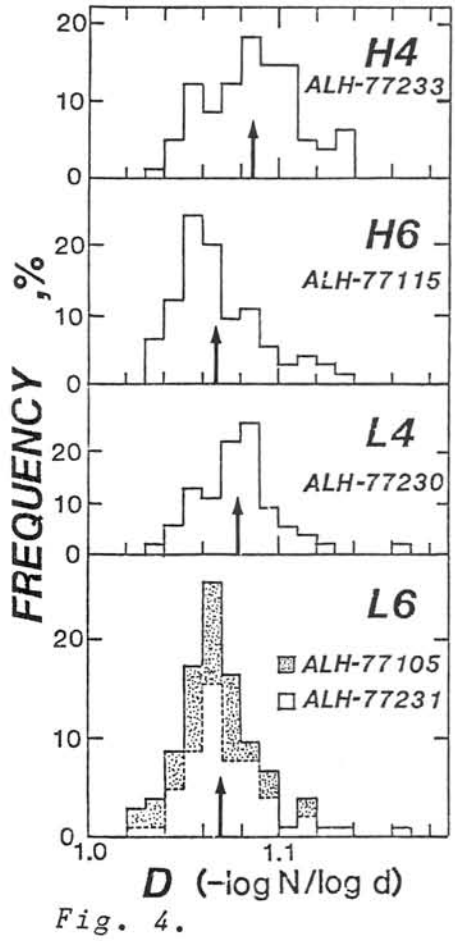

Fig. 4.

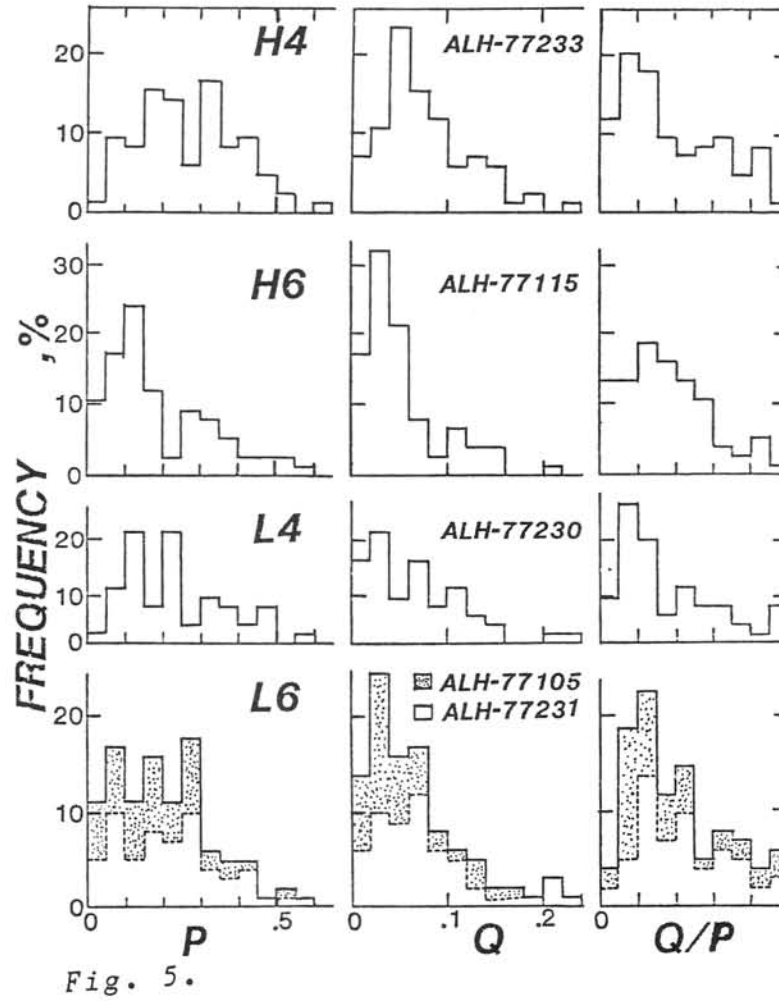

Fig. 5.

15—1

OPAQUE MINERALS IN SEMARKONA CHONDRITE

Yoshie INOUE: Geological Institute,University of Tokyo, Tokyo 113.

Microscopic and SEM observations were carrid out on the opaque minerals in highly unequilibrated Semarkona (LL3.0) chondrite. Mineral assemblage, texture and chemistry show that these minerals preserve a relatively unaltered record of formation in the solar nebula.

Opaque minerals encountered are low-Ni metal, high-Ni metal, troilite, Ni-bearing iron sulfide (Ni<5wt%), high-Ni iron sulfide(Ni~17wt%) and iron oxides. They often form complex aggregations and there are intimate relationships among size, texture, mineral assemblage and occurrence. These relationships are shown in Fig. 1. Modal composition of metal is lower than those of sulfides and iron oxides. Iron oxides are much as sulfides and there are two kinds of oxides; Ni-bearing and Ni-free.

Based on the size and texture, opaque minerals were classified into three types; (1) the small and simple type which are irregular or spherical in shape, (2) the large and simple type, most of which are spherical or round in shape, (3) the large and complex type which are irregular in shape.

(1) The small and simple type chiefly occurs inside porphyritic or non-porphyritic chondrules or on the chondrule surfaces. Those inside the chondrules are composed of kamacite, troilite and Ni-bearing iron sulfide. There are small FeNi-metal grains with Ni content of 10%, but it is not known whether they are single phase or mixture of two phases. Those on the chondrule surfaces are composed mainly of low-Ni metal, taenite, troilite, Ni-bearing iron sulfide and high-Ni iron sulfide.

(2) The large and simple type occurs chiefly in the matrix and inside the "lithic" fragments (fragments showing olivine microporphyritic texture with fine-grained groundmass, which are considered to be precursors of chondrules). There is Ni-bearing iron sulfide or troilite. The shape of this type is rounded showing the possibility of melting.

(3) The large and complex type occurs mainly inside the "lithic" fragments and their rims, and in the matrix. They are composed of kamacite, taenite, troilite, high-Ni sulfide and inon oxides.

Type (3) aggregates (large and complex type), show the most interesting texture. The typical one is observed inside one of the "lithic" fragments. The whole size is 100~700 microns in diameter. It shows a complex structure (Figs.2 and 3); spherical or irregular patches (S) of 10~50 microns in size with layered structure (P) are embedded in sulfides and iron oxides which often contain Si or Ni. Kamacite(K) and taenite are sporadically present in sulfides and iron oxides suggesting that sulfides and oxides were derived from metal through sulfidation and oxidation.

The spherical and irregular patches show layered structures as shown in Fig. 4, which consist mainly of A, patches of B and kamacite with rim layers of C and D.

A presents heterogeneous appearance containing Fe, Si, Ni, P, and S in decreasing order which might be a mixture of several phases.

B forms an alignment concordantly with the shape of the spherical patch. B contains mainly Si with subordinate Fe Ni, P, Co and S with or without Mg, Mn. B may be derived from phosphide schreibersite.

C is the inner layer of the rim surrounding A and B. C is heterogeneous consisting mainly of Fe and subordinate Si with small amount of S, P and Mg, Mn. This layer is richer in S and poorer in P in the inner part.

D is the outer layer surrounding the inner layer C. This layer looks like one phase. It contains mainly Fe with small amounts of S, Ni and Si.

Highly heterogeneous metal-sulfide-oxide aggregates show that they are in gross disequilibrium, and that have not experienced a heating after formation. Compositional variation from A to D might be due to the decrease of formation temperature, and the formation process of those aggregates might reflect the chemical process happened in the early solar nebula.

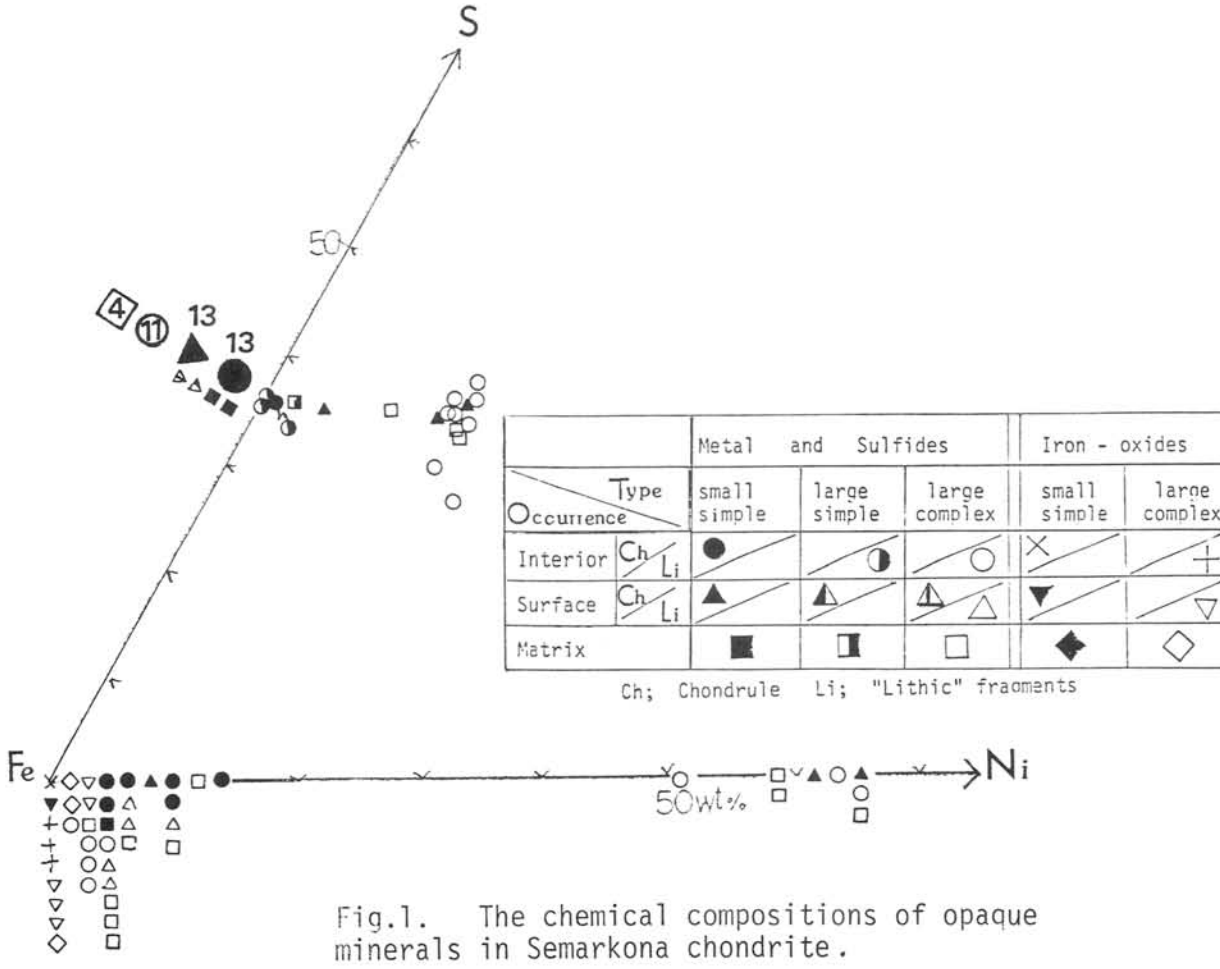

Fig.1. The chemical compositions of opaque minerals in Semarkona chondrite.

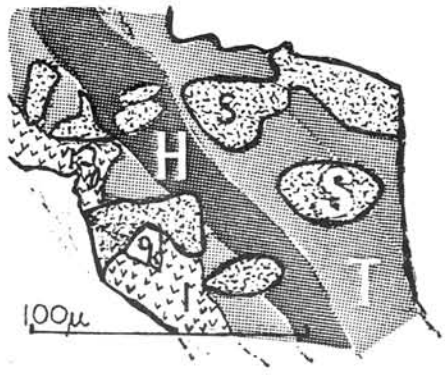

S: Spherical or irregular patches
H: High-Ni iron sulfide
T: Troilite
I: Iron-oxides
K: Kamacite

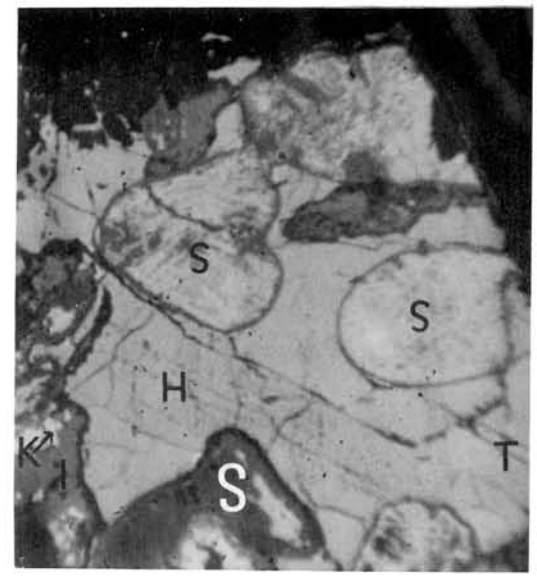

Fig.2.

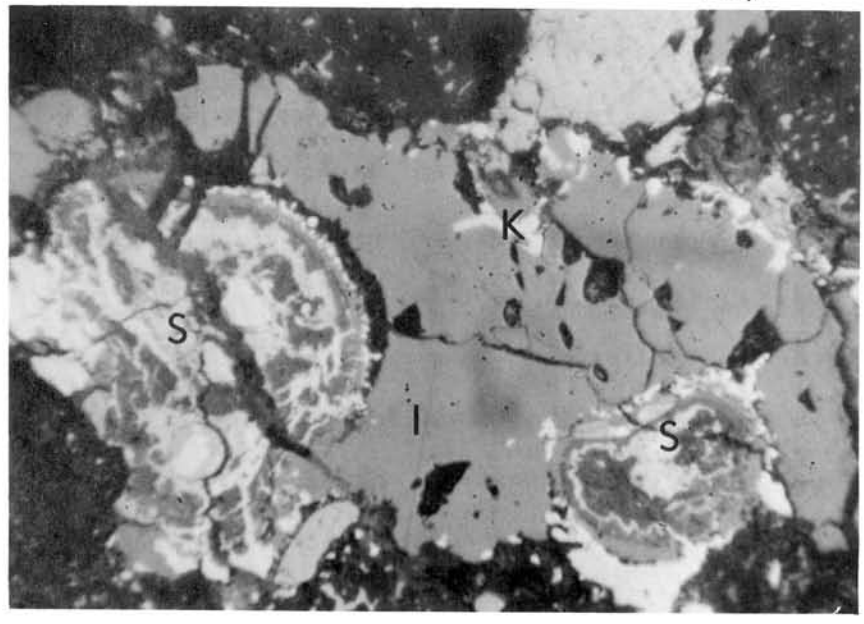

Fig.3.

Fig.2.,3.
Complex structure observed in type(3) aggregates(large and complex type).

Layered structure (P).

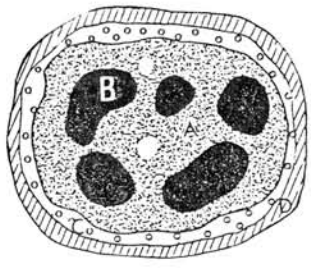

Kamacite graine
A: Fe-rich part
B: Si-rich patches
C: The inner layer
D: The outer layer

Fig.4. Layered structure (P) of the spherical or irregular patches (S).

Opaque Minerals in Y-691 Enstatite Chondrite

Makoto Kimura
Ibaraki University, Mito 310

Opaque minerals in enstatite chondrites have unique features such as their chemical compositions and mineral assemblages, which characterize unique condition of the origin of enstatite chondrites. This paper discusses the genetic relations between opaque minerals in Y-691 chondrite on the basis of their petrographic and chemical features.

Y-691 chondrite consists of chondrules, and silicate and opaque mineral fragments. This chondrite do not include the same matrix materials as ordinary chondrites do. Instead of such a matrix, fine-grained silicate and opaque minerals fill the interstices among relatively coarse fragments and chondrules. Opaque minerals, which occur as opaque mineral fragments (OMF's hereafter) and in chondrules, are Fe-Ni metal, graphite, perryite, schreibersite, troilite, niningerite, oldhamite, daubreelite, djerfisherite, sphalerite, and alkali-Cr-sulfide (mineral B of Ramdohr [1]). In this paper opaque minerals in OMF's are discussed.

Y-691 is classified as E3 [2]. This contains sharply defined glass-bearing chondrules in which clinoenstatites occur as phenocrysts [3]. Plagioclase hardly occurs in this chondrite. The chemical compositions of opaque minerals in Y-691 are generally similar to those in Qinzhen (E3) [4]. and different from those in equilibrated enstaite chondrite [5], e.g, Cr in troilites, P in Fe-Ni metal, and Fe in niningerites. The equilibration temperatures of sphalerites with Fe-Ni metal and troilite in Y-691 are estimated as about 300-400 C from the method of Hutchison and Scott [6], and those of ninigerites with troilite are below about 400 C from the phase equilibria of (Ca,Mg,Mn,Fe)S of Skinner and Luce [7]. All these observation and mineralogical features show that Y-691 is a primitive enstatite chondrite.

The phase assemblages and textures of OMF's, above about 50 microns in size, in Y-691 were observed. In general OMF's consist mainly of Fe-Ni metal with various abundance of troilite, perryite, and schreibersite. Such a mineral assemblage is comparatively common in spite of the size and shape of OMF's. Ninigerite is also common mineral in OMF's, whereas the others occur rarely. Spherical OMF's like chondrules are often present in Y-691.

Fig. 1 shows the outline of petrographic relations between opaque minerals in OMF's. Although Fe-Ni metals are most common minerals in OMF's, they are almost accompanied by the other minerals. They are kamacite, and average Si-content in them is about 2.1wt.%. Troilites are abundant next to Fe-Ni metal in opaque minerals, and occur in OMF's in which

troilites frequently rim Fe-Ni metal. In some OMF's, troilites are dominant with minor amount of Fe-Ni metal and others. Rarely OMF's comprise only Fe-Ni metal or troilite, respectively. Troilites contain small amounts of Ti (about 0.2%) and Cr(1.3%). Perryites necessarily accompany Fe-Ni metal and/or troilite in OMF's. They are typically intergrown with troilite in any OMF's, and especially they form as thin bands along the boundary between Fe-Ni metal and troilite in a few OMF's. Some perryite are independently included in Fe-Ni metal. Schreibersites, as well as perryite, do not occur independently as an OMF. Most of them are included in Fe-Ni metal. Although intimate intergrowth between schreibersite and troilite is rarely, troilites surround them in a few OMF's. Irregular-shaped graphites are also included in Fe-Ni metal and rarely troilite. Modal abundances of graphites in OMF's are below about 2 wt.%. Niningerites are common sulfide mineral next to troilite, and typically attach to OMF's which mainly consists of Fe-Ni metal with the other minerals. In some OMF's they occur in the boundary between Fe-Ni metal and troilite. Rarely coarse-grained niningerites are surrounded by troilite. Niningerites contain about 13.3% Fe. The occurrence of oldhamite is similar to that of niningerite, although oldhamite is less common. Some OMF's conatin both oldhamite and niningerite. The abundance of daubreelites is poor, and they necessarily occur in troilite as thin exsolution lamella in both Fe-Ni metal and troilite-rich OMF's. The poor abundance and mode of occurrence of daubreelites are different from those in Y-74370 equilibrated enstatite chondrite. On the other hand, Cr-content of troilite in Y-691 is generally higher than that in Y-74370 (Kimura, unpublished data). Sphalerites accompany troilites which attach to Fe-Ni metal and/or are included in metal. Sphalerites contain about 0.8% Mg and 1.3% Mn. Djerfisherites necessarily occur with troilite. An alkali-Cr-sulfide occur with troilite and niningerite in an OMF. Its chemical composition is comparatively similar to those in Qinzhen (8). The bulk compositions of some OMF's were calculated from the modal and mineral compositions.

The origin and genetic relations between opaque minerals in OMF's can be estimated from the above mineral features and phase equilibria, although our knowledge about experimental phase relations between unique phases in enstatite chondrites is not yet enough. From the modal compositions of graphite in OMF's, it is probable that graphite (primarily cohenite ?) exsolved from Fe-Ni metal at about 900 C. The occurrence and bulk compositions of OMF's show that schreibersites exsolved from Fe-Ni metal at about 700 C on the basis of the Fe-Ni-P phase equilibria (9). Troilites frequently form around Fe-Ni metal in OMF's, which suggests that troilites formed through the reaction between Fe-Ni metal and sulfur gas. Since troilites surround schreibersite in a few OMF's, it is evident that troilite formed below about 700 C. Such an inference

about the formation of troilite is not inconsistent with the estimated condensation temperature (10). Since perryites are typically intergrown with troilite, it is probable that most of them formed simultaneously with troilite. Especially, the thin bands of perryite along the boundary between troilite and Fe-Ni metal support this idea. It seems that the origin of sphalerites is also related to that of troilite in OMF's, since they occur with troilite in OMF's. The occurrence of daubreelites shows that they exsolved from troilite. Although the exsolution temperature of daubreelite can not be determined accurately, it is probable that daubreelite formed at comparatively low temperatures (below about 600 C at least), on the basis of the phase equilibria of Fe-Cr-S (11). The occurrence shows that niningerite and oldhamite probably condensed and attached to Fe-Ni metal. Later troilite formed around OMF's. Fig. 2 summarizes the genetic relations between all these opaque minerals. It is concluded that these minerals formed through various kinds of reactions from the primitive Fe-Ni metal at lower temperatures. Most of these reactions took place in the primitive solar nebula, and various OMF's accumlated to the parent body of enstatite chondrite.

References: (1) Ramdhor P. (1963): J. Gophys. Res., 68, 2011. (2) Prinz M. et al. (1984): Abs. Ninth Symp. Ant. Meteorite NIPR, 14. (3) Okada A. (1975): Mem. Natl. Inst. Polar Res., 5, 14. (4) Rambaldi E. R. et al. (1983): Lunar Planet. Sci. XIV, 626. (5) Keil K. (1968): J. Geophys. Res., 73, 6945. (6) Hutchison M. N. and Scott S. D. (1983): Goechim. Cosmochim. Acta, 47, 101. (7) Skinner B. J. and Luce F. D. (1971): Am. Mineral., 56, 1269. (8) El Goresy A. et al. (1983): Meteoritics, 18, 293. (9) Doan A. S. and Goldstein J. I. (1970): Met. Trans., 1, 1759. (10) Sears D. W. (1980): Icarus, 43, 184. (11) El Goresy A. and Kullerud G. (1969): in Meteorite Research, 638.

Fig. 1 Schematic illustration for the petrographic relations between opaque minerals in OMF's.

Fig. 2 The diagram for the genetic relations between opaque minerals.

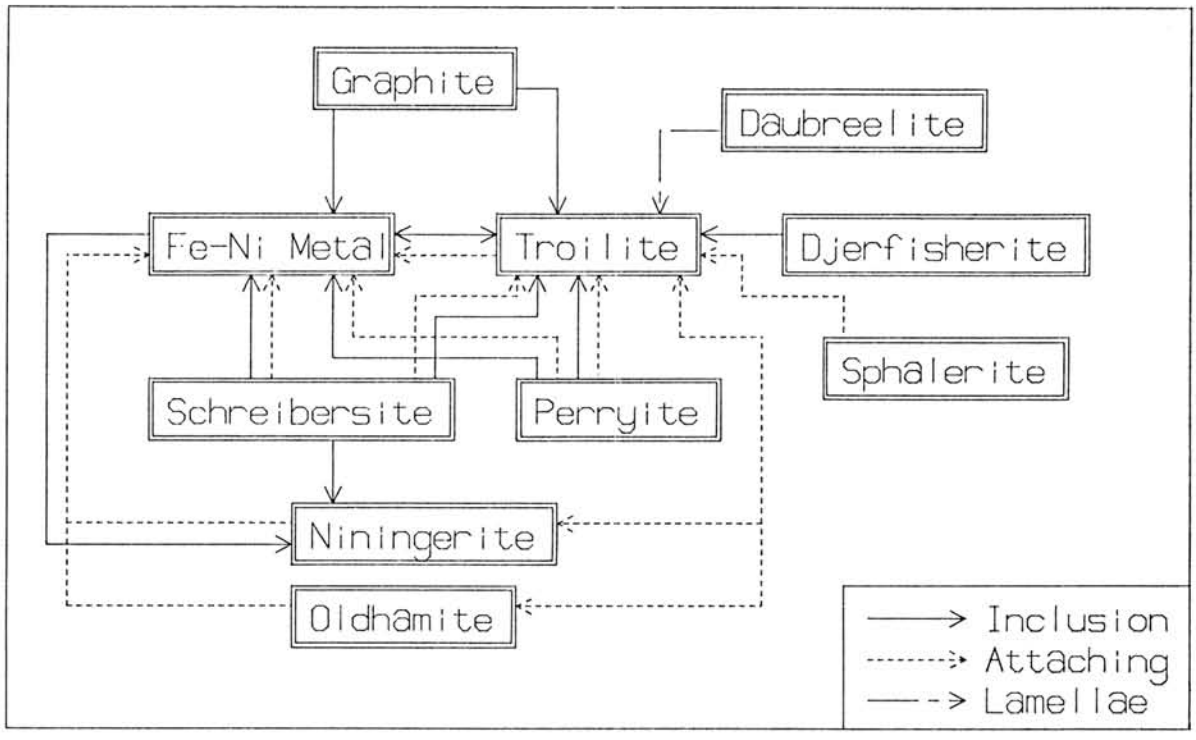
Graphite
Daubreelite
Fe-Ni Metal
Troilite
Djerfisherite
Sphalerite
Schreibersite
Perryite
Niningerite
Oldhamite
Inclusion
Attaching
Lamellae

Fig. 1

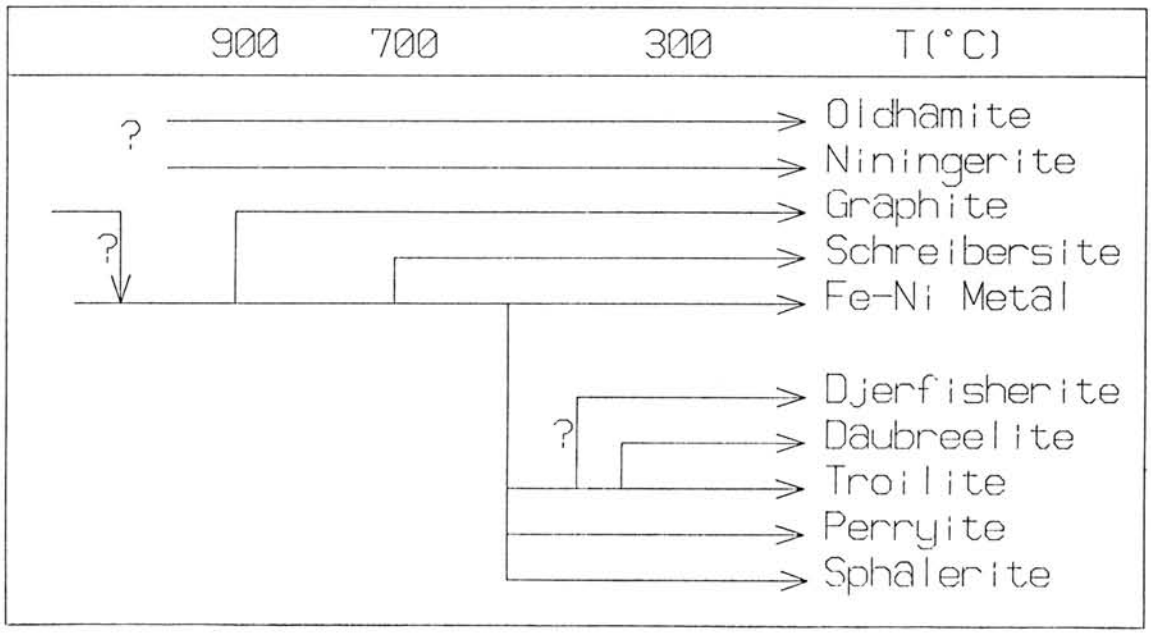
900
700
300
T(°C)
?
Oldhamite
Niningerite
Graphite
?
Schreibersite
Fe-Ni Metal
Djerfisherite
?
Daubreelite
Troilite
Perryite
Sphalerite

Fig. 2

METAL - SULFIDE EQUILIBRIUM IN YAMATO-74, -75 CHONDRITES (PRELIMINARY REPORT)

Hiroharu MATSUEDA and Tomoji SANGA

Institute of Mining Geology, Mining College,
Akita University, Akita 010, JAPAN

Metal-sulfide equilibrium was studied on 32 Antarctic chondrites(13H,12L,7LL) in order to clarify the thermal-pressure histories on the basis of their textures, parageneses and chemical compositions.

Textural Features

Textural features and paragenetic relationships of metals and sulfide are summarized in Fig. 1.

Metals and sulfide are universaly found in any petrologic types of chondrites. Troilite show various kinds of textures as follows; i)isolated grains, ii) aggregated crystals, iii) aggregations of fine-grained crystals, iv)veinlets and/or networks. Especially in unequilibrated chondrites, troilites are apt to show the textures iii) and iv). Overgrowth texture surrounding chondrules by metals and troilite is also recognized in unequilibrated ones. On the other hand, 3-phases assemblage composed of kamacite -taenite-troilite are also occurred in equilibrated chondrites. The modes of occurrence of troilite well correspond to the equilibration grade of chondrites.

As a secondary texture, troilites in some chondrites show the textures such as lamallae- or lattice-like twin, wavy extinction, brecciation and stretched texture with maskelynite.

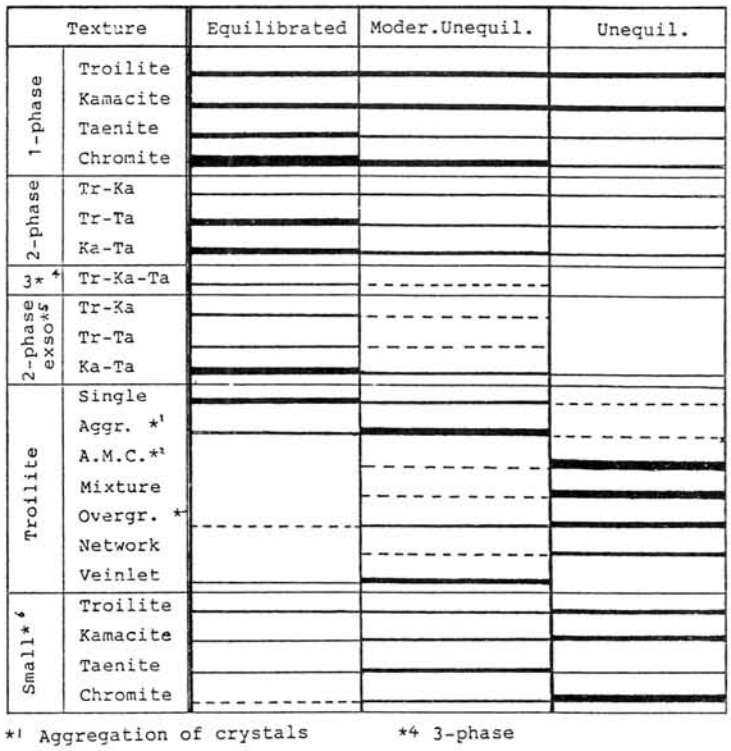

*1 Aggregation of crystals
*2 Aggregation of micro crystals
*3 Overgrowth on chondrule
*4 3-phase
*5 2-phase exsolution
*6 Small grains in chondrule

Exsolution Textures

Exsolution textures among metals and troilite are generally disposed to be observed in relatively equilibrated chondrites.

In the type of 2-phases exsolution, troilite in metal phases, are inclined to be found in relatively equilibrated chondrites. But the type of kamacite in taenite is occurred in any equilibration grade.

Genetical special attention should be paid to the reversed exsolution type such as taenite in kamacite as shown in Fig.2.

Fig. 1 Paragenetic relationships and textural features of metals and troilite in Yamato-74, -75 chondrites.

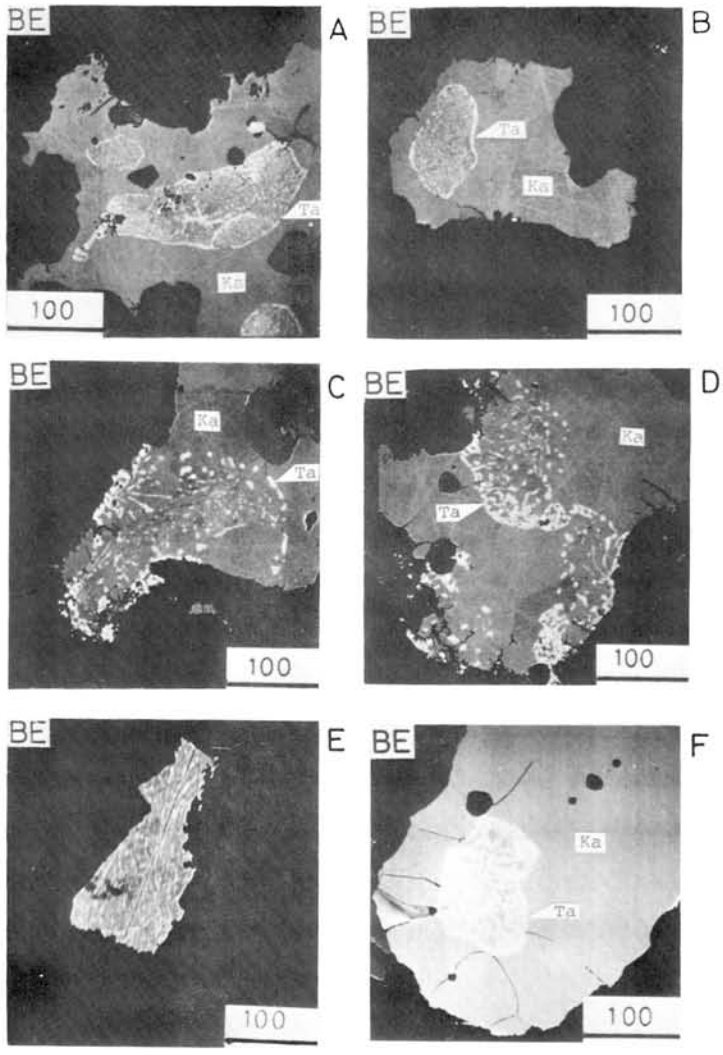

Fig. 2 EPMA back scattering elctron images(BE) of reversed exsolution textures in chondrites.
A & B : Y-74379
C & D : Y-74236
E : Y-74070
F : Y-75145

Compositional Heterogeneity

In spite of L5 petrologic type, metal phases in Y-74015 chondrite show a remarkable compositional heterogeneity as shown in Fig. 3. Most of metal grains in this chondrite show more or less similar heterogeneity on Nickel distributions.

Unique cooling history of Y-74015 chondrites should be considered to expalin the construction of these heterogeneity in metal phase.

Partition of Co between kamacite and taenite

Partitional relationships of Cobalt between kamacite and taenite were investigated by EPMA quantitative analyses. As shown in Fig. 4, partition ratios between both phases do not depend on the petrologic type but depend on the chemical type of chondrites.

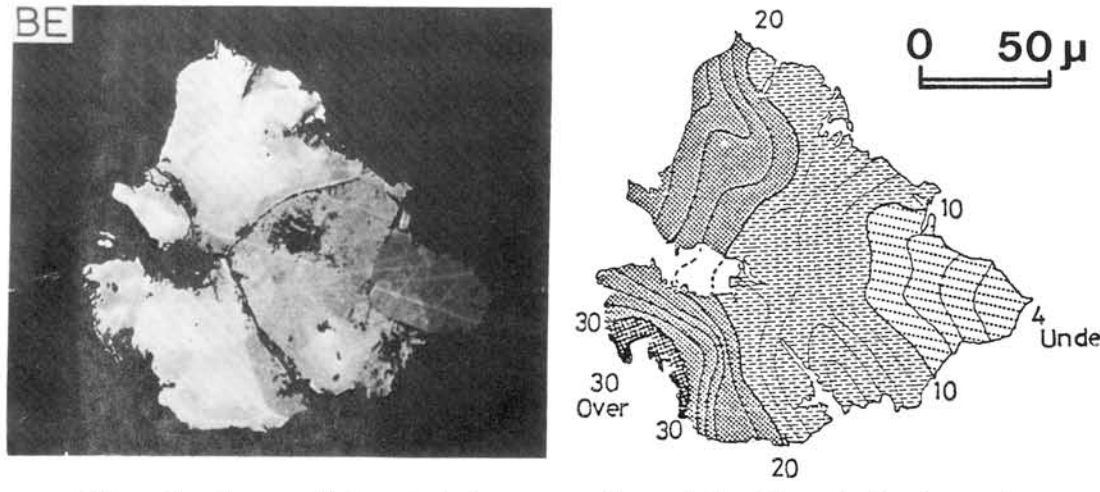

Fig. 3 Compositional heterogeneity of Fe-Ni metal phase in Y-74015 chondrite. Numerical numbers show the concentrations of Ni.

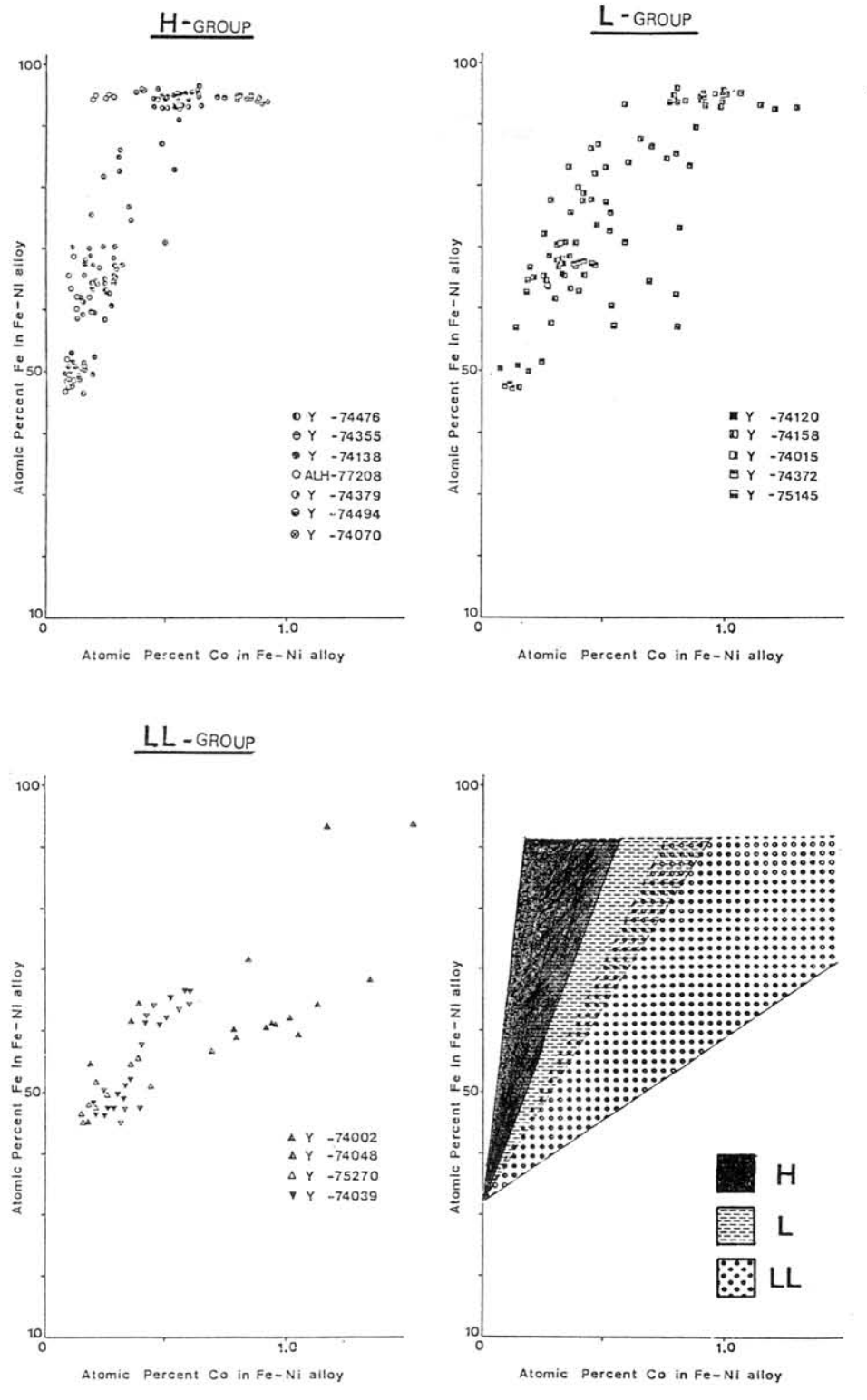

Fig. 4 Partitional relationships of Cobalt between kamacite and taenite in Yamato H, L and LL type chondrites.

Partition of Nickel among Metal Phases and Troilite

Equilibrated temperatures of chondrites were obtained on the basis of Nickel partitional relationships among kamacite-taenite -troilite by Bezmen et al.(1978). Minimum equilibration temperatures are nearly identical around 500 °C having no relation to the equilibration grade. Accordingly, cooling rate of chondrites might be roughly similar in them.

From a viewpoint of distribution pattern of equilibration temperatures, two types of "Concentration" and "Dispersion" are distinguished in the equilibrated chondrites as shown in Fig. 5. "Dispersion" type of chondrite show a wide temperature range in the same specimen notwithstanding the equilibrated chondrites. Both types are also recognized in equilibrated chondrites.

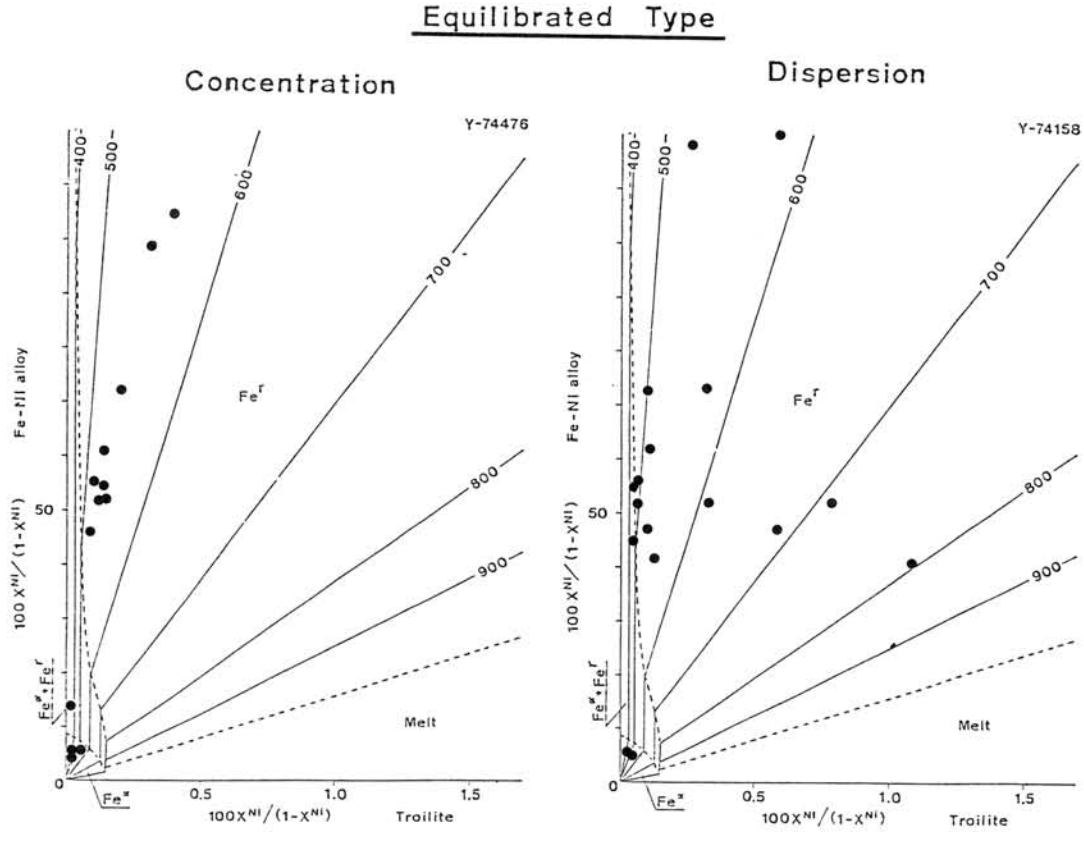

Fig. 5 Nickel partitional relationships among metals and troilite in equilibrated chondrites based on the Bezmen et al.(1978).

Providing the apparent reheating process caused by shock events and rapid cooling history in cosmic space, it might be well explained the unusual textures of troilites, reversed exsolution phenomena between metal phases and apparent dispersed equilibration temperatures in the same specimen.

GEOCHEMISTRY OF CHONDRULES FROM CARBONACEOUS, ORDINARY, AND E CHONDRITES.

Gero Kurat

Naturhistorisches Museum, A-1014 Vienna, Austria

Major, minor, and trace element data of individual chondrules show a remarkable variability of chondrule compositions (1, 2). This variability apparently reflects a variety of fractionation processes which were active before, during, and after the chondrule forming event. Data are now available for chondrules from a variety of chondrites. Major and minor element data have been discussed already by several authors (e.g.2-5). Here I make an attempt to compare trace element data of chondrules from a few chondrites: Allende (6), Qingzhen (7), Tieschitz (8,9), Chainpur (9,10), and Semarkona (11,12). Selected elemental patterns - normalized to CI (13) - are shown in Figs. 1-3.

Lithophile elements display generally complex distribution patterns. The refractory lithophile elements (RLE) are normally enriched in chondrules as compared to CI (Table). Chondrules from ordinary chondrites (OC) and enstatit chondrite (EC) Qingzhen have RLE abundances mostly between 1x and 2x CI. Allende chondrules are on average clearly more refractory (2-8x CI). They also show uniform enrichments of RLE which is commonly not the case in all other chondrites. Several anomalies in elemental abundances are frequently observed: Ca/Sc,La shows commonly positive and negative anomalies in most OC's and in EC, except for Semarkona and Allende. There are no Eu/Sm anomalies in Allende, very common - in EC and common + or - in OC's. Interestingly, there are only few and mostly weak Yb/Lu anomalies, most of which are unrelated to the Eu-anomaly. The moderately volatile lithophile elements Cr and Mn are either unfractionated as compared to the RLE (most OC chondrules) or regularly depleted (Allende and refractory OC and E chondrules) or show complex patterns. EC chondrules generally show strong - Cr/Lu anomalies, which are also present but weaker among some OC chondrules. Cr/Mn is mostly unfractionated among EC and OC chondrules except for the refractory chondrules and a few others which show either + or - anomalies.

The volatile lithophile elements Na and K show characteristical fractionations. Na/Sm is always - in Allende, always + in Qingzhen, commonly + or - in Chainpur and unfractionated in Tieschitz and Semarkona (with exceptions). Na/K fractionation is strong in Qingzhen (all K-), common among Chainpur chondrules (K+ and K-), and weak or not present among Allende and Semarkona chondrules. The Na/K fractionation appears to be related to halogen abundances in Allende and Qingzhen chondrules (6).

Siderophile elements are generally strongly depleted in chondrules as compared to CI and are almost always fractionated (Figs.1-3). The most common fractionation is that of Ir/Ni which ranges from highly - to highly +. Most chondrules from all chondrites show Ir-, except those of Qingzhen which have mostly chondritic Ir/Ni, similar to some chondrules from Allende and some metal-rich chondrules from OC's. Refractory chondrules from OC's tend to show Ir > Ni, some chondrules from Allende and OC's have Ir ≫ Ni. Ni/Co fractionations are less common and well developed

mostly only among chondrules with very low metal contents: Chainpur, Semarkona and Allende - all with Co > Ni. The Fe/Co ratio is chondritic only in most Allende chondrules. All other chondrules and two RP chondrules from Allende show variably strong Fe+ anomalies. Au contents are surprisingly high and the Au/Ni ratio is mostly close to CI, despite the very strong Ir/Ni fractionations. Only some refractory chondrules show Au-, and RP chondrules from Allende and a few others Au+.

Conclusions: Trace element contents of chondrules from CV, E, and ordinary chondrites reflect complex fractionation processes before, during and after chondrule formation:

1) Partitioning of trace elements into different pre-chondritic phases and subsequent non-representative sampling (anomalies among RLE, Cr/Mn fractionation, Na/K fractionation and link with halogen abundances, very strong Ir+ anomaly, siderophile-lithophile element fractionation (?)).
2) Vapor fractionation via evaporation (depletions of Na and K, Cr and Mn, Ir > Ni,Co-fractionation) and via condensation (Sc,Lu < RLE,Ir < Ni < Co < Au).
3) Metal-silicate fractionation during melting event (Ir RLE).
4) Oxidizing conditions are indicated by Ir< Ni < Co < Fe (all OC chondrules, some Allende chondrules). Reducing conditions are indicated by (Ir) ~ Ni ~ Co ≲ Fe (Qingzhen and some Allende chondrules).

References: (1) For references see: Kurat,G.(1984), Proc. 27th Internat.Geolog.Congress, vol.11, 155-197. (2) Ikeda,Y. (1983), Mem.Nat.Inst.Polar Res.,Spec.Iss.30, Tokyo, 122-145. (3) Dodd,R.T. and L.S.Walter (1972), In: L'Origin du Systeme Solaire, H.Reeves (ed.) Paris, C.N.R.S., 293-300. (4) Fredriksson,K.(1982) Lunar Planet.Sci. XIII, 233-234. The Lunar Planet.Inst.Houston, TX. (5) Dodd,R.T.(1981), Meteorites. Cambridge Univ.Press, Cambridge, 368 pp. (6) Kurat,G., H.Palme, F.Brandstätter, B.Spettel, and V.P.Perelygin (1985), Lunar Planet Sci.XVI, The Lunar Planet. Inst.Houston, TX, in the press (7) Grossman,J.N., A.E.Rubin, E.R. Rambaldi, R.S.Rajan, and J.T.Wasson (1984), preprint. (8) Gooding,J.L.(1979), Ph.D.Thesis, Univ.New Mexico, Albuquerque, 392 pp. (9) Unpublished data, MPI Heidelberg (10) Kurat,G., E. Pernicka, and I.Herrwerth (1984), Earth Planet.Sci.Lett.68, 43-56. (11) Grossman,J.N. and J.T.Wasson (1983), Geochim.Cosmochim. Acta 47, 759-771. (12) Grossman,J.N. and J.T.Wasson (1984), preprint. (13) Unpublished data, MPI Mainz.

Table 1 : Common lithophile element fractionations in chondrules.

Fractionation	Allende (CV)	Qingzhen (E-3)	Tieschitz (H-3)	Chainpur (LL-3)	Semarkona (LL-3)
Refractories/CI	2-8x	mostly 1-2x, a few up to 3x	1-2.5x	1-2x rare up to 5x	1-2x a few up to 3x
Ca/Sc,La	weak Ca-common	common Ca+ and Ca-	common Ca+ and Ca-	very common Ca-	very common no anomaly
Eu/Sm	no	very common Eu-	common weak Eu-, a few Eu+	Eu+ and Eu- common	common weak Eu+
Yb/Lu	no one strong Lu-	mostly no, some weak Yb+,Yb-	mostly no,some Yb+,Yb-	mostly no,some weak Yb+	mostly no,some weak Yb+,Yb-
Cr/Lu	mostly strong Cr-	mostly strong Cr-, one strong Cr+	mostly no, a few Cr+,Cr-	mostly no,a few Cr+,Cr-	mostly no,a few Cr-
Cr/Mn	mostly strong Mn-	unfractionated some Mn+, a few Mn-	unfractionated few Mn+,Mn-	unfractionated, few Mn+, one Mn-	unfractionated few Mn+.Mn-
Mn/Na	RP weak Na-, others strong Na+	mostly strong Na+, few unfr. or Na-	mostly Na+ or Na-	unfract. and Na+,Na-	unfract. common Na-, rare Na+
Na/Sm	all Na-	all Na+	common unfract. or weak Na+,Na-	common Na+,Na-	unfract. Na+,Na-
Na/K	unfract.weak K+,K-	all K-	-	unfract.K+,K-	mostly unfract. few K+,K-

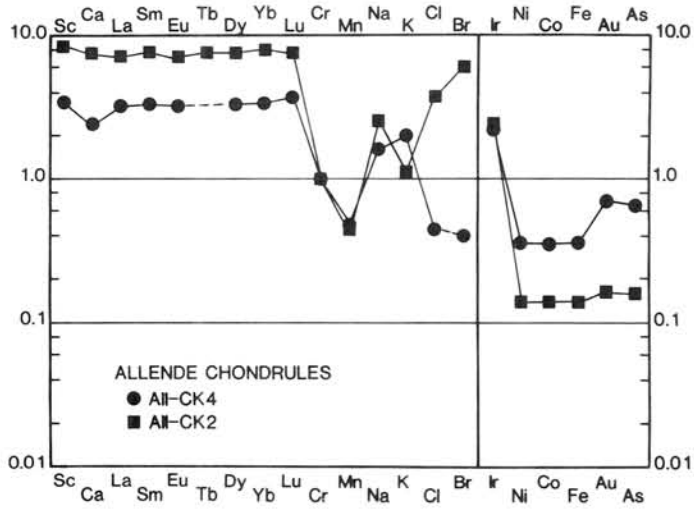

Fig.1(left): CI-normalized elemental abundances of two chondrules from Allende (6).
Fig.2(lower left): CI-normalized elemental abundances of refractory chondrules from Chainpur (9,10).
Fig.3(lower right): CI-normalized elemental abundances of K-rich chondrules from Chainpur (9,10).

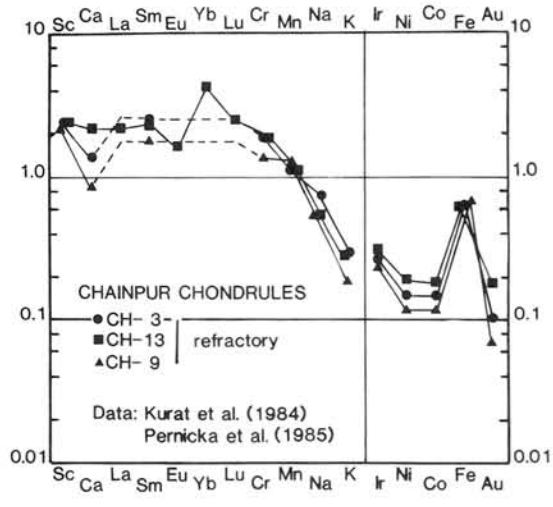

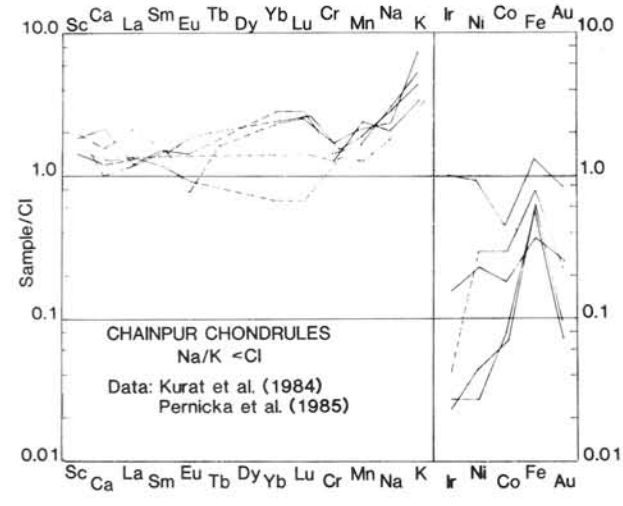

THERMOANALYTICAL STUDY OF CARBONACEOUS CHONDRITES: YAMATO-74662 - KAINSAZ - ALLENDE

B.Lang[1], A.Grodziński[2], M.Żbik[3] and L.Stoch[4]

1) Warsaw University, Department of Chemistry, 02-089 Warsaw
2) Institute of Electronic materials, 02-075 Warsaw
3) Warsaw University, Department of Geology, 02-089 Warsaw
4) Technical University of Mining and Metallurgy, 30-059 Cracow

Our thermoanalytical study of a number of meteorites [see Lang et al., 1981; Lang et al., 1983; Żbik et al., 1984] has been extended over carbonaceous chondrites: Yamato-74662 C 2, Kainsaz CO 3 and Allende CV 3. The features on the differential thermal (DTA) and thermogravimetric (TG) curves were regarded as thermochemical response of the respective meteoritic bulk material to heating both in air and in oxidation suppressing atmosphere of argon. Superimposed partially or resolved oxidation and/or volatilization events observed as features on the DTA-curves were monitored along the TG-curves. As previously the thermoanalytical curves were obtained with Rigaku Denki Thermocontroller, high purity Al_2O_3 being used as reference material. Heating up to 1000°C and cooling down were performed at the rate of 10°C per minute. For heating in argon the TG-curves were not available. An auxiliary microstructural information was provided by SEM. To illustrate the latter the microphotographs of the Yamato-74662 and Kainsaz samples are given below.

The microstructure of the Yamato-74662 is characterized by occurrence of very fine closely-packed grains as constituents of the matrix. With their size of ultrapores the intergranular void spaces in matrix do not give any clear view. Single vugs, intercrystalline pores and rare larger cracks were noticed in the microphotographs. Fine acicular mineral forms are also viewed in vugs. The matrix material of Kainsaz is composed of similar fine grains. Irregular porous white inclusions, rounded or tubular, as that single one exposed in the microphotograph, occur in Kainsaz.

Thermoanalytical features of the Yamato-74662 deserve a special attention. Heated in air to 900°C sample of this meteorite lost smoothly enough 9.3% of its original mass. The losses at lower temperatures are likely to be attributed to volatilized water and carbon compounds. At higher temperatures the losses can be presumably referred to products of weathering converted at heating into volatiles..Such an explanation seems to be supported by Fig.1a. However, on the DTA-curve in Fig.1b a peculiar peak is seen recorded at 686°C. It reminds by shape typical oxidation peaks, obtained from heating in air. But in terms of heating in argon an alternative arises: either some unidentified topochemical exothermic reaction occurred or the recorded thermal effect is due to some phase transition to be defined. In any case it seems reasonable to suspect an involvement direct or indirect of the behaviour of phyllosilicates.

Looking at the thermoanalytical curves for the Ornans-type Kainsaz C 3 and the Vigarano-type Allende C 3 it is easy to realize the difference in their response to heating in air. Compared to Allende the oxidation capability of Kainsaz is remarkably

lower and shifted towards higher temperatures. This is proved by comparisonof Figs.2a and 3a. In Fig.3a two large peaks from heating in air are seen on the DTA-curve for Allende at 292°C and 511°C. They are lacking on the curve in Fig.3b, obtained from heating in argon. This argues for oxidation as their nature. The magnitudes of the appropriate thermal effects were determined with Perkin-Elmer differential scanning calorimeter (DSC). They are 103.1 J/g and 389.3 J/g respectively (Fig.3c). While the first peak is not accompanied by any per saldo mass increase, the second has been recorded against sloping up rising mass which reached its peak value of 4.45% at 774°C. Heated in air Kainsaz exhibited remarkably slower oxidation reaching the peak value of mass increase of 5.3% at 960°C. This low rate of oxidation is likely to explain the lacking larger peaks on the DTA-curve in Fig.2a.

References: B.Lang, A.Grodziński and L.Stoch (1981) Meteoritics 16, 345 - 346; B.Lang, A.Grodziński and L.Stoch (1983) Mem.Natl Inst.Pol.Res., Spec.Issue, 30, 378 - 388; M.Zbik, B.Lang, A. Grodziński and L.Stoch (1984) Papers presented to the Ninth Symposium on Antarctic Meteorites.

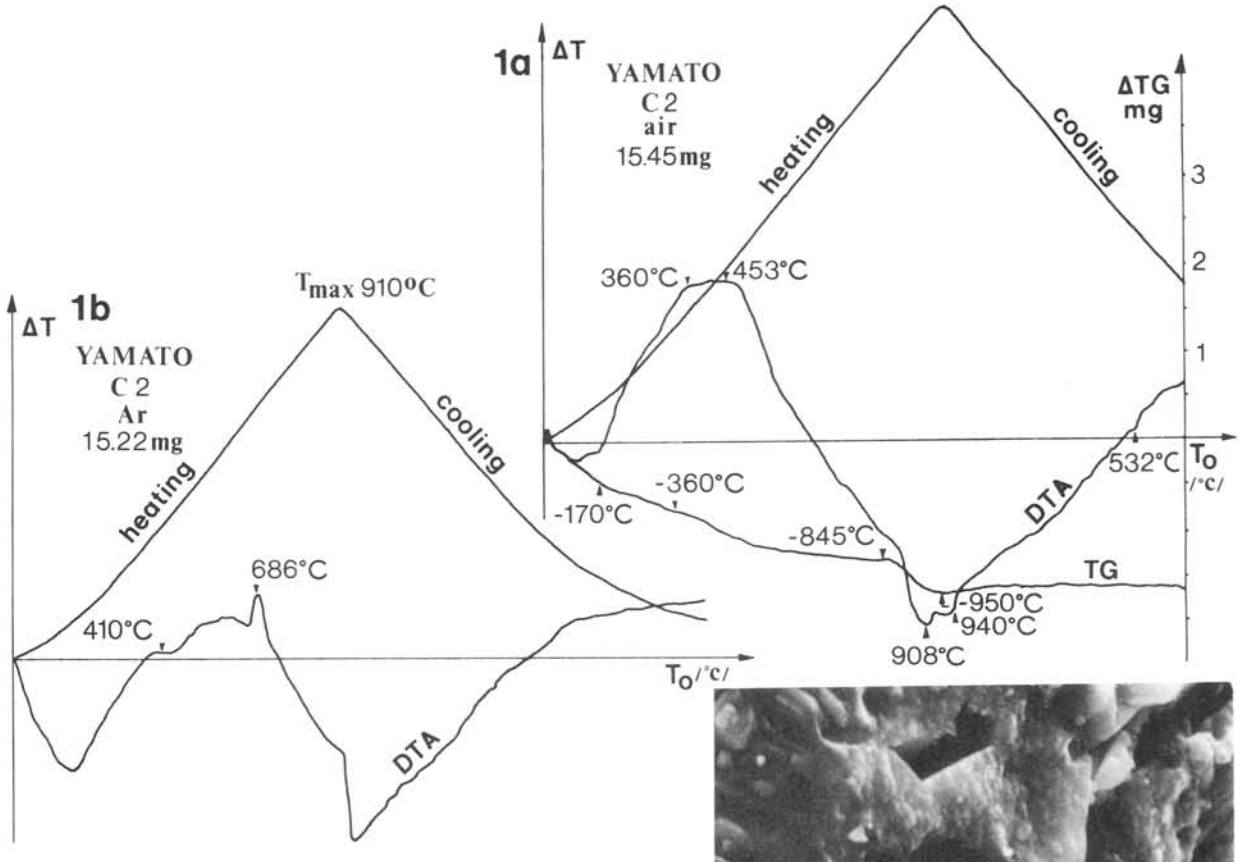

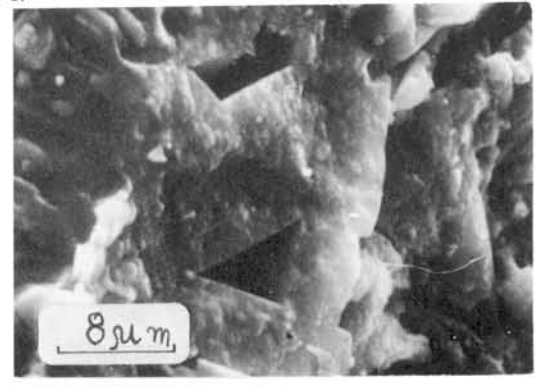

Yamato-74662

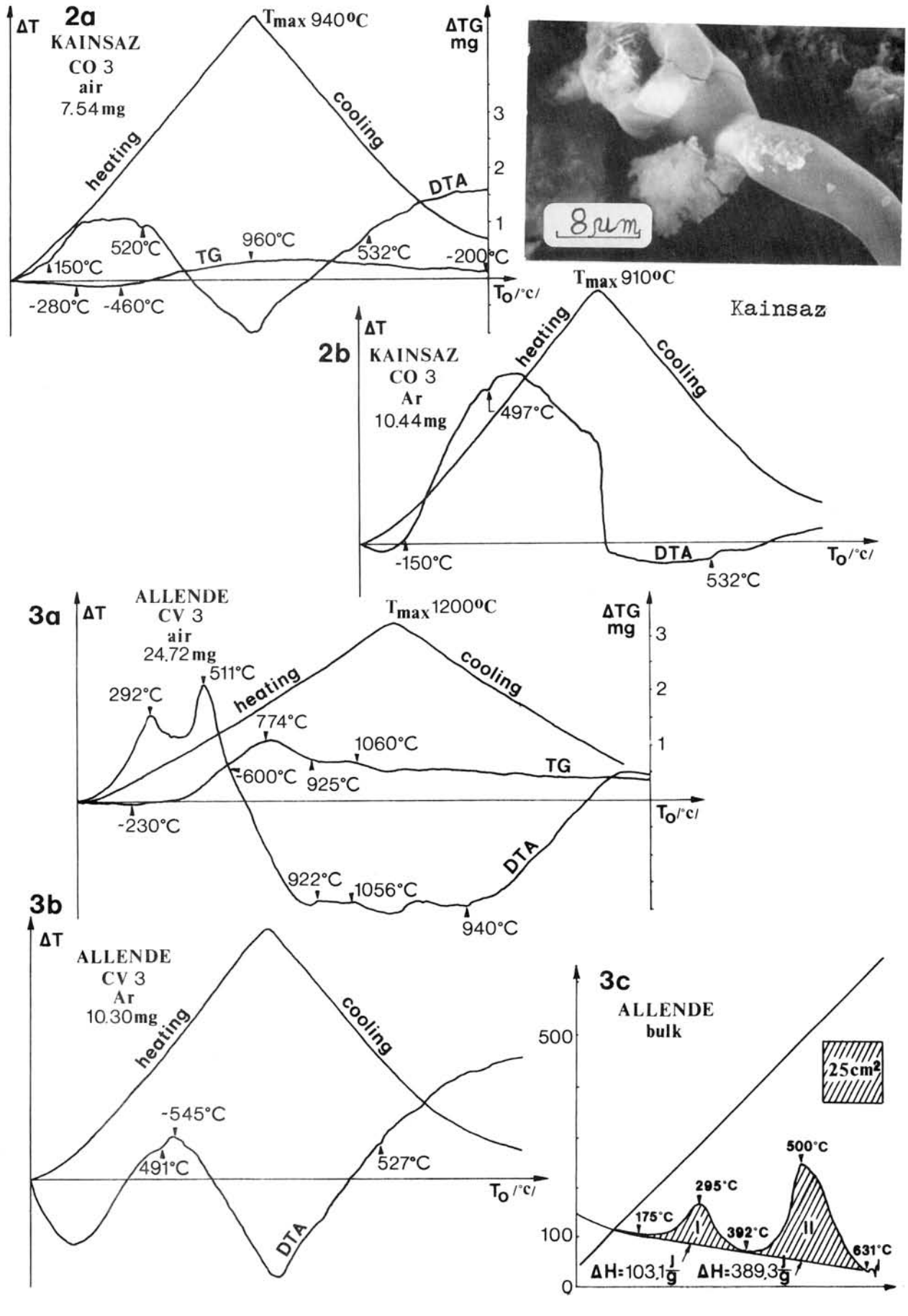
2a
KAINSAZ
CO 3
air
7.54mg
ΔT
ΔTG
mg
Tmax 940°C
heating
cooling
DTA
TG
520°C
960°C
532°C
150°C
-200°C
-280°C
-460°C
To/°c/
8μm
2b
KAINSAZ
CO 3
Ar
10.44mg
Tmax 910°C
Kainsaz
497°C
-150°C
DTA
532°C
3a
ALLENDE
CV 3
air
24.72mg
Tmax 1200°C
511°C
292°C
774°C
1060°C
600°C
925°C
-230°C
922°C
1056°C
940°C
3b
ALLENDE
CV 3
Ar
10.30mg
-545°C
491°C
527°C
3c
ALLENDE
bulk
25cm²
500°C
295°C
175°C
392°C
631°C
ΔH=103.1 J/g
ΔH=389.3 J/g

Chromium distribution in type 3 ordinary chondrites

Hideyasu Kojima, Keizo Yanai and Satsuki Ikadai
National Institute of Polar Research, Tokyo 173

Ordinary chondrites include 0.4-0.6% of Cr_2O_3, regardless of the chondrite chemical group. On the other hand, equilibrated ordinary chondrite contains about 0.3 wt% of chromite (Bunch et al, 1967). The main constituents of equilibrated ordinary chondrites, such as silicate, FeNi metal and sulphide include very little Cr. It is inferred that almost all chromium occurrs as chromite in the equilibrated ordinary chondrites. However the amount of chromite is very low in the type 3 ordinary chondrites. It is a question what phases contain the chromium in the type 3 chondrites. Olivines in Sharps H3 chondrite contains 0.03-0.21% (mean 0.09%) of Cr_2O_3 (Dodd, 1973). Snellenburg (1977) described much chromium occurred in the silicates of Semarkona LL3 chondrite. But the detail of the distribution of chromium in type 3 chondrite is not clear. The present study focuses on chromium in silicates in Antarctic type 3 ordinary chondrites.

Table 1 shows the mean Cr_2O_3 contents in olivines and low-Ca pyroxenes of type 3 ordinary chondrites. The Meteorites studied have been divided into 4 groups on Cr_2O3 contents. These groups parallel the thermoluminescence classification of Sears (1982 and 1983). Olivines in group 1 meteorites contain 0.2 -0.3% of Cr_2O_3 and the co-existing low Ca-pyroxenes contain 0.6-0.7% Cr_2O_3. However olivines in group 4 (Table 1) have much lower Cr_2O_3 contents, as do the co-existing low-Ca pyroxenes. This value may be the initial content in low-Ca pyroxenes of the most unequilibrated ordinary chondrites. Table 1 shows that more chromium is included in silicates of group 1, than group 2-4 does. In group 2, Cr_2O_3 in olivines is lower (0.05 to 0.1 %) but Cr_2O_3 in low -Ca pyroxenes is the same as in group 1. This fact shows that the group 1 to group transition only olivine loses Cr. In group 3, however, the low-Ca pyroxene has significantly lower Cr_2O_3 content than gruop 2. In group 4, Cr_2O_3 in olivines is about 0.02%, a value similar to that for in olivines of equilibrated ordinary chondrites. Cr_2O_3 in low-Ca pyroxenes ranges 0.15 to 0.33.

In conclusion, much chromium is included in olivines and low-Ca pyroxenes of low grade type 3 ordinary chondrites. The value of Cr_2O_3 in them is 0.3% in olivines and 0.65% in low-Ca pyroxenes. Chromium is gradually expelled from silicates in order from group 1 to group 4, reflecting increasing degree

of silicate in "metamorphism". Cr in olivines is expelled at an earlier stage than Cr in low-Ca pyroxenes. Cr released by the silicates forms chromite. This is consistent with the observations of Bunch et al.(1967) and Huss et al. (1980) that chromite is present in crystallized matrix but not in opaque matrix.

References

Bunch T. E., Keil K. and Snetginger K. G. (1967), Geochim. Conmochim. Acta 31, 1569-1582.

Dodd R. T.(1973), Contr. Mineral. and Petral. 42, 159-167.

Hess G. R., Keil K. and Taylor G. J. (1981), Geochim. Cosmochim. Acta 45, 33-51.

Sears D. W. G., Grossman J. N. and Melcher C. L. (1982), Geochim. Cosmochim. Acta 46, 2471-2481.

Sears D. W. G. and Weeks K. S. (1983), Proc. Lunar Planet Sci. Conf., 14th, Partl. in J. Geophys. Res., 88, B301-B311.

Snellenburg (1977), Meteoritics 12, 364-365.

Table.1

Name	Type	Cr_2O_3%		%M.D.	TL	Group
		olivines	pyroxenes			
Y-74660	LL3	0.31	0.63	63.4		
ALH-77176	L3	0.25	0.61	54.6	3.2	1
Y-790448	LL3	0.24	0.71	42		
ALH-764	LL3	0.09	0.67	51.2	3.3	
Y-74441	L3	0.08	0.62	44.7		
ALH-77167	L3	0.06	0.64	51.6	3.4	2
Y-74417	L3	0.09	0.61	45.6		
ALH-77011	L3	0.06	0.60	49.7	3.5	
ALH-77299	H3	0.07	0.46	18.3	3.7	
ALH-77278	LL3	0.08	0.41	37.9	3.6	3
Y-791429	L3	0.08	0.38	6.9		
Y-790461	H3	0.03	0.33	6.0		
Y-791428	H3	0.03	0.33	2.0		
ALH-77304	L3	0.02	0.33	1.3	3.8	
ALH-78084	H3	0.02	0.27	1.9	3.9	4
Y-791047	H3	0.03	0.24	2.4		
Y-791087	H3	0.02	0.23	1.8		
ALH-77216	L3	0.02	0.15	5.8	3.8	

COMPOSITIONAL COMPARISONS OF METAMORPHOSED CARBONACEOUS CHONDRITES

Gregory W. Kallemeyn
Institute of Geophysics and Planetary Physics, University of California, Los Angeles, CA 90024

Recent petrographic studies of four carbonaceous chondrites: Coolidge, Karoonda, PCA82500, and YAM6903 show the first 3 of these to be of petrologic type 4, while the latter is possibly of type 5(1,2). Of these chondrites, Coolidge appears to be petrographically most dissimilar from the other 3(1), while the others have closely related mineralogies (2). New compositional studies of PCA82500 and YAM6903 using instrumental neutron activation techniques are reported here. Combined with previous studies of Coolidge and Karoonda from this lab (3),these provide a basis for determining whether the compositional trends mirror the petrographic trends.

CI-normalized abundances are plotted in Figs. 1-2 for lithophile and for siderophile and other nonlithophile elements, respectivley. Magnesium is used as a normalizing element for both plots, and elements are placed in approximate order of decreasing condensation temperatures.

Refractory lithophile and siderophile abundances for Coolidge are quite similar to those for CV chondrites, and on that basis Kallemeyn and Wasson (3) classified it among the CV clan. Its low common siderophile abundances relative to CV3 are probably the result of weathering effects, but the very low volatile abundances cannot be explained by such a mechanism and are likely due to open-system metamorphism. A classification of CV4 is supported by the data.

YAM6903 also has refractory lithophile abundances similar to CV, but refractory and common siderophiles are enriched by 10-15%. Volatile abundances are surprisingly at normal CV3 levels. Our replicates were quite heterogeneous in refractory siderophiles and Au, if only one of the replicates were used for these data, agreement with CV would be improved. Refractory siderophiles are probably sited mainly in phases different from those for other siderophiles, and these phases are apparently inhomogeneously distributed on the scale of our sample size (300 mg). YAM6903 appears to belong to the CV clan, but its normal CV3 levels of volatiles support a classification closer to CV3 than to CV5.

Karoonda has refractory lithophile abundances intermediate between those of the CM-CO and CV clans (3). Volatile abundances are consistently lower than both CO3 and CV3 chondrites, supporting the higher petrologic type 4. Kallemeyn and Wasson (3) left Karoonda ungrouped, forming its own grouplet of one.

PCA82500 is highly weathered, with numerous cracks and cavities, and this seems to be reflected in the high variability seen in the abundance data. Despited this, some important points can be noted from the plots. Refractory lithophiles Al, Ca, and V and common siderophile Fe have abundances only slightly lower than in Karoonda. Refractory siderophiles and REE are very low, possibly from selective weathering of phases containing those

elements. Volatile abundances in PCA82500 are generally quite similar to those in Karoonda, supporting a similar petrologic type 4.

Overall, the compositional data appear to support assignment of Coolidge and YAM6903 to the CV clan, although YAM6903 appears to be a more normally grouped CV3 rather than a CV4 as Coolidge. PCA82500 is possibly related to Karoonda as a member of a clan intermediate to the CM-CO and CV clans. It is also possibly a second member of the grouplet represented by Karoona, although this is rather specualtive due to the compositional variability of this weathered meteorite. Analysis of a second replicate of PCA82500 is planned, which will hopefully clear up this issue a little better.

References: (1) Scott E.R.D., Taylor G.J. and Keil K. (1984) LPSC XV, 740-741. (2) Scott E.R.D. (1985) LPSC XVI, in press. (3) Kallemeyn G.W. and Wasson J.T. (1982) GCA 46, 2217-2228. (4) McSween H.Y. (1977) GCA 41, 1777-1790.

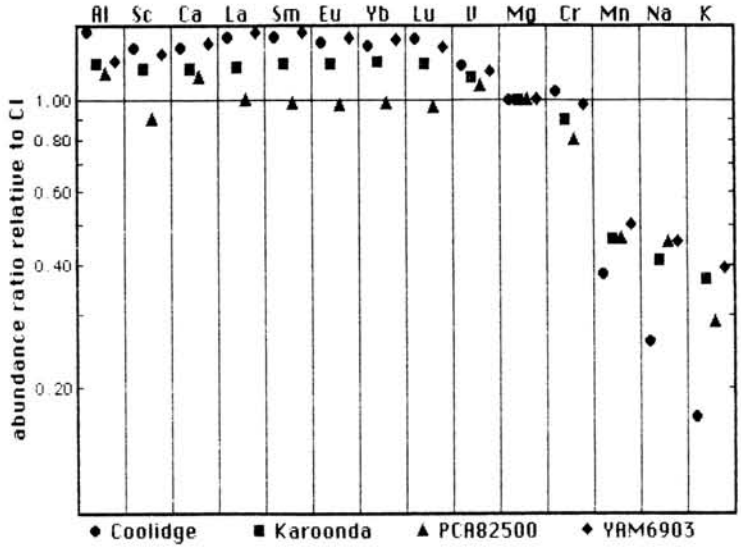

Fig. 1

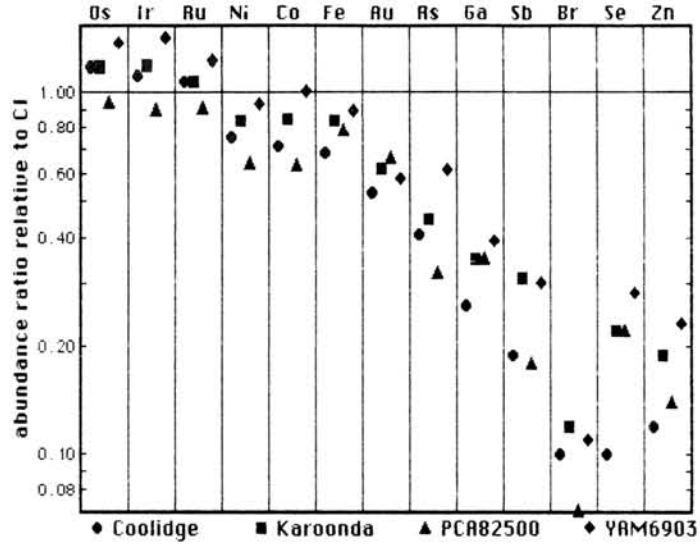

Fig. 2

Mineralogical study of matrix phyllosilicates and isolated olivines in Yamato-791198 and -793321

Junji AKAI and Jinko KANNO
Faculty of Science ,Niigata University,950-21 Niigata,Japan

High resolution electron microscopic (HREM) investigations of phyllosilicates and other closely related layer minerals in the matrix of carbonaceous chondrites shed light on the characterization of these minerals and further on these meteorite origin. However, many problems concerning to the carbonaceous chondrites remain ; for example ,in the genetic relations among C1,C2 and C3 types and in the formative condition of the matrix phyllosilicates . The results of HREM study on the matrix phases of Y-793321 have been reported at the ninth Symposium on Antarctic Meteorites (Akai,1984). Then,we report the results on Y-791198 together with the zoning pattern analysis of isolated olivines in Y-793321.

General description of Y-791198

Dispersed throughout the matrix , are chondrules and isolated olivine and pyroxene grains. The ratio of these chondrules and grains to the matrix is similar to the other C2 chondrites. Chondrules were classified into 4types ; the one composed of barred olivines, the one composed of small anhedral olivine grains, the one composed of pyroxenes with radial textures and the one consisting of euhedral olivines. Green 'phyllosilicates' (spinach phase) are present in or around the chondrules or mineral grains. Isolated olivines are angular olivine grains ranging from 2.5μm to 0.8mm in size and homogeneously distributed in the matrix. In contrast to this, isolated pyroxene grains were rarely found. X-ray powder diffraction pattern showed relatively strong 7 Å serpentine diffraction peak.

Zoning pattern of isolated olivines

The mode and the compositional range of the isolated olivines in Y-793321 are shown in Fig.1. The results on Y-791198 were essentially similar to this pattern. In the figure, two distinct types were recognized ; that is, magnesian olivines which have a narrow compositional range, and most of them are nearly homogeneous and the iron -rich olivines which show a wide compositional range. The modal ratio of the two olivines is nearly the same in Y-793321 and more magnesian olivines than iron olivines are in Y-791198. These results on isolated olivines strongly suggest the similarity of C2 (especially Y-793321) and C3 (ALH-77307).

EM & AEM investigation of Y-791198

Micron-size Fe-sulfide grains, olivine and pyroxen grains were found by EM (Fig.2). The tendency of accumulation of same type grains in narrow regions was observed.Phyllosilicates found in Y-791198 matrix can be divided into four types in structure and morphology : A) 7 Å platy phyllosilicates (Fig.3). B) 7 Å-poorly organized tubular phyllosilicates (Fig.4). C) 7 Å-poorly organized phyllosilicate with only a few 7 Å lattice fringes. D) 17 Å platy phyllosilicates which was ,at first,inferred to be composed of 7 Å serpentine layer and two brucite layers but was recently characterized to be the mixed layer minerals composed of serpentine layer

plus tochilinite layer.(Tomeoka and Buseck,1983 ,Mackinnon,1984). In addition to these four types, 11 Å layer minerals which are recently identified to be tochilinite were found. This 11 Å minerals are often found with parallel intergrowth with the type A 7 Å phyllosilicates (Fig. 3). Type B and C are often found in the same regions(Fig.4). All these features of phyllosilicate types lead us to conclude that characteristic of phyllosilicates in Y-791198 is same as that in Murchison and Y-74662.

AEM study of type A 7 Å phyllosilicate showed considerable compositional (especially Fe/(Fe+Mg) ratio) fluctuation. The tendency of accumulation of the same type phyllosilicates in narrow regions was also recognized.

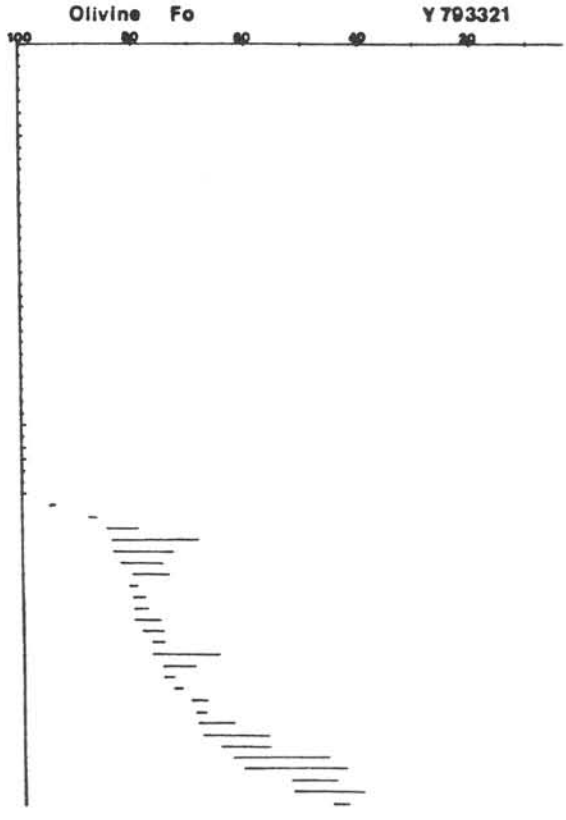

Fig.1 Compositional range of isolated olivines in Y793321. One bar represents one grain selected at random.

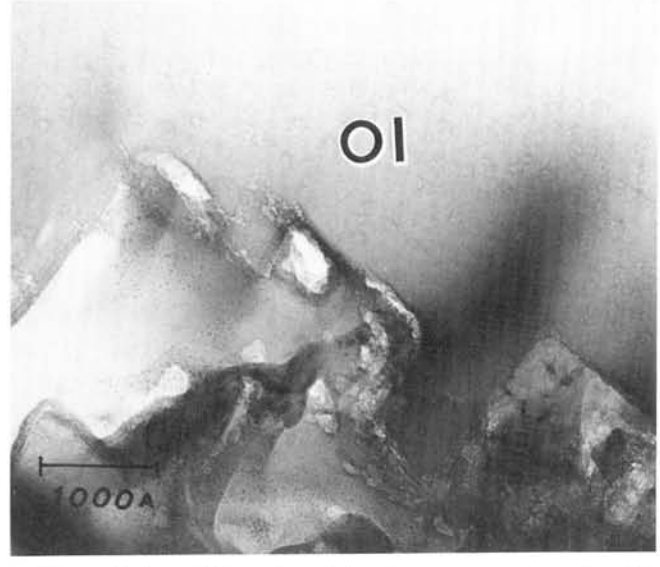

Fig.2a EM of olivine grain in Y-791198 showing irregular outline suggestive of erosion by some fluid phase.

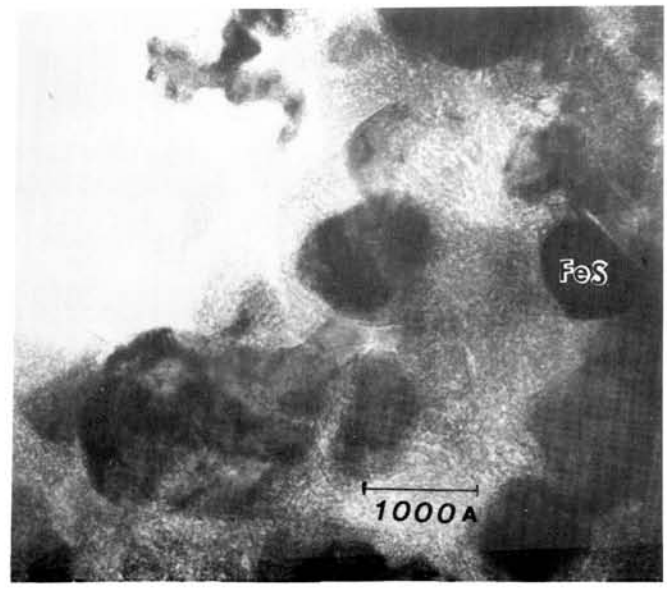

Fig.2b EM of matrix texture in Y-791198 indicating the presence of many FeS grains in this region.

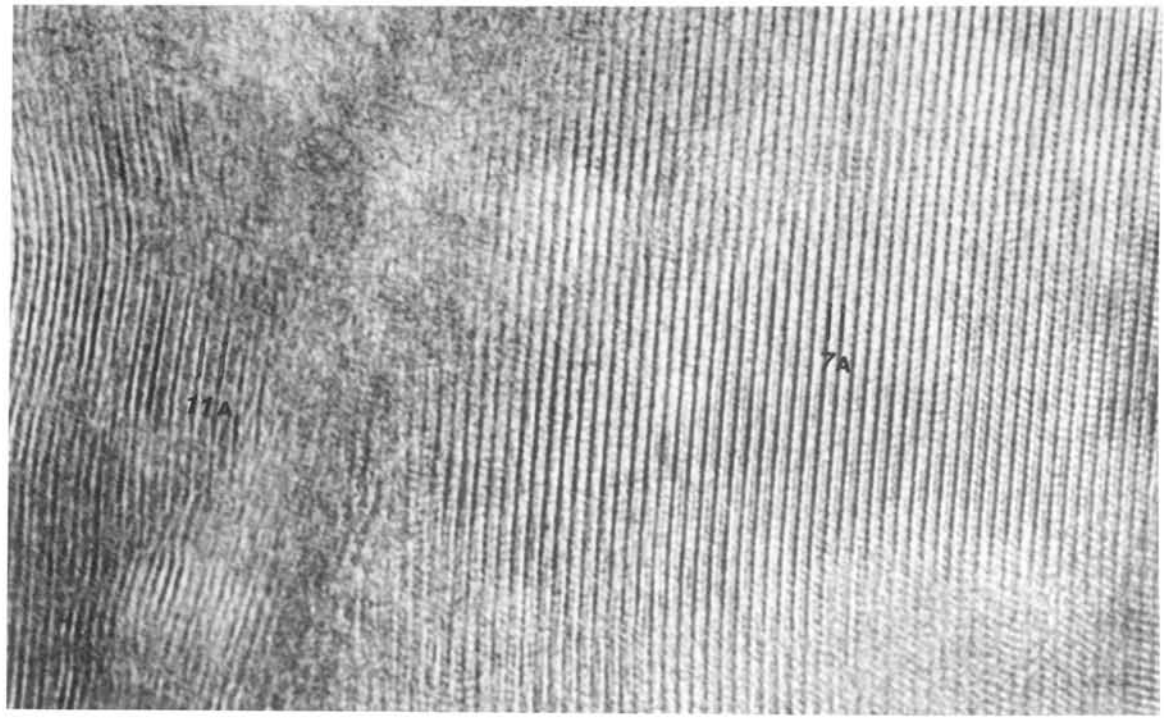

Fig.3 Electron micrograph of 7 Å phyllosilicates (serpentine structure) in Y-791198. Stacking disorder of n·b/3 type is found. 11 Å layer structure (tochilinite?) is parallel intergrown.

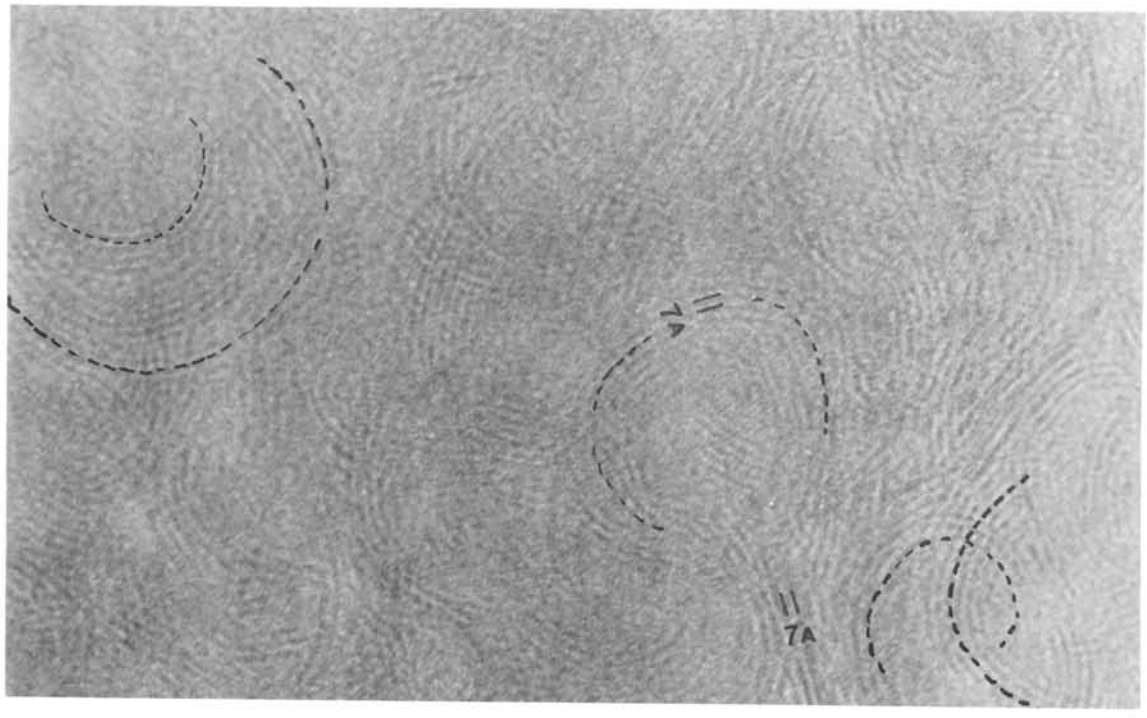

Fig.4 Electron micrograph of a section of poorly organized tubular phyllosilicates with 7 Å structure.

POSSIBILITY OF CLASSIFICATION OF CARBONACEOUS CHONDRITE BASED ON CARBONACEOUS MATTER

Murae, T., Masuda, A., and Takahashi, T.
Department of Chemistry, Faculty of Science, University of Tokyo, Bunkyo-ku, Tokyo 113

Carbonaceous chondrites have been classified by chemical and petrographic correlations (e.g. Wiik (1956), Clayton et al. (1973), Schmus and Hayes (1974), Kallemeyn and Wasson (1982)). Quantitative analyses for organic matter in carbonaceous chondrites by pyrolysis reveals that the meteorites analyzed in this work can be classified into three subgroups which were different from the conventional classifications. The investigation on the nature of carbonaceous matter in the carbonaceous chondrites may afford a new classification reflecting the formation process of this kind of meteorite in the solar nebula.

Four Antarctic carbonaceous chondrites Y-74662(C2), ALH-77307(C3), B-7904(C2), and Y-79332(C2) along with two carbonaceous chondrites Allende(C3) and Murchison(C2) were pyrolyzed at 740 ^{o}C using Curie point pyrolyser and the pyrolysis products were analyzed by GC (column: 25m x 0.25mm i.d. open tubular fused silica column coated with silicone OV-101, detector FID). The examples of gas chromatogram are shown in Fig. 1. Primary products on the pyrolysis are considered to be essentialy the same for all samples.

The carbon contents before the pyrolysis were determined by a CHN analyzer for all samples. The amount of naphthalene (typical and main pyrolysis product for all samples) was determined by GC. The ratios of naphthalene produced on the pyrolysis to the amount of total carbon originally contained in the meteorite were calculated (Table 1). Remarkable difference in the ratio between for groups I (Y-74662, Allende, Murchison), II (B-7904, ALH-77307), and III (Y-79332) were observed. The results can be considered to reflect the thermal history of the carbonaceous chondrites.

References:
Clayton, R. N. et al. (1973), Science, 182, 485.
Kallemeyn, G. W. and Wasson, J. T. (1982), Geochim. Cosmochim. Acta, 46, 2217.
Van Schmus, W. R. and Hayes, J. M. (1974), Geochim. Cosmochim. Acta, 38, 47.
Wiik, H. B. (1956), Geochim. Cosmochim. Acta, 9, 279.

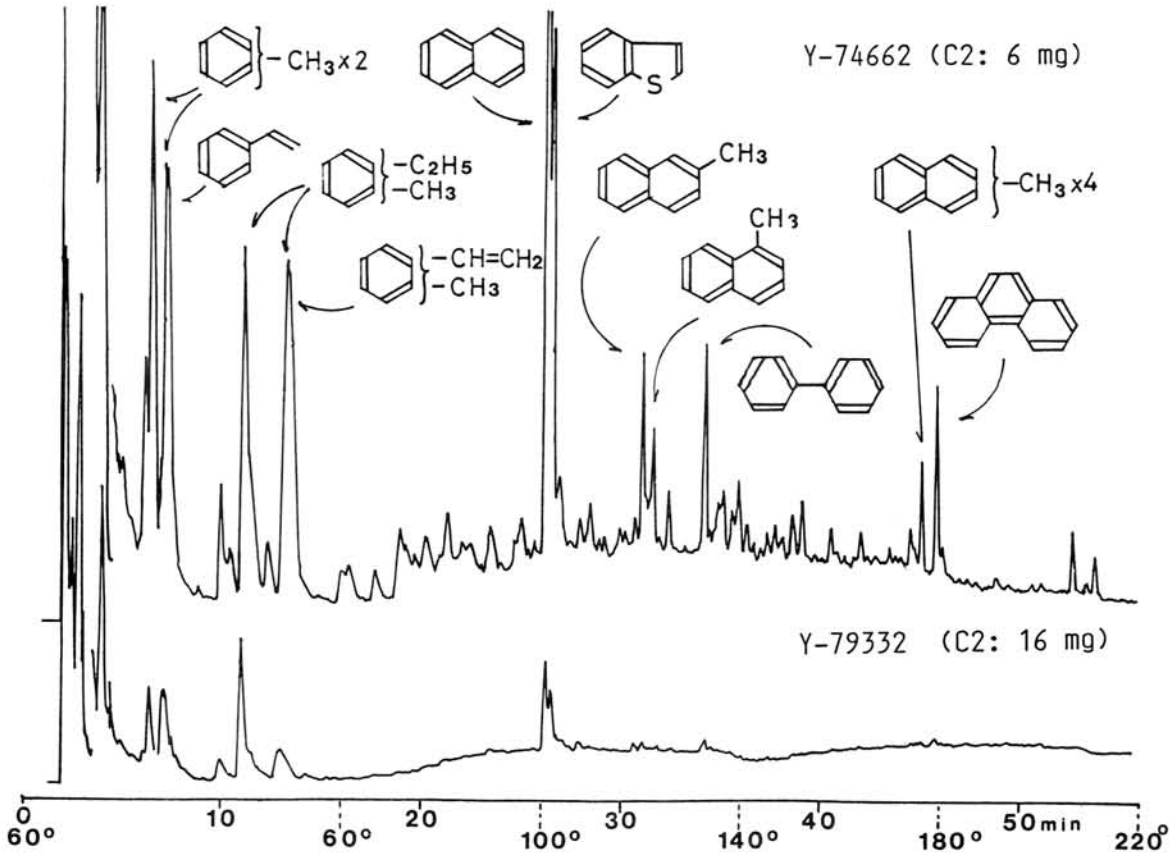

Fig. 1 Gas chromatograms of the products afforded at 740 °C pyrolysis for Y-74662 (C2: 6 mg) and Y-79332 (C2: 16 mg). The attenuation and the sensitivity of GC are the same for the both samples.

Group	Meteorite	Class	Sample weight (mg)	Carbon content (%)	Total carbon (μg)	Observed naphthalene (ng)	Naphthalene / Original carbon (%)
I	Y-74662	C2	5	1.89	95	100	0.11
	Murchison	C2	2	1.98	40	50	0.13
	Allende	C3(V)	15	0.23	35	50	0.14
II	B-7904	C2	15	0.96	144	20	0.014
	ALH-77307	C3	20	0.74	148	20	0.014
III	Y-79332	C2	15	1.77	266	9	0.003

Table 1 The amount of total carbon in the samples and the amount of naphthalene yielded on pyrolysis at 740 °C.

INDIGENOUS AMINO ACIDS FROM THE YAMATO-791198 CARBONACEOUS CHONDRITE

SHIMOYAMA, A.[1], HARADA, K.[1], and YANAI, K.[2]
1 Department of Chemistry, University of Tsukuba
Sakura-mura, Ibaraki 305
2 National Institute of Polar Research, Kaga-cho
Itabashi-ku, Tokyo 173

It has been thought that amino acids could be found in hot-water extract of C2 chondrites from Antarctica, which was supported by the studies of the Y-74662(1) and the ALH-77306(2,3,4). However, most recently, it was found that two C2 chondrites, namely the Y-793321 and B-7904 yielded little amino acids(5). This new finding shows that the carbon content is not always a good indicator for, at least, Antarctic carbonaceous chondrites as to whether they yield detectable amounts of amino acids. Therefore, it is necessary to examine, further, carbonaceous chondrites from Antarctica in order to know if indigenous amino aicds are found and to better-understand organic chemistry in the early solar nebula.

We analyzed C and N contents and amino acids from a C2 chondrite(sample No. Y-791198,23 and Y-791198,73). It was found that this chondrite showed a typical C-N content for C2 as below,

Sample No.	C(%)	N(%)
Y-791198,23	2.33, 2.31	0.12, 0.13
Y-791198,73	2.26, 2.26	0.13, 0.12

(Duplicated results)

For amino acids, the two samples were extracted with hot-water and the extracts were divided into two fractions, one unhydrolyzed, one hydrolyzed by 6 M HCl. Both fractions showed amino acids as revealed by fluorescent detection(Fig. 1) and by ninhydrin detection(particulary for sarcosine). A total of 18 amino acids were detected among which nine are proteinous and nine are non-proteinous. Amounts of some amino acids in the hydrolyzed fraction per gram of the Y-791198,23 were 98 n mole glycine, 50 n mole alanine, 15 n mole β-alanine, and tentatively 360 n mole α-amino-i-butyric acid. The acid hydrolysis increased amounts of amino acids found in the unhydrolyzed fractions, but the increase was less than twice except dicarboxylic amino acids. Upon hydrolysis, aspartic acid increased at least 100 times, glutamic acid 8 times and α-aminoadipic acid 5 times. A similar increase of dicarboxylic amino acids was repoted in previous work of the Y-74662(1).

Gas chromatographic analysis with a Chirasil-Val column and a nitrogen-phosphorous detector found nearly all amino

acids detected by the amino acid analyzor. Further, D- and L-enantiomers were found with such amino acids as alanine, α-amino-n-burytic acid, valine, norvaline, aspartic acid, glutamic acid and α-aminoadipic acid.

The amounts of amino acids found from the Y-791198 are larger than those for the Y-74662 and show the Y-791198 the richest amino acid-yielding carbonaceous chondrite ever found in Antarctica. The amounts is similar to those for the Murchison(2), e.g., 98 n mole/g glycine for the Y-791198 and 96 n mole/g glycine for the Murchison. The Y-791198 yielded various

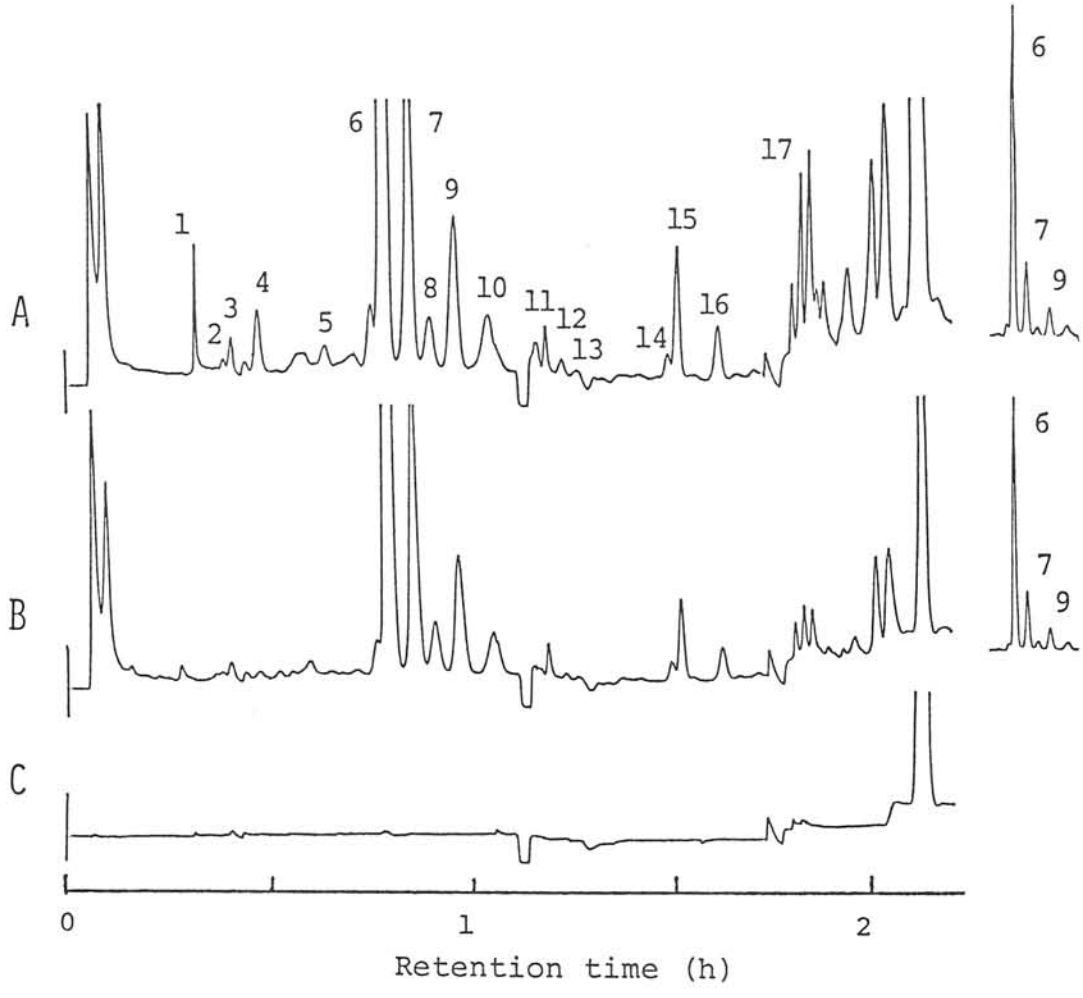

Fig.1 Amino acid chromatograms of Y-791198, A) acid-hydrolyzed fraction, B) unhydrolyzed fraction, and C) procedural blank.
Peak No., 1. aspartic acid, 2. threonine, 3. serine, 4. Glutamic acid, 5. α-aminoadipic acid, 6. glycine, 7. alanine, 8. α-amino-i-butyric acid, 9. α-amino-n-butyric acid, 10. valine, 11. norvaline, 12. isoleucine, 13.leucine, 14. β-amino-n-butyric acid, 15. β-alanine, 16. β-amino-i-butyric acid, 17. γ-aminobutyric acid.

structural isomers of amino acids, e.g., for C_4 amino acids, α-amino-n-butyric acid, α-amino-i-butyric acid, β-amino-n-butyric acid, β-amino-i-butyric acid and γ-aminobutyric acid. These isomers clearly indicate that the amino acids found are abiotic in origin and therefore, indigenous to the Y-791198. Likewise, the finding of D- and L-enantiomers support the abiotic origin. It appears that the terrestrial biologic contamination is nil from the enantiomeric ratios as observed in other Antarctic carbonaceous chondrites

References

1. A. Shimoyama, C. Ponnamperuma, and K. Yanai(1979) Natl. Inst. Polar Res. Sp. Issue, 15, 196.
2. J.R. Cronin, S. Pizzarello, C.B. Moore(1979) Science, 206, 305.
3. R.K. Kotra, A. Shimoyama, C. Ponnamperuma, and P.E. Hare(1979) J. Mol. Evol., 13, 179.
4. G. Holzer and J. Oro(1979) J. Mol. Evol., 13, 265.
5. A. Shimoyama and K. Harada(1984) Geochem. J., 18, 281.

Genetic bases in carbonaceous chondrites

Cryil Ponnamperuma
Institute of Fundamental Studies, Republic of Sri Lanka

EVIDENCE REGARDING THE ORIGIN OF CHONDRULES

John T. Wasson
Institute of Geophysics and Planetary Physics, University of California, Los Angeles, CA 90024 USA

During the past 5 years numerous advances have been made in our knowledge regarding the origin of chondrules. Researchers have recognized that the record of solar-nebula processes is best preserved in the highly unequilibrated type-3 chondrites, and have focused their research on them. Bulk chemical compositions have been determined on suites of petrographically characterized chondrules. Oxygen-isotopic compositions have been determined on individual chondrules. Detailed petrographic studies have demonstrated the presence of relict grains that were not melted during the chondrule forming process. Chondrule textures have been mimicked by laboratory simulations, thus providing information about crystal nucleation and rates of cooling. The investigated chondrules were mostly from ordinary chondrites, but some very recent work involved chondrules from EH3, CV3, CO3 and CM2 chondrites. Calculations have been carried out for chondrule melting models including lightning discharge and the heating of interstellar grains during infall into the nebula.

The isotopic and chemical studies show great diversity in composition among individual chondrules. This diversity is inconsistent with formation by condensation; it is best explained by the remelting of grains and grain-aggregates. Factor analysis of the ordinary-chondrite-chondrule (OCC) chemical data revealed the presence of two major components, a refractory-lithophile and a nonrefractory-siderophile component. The refractory lithophile component correlates positively with olivine content and with MgO/(MgO + FeO) ratio in the mafic minerals. It has the characteristics expected of the nebular component required to explain the lower refractory abundance in ordinary chondrites relative to CI or solar abundances. In the nonrefractory siderophile component siderophiles are relatively unfractionated; a few chondrules with exceptionally low metal contents show evidence of a refractory metal component.

The volatile elements provide an important constraint on models of chondrule origin. Analysis following the removal of chondrule surfaces by etching or abrasion shows that major fractions of the volatiles are in chondrule interiors and were thus part of the original chondrule material. Modal analysis of volatile FeS confirms the high concentration of volatiles in the interior. This requires (a) that chondrule formation have occurred after nebular temeratures had fallen below 600 K, and (b) that the melting was produced by flash heating, with the period spent near the melting point very brief, of the order of seconds. Simulation of chondrule textures indicate relatively slow cooling at rates as low as 1 K/hr, in apparent conflict with this interpretation. It may be that this discrepancy reflects an inadequate understanding of the processes involved. For example,

volatilization may mainly occur near the peak temperature, whereas appreciable crystal growth may occur at temperatures 200-300 K lower.

A key recent discovery is that many chondrules were incompletely melted during the formation event. Relict, unmelted olivine grains can be recognized in porphyritic chondrules because their properties (dusty, Ni-poor metal inclusions, lower MgO/(MgO + FeO) than the surrounding mafic minerals) are inconsistent with crystallization from a melt. About 85% of ordinary-chondrite chondrules are porphyritic, and about 40% of these have relict or poikilitically enclosed olivine. Because it is difficult to recognize relict grains having high MgO/(MgO + FeO) ratios, the fraction of porphyritic chondrules that were incompletely melted probably approaches 100%.

We recently obtained chemical-petrographic data on a suite of chondrules from the unequilibrated enstatite chondrite Qingzhen. These chondrules also formed by melting nebular grains and grain-assemblages. In addition to siderophile and refractory components similar to those in ordinary chondrites we find evidence of a Na-rare-earth-rich component and a oldhamite-rich component. In a recent study of chondrules from carbonaceous chondrites we find that the refractory-lithophile abundances correlates with modal pyroxene rather than olivine as in the analogous OCC component; we attribute this to incomplete vaporization of pyroxene during solar-nebula formation at the carbonaceous-chondrite formation location.

Chondrule formation by heating during infall of interstellar materials into the nebula would have vaporized much material (leading to a matrix/chondrule ratio that increased with decreasing distance from the Sun) and produced complete volatile loss in the remainder. If the presolar solids are fine grained and well mixed, this mechanism would have led to uniform chemical composition in the chondrules at all distances from the Sun.

In contrast, the lightning-discharge mechanism can yield the energy flash needed to provide the rapid heating of nebular grains. It appears that turbulence at the interface between the dusty midplane and the overlying and underlying gas-rich regions is energetically capable of generating the required amount of lightning.

Tuesday, March 26, 1985

0900 - 1200	Symposium, Auditorium
1300 - 1720	Special session: Lunar meteorites
1720 - 1805	Special lecture Professor Klaus Keil (University of New Mexico)

MELTING OF A PERIDOTITE AND A CHONDRITE UNDER ULTRAHIGH-PRESSURE

Takahashi,E., Matsui,Y. and Ito,E.

Institute for Study of the Earth's Interior*
Okayama University, Misasa, Tottori-ken, 682-02, Japan

*The name of the institute has been changed from
Institute for Thermal Spring Research, after April 1, 1985

In order to study the early evolution of the terrestrial planets, melting phase relation of a fertile lherzolite KLB-1 and that of a L3 chondrite (Y74191) have been studied in the pressure range 1 atm to 14 GPa (140 kilobar) under dry condition. A 1/2-inch diameter piston-cylinder apparatus was employed for the experiments up to 3.5 GPa. A 5000 ton uniaxial split-sphere apparatus of Okayama University was employed for the experiments above 5 GPa, using semisintered octahedron of MgO pressure media with 18 mm edge length up to 7.5 GPa and 14 mm edge up to 14 GPa. A computer aided temperature controller was employed and the run temperature was controlled to within less than ±5°C of the desired values. The sample was quenched by cutting off the electric power supply and recovered by releasing the oil pressure slowly. Run products were identified with BEI (Back scattered Electron Image) technique and chemically analysed by an electron microprobe.

At 1 atm, the solidus of the peridotite KLB-1 is about 1150°C and the liquidus is about 1750°C. The dT/dP slope of the dry solidus is about 100°C/GPa in the pressure range between 1 atm and 5 GPa, whereas it is less than 50°C/GPa for the liquidus in the same pressure range. As a result, the melting temperature of the peridotite is about 600°C wide at 1 atm but narrows to about 100°C at 10 GPa (Figure 1). Olivine is the liquidus phase at all pressures studied. The second liquidus mineral changes with increasing pressure; chromian spinel (1 atm), Ca-poor orthopyroxene (1.5 GPa), pigeonitic clinopyroxne (3 and 5 GPa), pyrope-rich garnet (7.5 and 11 GPa). The partial melts along the peridotite solidus become increasingly more MgO-rich (normative olivine rich) as pressure increases, so that partial melts formed within 50°C from the solidus at 5 to 7 GPa contain more than 30 wt% MgO and are very similar to Al-undepleted komatiite which is common in Archean volcanic terrains.

The melting relation of the L3 chondrite is similar to that of the peridotite, although both the solidus and liquidus of the silicate minerals are 100°-200°C lower than those of the peridotite due to the high Fe-Mg ratio in the chondrite. The solidus for the Fe-Ni-S is about 1000°C even at pressures above 10 GPa and is more than 500°C lower than the silicate-solidus. In experiments above about 7 GPa, transition of graphite (sample container) to diamond occurr at temperatures above about 1500°C. The Fe-Ni metal in the chondrite acts as a catalyser to the above reaction and is absorbed in the grain boundary of the newly formed diamond container within less than 1 minutes. In order to carry out well controlled melting experiments with the chondrite, therefore, it is necessary to introduce an appropriate material for its container.

Implication of the present experimental results are as follows;

1) The upper mantle peridotite (UMP) which is the representative composition of the earth's lithosphere has a very narrow melting temperature interval at pressures above 10 GPa.
2) The UMP, therefore, could have been formed from a high pressure melt.
3) Global uniformity of the UMP composition is in accord with the idea such that the UMP represents terrestrial magma ocean solidified.
4) From the Fe/Mg partitioning between olivine and silicate melts, it is expected that the residual materials of the magma ocean would be more Mg-rich [Mg/(Mg+Fe)≃0.05] than UMP.
5) If the source materials for the earth were chondritic, it may be similar to the iron-rich variety of E-chondrite.

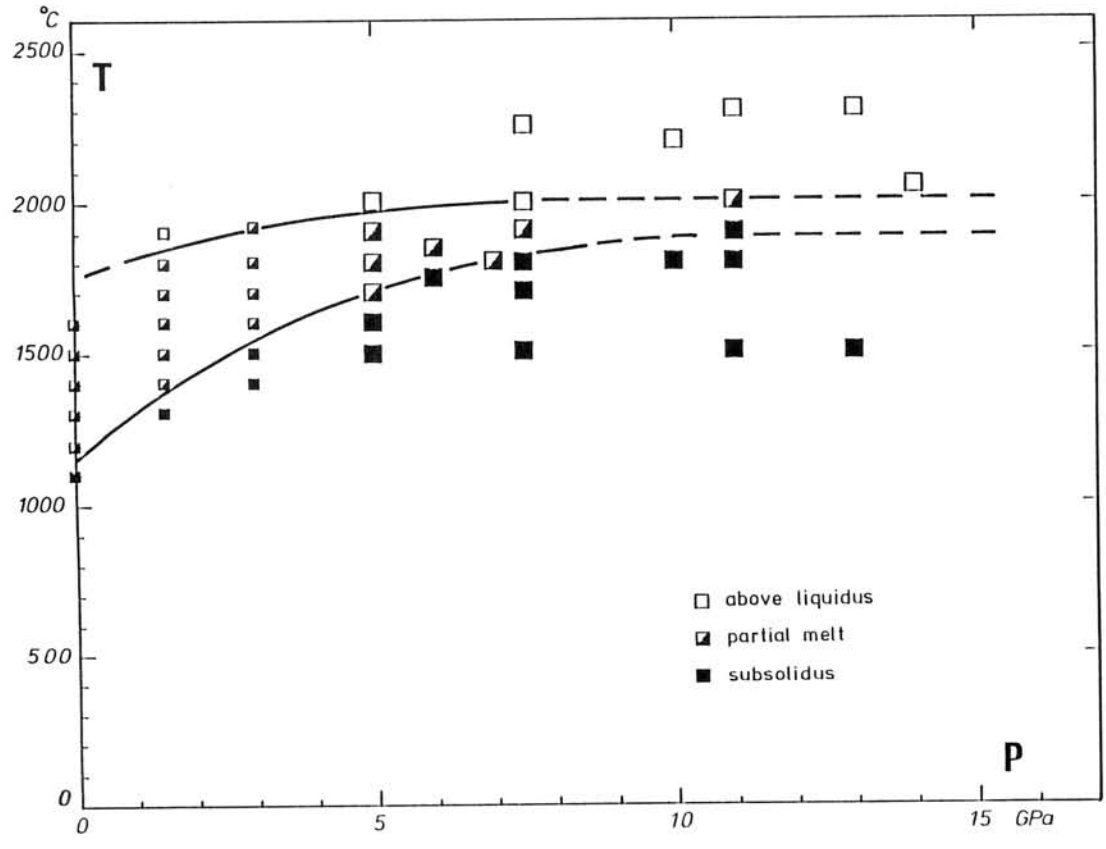

Fig. 1 Solidus and liquidus of a dry peridotite KLB-1 up to 14 GPa (140 kbar). The peridotite shows a wide melting temperature interval at low pressures but the solidus and liquidus converge to narrow temperature interval above 10 GPa.

COMPOSITIONAL VARIATIONS OF MATRIX OLIVINE IN EXPERIMENTALLY HEATED ALH-77214 (L3.4) CHONDRITE:

Satoshi MATSUNAMI, Hiroko NAGAHARA and Ikuo KUSHIRO;
Geological Institute, University of Tokyo, Tokyo 113.

Several authors have suggested that the composition of matrix olivine and the texture of matrix in some UOCs would have been affected remarkably by thermal metamorphism (1,2,3,4). To examine the metamorphic process qualitatively, heating experiments of ALH-77214 (L3.4) chondrite have been carried out in the temperature range where equilibrated chondrites would have been metamorphosed (800-1000 °C; e.g., 5) to obtain information on the equilibration kinetics of matrix olivine at the early stage of recrystallization processes of UOC. In this study, small chips of ALH-77214 chondrite samples (about 3 mm in diameter) were attached to Pt-wire loops, placed in a vertical gas mixing furnace, and heated for various durations (4-100 hrs) in the temperature range 900-1100 °C and the PO_2 range 10^{-18} - 10^{-13} atm in a constant H_2/CO_2 gas stream. Polished thin sections of these heated samples were examined in detail by scanning electron microscope. The analyses of olivine, pyroxenes and Fe-Ni metal grains in the matrix were made by the SEM-EDS technique (4).

Overall textural changes of matrix due to heating are particularly remarkable in 1100 °C experiments. The matrices have some marked evidences showing sintering (e.g., formation of neck), grain growth and/or partial melting. The matrix in 1000 °C experiments shows a well-sintered texture. The matrices in 900 °C experiments also show the textural variations similar to those under higher temperature conditions, while the samples in shorter experiments (~24 hrs) preserve some original features such as fine-grained, less-sintered nature. Spherical to subround (or sometimes vein-like) Fe-Ni metals are commonly observed, some of which might have been formed by melting within the metal-rich portion of the Fe-Ni-S system (6), the subsequent reduction of troilite to metal through sulfur loss, as suggested previously in the heating experiments of the Krymka chondrite (7), and/or the reduction of iron oxides such as magnetite to metal. Micron-sized spherules of S-bearing metal are scarcely observed in short experiments.

Representative frequency diagrams of Fa content of matrix olivine in experimentally heated samples are shown in Fig. 1. Average Fa mole% and "percent mean deviation" (PMD) (8) of matrix olivine in each experiment are listed in Table 1. In 1100 °C experiments, average Fa mole% appears to be sensitive to the change of PO_2 condition. When PO_2 increases from 10^{-14} to 10^{-13} atm a little above iron-wüstite buffer curve, average Fa mole% increases from about 30 to 40 mole% (Fig. 2). Similar tendency is also observed in 1000 °C experiments. It is suggested that in the higher temperature range (1000-1100 °C), compositional variation of matrix olivine is strongly controlled

by ambient PO_2 condition. Taking the compositions of Fe-Ni metals and pyroxenes into account, it is suggested that in the high temperature region, the reaction ($En+Fe+O_2=Fa_{50}$) is so rapid that the production rate of the Fa_{50} components would be sufficiently large. On the other hand, in 900°C experiments the composition of matrix olivine does not seem to be sensitive to PO_2 condition (Fig. 2). However, they show a remarkable dependence on heating duration; that is, matrix olivine in 72-100 hrs runs becomes more magnesian in the course of heating up to 30 mole% Fa in average. And the composition of matrix olivine shows much wider variability than those in shorter 24 hrs experiment (Figs. 1 and 3; Table 1). It is suggested that the increase in variability of matrix olivine composition may be due to the advance of Fe/Mg exchange reaction with more magnesian olivines in chondrules; however, further experiments are required over wider ranges of heating duration and T and PO_2 conditions.

The texture of matrix and the composition of matrix olivine are the most sensitive indicators of equilibration during thermal metamorphism of UOCs. This study experimentally shows that these features are sensitively affected by heating conditions such as temperture, PO_2 and heating duration. Therefore, the extent to which matrix olivine equilibrates with chondrule olivine may be a potential indicator of heating duration, if the heating temperature is known, because the composition of matrix olivine is not so strongly affected by the PO_2 condition, especially, in a lower temperature range ($\lesssim$ 900°C).

References:

(1) Van Schmus, W.R. and Wood, J.A. (1967): G.C.A., 31, 747-765.
(2) Dodd, R.T. (1969): G.C.A., 33, 161-203.
(3) Huss et al. (1981): G.C.A., 45, 33-51.
(4) Matsunami, S.(1984): Mem.Natl.Inst.Polar Res.,Spec.Issue, in press.
(5) Dodd, R.T. (1981): Meteorites. Cambridge Univ. Press, 368pp.
(6) Kullerud, G. (1963): Carnegie Inst. Wash. Yearb., 62, 175-189.
(7) McSween, H.Y.,Jr. et al. (1978): Proc.Lunar Planet.Sci.Conf., 9th., 1437- 1447.
(8) Dodd, R.T. et al. (1967): G.C.A., 31, 921- 951.

Table 1. List of heating conditions of experimentally heated samples of ALH-77214 chondrite. The average Fa mole% of matrix olivine and the PMD, obtained by the SEM-EDS technique, are also shown. N is the number of olivine analyses averaged.

No.	Temperature(°C)	PO_2	t (hrs)	av. Fa mole% (N)	PMD
M-2	1100	10^{-13}	8	39.9 (42)	8.28
M-5	1100	10^{-14}	8	29.3 (40)	5.12
M-6	1100	10^{-14}	4	31.3 (10)	13.25
M-7	1000	10^{-13}	48	38.0 (44)	11.02
M-4	1000	10^{-14}	23	39.9 (38)	6.68
M-1	1000	10^{-15}	9.5	31.1 (37)	11.93
M-3	1000	10^{-15}	22	34.3 (41)	14.32
M-10a	900	10^{-17}	24.5	37.0 (37)	7.33
M-10b	900	10^{-17}	100	28.5 (45)	18.12
M-11a	900	10^{-18}	24	37.5 (42)	5.42
M-11b	900	10^{-18}	72	31.3 (35)	15.22

Figure 1.

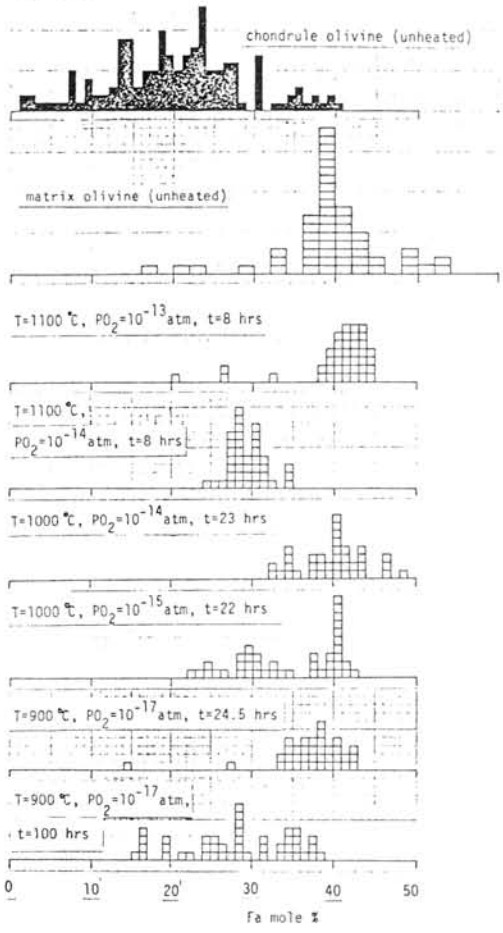

Figure 2.

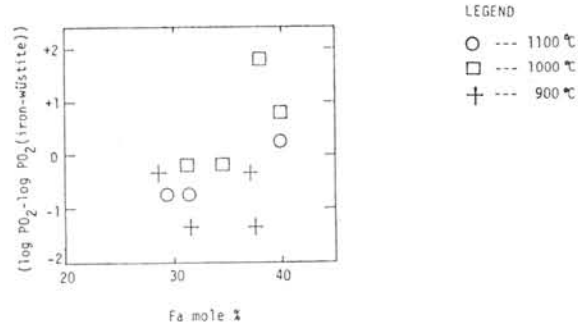

Figure 3.

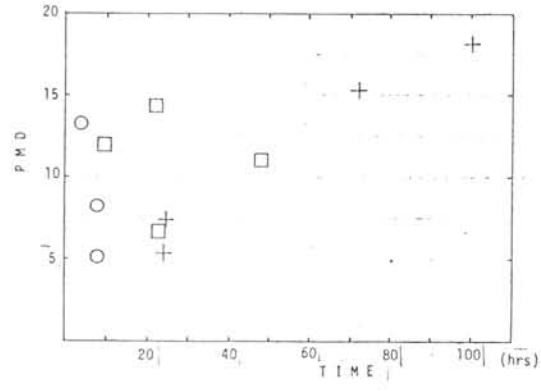

Figure 1. Representative frequency diagrams of Fa content of matrix olivine in experimentally heated ALH-77214 chondrite. One square represents one analysis.

Figure 2. Dependence of average Fa mole% of matrix olivine on PO_2 condition.

Figure 3. Dependence of PMD on heating duration.

29—1

ORIGIN OF IRON-RICH OLIVINE IN THE MATRICES OF TYPE 3 ORDINARY CHONDRITES

Ikuo Kushiro and Hiroko Nagahara
Geological Institute, University of Tokyo, Tokyo 113, Japan

The composition of olivine in the fine-grained matrices of Type 3 ordinary chondrites varies widely (e.g., Fo92-Fo14 in Krymka; Fo99-Fo15 in Chainpur; Fo89-Fo7 in ALH77278)(Huss et al., 1981; Nagahara, 1984). The process of formation of olivine with such a wide compositional range is discussed based on the experiments on the reaction among metallic iron (M), enstatite(En) forsterite (Fo) and silica mineral (Sm) and the possible vaporus phase relations of these minerals at pressures below 10^{-3} atm.

The experiments were carried out at temperatures between 1000^{o} and 1150^{o}C and at Po_2 between 10^{-16} and 10^{-13} atm. The preliminary results have been reported by Nagahara and Kushiro (1984). In these experiments olivine with intermediate compositions (Fo48) is formed within a short period (0.5 hr) at 1000^{o}C by reaction between M and En. Magnesian olivine (Fo72-Fo50) is formed by reaction among M, En and Fo, its composition becoming more magnesian with increasing Fo/En ratio in the starting material. Relatively iron-rich olivine (Fo50-Fo28) is formed by reaction among M, En and Sm, its composition becoming more iron-rich with increasing Sm/En ratio. It is evident that the presence of Sm is essential to form iron-rich olivine by sub-vaporus reactions. From these experimental results it is suggested that the wide compositional range of olivine in the matrices of Type 3 ordinary chondrites would have resulted from heterogeneity of the precursor materials condensed from the nebular gas, especially the variations in the proportion of M, Fo, En and Sm. At lower temperatures and at higher oxygen fugacities the above minerals with variable ratios reacted to have formed olivine with variable compositions probably before the aggregation into chondrites. Iron-rich olivine may have formed from the precursor materials containing Sm.

Silica mineral may have condensed from the nebular gas by a process of fractional condensation.

Another possibility is that the iron-rich olivine was formed by reaction of M and En with a silica-rich gas in the nebula. Such a silica-rich gas may have been formed also by the fractional condensation process. In either case, the fractional condensation to produce Sm or silica-rich gas is essential to form iron-rich olivine in the matrices of Type 3 ordinary chondrites. The extensive fractional condensation probably took place locally in the nebula.

The compositions of the fine-grained matrices of Type 3 ordinary chondrites (Bishunpur, Chainpur, Krymka, Ngawi, Semarkona and Sharps) (Huss et al., 1981; Matsunami, 1984) are significantly more silica-rich than the bulk compositions of these Type 3 ordinary chondrites and the cosmic abundance. This evidence strongly suggests that some fractionation took place in the formation of the matrices of these ordinary chondrites and that the fractionation was toward silica-rich compositions. The fractional condensation of the nebular gas suggested above would be the most probable process for the fractionation observed in the Type 3 ordinary chondrites.

References: Huss, G. R., K. Keil and G. J. Taylor, Geochim. Cosmochim. Acta, 45, 33-51, 1981; Nagahara, H., Geochim. Cosmochim. Acta, 48, 2581-2595; Nagahara, H. and I. Kushiro, Lunar Planet. Sci., 15, 585-586, 1984; Matsunami, S., Mem. Nat. Inst. Polar Res.(in press), 1984.

30—1

COMPOSITION AND STRUCTURAL SUBSTITUTION OF METEORITIC PLAGIOCLASES (II)

Miura, Yasunori[1], Yanai, K.[2] and Tanosaki, T.[1]
1 Dept. of Mineral. Sci. & Geol., Faculty of Science
Yamaguchi University, Yoshida, Yamaguchi, 753.
2 National Institute of Polar Research, Tokyo, 173.

Meteoritic plagioclases have higher Mg and Fe contents than those of terrestrial and lunar plagioclases, resulted in much more Fe and Mg substitution for T and M site (M=K,Na,Ca,etc.; T= Si,Al,Mg,Fe etc.) (Miúra, 1984; Miúra and Tomisaka, 1984).

Plagioclases in eleven meteorites (Y-74640,81-3; Y-74647,95-3; ALH-768,65-2; ALH-77288,64-2; Y-74190,72-3; Y-74362,84-3; Y-75102,74; Y-75115,91-2; ALH769,85-3; ALH77214,93-1; Y-74646,93) were analyzed by using the JXA-50A electron microprobe analyzer.

Substitution vectors obtained by computer simulation plotted in the Al+Si vs. Si-(Na+K) diagram show that Fe and/or Mg cations substitute T and/or M site (in Y-74674,95-3, ALH-77214,93-1 and Y-74646,93), and that excess T cations substitute M site (in Y-74362,84-3, ALH-768,65-2, ALH-769,85-3 and ALH-77288,64-2), as shown in Fig. 1.

It is found in Fig. 2 that An-rich chondrites have much more Mg-substitution mainly to Al-site, and that An-poor chondrites have much more Fe-substitution. In this study, the maximum contents of Mg and Fe are 0.338 (MgO=5.01 wt.% in the Y-74647,95-3 chondrite) and 0.181 (FeO=4.81 wt.% in the Y-74646,93 chondrite) per formula unit in O=8, respectively.

The largest value of $Ca(Fe,Mg)Si_3O_8$ is 16.9(mol%) in $An_{13.1}$ plagioclase of the Y-74646,93 (LL5-6) chondritre, whereas those of $(Fe,Mg)Al_2Si_2O_8$ is 31.9(mol%) in $An_{31.0}$ plagioclase(-like) grain in the Y-74647,95-3 (H5-6) chondrite.

Almost all data are plotted in three different regions of the An-content vs. Fe/(Fe+Mg) diagram; that is, Fe/(Fe+Mg)=0.38 to 0.46, 0.54 to 0.68, and 0.83 to 0.99, which have been reported by Miúra (1984). Some data in this study, however, are plotted out of these regions; that is, Fe/(Fe+Mg)=0.10 to 0.29 with An-rich composition of $An_{31.1}$(Fe/(Fe+Mg)=0.10) and $An_{17.5}$ (0.29) in the Y-74647,95-3 (H5-6) chondrite (cf. Fig. 2).

If the compositional data of plagioclase in the ALH-77307,85 (C3) and Allende (CV3) chondrites are plotted in the An-content vs. Fe/(Fe+Mg) diagram (cf. Fig.4 of Miúra, 1984), it is found that the progressive change of Mg-substitution for the Al site with an ordinary An-content is obtained in the overall plagioclase(-like) grains in the chondritic meteorites (Fig. 3). The petrologic type (from 3 to 6) of the chondrite is surely increased with the value of Fe/(Fe+Mg) in plagioclase(-like) grain, though Miúra (1984) has pointed out the small increase of the petrologic type from 4 to 6 with the value of Fe/(Fe+Mg) in the Y-75 chondrites. This indicates that the difference between type 3 and 4-6 is not only cooling rate but also "compositional change (such as Mg and Fe contents)" of plagioclase(-like) grain in the chondrites.

The chemical heterogeneity of chondritic meteorites and the mixing up of the fragments are supported by the experimental result that the values of Fe/(Fe+Mg) of every petrologic type are plotted at random into these isolated regions of Fe/(Fe+Mg) in Figs. 2 and 3.

[Reference]
Miúra, Y. (1984): Mem. Natl Inst. Polar Res., Spec. Issue, 35, 224-240.
Miúra, Y. and Tomisaka, T. (1984): Mem. Natl Inst. Polar Res., Spec. Issue, 35, 208-223.

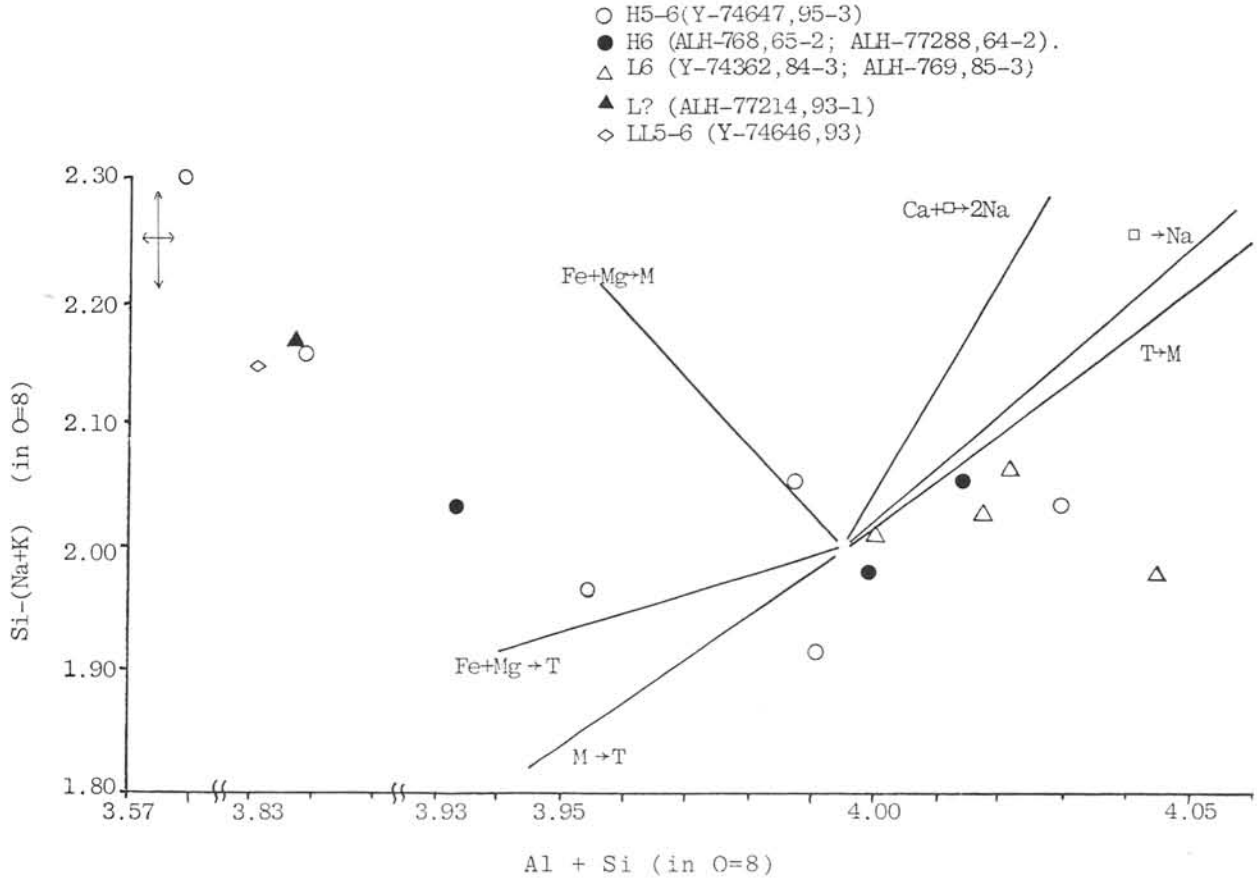

Fig. 1. Variation of Si-(Na+K) and Al+Si in seven chondrites.

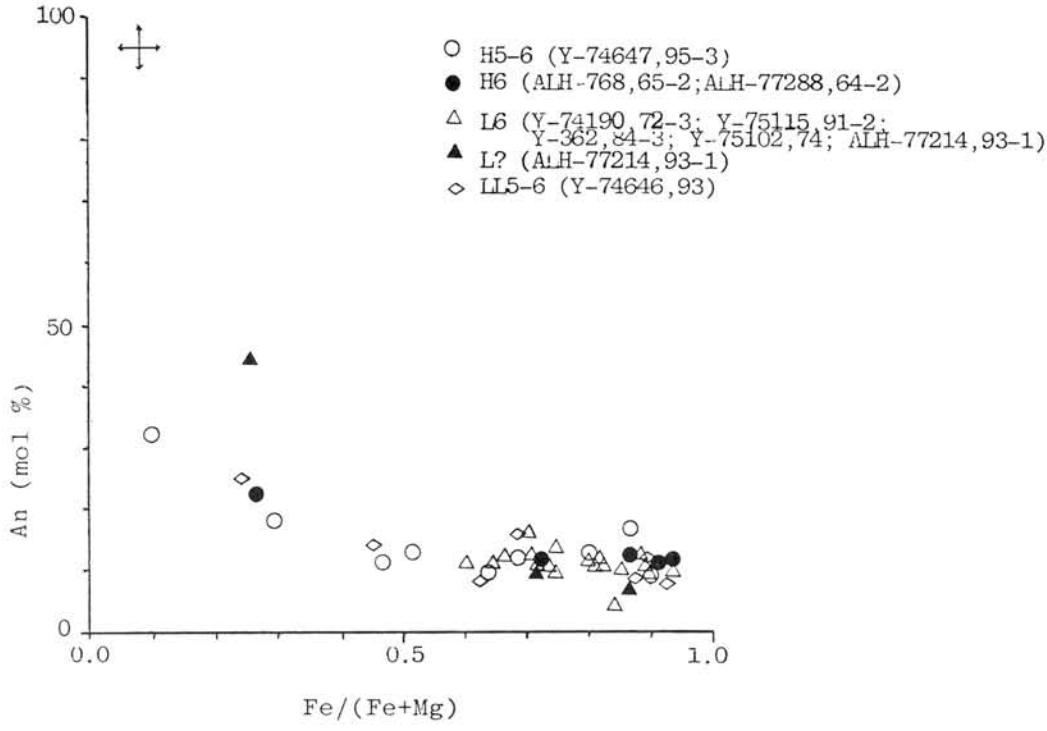

Fig. 2. An-content vs. Fe/(Fe+Mg) in the ten chondrites.

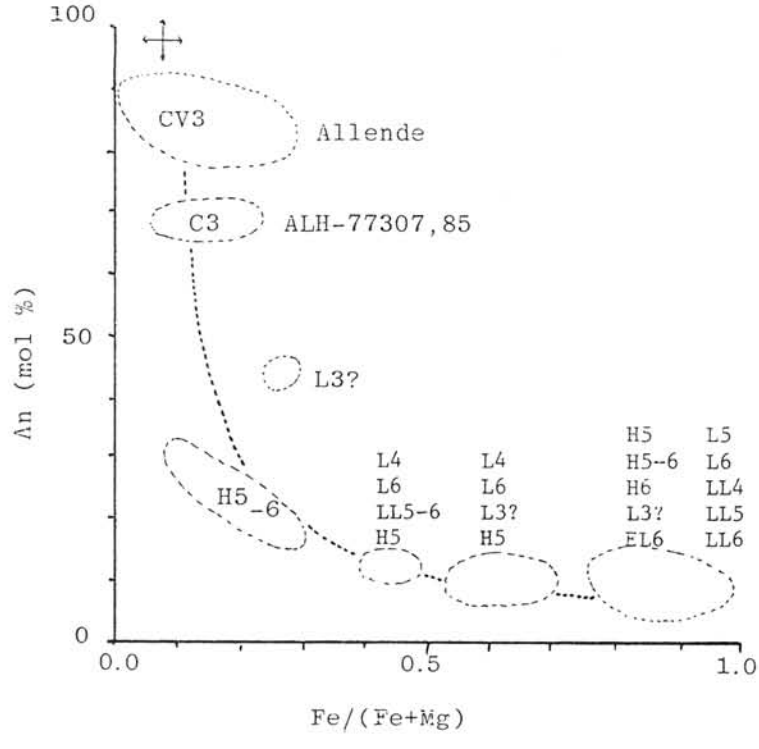

Fig. 3. An-content vs. Fe/(Fe+Mg) in various petrologic types of chondritic meteorites.

NORTON COUNTY ENSTATITE ACHONDRITE AND ITS LITHIC FRAGMENTS

A. OKADA*, K. KEIL** and G. J. TAYLOR**

* The Institute of Physical and Chemical Research, Wako, Saitama
**Department of Geology and Institute of Meteoritics, University of New Mexico, Albuquerque, NM 87131, U.S.A.

The Norton County enstatite achondrite is largely made up of brecciated pyroxenitic material. The recent study has revealed that Norton County contains unbrecciated pyroxenitic rock fragments, feldspathic clasts and impact melt rock clasts (OKADA, KEIL and TAYLOR, 1980, 1985). The pyroxenitic rock fragment is a crystalline mass, up to 8 cm in size, consisting essentially of coarse, xenomorphic enstatite crystals ($En_{99}Wo_1$) ranging up to 3 cm in size. Diopside ($En_{55}Wo_{45}$) occurs both as individual crystals and as exsolved grains displaying blebby, septal, vermicular and irregularly curved shapes. The content of exsolved diopsides within the host enstatites varies from 9 up to 25 vol.%, 20 vol.% on average in the thin section. The exsolved crystals appear to be crystallographically misoriented to the host. The apparent equilibration temperature of the pyroxene pair is about 1000°C based on the 1 atm enstatite-diopside phase diagram. The pyroxenitic rock fragment includes very minor, anhedral plagioclase ($Ab_{78\sim88}$). It also contains metal grains of zoned taenite in contact with kamacite. The cooling rate obtained from the maximum Ni content, about 48 wt. %, of zoned taenite at the boundary with kamacite gives about 1°C/m.y. The slow cooling rate and exsolution texture indicate that the rock crystallized at depth. The feldspathic clast, 1.4-3.2 mm in size, consists of major plagioclase ($Ab_{85\sim97}$) and minor silica (possibly tridymite). In contrast with the pyroxenitic rock fragment, the feldspathic clast contains more albite-rich plagioclase having subhedral and platy shapes. Two kinds of impact melt rock clasts occur in the brecciated area. One is a clast, up to 1 mm in size, having a micro-porphyritic texture consisting of ortho- and clinoenstatites (~ 85 vol.%), olivine (~8 vol.%) and fine-grained mesostasis (~6 vol.%). A few angular enstatites ($En_{99}Wo_1$), up to 1 mm in size, coexist as relict grains. Microphenocrysts of enstatites and olivines are slightly higher in FeO content, Fs:0.3-0.5 and Fa: 0.6-0.8 mol.% respectively, in comparison with nearly iron-free enstatites ($En_{99}Wo_1$) and olivines (Fo_{100}) in the brecciated area. Many pyroxenes enclose tiny olivines, and olivine microphenocrysts contain melt inclusions. The second type of impact melt rock clast is composed of fine-grained, granular diopside, plagioclase and silica mineral. It is about 0.3 mm in size, and fragments of diopside ($En_{52}Wo_{48}$) and anorthite ($An_{92\sim93}$) are sporadically mixed in the albite-rich plagioclase ($Ab_{93\sim94}$) and silica matrix. The clast could be a shock-induced product by physical mixing of melted albite- and silica-rich rock with crystalline diopside- and anorthite-rich material(s). From these results,the following history is proposed for the Norton County enstatite achondrite. The

sequential crystallization differentiation process produced olivine-rich rock, pyroxenitic rock and feldspathic rock from the silicate-rich melt formed by melting or partial melting of nebular condensates at depth in the parent body, as indicated by the presence of big, forsterite single crystals, pyroxenitic rock fragments and feldspathic clasts in the brecciated area. During slow cooling at depth, the intergrowth of zoned taenite and kamacite and the pyroxene exsolution texture developed. The impact events on the parent body excavated rocks and brecciated and mixed them, and also produced impact-melted rocks.

OKADA, A., KEIL, K. and TAYLOR, G. J. (1980): Meteoritics, 15, 34.
OKADA, A., KEIL, K. and TAYLOR, G. J. (1985): Chem. Erde (to be published).

SHOCK EFFECTS IN POLYMICT ACHONDRITE BRECCIAS Y-7308, Y-74450, Y-75032, AND Y-790260.

Ostertag, R.

Institut für Mineralogie, Corrensstraße 24, D-4400 Münster, FRG

Shock effects in mineral and lithic clasts of four Yamato achondrite breccias have been investigated in order to assess the variation of shock pressures for individual fragments and the breccias as a whole. These studies should yield insight into the intensity of the bombardement and the maximum shock pressures achieved on the achondrite parent body.

Y-7308,77-3 represents a polymict breccia consisting of mineral and lithic fragments which are clearly discernable from a fine-grained matrix. Lithic fragments are igneos rocks of eucritic and diogenitic compositions and recrystallized impact breccias with granoblastic textures. The matrix consists of angular to subrounded pyroxene and plagioclase clasts and minor amounts of chromite and other opaques. The range of shock effects in lithic clasts extents from unshocked to whole-rock melting. Most of the clasts are unshocked or only moderately shocked displaying fracturing and wavy extinction of pyroxene and plagioclase crystals. Mechanical twinning of pyroxene is rare. Diaplectic plagioclase glass was reported by (1) from a different thin section of Y-7308. The most conspicuous evidence of shock metamorphism is the occurence of glass beads and sherds, and impact melt rocks. These components can be classified into three groups: (1) glass beads and sherds with or without recrystallization textures, (2) glassy or microcrystalline melt rocks containing abundant mineral fragments, (3) crystalline impact melt rocks consisting of mineral fragments in a matrix of lathy orthopyroxene crystals. The shapes and the variable chemical compositions of the glass beads and sherds indicate that they did not form in situ. Agglomerates have not been observed. The clast-rich melt rocks have a composition and texture very similar to the melt in Y-75032 although the fragments are not recrystallized. The matrix of Y-7308 is compacted but does not show evidence of recrystallization. Y-7308 is a fragmental breccia composed of eucritic and diogenitic lithologies and recrystallized breccias which incorporated more highly shocked components. The occurrence of glass beads indicates an origin of the breccia very close to the surface of the parent body, similar to, e.g., Kapoeta.

Y-74450,94-3 is a fragmental breccia almost exclusively consisting a eucritic lithology and pyroxene clasts. The grain size distribution is seriate and a distinction between the eucritic clasts and the matrix is difficult. The dominant lithology was classified as Pasamonte-type eucrite (2) and consists of lathy plagioclase crystals nucleating at isometric clinopyroxenes. The interstices are filled with clinopyroxene and a silicate mesostasis which typically contains 2-3 different opaque phases. Shock effects are minor, polysynthetic twinning of clinopyroxene and wavy extinction in plagioclase indicate shock pressures of the order of 10 GPa. One angular piece of a brownish glass with spherulitic crystallization textures indicates shock pressures of >60-70 Gpa but evidently did not form in situ. Y-74450 therefore is a polymict fragmental breccia consisting of predominantly low-shocked components.

Y-75032,5-2 is a thin section of a melt-rich part of this meteorite and consists of orthopyroxene and plagioclase clasts and fragments of a coarse-grained opx-plagioclase rock embedded in a microcrystalline brownish melt. All small mineral clasts embedded in the melt are recrystallized.

The plagioclase minerals in the coarse-grained rocks and the plagioclase clasts in the melt show variable recrystallization textures which indicate that they have been shocked to various peak pressures before annealing. In comparison to experimentally shocked and annealed plagioclase crystals (3) the range of shock pressures can be determined to extend from >25 to >45 GPa. Some plagioclases show vesicles indicating shock-induced melting at peak pressures exceeding 52 GPa (4). One micropoikilitic clast-free impact melt clast consisting of pyroxene and plagioclase has been found. The brownish melt is a mixture of orthopyroxene and plagioclase. This portion of the Y-75032 meteorite is a glassy melt breccia, according to (5).

Y-790260,78-1 is different from the other samples investigated as it contains a large number of impact melt clasts in a compacted and recrystallized matrix. The compaction of the matrix is the result of an impact event which shocked the breccia as a whole and which is evident from a pseudotachylite vein cutting through the sample. This vein consists of brownish glassy or microcrystalline material and is lined by partially isotropic plagioclase crystals. This indicates local shock pressures in excess of 30 GPa, probably as high as 60-70 GPa. The other plagioclase crystals in this meteorite are only moderately shocked. The impact melt clasts in Y-790260,78-1 are variable in texture and in part different from those in Y-7308. There are (1) clast-bearing fine-grained melt rocks with poikilitic textures, (2) clast-poor or clast-free devitrified glasses with spherulitic textures, and (3) very fine-grained eucritic rocks with acicular plagioclase crystals which are tentatively interpreted to be impact melt rocks. Y-790260 is a shocked and recrystallized polymict fragmental breccia containing eucritic and diogenitic clasts and several impact melt lithologies.

Although most of the breccias are unshocked as a whole, the individual fragments display variable degrees of shock metamorphism and recrystallization. The shock pressures on the parent body of differentiated meteorites span the range from unshocked to whole-rock melting, i.e., from 0 GPa to >70 GPa. The occurrence of a variety of impact melts, glasses, and recrystallized breccias implies a multiphase shock and annealing history of rocks on the achondrite parent body.

References: (1) Yagi, K. et al., (1978) Mem. Natl. Inst. Pol. Res., Spec. Issue, 8, p.121-141. (2) Takeda, H. et al., (1978) Proc. Lunar Planet. Sci. Conf. 9th, 1157-1171. (3) Ostertag, R. and Stöffler, D. (1982) Proc. Lunar Planet. Sci. Conf. 13th, J. Geophys. Res., 87, Suppl., p. A457-A463. (4) Ostertag, R. (1983) Proc. Lunar Planet. Sci. Conf. 14th, J. Geophys. Res., 88, Suppl., p. 364-376. (5) Stöffler, D. et al., (1980) Proc. Conf. Lunar Highlands Crust, p. 51-70.

ORIGIN AND SOME PROBLEMS OF PYROXENE CUMULATE ACHONDRITES

Takeda, Hiroshi
Mineralogical Institute, Faculty of Science, University of Tokyo, Hongo, Tokyo 113

In Yamato achondrite collection, there are two distinct group of low-Ca achondrite or pyroxene-rich achondrites, and they are classified as type A and B diogenite (1), respectively. Type A diogenites such as Y-74013 show shock recrystallized textures (2). Type B group such as Y-75032 collected by Prof. Matsumoto's party of JARE is characterized by shocked pyroxene fragments set in a dark brown glassy matrix (3).

Y-75032 is a pyroxene-rich achondrite, but contain low-Ca inverted pigeonite in addition to diogenitic orthopyroxene. The original PTS was particularly low in plagioclase content, which is within the known range of diogenite (3). A recently produced PTS of the interior portion contains more plagioclase-rich clast (4). Yanai and his party of JARE recovered several other meteorites which show characteristics similar to Y-75032 in hand specimen (1)(5). However, some of them contain true cumulate eucrite clast.

Takeda and Mori (4) have described the crystallization history of the primitive crust of the HED (Howardite, Eucrite, Diogenite) achondrite parent body from the microtextures and chemical compositions of their pyroxene and plagioclase. Delaney et al. (5) examined these Yamato-79 collections and proposed a new group of pyroxene-rich meteorites named pigeonite cumulate eucrites, because they contain more feldspar than diogenites and more pigeonitic pyroxene than the previously known orthopyroxene cumulate eucrite, Binda. However, Binda contains abundant low-Ca inverted pigeonite and the Y-75032 type contains diogenite-like orthopyroxenite and true plagioclase-rich cumulate eucrite clasts. To obtain a better understanding of this diogenite-eucrite link problem, we reinvestigated several meteorites of this type, and propose that basic pyroxene mineralogy and crystallo graphy have to be straightened out before we debate this problem and that important problem is a crystallization process producing these suite of pyroxenes.

In order to understand this problem, we have to be familiar with what is a criterion to distinguish primary orthopyroxene and orthopyroxene inverted from low-Ca pigeonite. Primary orthopyroxene displays regular fine lamellae of exsolved augite with (100) in common, upon slow cooling (6). Some pyroxenes in a clast or as a fragment which are candidates for a primary orthopyroxene found in Y-75032, Y-791199, Y-791422, and Y-791073 contain only rare augite blebs. The TEM and optical studies (1) detected thin augite lamellae on (100). A clast in Y-75032 displays well developed grain boundaries and subgrain boundaries decorated with fine blebs of augite and chromite (1). Such precipitates have been found in diogenites by Mori and Takeda (7). The chemical composition is generally more Mg-rich and Ca-poor than the low-Ca inverted pigeonite.

Low-Ca pigeonite produces blebby augite inclusions known in Binda, aligned mostly along one orientation, as the result of a 'pearlite transformation', upon decomposition to orthopyroxene and augite, at or a little below the pigeonite eutectoid reaction (PER) line (4). The textures displayed by some pyroxenes, with Wo = 100 x Ca/(Ca+Mg+Fe) nearly equal to 5, are intermediate to the above two cases. The precipitates are lamella

-like but the boundaries are not regular and straight and are sometimes discontinuous, forming a aurora-curtain-like texture. The major plane in common with the host orthopyroxene is (100). A mechanism to make such precipitates has been proposed by Takeda and Mori (4). A few Fe-rich pyroxene in Y-791073 and Y-791201, show thick augite exsolution lamellae on (001) similar to that found in a true cumulate eucrite, Moore County.

In addition to this complex texture, the microtexture is more complicated by the facts that clinopyroxene (pigeonite)-like stacking sequences were produced in the host orthopyroxene and that recrystallization of orthopyroxene took place in a shocked portion. The pigeonite observed by Delaney et al. (5) are not well characterized on these textures. It is possible that it may not be a true pigeonite. These four types of pyroxene, three inverted pigeonites and one primary orthopyroxene, are intimately mixed in the brecciated Y75032-type achondrite suites. In addition, shock compression and heating made the textures of these meteorites more complex and obscured the original textures and origin. Therefore, their structural state should not be used in classification.

These pyroxenes may form five differnt rock types: true diogenite with a primary orthopyroxene, a rock with primary orthopyroxene and small amounts of plagioclase (clasts in Y-75032 and Y-791422), a rock with low-Ca inverted pigeonite with minor plagioclase, a similar rock with considerable plagioclase (more than 10 %), and true cumulate eucrite.

In a recent proposal on nomenclature of the polymict achondrite breccias (8), a 10 per cent divide for the amount of orthopyroxene was employed to set a boundary between howardite and polymict eucrite. To apply this principle to crystalline rocks the presence of 90 per cent or more orthopyroxene may be used as a criterion for diogenite. However, since the identification of primary orthopyroxene is essentially impossible as pointed out in the above discussion, such a criterion cannot be used in this case. Since we have to disregard the pyroxene structure-type, the 10 per cent divide for plagioclase is the best candidate for the distinction between diogenite and eucrite, if we insist on classifying a continuum into one of two categories.

The bulk chemical compositions of the Y75032-type achondrites plot in the intermediate region between diogenite and cumulate eucrite or howardite, for both CaO vs. Al_2O_3 and CaO vs. FeO/(FeO + MgO) According to Mason's plot (Fig. 1), of CaO vs. FeO/(FeO + MgO), The Y75032-type achondrites would be characterized chemically by his method as diogenite, but anyone cannot hope to distinguish polymict rocks chemically.

It is certain that there are true cumulate eucrite clasts in Y791200 and Y791201, but diogenitic clasts with Mg/(Mg + Fe) a little lower than those of common diogenite are also present in the Y-75032 type achondrites. which are special kinds of diogenite. Because lithic clasts and mineral fragments in the Y75032-type achondrites are genetically related by crystal fractionation, genomict diogenite, cumulate eucrite breccia may be the proper name to be used. These names show the futility of arbitrary classification schemes.

In any case, the Y75032-type achondrites are truly intermediate between diogenites and cumulate eucrites and it may not be fruitful to debate the classification of these achondrites and simply Y-75032 type achondrite may be sufficient name. What is important is the fact that there are achondrites intermediate between these two groups. The sequence of mineral compositions and textures appears to be continuous and these

clasts appear to be related by fractional crystallization (10), dominantly of pyroxene from a eucritic partial melt of Stolper (9). The relation between anorthite content of plagioclase and Mg/(Mg+Fe) of coexisting pyroxene in HED achondrites of the howardite parent body (11) displays two trends, the origin of which may require further study.

Acknowledgment. We thank Y. Matsumoto, K. Yanai and their parties and National Inst. of Polar Res. (NIPR) for providing us with Yamato meteorite samples. We are indebted to Y. Ikeda, B. Mason, E. Stolper, J. S. Delaney, M. Prinz, H. Wänke, L. E. Nyquist, R. H. Hewins, T. Ishii, M. B. Duke, and M. Miyamoto for discussions. A part of this study was supported by a Fund for Scientific Research from the Ministry of Education.

References: (1) Yanai K. compiler (1983) Tentative Catalog of Yamato Meteorites, pp. 63, NIPR, Tokyo. (2) Takeda H., Mori H., and Yanai K. (1981) Mem. Natnl. Inst. Polar Res. Spec. Issue No. 20, p. 81-99, NIPR, Tokyo. (3) Takeda H., Miyamoto M., Ishii T., Yanai K., and Matsumoto Y. (1979) Mem. Natnl. Inst. Polar Res., Spec. Issue No. 12, p. 82-108, NIPR, Tokyo. (4) Takeda H. and Mori H. (1984) Proc. Lunar Planet. Sci. Conf. 15th, in J. Geophys. Res., in press. (5) Delaney J. S., O'Neil C., Nehru C. E., Prinz M., Stokes C. P., Yanai K. and Kojima H. (1984) Abstr. 9th Symp. Antarctic Meteorites, Natnl. Inst. Polar Res., Tokyo. (6) Ishii T. and Takeda H. (1974) Mem. Geol. Soc. Japan, No. 11, p. 19-36. (7) Mori H. and Takeda H. (1981) Earth Planet. Sci. Lett. 53, 266-274. (8) Delaney J. S., Takeda H., Prinz M., Nehru C. E. and Harlow G. E. (1983) Meteoritics 18, 103-111. (9) Stolper E. (1977) Geochim. Cosmochim. Acta 41, 587-611. (10) Ikeda Y. and Takeda H. (1985) Proc. Lunar Planet Sci. Conf. 15th, in J. Geophys. Res., in press. (11) Takeda H. (1979) Icarus 40, 455-470.

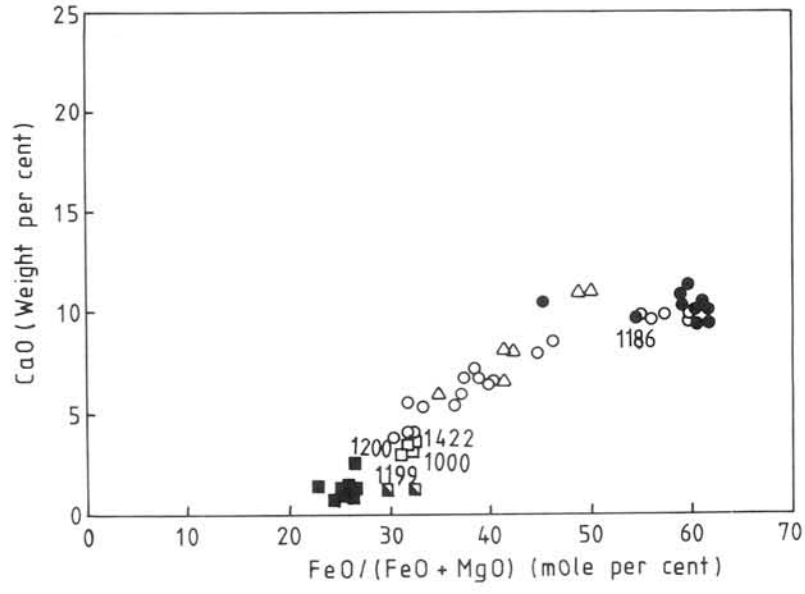

Fig. 1. CaO versus FeO/(FeO + MgO) plot of the HED achondrites. Solid square: diogenite, other squares: inermediate group, open circle: howardite, triangle: cumulate eucrite, and solid circles: eucrite. Four-digit numbers are Y-79 achondrites.

34—1

ORIENTED CHROMITE INCLUSIONS IN PIGEONITE CRYSTALS OF EUCRITE METEORITES

H. Mori and H. Takeda

Mineralogical Institute, Faculty of Science, University of Tokyo, Hongo 7-3-1, Tokyo 113

Eucrites are achondritic meteorites consisting mainly of pigeonite and plagioclase. In spite of their rapidly cooled textures, most of eucrites show no chemical zoning and exsolution of augite lamellae is extensive in pigeonite. Thermal annealing or metamorphism has been suggested as the cause for the features [1]. Reid and Barnard [2] characterized equilibrated and unequilibrated eucrites. Extensive study of the chemical zoning of mineral grains in eucrites from Antarctic and non-Antarctic specimens revealed various degree of the homogenization of the chemical zoning [3].

The clouded appearance of pigeonite crystals is a very prominent feature found in petrographic thin sections of the several equilibrated eucrites. Harlow and Klimentidis [4] examined some eucrites with a polarizing light microscope and electron microprobe to determine the nature of clouding phases in pigeonite and plagioclase. They found clouding of pigeonite is caused by minute grains of ilmenite and chromite concentrated primarily on healed microfractures in their host. The clouding was interpreted to be the results of exsolution of minor components which became incompatible and crystallized on microfractures during post-brecciation metamorphism.

To gain better understanding of clouding phenomena in eucritic pigeonites we conducted transmission electron microscope (TEM) study. We have selected three eucrites (i.e., Juvinas, Yamato 75011, Yamato 790266) with different degree of clouding or homogenization of chemical zoning.

Juvinas : This eucrite is classified into completely equilibrated eucrite [3]. Clouding of the Juvinas pigeonite is caused by very fine grains (submicron size) of chromite. When the pigeonite crystal is viewed down along b-axis, chromite inclusions concentrated on banded zones subparallel to the $(20\bar{1})$ plane and exsolution lamellae of augite on the (001) plane give pigeonite a grid appearance. Coarse irregular grains of ilmenite and chromite occur along large cracks. TEM observation revealed the chromite inclusions have rod-like shapes and two different kinds of orientation. One is elongated parallel to the pyroxene c-axis and the other parallel to the pyroxene a-axis approximately. The former is more abundant than the latter. We could find no compositional difference between the two kinds of chromite inclusions. The chromite inclusions seem to be aligned on a line. However, we could not find any traces of linear features (e.g.,fracture, crack), which may have been healed.

Yamato 790266 : Pyroxene crystals in Y790266 show a chemical zoning trend from pigeonite core ($Wo_6En_{36}Fs_{58}$) to augite rim ($Wo_{28}En_{32}Fs_{40}$). Takeda et al. [3] interpreted the trend as being partially homogenized from the original chemical zoning produced during crystallization. Clouding such as those observed in the Juvinas pigeonite is not obvious in the Y790266 pyroxene, but the pyroxene crystals are not so clear as those in the Y75011 eucrite. TEM observation revealed similar array of chromite inclusions aligned on the pyroxene $(20\bar{1})$ plane to that of Juvinas, but the size of the chromite rods is smaller (up to 0.1μm in length) than in Juvinas. We found another type of occurrence of chromite inclusions which are always associated with (often included in) augite lamellae and have coarser grain size (up to 0.7μm in length) than that of chromite aligned on the $(20\bar{1})$ plane.

Yamato 75011 : Pyroxene crystals in Y75011 show extensive chemical zoning. The trend is $Wo_5En_{65}Fs_{30}$ (core) to $Wo_{25}En_{19}Fs_{56}$ (rim). Takeda et al.[3] interpreted the feature might represent the most pristine eucrite basalt type, which preserves the original chemical zoning developed during crystallization. The pyroxene crystals are very transparent without clouding. However, we can find abundant planar microfractures developed on the $(20\bar{1})$ plane. Chromite inclusions were observed only associated with the exsolution lamellae of augite with TEM. The size of chromite is up to 0.6μm in length. We could find no such chromite inclusions aligned on the pyroxene $(20\bar{1})$ plane in Y75011 as those observed in both Juvinas and Y790266.

Oriented chromite inclusions in pigeonite crystals of the eucrites were confirmed to be the result of exsolution by TEM observation. Most of Cr in the basaltic eucrites may have been incorporated into pigeonite during the initial crystallization. According to the melting experiments on eucrites [5], the temperature of spinel appearance drops sharply with decreases in fO_2 below metal-saturation redox conditions (i.e., $fO_2 < 10^{-14}$ at 1170°C) and crystallization of spinel is suppressed well below that of pigeonite and plagioclase. This is primarily due to increases in the Cr^{2+}/Cr^{3+} ratio of the melts with decreasing fO_2. Thus some of Cr may have crystallized as Cr^{2+} in the pigeonite structure. During subsequent subsolidus cooling the Cr in the pigeonite structure may have become incompatible and crystallized in chromite precipitates. A possible mechanism is a redox reaction between Fe and Cr of the form

$$\underset{\text{"pyroxene"}}{2Cr^{2+}Fe^{2+}Si_2O_6} \longrightarrow \underset{\text{chromite}}{Fe^{2+}Cr_2^{3+}O_4} + \underset{\text{metal}}{Fe^{0}} + \underset{\text{silica}}{4SiO_2}$$

However, we could find no composite precipitates of the three phase groupings (i.e., chromite, Fe-metal, silica) in the eucritic pigeonites. Indirect redox reaction may have occurred without movement of metallic-Fe and SiO_2.

Clouding, augite exsolution and homogenization of chemical zoning in pigeonite crystals of eucrites are considered to be indicative of subsolidus re-equilibration. The occurrence of chromite inclusions associated with augite lamellae in the Y75011 pigeonite which shows extensive chemical zoning and no clouding indicates that augite is more susceptible to chromite exsolution than pigeonite host because of its higher concentration and diffusivity of Cr. Nucleation and growth of chromite in pigeonite host primarily occurred at the $(20\bar{1})$ planar microfractures which may have been induced by impact events, and probably needed more extensive thermal annealing than that in augite.

REFERENCES

[1] Duke M.B. and Silver L.T.(1967) Geochim. Cosmochim. Acta 31, 1637-1665.
[2] Reid A.M. and Barnard B.M.(1979) Lunar and Planetary Science X, 1019-1022.
[3] Takeda H., Mori H., Delaney J.S., Prinz M., Harlow G.E. and Ishii T. (1983) Proc. 8th Symp. Antarctic Meteorites, 181-205.
[4] Harlow G.E. and Klimentidis R.(1980) Proc. 11th Lunar Planet. Sci. Conf., 1131-1143.
[4] Stolper E.(1977) Geochim. Cosmochim. Acta 41, 587-612.

35—1

CATION DISTRIBUTION AND MINERAL CHEMISTRY OF PCA82506 AND RELATED UREILITES

Toyoda, H., Haga, N., Tachikawa, O., Takeda, H., and Ishii, T.*
Mineralogical Institute, Faculty of Science, University of Tokyo, Hongo
*Ocean Resarch Institute, University of Tokyo, Nakano-ku, Tokyo

Pecora Escarpment 82506 (PCA82506) is classified into ureilite which is a rare group of achondrites with olivine, pigeonite and C matrix including graphite, lonsdaleite and diamond. It is generally understood that most ureilites experienced a high temperature condition, a shock event and rapid cooling. This work was undertaken in order to investigate the thermal history of the ureilite in a hope that it might reveal its origin. As PCA82506 is relatively unshocked compared to most ureilites (Mason, Antarctic Meteorites Newsletter, 1983), large unshocked crystals are available for detailed mineralogical studies. They were examined with single crystal X-ray diffractometer, microprobe, analytical transmission electron microscope (ATEM). The polished thin section (PTS) of PCA 82506,24 is investigated with an optical microscope and an electronprobe X-ray microanalyzer. The quantitative chemical analysis of grains and zoning profiles were made with an automated model 733 electronprobe X-ray microanalyser with a 40·take off angle to carry out point analysis.

The modal abundance of mineral of PCA82506 obtained by line analyses, is olivine (50%), pigeonite (45%) and dark C matrix and others (5%). Several grains show undulatory extinction and some of the pigeonite crystals display (100) twinning. Quantitative analysis with EPMA revealed that the chemical composition of the pigeonite crystal is very homogeneous and uniform $Ca_6Mg_{76}Fe_{18}$. Average olivine core compositions is Fa_{20} and the area about 4 microns from the rim is reduced by C matrix. The nearer to rim, the composition is richer in Mg and sometimes metal and enstatite were observed at the rim. The same facts were confirmed by analytical TEM. From the diffusion profiles of olivine crystal, cooling rate of 10-15·C/hr has been estimated by computer simulation method of Miyamoto [1]. A pigeonite crystal which was about 0.2mm in diameter were selected to measure diffraction intensities with 4-circle, single-crystal diffractometer using graphite-monochromatized MoKα radiation (λ=0.71069A). The ω-2θ technique was used to collect the intensity data up to 2θ =90· at room temperature. A set of 3341 independent reflections was measured and corrected for Lorentz and polarization factors. Cell dimensions were determined from 23 reflections: a 9,669(9) b 8.8719(6) c 5.2134(5) β 108.51(1). To obtain site occupancy factors for Mg and Fe in the M1 and M2 site of the pigeonite taken from PCA82506, the refinement of the structure was carried out with the full-matrix least-squares program RADY (Busing, Levy, Coppens, Hamilton, Ibers and Sasaki, 1981) using 2255 reflections ($F>2.5\sigma(F)$). The starting parameters were those from the previous structural work of lunar pigeonite [2]. The final R value was converged to 0.080. The site occupancy factors of PCA82506 is M1(Mg 0.064, Fe 0.936); M2(Ca 0.116, Mg 0.568, Fe 0.316) and were compared with others which are derived from Takeda [2] and Yajima and Hafner [3]. Equilibrium temperature of 620·C is obtained by plotting the value of PCA82506 on the distribution isotherm of orthopyroxene [4]. Furthermore, the value of PCA82506 and the data obtained experimentally demonstration by Yajima and Hafner [3] is plotted in Fig. 1 to estimate the equilibrium temperature of the PCA82506 pigeonite.

The variation of k value for cation distribution among the M1 and M2 sites of pigeonite results from primarily variable cooling history of a meteorite which contain pigeonite, but an effect of the variable ferrosilite component in pigeonite on k at constant temperatures, effects of small concentrations of foreign atoms, differences in domain structure, or multiple cooling history etc. have to be considered [3]. The equilibrium temperature estimated from the orthopyroxene diagram may include an error of the difference in the crystal structure. Because there is not a complete disturbution isotherm for pigeonite at present, the equilibrium temperature was estimated by comparing the information of several pigeonite crystals of known cooling history.

As the data point of PCA82506 is plotted a little below the line of k=0.11, which is drawn through the points C1, C6 and C8, the equilibrium temperature may be higher than 650·C. Because the equilibrium temperature proposed for basalt 15597, whose chemical composition and k-value are similar to that of PCA82506, is 650·C [3], that of PCA82506 should also be about 650·C.

The cooling rate 10-15·C/hr, obtained by the diffusion profile described in the previous section is in agreement with that estimated for Y-74130 and Y-790981 pyroxenes (3 to 20·C/hr) from the wave length of the spinodal decomposition of Ca-rich pyroxenes by Mori and Takeda [5]. These data indicate that the thermal history at higher than 800·C is very rapid and that the Fe cation can move in an olivine grain.

The quenched temperature obtained by Fe-Mg cation distribution of pigeonite suggests two cooling history models. One is the equilibium temperature before rapid cooling, and the other is an apparent temperature when the cation distribution was fixed during the course of continuous cooling. The cooling at temperature about 650·C may not be more quicker than the rate expected from 10-15·C/hr.

Rapid cooling from 1250·C at the rate of 10-15·C/hr and below 800·C continuous cooling with the cooling rate expected for the natural cooling of the black body in a planetary enviroment may give 650·C which is an apparent equilibrium temperature where the cation migration is ceased during the last cooling. All these results are in agreement with a hypothesis that the ureilite parent body experienced a breaking of the body at the end of its history.

Acknowledgments We thanks the Meteorite Working Group for the sample.

References: [1] Miyamoto M., Duke M. B. and Mckay D. S.(1985), Proc. Lunar Planet. Sci. Conf. 15th in J. Geophys. Res. in press. [2] Takeda H. (1972) Earth and Planet. Sci. Lett. 15, 65-71. [3] Yajima T. and Hafner S. S. (1974) Proc. Lunar Planet Sci. Conf. 6th, 769-784. [4] Ganguly J.,Thermodynamics, Kinetics, and Geological applications. Advances in Physical Geochemistry vol.2. [5] Mori H. and Takeda H. (1983) Meteoritics 18, 358-359.

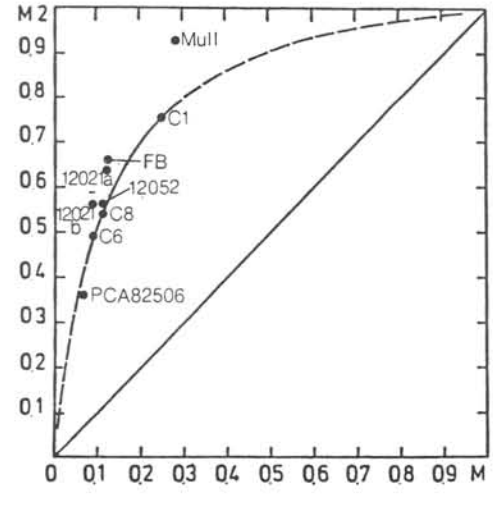

Fig. 1. Distribution isotherm of pigeonite.

FRACTIONAL TREND OF BULK CHEMISTRY OF CHONDRULES IN THE ALLENDE METEORITE

Hiroshi ISOBE, Masao KITAMURA and Nobuo MORIMOTO.
Department of Geology and Mineralogy, Fuculty of Science, Kyoto University, Sakyo, Kyoto, 606, Japan

Allende meteorite is a type 3 unequiliblrated carbonaceous chondrite, which contains chondrules and inclusions. The chemistry of chondrules is considered to reflect the chemistry of chondrule precursor materials, preserving information before its accretion to a parent body. Kitamura et al.[1] reported a relict pyroxene in a chondrule of the Allende meteorite which implied that the precursor material of the chondrule had been brought from grandparent bodies. In order to investigate the chemistry of the precursor materials, bulk analyses of the chondrules and inclusions of the Allende meteorite have been carried out.

Bulk chemistry of the chondrules were obtained after the correction [2] of the data by EPMA with a defocussed beam of 30 um in diameter. The chondrules were classified into four types defined by McSween [3] ; type I (granular olivine), type II (porphyritic or barred olivine), type III (excentroradial pyroxene) and type IV (anorthite, spinel & melilite). Among these types, the type IV chondrules are rare. Most of the type I-III chondrules have less amounts of alkali, Al and Ca than the solar abundance. On the other hand, CAIs are alkali-free and have less amounts of Mg, Fe and Si.

Several chondrules with no correspondence to the McSween's classification are also found (type V, hereafter). Their texture is porphyritic. Phenocrysts are olivine, enstatite, augite and clinoenstatite. Groundmass is inhomogeneous glass including microcrystals of albite, nepheline and sodalite (Fig.3). Volume ratios of the phenocrysts to the groundmass vary from chondrule to chondrule. Bulk composition of the type C chondrule without no phenocrysts reported by Clarke et al. [4] is similar to those of this type.

All of the bulk compositions were plotted in Figs. 1 & 2. Type I-III are plotted near the Si-end. The type V distributes in the alkali-rich region. The data of type I-III and V form a straight line. The groundmass-phenocryst assemblages of the type V chondrules (Fig. 2 a) are also on this straight line. The type IV distributes between CAIs and this straight line. This straight line of the bulk compositions implies the trend of chemical fractionation of the chondrule precursor materials. This fractionation was caused by the concentration of alkali and other elements to the melt phase formed by the sequential crystalization or partial melt. In order to maintain volatile elements of such as Na and Cl, it is necessary that the fractionated melt was covered by dense gas or was in the interior of a grandparent body.

[1] Kitamura,M. et al.: Abst. 9th Symp. Antar. Meteo.,50-51, 1984
[2] Ikeda,Y.:Mem. Natl Inst. Polar Res., Spec.Issue,**17**,50-82,1980
[3] McSween, H.Y.:Geochim. Cosmochim. Acta, **41**, 1843-1860, 1977
[4] Clarke,R.S. et al.:Smithon. Contrib. Earth Sci.,**5**,1-53, 1970

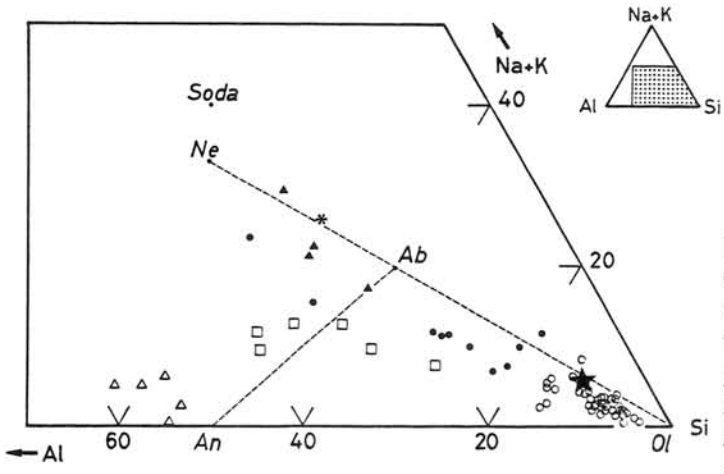

○ Type I-III McSween (1977d)
□ Type IV as above
✱ Type C Clarke et al (1970)
△ CAI
● Type V this work
▲ Groundmass of type V chondrule
★ Solar abundance

Figure 1. Atomic plotting of Na+K - Al - Si for bulk chemistry of chondrules. Type V chondrules which plotted outside of the Ab-An-Ol triangle exist. Ab, An, Ol, Ne and Soda represent albite, anorthite, olivine, nepheline, and sodalite, respectively.

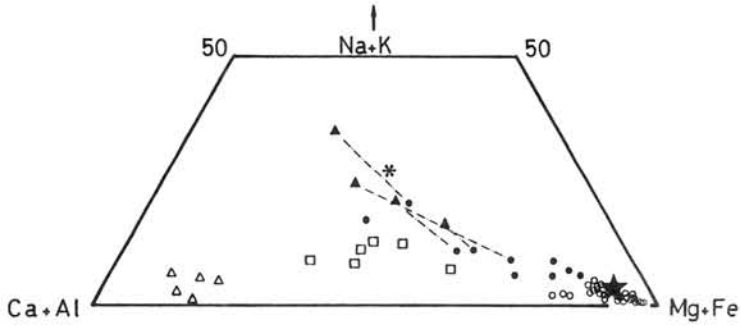

Figure 2a. Atomic plotting of Na+K - Ca+Al - Mg+Fe. Symboles are the same as in Fig. 1. Dashed lines are bulk-groundmass assemblages of each chondrules.

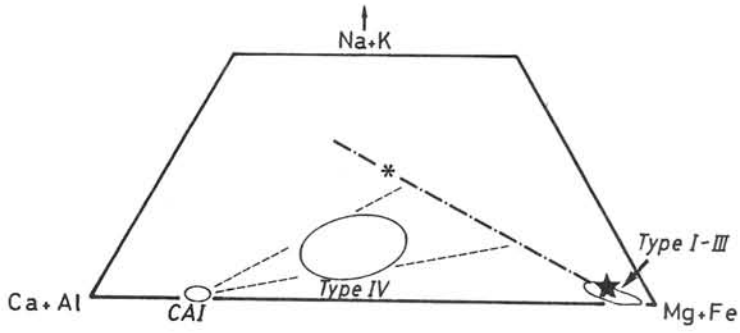

2b. Schematic drawing of Fig. 1 a. Dot-and-dashed line from the Mg+Fe apex stands for the fractional trend. This line is not a mixing line, because the end-component against to the Mg+Fe end-component does not exist.

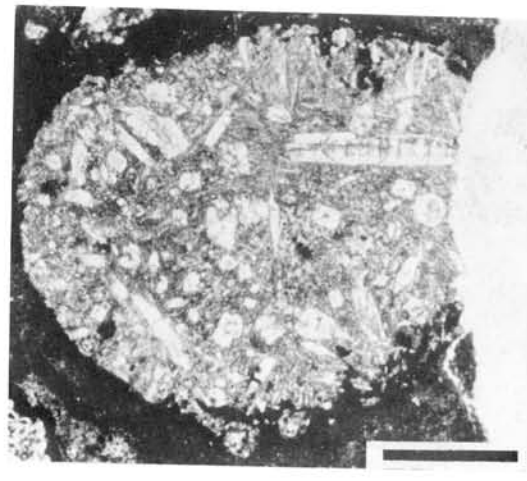

Figure 3. Photomicrograph of type V chondrule (plane polarization, scale bar is 0.3 mm). Phenocrysts are rectangular pyroxenes (core opx - En_{95} Fs_1 Wo_{40}, rim cpx - En_{59} Fs_1 Wo_{40}) and clinoenstatites (En_{98} Fs_1 Wo_1).

PHOSPHATE-BEARING MICROSPHERULES IN CHONDRULES OF UNEQUILIBRATED ORDINARY CHONDRITES

Yabuki, H.[1] and El Goresy, A.[2]

[1] The Inst. Phys. Chem. Res., Wako, Saitama, 351-01 Japan
[2] Max-Planck-Inst. f. Kernphys., 6900 Heidelberg, FR-Germany

The existence of primitive phosphate has been first confirmed by Rambaldi and Rajan (1982) in the matrix of some unequilibrated chondrites. We found that metallic globules frequently seen in porphyritic chondrules of unequilibrated chondrites often include various amount of phosphate at the margin. Their occurrence and features should be significant for the event of chondrule formation.

Size of those spherules range from submicron to 200 micrometers. Along with metallic iron, often troilite, sometimes chromite and rarely schreibersite are seen in the core of spherules. Phosphate is usually idiomorphic against metal. In some cases, phosphate forms a thick rim around the metal core (see Fig. 1), and its volume sometimes reaches over a half of the spherule. Very fine to dust-sized grains of chromite (probably) are frequently aggregating along the outer rim of phosphate. The phosphate observed in unequilibrated chondrites is mostly whitlockite, which is fairly homogeneous in composition. Apatite was found in metal-sulphide nodules in equilibrated Arapahoe (L5).

Two unusual microspherules recognized are as follows. One is a complex assemblage of metal, troilite, chromite, native copper, iron-chloride (probably lawrencite), iron-oxide and whitlockite. The other one is with a coarce whitlockite core enclosing diopside globules, and metal, troilite and chromite as a rim. The core is partly occupied by apatite.

Noteworthy is that primitive phosphate is always associated with metallic iron. It strongly implies that phosphorous was originary dissolved in metal or from schreibersite. We also detected phosphate in many of globular inclusions in metal in matrices of unequilibrated chondrites.

Though the origin of these microspherules has not been thoroughly deciphered yet, there seems to be several negative evidences to regard that they formed in situ from metal melt by reacting with chondrule materials; e.g., some spherules appear to have been partly destroyed by collision in space (Fig.2); Crystallization of phosphate by reaction with CaO and FeO attends significant increase of volume in microspherules. It would be impossible, especially for those with ample amount of phosphate, to maintain their spherical outline in porphyritic chondrules.

We would rather consider that they are exogenic. Metal, sulphide and phosphide would have been heated and formed droplets in the event forming silicate chondrules. Assuming that the melt passed the region with enough f_{O_2} and f_{CaO}, they could be readily dephosphorized and formed whitlockite by following reaction: $2Fe_xP + 3CaO + \frac{5}{2}O_2 = (CaO)_3P_2O_5 + 2xFe$. After solidification, they had a chance to be captured by much larger silicate melt. When the temperature of silicate melt was not so high compared with melting point of metal (ca. 1530°C), as is expected in porphyritic chondrules, they could have survived.

Rambaldi, E.R. and Rajan, R.S. (1982): Abstract of Lunar Planet. Sci. Conf., XIV-3.

Table 1. Microprobe analyses of phosphate in microspherules in chondrules from Chainpur (14 grains), Mezö Madaras (12 grains) and Saratov (22 grains).

	P_2O_5	CaO	FeO	MnO	MgO	Na_2O	Cr_2O_3	Al_2O_3	Total
Chainpur	46.37	44.05	1.82	0.05	3.51	2.73	0.10	0.02	98.65
Mezo Madaras	46.04	44.72	2.72	0.02	3.30	2.69	0.00	0.00	99.50
Saratov	46.07	44.82	1.06	0.05	3.50	2.72	0.06	0.05	98.33

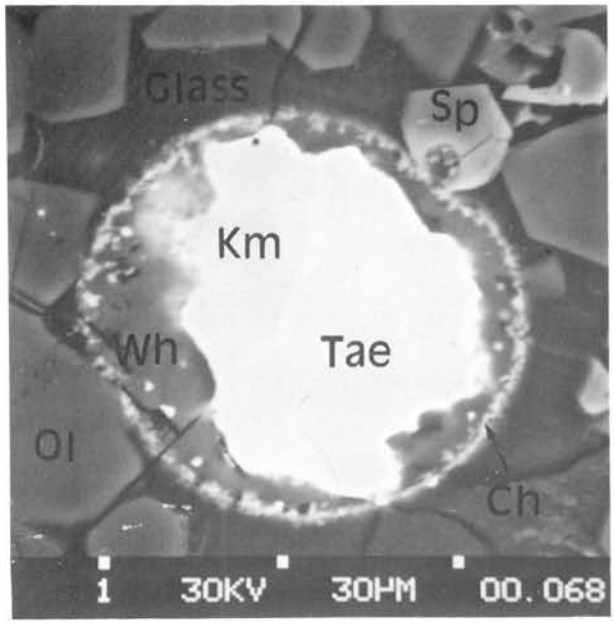

Fig. 1 A microspherule thickly rimmed by whitlockite (Wh). Dust-sized chromite (Ch) is aggregating along the outer rim. The outline is slightly bent by phenocrysts of olivine (Ol) and spinel (Sp). Saratov. Backscattered electron image. Km and Tae indicate kamacite and taenite, respectively.

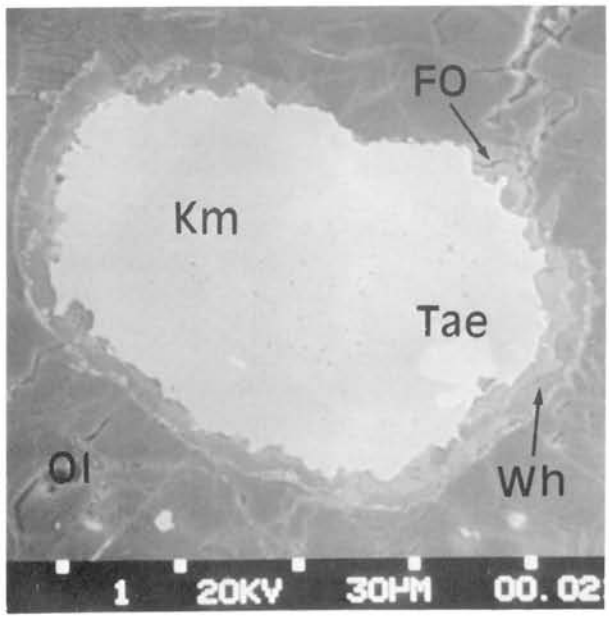

Fig. 2 A phosphate-bearing microspherule which shows an appearance having been partly destroyed by collision in space. Metal core is covered by iron-oxide (FO) and whitlockite (Wh). Mezö Madaras. Back scattered electron image.

THEORETICAL APPROACH TO DETERMINE SPECTRAL REFLECTANCES OF MINERAL MIXTURES

Kinoshita, M., Miyamoto, M., and Takano, Y.
Dept. of Pure and Applied Sci., Coll. of Arts and Sci., Univ. of Tokyo, Komaba, Tokyo 153.

We developed a model to determine spectral reflectances for mineral mixtures on the basis of the optical properties of mineral components[1]. The optical properties of each mineral component are determined from spectral reflectance and spectral transmittance of the component. The model gives spectral reflectances for mineral mixtures as a function of relative amounts of mineral components. It is important to examine the systematic variation of spectral reflectances for mixtures composed of coexisting mineral components which are separated from meteorites, in order to interpret the spectral reflectances of asteroids[2]. We measured diffuse spectral reflectances and diffuse transmittances of olivine sample and pyroxene sample separated from Nuervo Mercurio ordinary chondrite(H5), and calculated spectral reflectances for olivine-pyroxene mixtures from Nuervo Mercurio. We measured spectral reflectances of the olivine-pyroxene mixtures from Nuervo Mercurio in order to check the varidity of the model. We also applied the model on the olivine-pyroxene mixtures from olivine sand from Hanauma Bay, Hawaii for another test.

Multilayer model We assume that the mineral is composed of plane parallel layers, where thickness of each layer is equal to the mean dimension of the grains in the mixture[e.g. 3]. Further we assume that each layer is composed of unit cells whose optical properties are shown in Fig. 1 [1]. Let scattering activity s and transmitting activity t of the unit cell denote total intensity of scattered light and transmitted light for unit incident light, respectively. Then reflectance R and transmittance T of a single layer for perpendicular incident light are

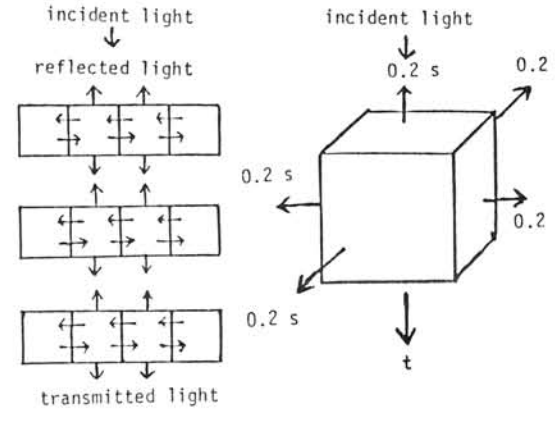

Fig. 1 Multilayer model and optical properties of cubic unit cell.

$$R = 0.2\,s + 0.2(1-0.2)s^2 / (1-t-(1-2\times0.2)s)$$
$$T = t + 0.2(1-0.2)s^2 / (1-t-(1-2\times0.2)s) \qquad (1)$$

Mean scattering activity s_{mix} and mean transmitting activity t_{mix} for mineral mixture are

$$s_{mix} = \Sigma\, c_i\, s_i, \quad t_{mix} = \Sigma\, c_i\, t_i \qquad (2)$$

where s_i and t_i are scattering activity and transmitting activity of a unit cell of mineral component i, respectively, and c_i is volume fraction of mineral component i. Reflectance and transmittance of a single layer for the mixture are given by substituting Eq.(2) in Eq.(1).

Reflectance R_N and transmittance T_N of the multilayer which consists of N layers are

$$R_N = (A^N)_{21} / (A^N)_{11}, \quad T_N = 1 / (A^N)_{11}, \quad A = \frac{1}{T}\begin{pmatrix} 1 & -R \\ R & T^2-R^2 \end{pmatrix} \tag{3}$$

where R and T are reflectance and transmittance of a single layer. If we let N approach to infinity, reflectance R_∞ is given by

$$R_\infty = 2R / \left(1+R^2-T^2+\sqrt{(1+R^2-T^2)^2-4R^2}\right) \tag{4}$$

Measurements were made with a Beckman UV 5240 spectrophotometer with an integrating sphere. Halon was used as a standard. Olivine and pyroxene were separated from Nuervo Mercurio by using a isodynamic magnetic separator and Clerici's solution. Separation was not perfect, each sample contained small amount of the other sample. Chemical analyses of the samples with a JEOL JXA-733 electron microprobe showed that about 20 percents of the grains in the olivine sample were pyroxene grains, and that about 10 percents of the grains in the pyroxene sample were olivine grains. We obtained reflectance and transmittance for a single layer(45μm in thickness) for each sample by using Eqs (3) and (4), on the basis of the reflectance and transmittance data for the sample, and determined scattering activity and transmitting activity for the unit cell for the sample by solving Eq.(1) for s and t. We substituted these scattering activities and transmitting activities for the unit cells for olivine and pyroxene in Eq.(2), and then computed spectral reflectances for olivine-pyroxene mixtures from Nuervo Mercurio by Eq.(4). Spectral reflectances for olivine-pyroxene mixtures from Hawaii(37-74μm in size) were calculated in the same manner as Nuervo Mercurio, where the thickness of a single layer for Hawaii samples was 55μm. Table 1 compares the calculated spectral reflectances for mixtures with the measured ones. Reflectances and wavelength positions of absorption bands agree well with those obtained by measurements.

We have obtained scattering activities and transmitting activities for Nuervo Mercurio samples which contain impurities. The effects of the impurities were reduced by means of the constructed scattering activities and transmitting activities for pure olivine and pure pyroxene by using Eq.(2) on the basis of the estimation of the amounts of the impurities. Fig.2 shows the calculated spectral reflectances for pure olivine and pure pyroxene from Nuervo Mercurio. Fig.3 compares wavelength positions of an absorption band around 1μm for olivine-pyroxene mixtures from Nuervo Mercurio with those from ALH-769 ordinary chondrite(L6) reported by Miyamoto et al.[2]. We have showed that spectral reflectances of mineral mixtures can be determined from spectral reflectances and spectral transmittances of mineral components.

References

[1]Kinoshita, M., Miyamoto, M., and Takano, Y.(1984) Lunar & Planet. Sci. Conf. 16th, [2]Miyamoto, M., Kinoshita, M., and Takano, Y.(1983) Mem. Natl. Inst. Polar Res., Spec. Issue, 25, p.367. [3]Wendlandt, W. WM. and Hecht, H. G.(1966) Reflectance spectroscopy, p.79, International Publishers, New York.

Table 1. Wavelength positions of band minimun around 1μm of olivine-pyroxene mixtures.
(1) From nuervo Mercurio, (2) From Hawaii

(1)	Pyroxene Content		0%	25%	50%	75%	100%
	Wavelength	Calc.	-	944	929	921	-
	Position (nm)	Obs.	1019	942	928	922	919
	$\sigma^* \times 10^3$		-	2.2	0.9	0.9	-
(2)	Pyroxene Content		0%	20%	50%	80%	100%
	Wavelength	Calc.	-	1051	1041	1028	-
	Position (nm)	Obs.	1057	1048	1041	1029	1019
	$\sigma^* \times 10^3$		-	3.1	3.1	3.8	-

* $\sigma = \left(\Sigma \left(R_{calc,i} - R_{obs,i}\right)^2 / N \right)^{1/2}$

$R_{calc,i}$: calculated reflectance at wavelength i. $R_{obs,i}$: observed

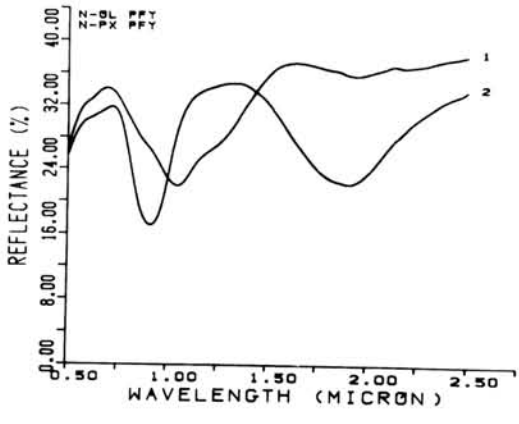

Fig. 2 Calculated spectral reflectances for pure olivine and pyroxene from Nuervo Mercurio.
1: olivine 2: pyroxene

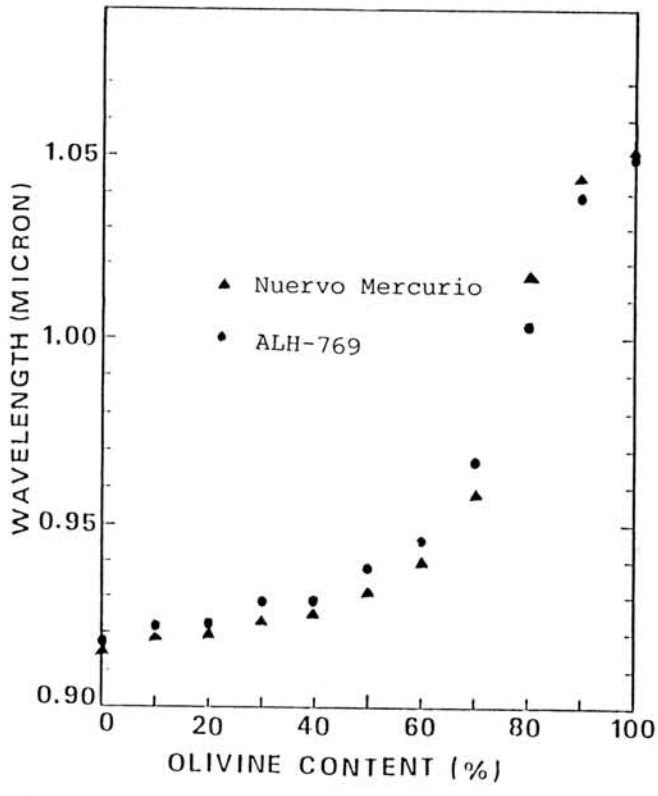

Fig. 3 Variation of wavelength positions of absorption band near 1μm shown in reflectance curves for olivine-pyroxene mixtures from Nuervo Mercurio(calculated) and ALH-769.

Special Session on Meteorites from Moon

Tuesday, March 26, 1985

1300 - 1720

Lunar meteorites; recovery, curation and distribution

Keizo Yanai and Kojima Hideyasu
National Institute of Polar Research, 9-10, Kaga 1-chome, Itabashi, Tokyo 173

Two lunar meteorites have been collected on the bare ice area near the Yamato Mountains, Antarctica. One is Yamato-791197, 52.40 grams, collected in November 1979 and the other is Yamato-82192, 36.67 grams, collected in January 1983. These meteorites were identified and classified as an anorthositic regolith breccia that originated on the lunar surface (Yanai and Kojima 1984, Yanai et al., 1984).

Yamato-791197 anorthositic regolith breccia: Yamato-791197 has been classified as an anorthositic regolith breccia. This specimen is an almost complete rounded stone, covered with a thick dusty-gray fusion crust. The interior consists mainly of angular clasts, dark gray to white in color, set in a black to dark brown glassy matrix(see figure). The meteorite was photographed at six directions. It measured 4.5 x 4.2 x 2.8 centimeters. The original volume of the meteorite was 18.45 cubic centimeters and specific gravity is 2.84 (g/cm). Most of clasts are smaller than 1mm across, but some clasts up to 4mm across were observed.

Petrographically Yamato-791197 is a polymict microbreccia containing clasts in a dark brown glassy matrix(see figure). Various types of clasts were observed in thin section, polyminerallic, monominerallic and melt clasts. Most larger clasts are polyminerallic, most frequently composed of calcic plagioclase, olivine, and pyroxene; less commonly plagioclase and pyroxene, and plagioclase alone. The smaller clasts are individual mineral fragments dominantly of plagioclase and with some pyroxene, and olivine and melted lithic fragments. The clasts also show a variety of textures(see figure), including troctolitic, gabbroic, diabasic, basaltic and shock-melted glassy clasts. Some of the clasts are similar to those of eucrites and howardites, but most clasts are more feldspathic.

Yamato-791197 appears to be a regolith breccia with glass spherules and an abundance of clasts, especially feldspathic clasts, set in a dark brown glassy matrix. From its texture, Y-791197 resembles the lunar regolith breccia of 64505 and 65787 (J. TAYLOR, personal communication). Swirly brown glass has not been in the Y-791197 meteorite.

Feldspar compositions range An92.0 to An98.2 with most analyses ranging from An95.5 to An97.5. Pyroxenes and olivines are also variable in composition. The compositional range in pyroxenes is En18.0-83.1 Fs9.0-58.9 Wo 1.7-44.1. Most olivines are Fo55-80, but several grains with Fo92.1 and Fo 13.3 have been found.

Yamato-82192 anorthositic regolith breccia: The third lunar meteorite, Yamato-82192 has been identified as an anorthositic regolith breccia by the present authors. Yamato-82192 was collected on the southern bare ice of the Minami-Yamato Nunataks, Antarctica by Mr. Takayoshi Katsushima, University of Hokkaido, geologist of the Japanese Antarctic Research Expedition Team in 1982-1983 field season. This specimen is nearly half of a stone, 36.67 grams, partly crusted, but it has some smmoth surface which is coated with yellowish-tan color. Fresh surfaces and the interior show grey to light grey color. This specimen consists of abundant clasts which range from millimeter to one centimeter across black and white in color in a light grey matrix. This meteorite measured 4.3 x 3.3 x2.3 cm. The original volume of of the meteorite was 12.87 cubic cm and the specific gravity is 2.85 (g/cm).

The thin section of the specimen shows numerous clasts of melted lithic fragments, crystalline fragments and brecciated lithic fragments in matrix. There are two types of clasts, polyminerallic and monominerallic in the section. The smaller clasts are individual mineral fragments mainly plagioclase, with some pyroxene and minor olivine. Most melted fragments showing brown color are divitrified and contain fine plagioclase and minor pyroxene. Rarely the specimen contains small glass spherules. The clasts of the crystalline rock fragments show a variety of textures including basltic and granulitic, and most of them have been shocked. The matrix of the specimen consists of two parts, a brown colored area and a light area which shows a divitrified and recrystallized texture. Feldspar ranges from An83.0 to 98.2 with most analyses between An93 and An98, with 1.3% (maximum) of Or component; pyroxene and olivine is variable in composition, pyroxene: Wo1.8-43.2, En13.8-79.4, Fs8.1-57.6 and olivine, Fo6.8-89.1. MnO content of both the pyroxene and olivine are lower than their equivalents in achondrites, but they are very similar to those of some lunar rocks, especially anorthositic regolith breccia.

This specimen shows a brecciated texture of numerous lithic fragments, which is a common occurrence in most polymict eucrites and howardites. It is however quite distenct from these meteorites.

Yamato-791197 is the subject of a consortium study, see following abstracts. Specimens have been provided to twenty research groups(see table). The distributed material was mainly from Yamato-791197,21, 8.858 grams and supplied as fragments or polished thin sections.

References:

Yanai, K. and Kojima, H.(1984), Proc. 9th Symp. Antarctic Meteorites, 18-34
Yanai, K., Kojima, H. and Katsushima, T.(1984), Meteoritics 19.

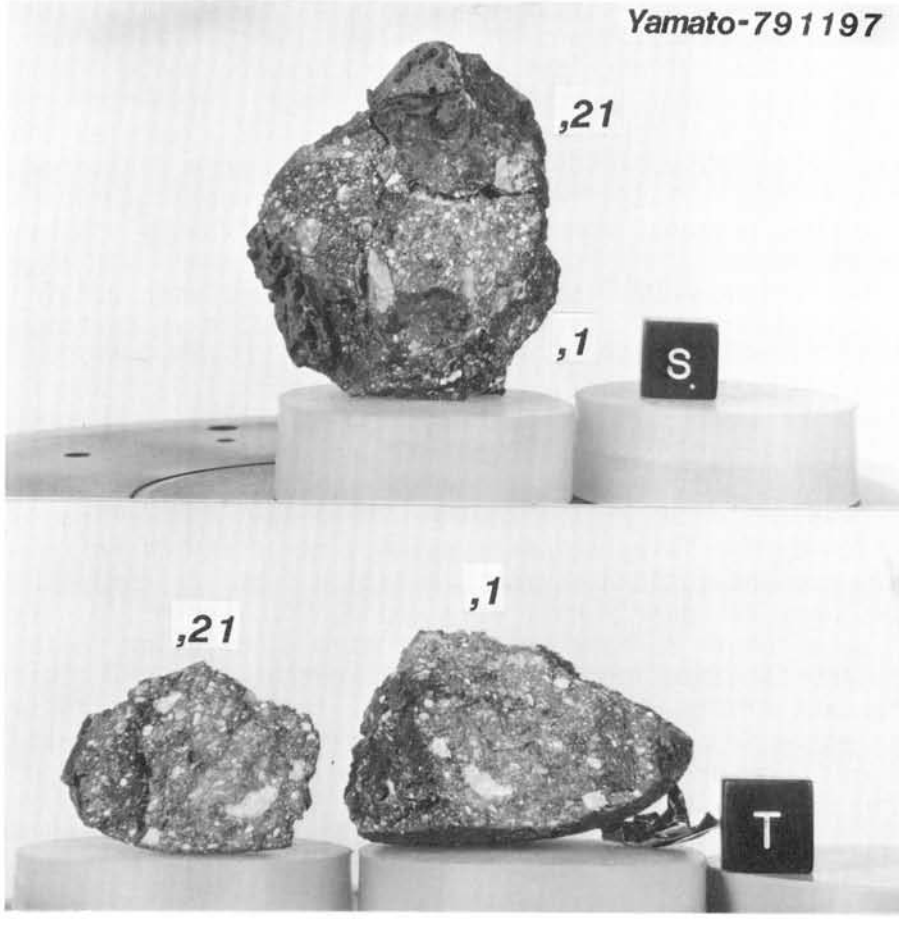

Figure

Table. Sample distribution of the Yamato-791197: Anorthositic regolith breccia

No.	Name	Sub.No.	sample(s)(type)	memo
1.	Yanai K.	0	52.40 g (whole rock)	Processing and preliminary studies
2.	Yanai K.	0	52.40 g (whole rock)	Physical description
3.	Kushiro I.	94	0.840 g (whole rock)	Bulk composition
4.	Lipschutz M.	88	0.112 g (whole rock)	Trace elements
5.	Takeda H.	120-1	P.T.S. (whole rock)	Mineralogy
6.	Clayton R.	150	0.026 g (whole rock)	Oxygen-isotope
7.	Warren P.	76	0.195 g (whole rock)	Petrology, chemistry and INAA
		100	0.047 g (clast)	
		103	0.047 g (clast)	
8.	Fukuoka T.	107	0.026 g (whole rock)	Chemistry and INAA
		148	0.042 g (whole rock)	
		99	0.010 g (clast)	
9.	Nishiizumi K.	75	0.350 g (whole rock)	Cosmic-ray and terrestrial age
10.	Masuda A.	108	0.031 g (whole rock)	REE
		109	0.060 g (clast)	
		115	0.045 g (clast)	
11.	Takaoka N.	105	0.150 g (whole rock)	Rare gases
		95	0.140 g (clast)	
12.	Tatsumoto M.	74	0.471 g (matrix)	Rb-Sr, Sm-Nd and REE
		84	0.030 g (clast)	
13.	Kaneoka I.	96	0.112 g (clast)	Ar-Ar age
		97	0.099 g (matrix)	
14.	McFadden L.	72	0.624 g (whole rock)	Reflectance spectra
		90	0.101 g (whole rock)	
15.	Haskin L.	89	0.120 g (matrix)	INAA, major & trace element and track & thermoluminescence
16.	Ikeda Y.	73-1	P.T.S. (whole rock)	Petrology
17.	Nagata T.	78	0.342 g (whole rock)	Magnetic
18.	Stoffler D.	73-2	P.T.S. (whole rock)	Petrolgy, bulk composition, and rare gasses
		87	0.202 g (whole rock)	
19.	Herzog G.	77	0.148 g (whole rock)	Terrestrial age
20.	Keil K.	73-3	P.T.S. (whole rock)	Petrology and chemistry

GEOCHEMISTRY OF LUNAR METEORITES YAMATO-791197 AND ALHA81005

Paul H. Warren and Gregory W. Kallemeyn

Institute of Geophysics and Planetary Physics
University of California, Los Angeles, CA 90024, USA

Yanai and Kojima [1] have described the petrography of Yamato-791197. These authors concluded from the high FeO/MnO ratios of its mafic silicates as well as its texture and anorthositic bulk composition that the parent body of Y-791197 was probably the Earth's Moon. Our instrumental neutron activation analysis supports this conclusion. In fact, this meteorite is so similar to lunar meteorite ALHA81005 [2], it seems possible that both meteorites were brought to Earth by a single impact onto the Moon's surface.

Our data for 33 elements in bulk-rock sample Y791197,76, and for a small white clast separated from the matrix, are shown in the Table. Some of these data are preliminary, as we have not quite completed gamma-ray counting of our samples. Parentheses around a datum indicate a relatively high (up to 35%) uncertainty. For comparison, the Table also shows averaged literature data for compositions of anorthositic (nonmare) lunar soils and lunar meteorite ALHA81005. Petrographic observations [1] (the texture of the matrix, especially the presence of a glass spherule) indicate that like ALHA81005, Y791197 is a regolith breccia, i.e., a breccia formed by consolidation of former lunar soil. Our analysis [3] of ALHA81005 was essentially identical to the weighted mean of the analyses from six different neutron activation laboratories [2], shown in the Table. The Luna 20 and Apollo 16 sites are generally considered to be our only sources of representative samples of lunar highlands soil. The Apollo 14 highlands region, with its extraordinary abundances of incompatible elements such as Th and K [4], certainly does not have a typical lunar highlands composition. But 73141, the most Al-rich soil from Apollo 17 [5], appears to be nearly free of mare material, and may be representative of an appreciable fraction of the central near side highlands.

The whole-rock Fe/Mn ratio (67.3, Table) is uncommonly low for a lunar regolith sample. As noted by Laul and Schmitt [6], Fe/Mn is nearly constant at 80 (± about 5) among all Apollo and Luna soils. The Fe/Mn ratio of the mean ALHA81005 data (73.6, Table) is slightly lower than usual for lunar regolith samples, but considerably higher than that of Y791197. The exact significance of these disparities is unclear, but we have no reason to suspect the accuracy of our new data. The lower Fe/Mn ratio for Y791197 vs. ALHA81005 might be an indication that these meteorites did not come from a single impact onto the Moon, their remarkable similarity in other respects notwithstanding. In any case, the Fe/Mn ratio of Y791197 is much closer to the mean lunar crustal Fe/Mn ratio than to the Fe/Mn ratios for plagioclase-rich meteorites from parent bodies other than the Moon: eucrites, howardites, and "SNC" achondrites, all have Fe/Mn ratios close to 40 [3].

Despite a limited amount of horizontal mixing by great impacts, the ancient, nonmare lunar crust manifests considerable lateral heterogeneity [4, 7]. As discussed in connection with ALHA81005 [2; especially 3], the Apollo and Luna missions only sampled a tiny region near the center of the Moon's near side. A polyhedron could be drawn around the sampled sites covering just 4.7% of the lunar surface. Although the exact sources of lunar meteorites can seldom or never be unambiguously determined, the vast majority are presumably not from the central near side region sampled by the Apollo and Luna programs. Lunar meteorites are therefore extremely valuable sources of information about lateral variations in the composition and petrology of the Moon's crust.

Incompatible element concentrations (Fig. 1; shown normalized to the KREEP component [8]) are remarkably similar to those of ALHA81005, and far lower than those of other lunar regolith samples. The crust in the region(s) that spawned Y791197 (and ALHA81005) was apparently close to, if not entirely, devoid of KREEP, a trait consistent with orbital spectrometry data [4] that indicate that abundant KREEP is found almost exclusively in the region of the central near side. Nonetheless, the pattern of incompatible element ratios is typically lunar. The similarity between Y791197 and ALHA81005 is further illustrated by a plot of the "plagiophile" ratios Eu/Al vs. Ba/Sr (Fig. 2).

Possibly significant differences between our analysis of Y791197 and the mean data for ALHA81005 do exist, however. The Fe/Mn ratios have already been discussed. Scandium, V and Zn all are considerably higher in Y791197. Aluminum is slightly higher in Y791197. The average plagioclase (i.e., Al) content of the ancient nonmare crust is the single most important constraint affecting the crucial issue of whether or not a magma "ocean" (or magmasphere)

	Y-791197 whole-rock 197 mg	ALHA81005 wtd. mean, ref. [2]	L20 soil ref. [3]	A16 avg. soil ref. [3]	A17 Al-rich soil 73141	Y-791197 Clast W 7.3 mg
Na mg/g	2.34	2.24	2.45	3.50	3.12	2.56
Mg mg/g	39	49.4	58	35	58.8	(49)
Al mg/g	142	136	121	143	113	151
K mg/g	0.232	0.194	0.59	0.92	1.17	0.14
Ca mg/g	108	107	103	112	92.9	120
Ti mg/g	(1.6)	1.57	2.8	3.4	7.3	-
Fe mg/g	44.4	42.7	60.0	41.0	62.3	49.4
Sc μg/g	12.5	9.1	16.4	9.3	16.2	13.0
V μg/g	29	24.6	27	20	37	(21)
Cr μg/g	890	890	1500	720	1480	840
Mn μg/g	660	580	800	530	840	770
Co μg/g	18.4	21.0	20.0	27.0	27.2	15.4
Ni μg/g	152	198	260	377	239	(83)
Zn μg/g	22	8.7	21	18	16	-
Ga μg/g	3.2	2.7	3.2	5.4	2.6	2.7
Sr μg/g	140	135	144	163	137	(205)
Zr μg/g	(26)	26.8	120	167	219	-
Ba μg/g	29	28.4	94	127	154	(53)
La μg/g	2.16	1.98	6.3	12.0	15.5	1.27
Ce μg/g	5.2	5.2	18.0	31.0	37.8	(3.6)
Nd μg/g	3.0	3.2	10.8	19.0	24.9	-
Sm μg/g	0.99	0.95	3.1	5.7	7.0	0.74
Eu μg/g	0.72	0.69	0.94	1.20	1.20	0.80
Tb μg/g	0.223	0.214	0.65	1.13	1.5	0.21
Dy μg/g	1.42	1.33	4.1	7.4	9.3	(1.7)
Ho μg/g	0.28	0.31	-	-	2.4	-
Yb μg/g	0.96	0.84	2.4	4.0	5.4	0.82
Lu μg/g	0.136	0.124	0.39	0.59	0.80	0.126
Hf μg/g	0.73	0.73	2.4	4.1	5.2	0.58
Ta μg/g	0.077	0.093	0.30	0.51	0.75	-
Ir ng/g	6.4	6.8	9.5	11.1	12	<8
Th ng/g	0.28	0.29	1.10	1.90	2.4	(0.18)
U ng/g	(0.079)	0.098	0.33	0.56	0.70	-

must be invoked to account for lunar crustal genesis. A magmasphere is probably the only plausible means of producing a crust with an average plagioclase content much greater than that of a basaltic partial melt (i.e., much greater than about 55 wt%). The CIPW norm of our Y791197 analysis has (assuming SiO_2 = 45 wt%) 74.5 wt% plagioclase. Thus, the high Al content of Y791197 strengthens the case for a primordial lunar magmasphere; especially if Y791197 and ALHA81005 are from separate lunar locations.

Another possibly significant difference between Y791197 and ALHA81005 is that the former appears to have a lower Mg/Fe ratio. Our Y791197 Mg datum has a relatively high uncertainty (nominally 10%); we hope to acquire a more precise Mg datum through further analysis. Yanai and Kojima [1] report an even lower Mg/Fe ratio. The Mg/Fe ratio of the mean ALHA81005 data (Table) is considerably higher than those of any other lunar regolith sample. Apparently in this respect Y791197 more closely resembles the central near side Apollo and Luna samples than ALHA81005 does. Nevertheless, the overall composition, especially the incompatible element contents, indicate that Y791197 originated far from the region of the Apollo and Luna samples, most likely on the Moon's far side, and very possibly via the same impact that spawned ALHA81005.

REFERENCES [1] Yanai K. and Kojima H. Mem. Natl. Inst. Polar Res., in press. [2] Bogard, D. et al. (1983) Geophys. Res. Lett. 10, No. 9 (special ALHA81005 issue). [3] Kallemeyn G. W. and Warren P. H. (1983) Geophys. Res. Lett. 10, 833-836. [4] Adler I. and Trombka J. I. (1977) Phys. Chem. Earth 10, 17-43. [5] Numerous authors (1974), all in Proc. Lunar Sci. Conf. 5. [6] Laul J. C. and Schmitt R. A. (1973) Proc. Lunar Sci. Conf. 4, 1349-1367. [7] Warren P. H. and Taylor G. J. (1981) in Multi-ring Basins (P. H. Schultz and R. B. Merrill, eds.), Houston: Lunar Planet. Inst., pp. 149-154. [8] Warren P. H. and Wasson J. T. (1979) Rev. Geophys. Space Phys. 17, 73-88.

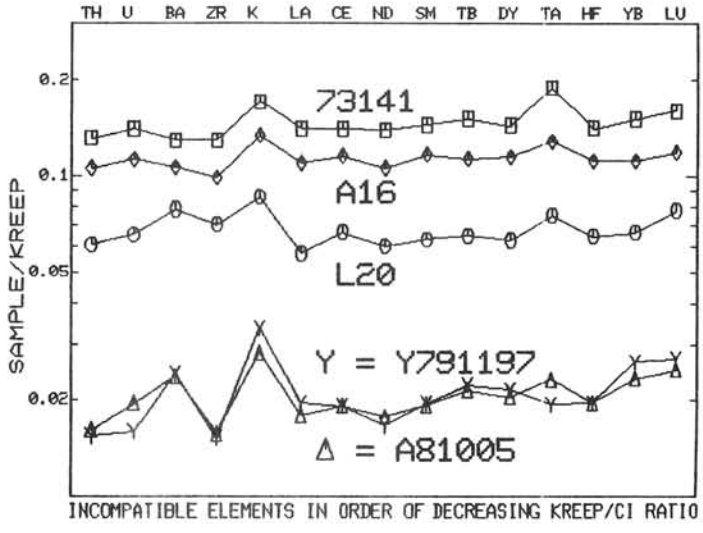

Figure 1

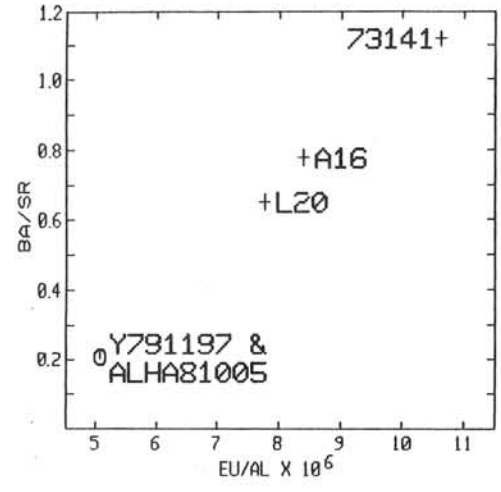

Figure 2

CHEMISTRY OF YAMATO-791197 METEORITE: EVIDENCE FOR LUNAR HIGHLAND ORIGIN

Fukuoka, T.[1], Laul, J. C.[2], Smith, M. R.[2], Hughes, S. S.[3] and Schmitt, R. A.[3]

1 Dept. of Chemistry, Gakushuin University, Toshima, Tokyo 171
2 Radiological Sciences Dept., Battelle, Pacific Northwest Laboratories, Richland, WA 99352
3 Dept. of Chemistry, Radiation Center, Oregon State University Corvallis, OR 97331

We analized more than 30 major, minor and trace elements in one white clast, two matrices and two bulk samples from Yamato 791197 meteorite by instrumental neutron activation analysis (INAA). Two whole rock samples (Sub. Nos. 107 and 148) and one white clast with dark matrix sample (Sub. No. 99) were provided from National Institute of Polar Research of Japan. We separated two matrix chips and one bulk samples from the Sub. No. 107 whole rock sample for the analysis. The white clast sample was purified with the exclusion of matrix prior to INAA.

The major chemical and siderophile elements abundances are shown in Table 1 with those of ALH81005 meteorite (1) for comparison. Fig. 1 shows the chondritic normalized abundance patterns of lithophile minor and trace elements with those of ALH 81005 (1). The bulk and matrices are the same in chemical composition and are anorthositic gabbro in nature. The chemical composition of the Y791197 matches closely with the ALH 81005 (Table 1 and Fig.1). The chemical composition of the ALH81005 was close to the Apollo 15 15418 and Luna 16 21013 highland rocks (1). Therefore it suggest strongly that the Y791197 is of highland origin.

The chondritic normalized REE patterns (Fig. 1) of the bulk and matrices are typical of lunar anorthositic gabbros with a positive Eu anomaly at 10 X (chondrite). The white clast is about 2 times higher in REE relative to the matrix and bulk without Eu anomaly.

The high content of siderophiles, Ni, Ir and Au in the most of matrix and bulk of Y791197 is similar to the siderophiles content in ALH81005 and other lunar highland breccias,while they are much higher in clast of Y791197, which strongly suggests that this rock was also subjected to a meteoritic impact on the moon.

Based on the well-established characteristic lunar and meteoritic ratios of FeO/MnO, Cr_2O_3/V and K/La, and REE patterns, Y791197 meteorite is undoubtedly of lunar highland origin like ALH81005 meteorite. Our conclusion is confirmed by trace element chemistry (2) and mineralogical (3) studies.

References:
(1) Laul, J. C., M. R. Smith and R. A. Schmitt (1983) Geophys. Res. Lett. 10, 825-828.
(2) Kaczaral, P. W., J. E. Dennison and M. E. Lipschutz (1985) this volume.
(3) Yanai, K. and H. Kojima (1984) Meteoritics (in press).

Table 1. Major chemical and siderophile elements abundances by INAA

		YAMATO 791197					ALH 81005 [1]		
		Clast	Matrix	Matrix	Bulk	Bulk	Clast	Matrix	Bulk
Wt	mg	5.39	5.65	6.57	21.4	23.2	9.3	23.0	20.5
TiO_2	%	0.15	0.36	0.35	0.30	0.32	0.30	0.30	0.30
Al_2O_3	%	24.7	28.9	27.8	27.7	26.0	25.9	25.6	26.3
FeO	%	6.91	6.60	6.55	6.70	6.84	5.90	5.60	5.60
MgO	%	8.0	5.1	4.5	5.8	5.0	9.0	8.0	8.0
CaO	%	16.1	15.0	14.5	15.3	15.5	16.7	15.2	15.2
Na_2O	%	0.30	0.35	0.36	0.34	0.32	0.31	0.31	0.31
K_2O	%	0.038	0.032	0.035	0.028	0.026	0.020	0.025	0.025
MnO	%	0.111	0.083	0.083	0.087	0.084	0.074	0.070	0.069
Cr_2O_3	%	0.20	0.12	0.12	0.12	0.11	0.12	0.12	0.12
Co	ppm	28.1	19.0	20.5	19.8	(174)	19.0	20.0	20.0
Ni	ppm	390	170	210	170	(1780)	160	190	190
Ir	ppb	13.8	6.0	8.0	6.0	4.5	6.0	6.2	6.1
Au	ppb	6.4	2.3	2.5	2.5	36.5	1.4	2.4	2.4

Values in parenthesis are suspect of contamination.
1) Laul et al. (1983).

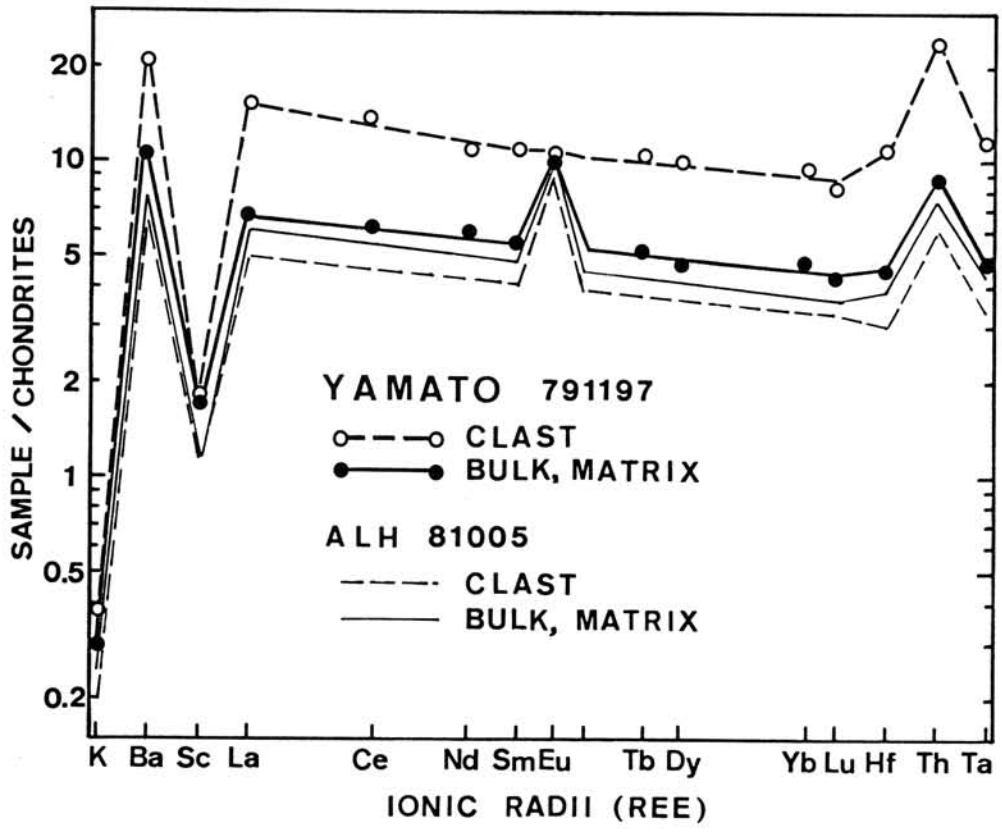

Fig.1. Chondritic normalized abundance patterns of lithophile minor and trace elements in bulk, matrix and clast of Y791197 and ALH81005.

LUNAR METEORITE Y-791197: A LUNAR HIGHLAND REGOLITH BRECCIA

Ostertag, R., Bischoff, A., *Palme, H., *Spettel, B., Stöffler, D., *Weckwerth, G., and *Wänke, H.
Institut für Mineralogie, Corrensstr. 24, D-4400 Münster; * MPI Chemie, Saarstr. 23, D-6500 Mainz, FRG

Yamato 791197 can be classified as a shocked regolith breccia from the lunar highlands. It is a polymict breccia containing a great variety of mineral and lithic clasts predominantly derived from feldspathic lithologies. The matrix of Yamato 791197 consists of densely compacted clasts with minor amounts of intergranular melt (brownish in thin section) which occasionally contains vesicles and appears to be an extremely fine-grained polycrystalline material. The amount of intergranular melt is somewhat variable. Melt-poor matrix continuously or discontinuously changes into very melt-rich matrix. Melt-rich matrix areas with distinct boundaries are interpreted as inclusions of older regolith breccias.

In thin section 791197,73-2 the meteorite is partially covered by a light yellow, highly vesiculated melt crust which displays a variolitic to subophitic crystallization texture with very elongated plagioclase laths and interstitial pyroxene. Beneath this crust the meteorite matrix is "annealed" and contains a large number of small vesicles. A second type of melt crust which is brown and still glassy occurs in a very limited region of the meteorite's rim.

Clast population studies: Thin section Y-791197,73-2 contains about 32 vol. mineral and lithic clasts larger than 0.1 mm. A total of 195 lithic clasts in the size range 0.1 to 2.0 mm were mapped and classified according to (1). Granulitic and recrystallized rocks and breccias and the dominant lithologies (56 vol.% of all clasts). Crystalline melt breccias and devitrified impact glasses amount to 25 and 6 vol.%, respectively, polymict fragmental breccias amount to 12 vol.%. Unrecrystallized glasses are rare (< 1 vol.%). Among the crystalline melt breccias three varieties dominate: (1) a light brown, fragment-laden, mafic-poor feldspathic melt breccia with a microporphyritic matrix, (2) a dark brown fragment-laden melt breccia with a very fine-grained matrix , and (3) subophitic crystalline melt breccias. Agglutinates, KREEP-bearing lithologies and eutectically crystallizing rocks (norites, troctolites) are lacking. The clast population of Y-791197 is similar to that of lunar meteorite ALHA 81005 except for the glass and agglutinate content which is higher in ALHA 81005. Petrographically, ALHA 81005 is a more mature regolith breccia than Y-791197.

Shock effects in Yamato 791197 related to the breccia-forming and any later shock event are moderate. Plagioclase and pyroxene show mosaic and undulous extinction throughout the breccia but severe shock-induced metamorphism such as deformation lamellae or diaplectic glass is absent. The breccias consolidated from loose regolith by moderate shock pressure which may have been in the order of 10 to 20 GPa, according to data of (2) and (3). The existence of highly feldspathic glass indicates that the breccia was never heated to very high temperature (at least not above 800 C, probably much less). The shock pressure during the event which caused the ejection of Y-791197 from the lunar surface did not exceed 25 GPa.

Chemical composition: Preliminary chemical data on a 59.3 mg piece of Yamato 791197 are listed in Table 1. A comparison with the ALHA 81005 lunar meteorite shows a striking similarity in composition. The P content in both lunar meteorites is low, and the P/Nd ratio in the two lunar meteorites immediately distinguishes them from any other meteoritic or terrestrial material (see Fig. 1 (4)). The pattern of incompatible elements (K, REE, etc.) is by about a factor of 1.3 higher in the Yamato meteorite, compared to ALHA 81005 (see Table). Within the error limits this factor is the same for all incompatible elements. We have argued that this pattern of incompatible elements is typical for the old lunar crust and may still be found in samples from the back side of the Moon. We therefore suggest that the Yamato meteorite also is an old crustal lunar rock.

The lack of a KREEP component in the pattern of incompatible elements supports a far side origin for Yamato 791197 similar to ALHA 81005. Siderophile trace elements (Ni, Co, Ir, and Au) point towards the same old meteoritic component as the ALHA data, a pattern perhaps diagnostic for the far side. In addition the Yamato data for Ni and Co lie on the same correlation line as those for ALHA 81005 and several granulitic impact breccias (4).

Differences in chemistry between Yamato 791197 and ALHA 81005 include a higher Sc content for the Yamato meteorite. The meteorite would therefore plot slightly off the highland correlation line of Fe vs. Sc (5). An even more pronounced difference is found for Ga. Yamato 791197 has the highest Ga content even found by us in a lunar sample (except metals). The reason for this enrichment is not clear. Parallel enrichment of Zn may point to volatility as a possible reason. However, since anorthite is the host phase of Ga in lunar highland rocks, we should expect a similar enrichment in Na, which is obviously not present. The ratios among Ca, Sr, and Eu are nearly chondritic, indicating the primitive composition of the plagioclase component (6). The chemical composition of ALHA 91005 did marginally fit into the multi-element highland mixing diagram (7). The deviation for Sc, Fe, Cr, and Ca of the Yamato 791197 meteorite from the ALHA 81005 composition are sufficient to make the Yamato composition completely incompatible with compositions covered by the mixing diagram. Since most of the Apollo highland breccias fit into this mixing diagram this observation may indicate that not only trace elements such as LIL-elements or siderophile elements are different on front and far side of the Moon, but that these differences may also extend to major elements.

Conclusions: Yamato 791197 was formed by shock lithification of lunar highland regolith which is less mature than the regolith from which ALHA 81005 is derived as indicated by the differences in the glass content. Lithologically both meteorites are similar. From the predominance of anorthosites and granulitic lithologies and from the chemical data (e.g. lack of KREEP) we conclude that Yamato 791197 originates from a highland site which differs dinstinctly from the Apollo highland landing sites. Consequently, a highland site such as that proposed for ALHA 81005 (8) is a viable candidate also for Yamato 791197. This meteorite therefore may provide additional evidence for the chemical composition of the lunar highlands away from the Apollo landing sites, in particular the large, so far unsampled, area of the far side of the Moon.

References: (1) Stöffler, D. et al., (1980) Proc. Conf. Lunar Highlands Crust, p. 51-70. (2) Kieffer, S.W., (1975) The Moon, 13, p. 301-320. (3) Schaal, R.B. and Hörz, F., (1980) Proc. Lunar Planet. Sci. Conf. 8th, p. 1679-1695. (4) Palme, H. et al., (1983) Geophys. Res. Lett. 10, p. 817-820. (5) Wänke, H. et al., (1975) Proc. Lunar Planet. Sci. Conf. 6th, p. 1313- 1340. (6) Palme, H. et al., (1984) Proc. Lunar Planet. Sci. Conf. 16th, submitted. (7) Wänke, H. et al., (1977) Proc. Lunar Planet. Sci. Conf. 8th, p. 2191-2213. (8) Ryder, G. and Ostertag, R., (1983) Geophys. Res. Lett. 10, p. 791-794.

Table 1: Preliminary data of major, minor, and trace elements in Yamato 791197 (59.3 mg, bulk sample) in comparison to ALHA 81005 (128 mg, bulk sample).

%	ALHA 81005	Y-791197	standard dev.	Y-791197/ ALHA 81005
Mg	4.78		5	
Al	13.4		3	
Si	21.72		3	
Ca	10.80	11.43	3	1.06
Ti	0.14		10	
Fe	4.20	5.06	3	1.20
ppm				
Na	2250	2408	3	1.07
P	90	100	25	1.11
K	230	291	5	1.26
Sc	9.24	16.5	3	1.78
V	26		8	
Cr	862	1034	3	1.20
Mn	587	734	3	1.25
Co	20.2	17.0	3	0.84
Ni	186	110 *	5	0.59
Zn	18 *	65	10	3.6
Ga	2.8	9.8	5	3.5
Se	<0.6	<0.6		
Rb	<1.5	<2.5		
Sr	128	120 *	10	0.94
Zr	30	<43		
Ba	34	32	20	1.06
La	2.44	3.3	3	1.35
Ce	6.9	9.1	5	1.31
Pr		1.48	30	
Nd	3.9	5.2	10	1.33
Sm	1.18	1.56	3	1.32
Eu	0.704	0.723	3	1.03
Gd	1.4	1.4 *	20	1.0
Tb	0.27	0.32	5	1.18
Dy	1.7	2.2	10	1.29
Ho	0.37	0.48	15	1.29
Er		1.7	25	
Tm	0.18	0.27	20	1.5
Yb	1.06	1.33	5	1.25
Lu	0.15	0.19	3	1.27
Hf	0.92	1.1	3	1.20
Ta	0.12	0.16	8	1.33
Ir	0.0073	0.006	10	0.82
Au	0.0021	0.0021 *	7	1.00
Th	0.35	0.45	8	1.28
U	0.103	0.129	15	1.25

Data for ALHA 81005 from (4); * accuracy reduced by a factor of two.

MINERALOGY OF ANTARCTIC LUNAR METEORITES AND DIFFERENTIATED PRODUCTS OF THE LUNAR CRUST

Takeda, H., Tagai, T. and Mori, H.
Mineralogical Institute, Faculty of Science, University of Tokyo, Hongo, Tokyo 113

The closest analogs in the Apollo lunar samples of lunar meteorites (1)(2)(3) have been proposed to be regolith breccias (1). However, these lunar rocks have not been too well characterized mineralogically to compare them with the lunar meteorites, except for probably 60016 studied by Takeda et al. (4). The distribution of pyroxene compositions of 60016 in the pyroxene quadrilateral is similar to those of ALH81005 (5) and Y-791197 (2), and they include almost all pyroxene types known to the lunar highland rock types. Studies of lunar meteorites, therefore, provide us with information of various samples of the lunar highland rock types of a wider area of the moon, from where the meteorite was derived. We planned to investigate pyroxene-rich clasts as a part of the consortium study of Y-791197, but clasts are relatively poorer than those of ALH81005.

Y-791197,120-1 is a relatively thick PTS (polished thin section) prepared for studying a brown pyroxene-rich clast (HPF) found during the sample preparation for the consortium study. The PTS is 7 x 4 mm in size and the plane of the PTS cut nearly perpendicular to a disk-like clast, which gives 2.2 x 0.4 mm in size on the PTS. In this PTS there is another large clast rich in plagioclase (AN1), 2.7 x 1.5 mm in size. Other portion consists of fine-grained fragments of plagioclase, glass and minor mafic minerals, set in dark brown glassy matrix. Some plagioclase fragments are shock darkened, or partly melted showing a suevite-like texture.

The HPF clast consists of dark yellow, brown, to reddish brown iron-rich pyroxene, small amounts of plagioclase, fayalite, and dark mesostasis-like materials including fayalite, minor silica mineral and ilmenite (Table 1). The pyroxene is zoned from Ca-rich pigeonite (or pyroxferrorite?) to hedenbergite (Fig. 1). The zoning trend is mainly Fe-Ca substitution trend, and the end product is almost pure hedenbergite. The plagioclase is Na-rich, and the composition is relatively constant with An about 90. Because the clast is very thin, it is difficult to visualize texture, but it is relatively coarse-grained.

The AN1 clast is fine-grained. A few subround plagioclase up to 0.2 mm in diameter are set in a fine grayish matrix. Very fine-grained (up to 30 microns) olivine and pyroxene are rarely found in the matrix. The plagioclase compositions range in An from 95 to 97. The Fa contents of olivine range from 36 to 49. Other small lithic clasts found in Y-791197 are: noritic and troctolitic anorthosites and shocked anorthosites. One clast (SA) consists of rounded euhedral pleonaste spinel enclosed in anorthite (Fig. 2). This clast could be a fragment of spinel cataclasite, which have lead many workers to ponder upon the possibility of a lower crustal or upper mantle origin as studied by Herzberg (6). However, SA does not contain olivine, high alumina orthopyroxene and cordierite. It could be a spinel-anorthite rock.

The relation between the anorthite content of plagioclase and the Mg number = Mg/(Mg + Fe) in co-existing mafic minerals in Y-791197 are plotted in Fig. 3. This trend is intermediate to that of the Mg-rich suites of the lunar highland crust and that of ferroan anorthosite. Similar trends were

shown in the ALH81005 (1). The SA clast is on the most Mg-rich portion of the trend. The HPF clast may not be on the extension of either of the trends, but it is possible that the most Ab-rich end of the ferroan anorthosite trend could approach the HPF clast. If it is the case, the HPF clast may be the last differentiated product of the anorthositic crust. Only such hederberite is reported for 14321,993 by Warren et al. (7). The coarse-grained texture may support the proposed origin. However, the presence of the chemical zoning in the pyroxene in the forbidden zone of pyroxene and of the mesostasis-rich portion suggest that the clast may be differentiated product of a lunar highland volcanism. It may be unlikely that this clast is the differentiated portion of a mare basalt, because the Mg-rich portion is not represented in the matrix elsewhere.

The bulk glass compositions of the matrix and clast types suggest that ALH81005 and Y-791197 are very similar. Their bulk rock compositions are also similar to those of 60016 and 60019. The only difference may be that the lunar meteorites contain lithic clasts more rich in mafic minerals than 60016 and 60019, as represented in their bulk chemisty. 60019 contains more glassy matrix than 60016. Considering the difference between 60016 and 60019, we cannot deny a hypothesis that two lunar meteorites were derived by the same impact event.

We thank Dr. K. Yanai and Mr. H. Kojima for the sample preparation and thin-sectioning of this interesting HPF clast. A part of this study was supported by a Fund for Scientific Research from the Ministry of Education.

References: (1) Warren P. H., Taylor G. J. and Keil K. (1983) Geophys. Res. Lett. 10, 779-782. (2) Yanai K. and Kojima H. (1984) Abstr. 9th Symp. Antarctic Meteorites. NIPR, p. 42-43, Tokyo. (3) Yanai K., Kojima H., and Katsushima T. (1984) Abstr. 9th Annual Meeting. Meteoritical Soc., Albuquerque. (4) Takeda H., Miyamoto M. and Ishii T. (1979) Proc. Lunar Sci. Conf. 10th, p. 1095-1107. (5) Ryder G. and Ostertag R. (1983) Geophys. Res. Lett. 10, 791-794. (6) Herzberg C. T. (1978) Proc. Lunar Planet. Sci. Conf. 9th, p. 319-336. (7) Warren P. H., Taylor G. J., Keil K., Shirely D. N., Wasson J. T. (1983) Earth Planet. Sci. Lett. 64, 175-185.

Table 1. Chemical Compositions of Minerals in the HPF clast.

Mineral	Hedenberg.	Pigenite	Plagiocl.	Fayalite	Silica	Glass
SiO_2	47.1	46.8	48.3	29.9	99.9	45.3
TiO_2	1.53	0.48	0.03	0.10	0.37	0.22
Al_2O_3	1.43	0.62	30.3	0.03	0.44	25.2
FeO	30.8	39.5	2.11	67.2	0.59	6.46
MnO	0.36	0.53	0.04	0.77		0.09
MgO	0.93	4.49	0.05	0.95	0.01	5.86
CaO	18.12	6.11	17.72	0.73	0.14	15.15
Na_2O	0.02	0.01	1.04	0.03	0.05	0.32
K_2O	0.00		0.04		0.00	0.03
Cr_2O_3		0.16		0.03		0.14
Total	100.24	98.64	99.67	99.66	101.48	98.91

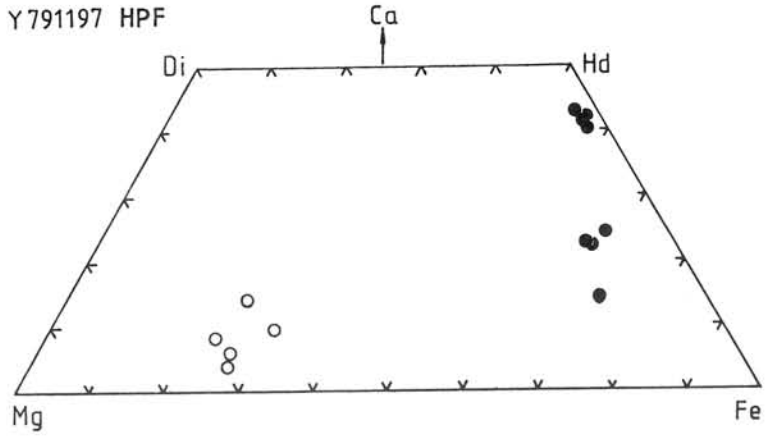

Fig. 1. Pyroxene quadrilateral of Y-791197. Solid circle: hedenbergite-plagioclase -fayalite (HPF) clast. Open circle: noritic and troctoritic clasts.

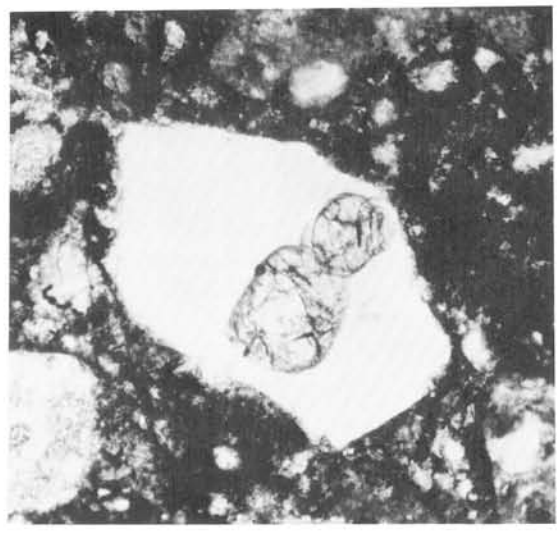

Fig. 2. Photomicrograph of SA clast in Y-791197. Unpolarized light. Width is 0.9 mm. PTS by courtesy of Y. Ikeda.

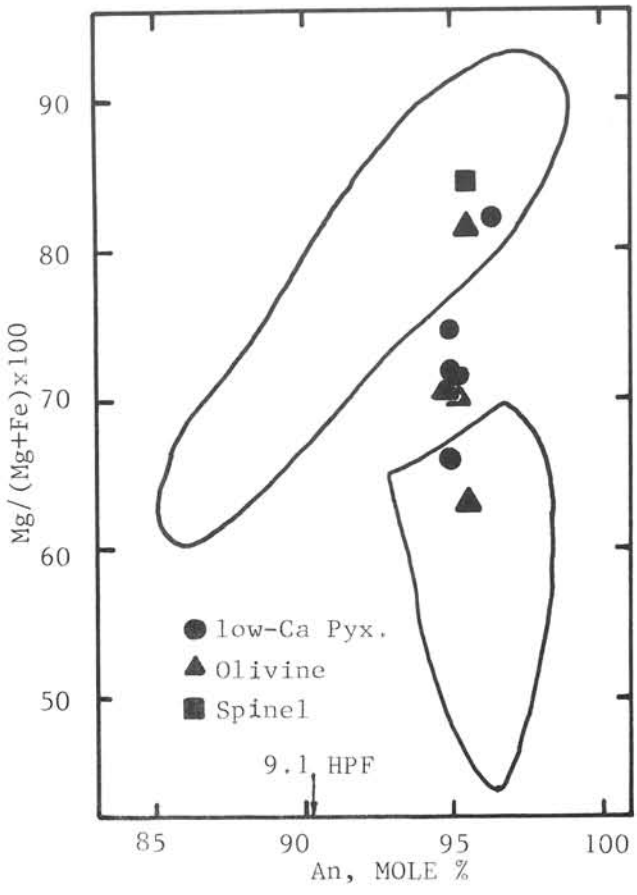

Fig. 3. The relation between the anorthite content (An) of plagioclase and the Mg number in coexisting mafic minerals in lunar meteorite, Y-791197 (solid circle for low-Ca pyroxene and solid triangle for olivine, and solid square for spinel in SA) and in lunar highland samples (curved lines). After R. S. Taylor (1981) Planetary Science: A Lunar Perspective, pp. 481, Lunar and Planet. Inst., Houston.

YAMATO 791197: A TRACE ELEMENT-RICH LUNAR HIGHLANDS SAMPLE

Patrick W. Kaczaral, Jane E. Dennison and Michael E. Lipschutz

Dept. of Chemistry, Purdue University, W. Lafayette, IN 47907 U.S.A.

We determined trace element contents of siderophilic Au, Co, Ga and Sb, volatile/mobile (mainly chalcophilic) Ag, Bi, Cd, In, Se, Te, Tl and Zn and lithophilic Cs, Rb and U by RNAA in two whole rock, interior samples of Y791197, an Antarctic lunar anorthositic breccia. These samples - designated ,88a and ,88b - were large and small chips (70.75 and 19.28 mg, respectively) received from NIPR.

The data are depicted in Fig. 1. Trace element contents differ widely in the two samples, 7 elements (Ag, Bi, Cd, Ga, Sb, Te and Zn) varying by about an order of magnitude. Except for highly mobile In and Tl ,88b is more enriched than ,88a. These differences greatly exceed those found in duplicate samples of Allan Hills 81005, the first Antarctic lunar meteorite identified (**1**), arguing for much greater compositional heterogeneity in Y791197. Lithophiles (Cs, Rb, U), most volatile/mobile elements (Ag, Bi, Cd, In, Te, Tl, Zn) and siderophilic Au are enriched in both portions of Y791197 relative to ALH A81005: ,88b is also enriched in Sb, Ga and Se (Fig. 1). Y791197,88 is among the most trace element-rich lunar material known: the unique Apollo sample 66095 ("Rusty Rock") compositionally seems to resemble it closely (**2-7**). As in ALH A81005, there is no evidence that mobile elements were lost from Y791197 during the impact that launched it earthward: In and Tl seem to have been mobilized while Y791197 was on the moon.

From our data, Y791197 and ALH A81005 did not come from the same lunar region, hence were launched from the moon in different impact events. Y791197 is a highlands sample which, like Apollo sample 66095, includes trace elements deposited heterogeneously during lunar volcanic outgassing. The lunar source region for Y791197,88 should be unusually rich in trace elements.

Yamato 82192 has not yet been studied extensively: physically, it appears very different from the other two known Antarctic lunar samples (**8**). If, indeed, all three derive from different lunar regions, so far Antarctica has sampled as many lunar sites as did the U.S.S.R. Luna program and half the number sampled by the U.S. Apollo program. Truly, Antarctica is yielding an unexpected bonanza of information on extraterrestrial bodies.

Acknowledgements: We thank the U.S. National Science Foundation (grant DPP 8111513) and the National Aeronautics and Space Administration (grant NAG 9-48) for partial support of this research and the U.S. Department of Energy for irradiation support (grant DEFG 0280 ER 10725).

References: (**1**) R. M. Verkouteren, J. E. Dennison and M. E. Lipschutz, Earth Planet. Sci. Lett. 10, 821-824 (1983); (**2**) A. R. Duncan, A. J. Erlank, J. P. Willis and L. H. Ahrens, Geochim. Cosmochim. Acta Suppl. 4, 1097-1113 (1973); (**3**) A. O. Brunfelt, K. S. Heier, B. Nilssen, and B. Sundvoll, ibid, 1209-1218; (**4**) S. Jovanovic and G. W. Reed, Jr., ibid, 1313-1324; (**5**) U. Krähenbühl, R. Ganapathy, J. W. Morgan and E. Anders,

ibid 1325-1348; (**6**) R. O. Allen Jr., S. Jovanovic and G. W. Reed, Jr., Geochim. Cosmochim. Acta Suppl. 5, 1617-1623 (1974); (**7**) N. J. Hubbard, J. M. Rhodes, H. Wiesmann, C.-Y. Shih and B. M. Bansal, ibid, 1227-1246 (1974); (**8**) K. Yanai and H. Kojima, Meteoritics, in press (1984); (**9**) U. Krähenbühl, J. W. Morgan, R. Ganapathy and E. Anders, Geochim. Cosmochim. Acta 37, 1353-1370 (1973); (**10**) B. Mason, Geol. Survey Prof. Paper 440-B-1 (1979); (**11**) E. Anders and M. Ebihara, Geochim. Cosmochim. Acta 46, 2363-2380 (1982).

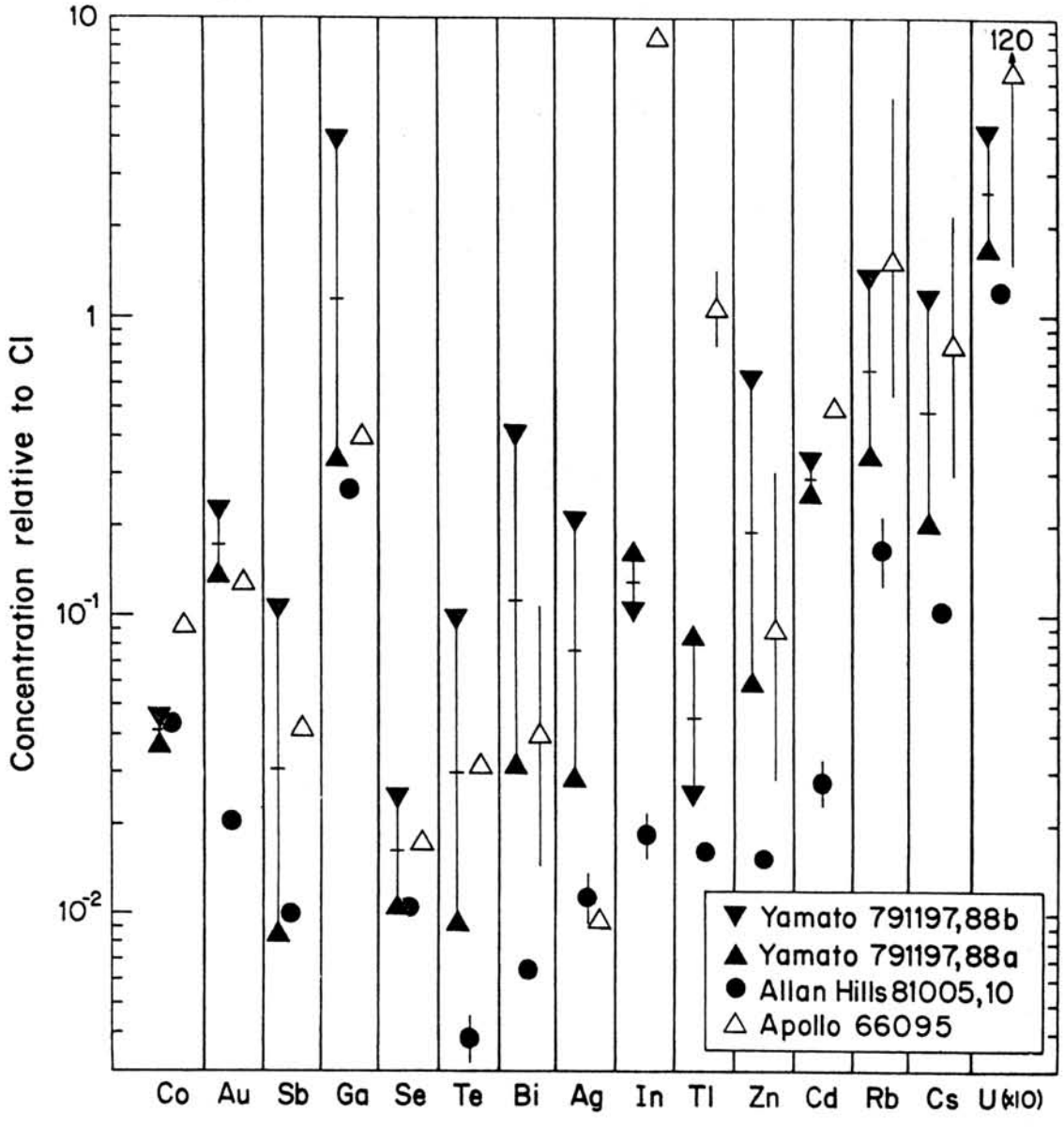

Fig. 1. Trace element data for lunar meteorites Y791197 and ALH A81005 (**1**) and Apollo "Rusty Rock", 66095, (**2-7**) normalized to mean Cl concentrations (**9-11**). Ranges are illustrated where replicate analyses exist and exceed symbol size. In Apollo sample 66095, only 1 datum each exists for Cd, In and the leftwards 5 elements. Trace element levels in Y791197 generally are enriched over those in ALH A81005 and resemble those in Apollo sample 66095 which seem to have been established by deposition of volatiles during lunar volcanism.

REE, Rb-Sr and U-Pb sytematics of "lunar" meteorite Yamato-791197

Noboru Nakamura[1], Daniel M. Unruh[2] and Mitsunobu Tatsumoto[2]

1) Dept. of Earth Sci., Kobe University, Nada, Kobe 657, Japan
2) U.S. Geological Survey, MS 963, Box 25046, DFC, CO 80226, U.S.A.

We have carried out analyses of Rb-Sr, U-Pb sytematics, and trace and some major elements including REE, Ca, Fe and Mg for the anorthositic breccia, Yamato 791197 meteorite in an attempt to confirm the suspected lunar origin of the meteorite (Yanai and Kojima, 1984), and to provide additional constraints on the type of mateiral that the meteorite may have originated from.

REE, Ba and Sr data for clast-80 (CL-80) and matrix material which includes numerous micro-clasts are shown in Fig. 1. Major element analyses are; CaO=17.5%, MgO=6.77% and FeO=6.95% for CL-80, and CaO=15.3%, MgO=5.52% and FeO=6.54% for MX-1, and thus similar to those of gabbroic anorthosite from the lunar highland. Both samples show slightly light-REE enriched, quite similar patterns with relatively low REE abundances and large positive Eu anomalies, which are almost identical with those of lunar anorthositic breccia, particularly to gabrroic anorthosite. Therefore, all the major and trace element compositions obtained for two specimens from the meteorite are consistent with a lunar origin of the meteorite.

The Pb isotopic composition analyses for 1N-HBr leached fraction (L) and the residue (R) of CL-80 are shown in Fig. 2, together with data from selected lunar samples taken from the linteratures. The leached fraction plots significantly above the geochron in the direction of lunar anorthositic rocks, but its Pb is not as radiogenic as that in typical lunar samples. The residue is much more radiogenic ($^{206}Pb/^{204}Pb$)~175), but plots only slightly above the geochron. The line connecting the L and R fractions corresponds to an age of 4.25 b.y., and the intersection of this line with 4.25 b.y. primary isochron corresponds to an initial $^{238}U/^{204}Pb$ ratio (μ) of 180, which is at least a factor of 2 lower than most lunar samples. Thus, if the meteorite did come from the moon, there must still be a significant amount of non-radiogenic non-lunar Pb (or Pb from unsampled lunar materials) in the meteorite. If the non-radiogenic component was derived from the projectile like unequilibrated chondrite and if Pb was homogenized during the impact event, then the 4.25 b.y. age may reflect this event. On the other hand, if Pb isotopes were not homogenized, or if the non-radiogenic Pb is of terrestrial origin, the apparent age has no significance. Thus, while the Pb isotopic data do not unambiguously confirm a lunar origin for this meteorite, they are consistent with a lunar origin and clearly indicate that this is not a "typical" meteorite in terms of Pb isotopes.

Rb-Sr analyses for two matrix materials and two clasts are shown in Fig. 3, together with analyses of plagioclase separate from the Moore County eucrite. The $^{87}Sr/^{86}Sr$ ratios for the samples are extremely low but within the range of those of lunar anorthosite to gabrroic anorthosite. Because of too small spread

of Rb/Sr ratios among the samples, only the inprecise apparent ages are calculated from the regrresion line; data for three most reliable data (MX-1, -2 and CL-80) give 3.9±0.5 b.y., and four data sets including CL-84 (tentative) yield 3.4±0.3 b.y. However, the corresponding initial $^{87}Sr/^{86}Sr$ ratios of 0.69907± 0.00009 (2σ) for the former age and 0.69916±0.00006(2σ) for the later are significantly low, even lower than those of most lunar mare basalts. If Rb-Sr system of the meteorite was in equilibrium among its components at the time of impact-brecciation event by which the glassy materials were formed, it is possible that the source material of the meteorite was formed under quite low Rb/Sr environment (usch as Rb/Sr=0.0003-0.001) possibly 4.25 b.y. ago and then brecciated at 3.9 b.y. ago. Thus, Rb-Sr data are reconcileed with the idea that the meteorite represents a lunar highland material.

In summary, REE, Rb-Sr, Pb analyses for the Yamato-791197 are consistent with the hypothesis that this meteorite represent a lunar highland breccia, particularly the gabbroic anorthosite.

References

Gray et al. (1973) Icarus 20, 213
Hubbard et al. (1974) Prof. Lunar Sci. Conf. 5th, Vol. 2, 1227
Lindstrom and Salpas (1983) Lunar Planet. Sci. XIV 440
Nyquist et al. (1974) Proc. Lunar Sci. Conf. 5th, Vol. 2, 1515
Yanai and Kojima (1984) Papers presented to 9th sympos. Antarctic Meteorites 42

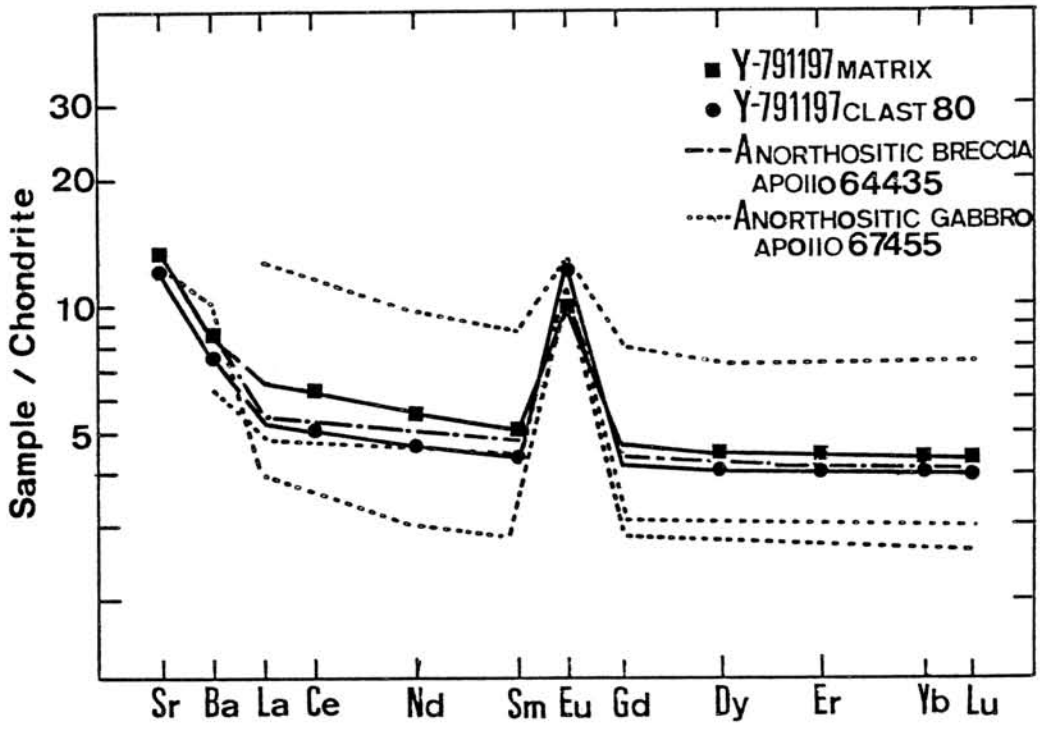

Fig.1. Chondrite-normalized trace element pattern for Y-791197. Data of anorthositic samples are from Lindstrome and Saalps (1983) and Hubbard et al. (1974).

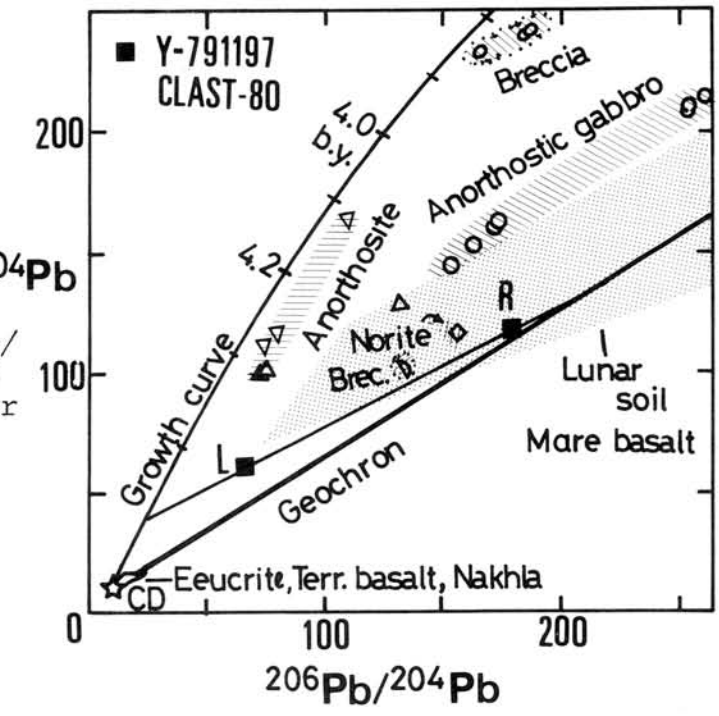

Fig. 2. $^{207}Pb/^{204}Pb$ vs $^{206}Pb/^{204}Pb$ diagram for Y-791197 clast-80 and selected lunar samples.

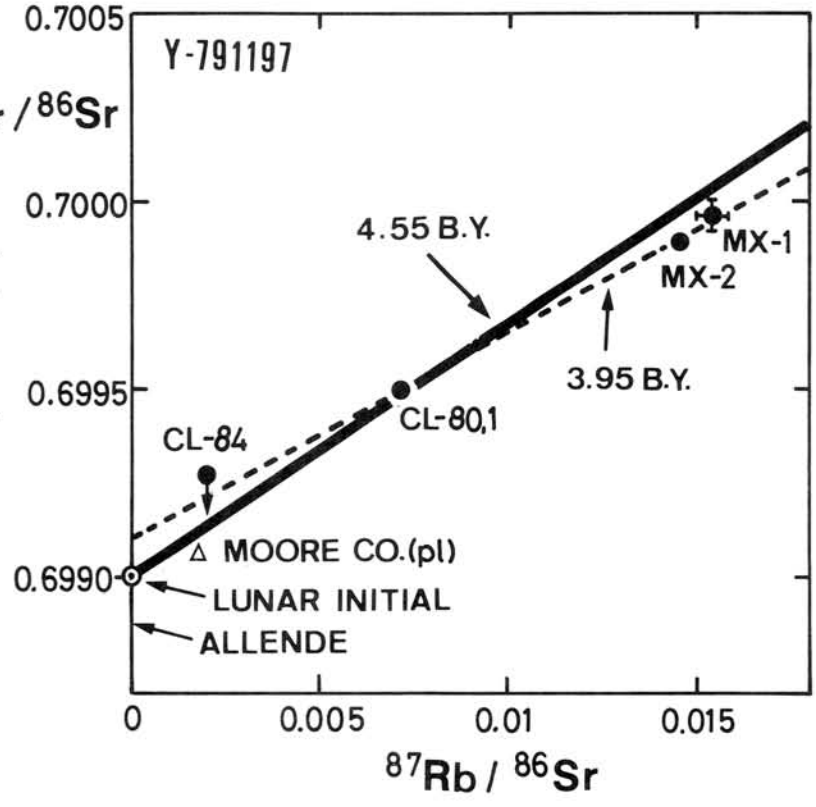

Fig. 3. ^{87}Rb-^{87}Sr diagram for Y-791197. Data of Lunar Sr initial (LUNI) and ALL, Allende initial are from Nyquist et al. (1974) and Gray et al. (1973), respectively.

46

REE abundances in the Yamato-791197,108

Kazuya Takahashi, Hiroshi Shimizu and Akimasa Masuda
Department of Chemistry, The University of Tokyo

We determined the REE, Sr and Ba abundances in the Yamato-791197,108, that represents the whole rock of the Yamato-791197. This meteorite has been considered to have the lunar origin.

Fig. 1 shows the the REE, Sr and Ba patterns of the Y-791197,108, ALH-81005, also classified as a lunar meteorite, and one sample of the lunar highlands. The data for ALH-81005 is quoted from Boynton et al.(1983) and the data for the lunar sample(65702,3,6c) from Haskin et al.(1973).

As shown in Fig. 1, the REE abundances for the sample in question are in good agreement with those for the 65702,3,6c, and all three patterns have some common features, i.e., positive Eu anomaly and enrichment toward the lighter REE. These observations suggest that the Y-791197 might have originated from the lunar highlands material, as ALH-81005 might. In addition, the positive Ce anomalies , which is common to these patterns, are characteristic and interesting. The REE patterns for the lunar rocks have been known (Masuda et al., 1972) to show the positive Ce anomalies frequently. The Ce anomaly of the pattern of the Y-791197,108 is about 5.5% and within the range obtained thus far for the lunar rocks.

We are going to add some data (major element compositions or isotopic data) for this specimen.

Fig. 1

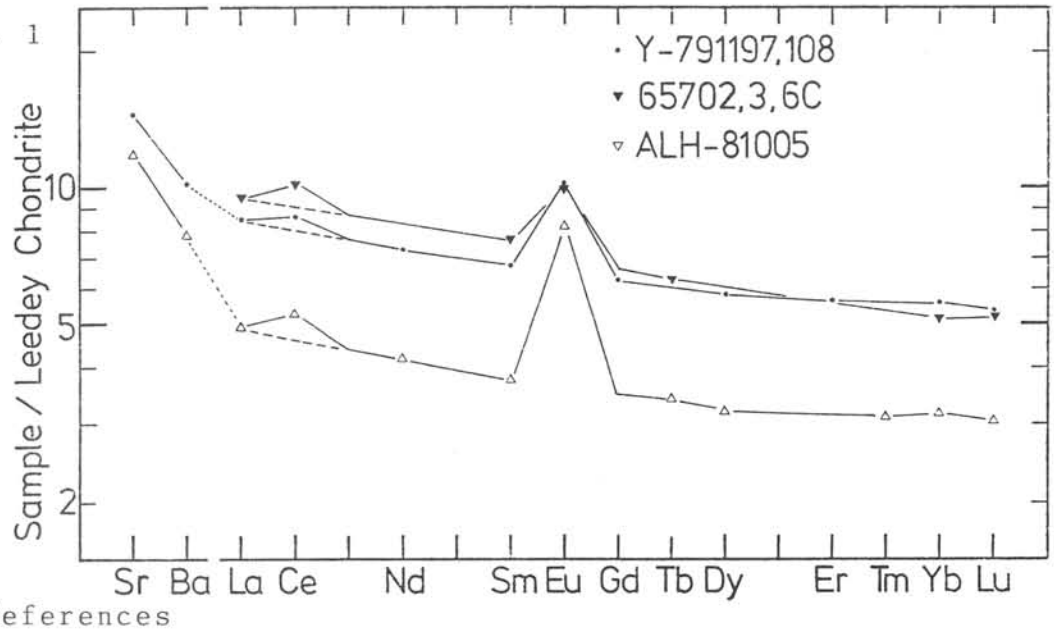

References

Boynton W. V. and Hill D. H.(1983) Geophys. Res. Lett. 10, 837-840

Haskin L. A., Helmke P. A., Blanchard D. P., Jacobs J. W., and Telander K. (1973) Proc. Lunar Sci. Conf., 4,1275-1296

Masuda A., Nakamura N., Kurasawa H. and Tanaka T. (1972) Proc. Lunar Sci. Conf. 3, 1307

^{40}Ar-^{39}Ar ANALYSES OF Yamato-791197

Kaneoka, I.* and Takaoka, N.**
* Geophysical Institute, Faculty of Science, University of Tokyo, Bunkyo-ku, Tokyo 113.
** Department of Earth Sciences, Faculty of Science, Yamagata University, Yamagata 990

Yamato-791197 has been classified as an anorthositic breccia, containing large amounts of angular clasts in a black matrix and reported to be similar to some of lunar rocks (1). Among a large number of Antarctic meteorites so far collected, only a meteorite Allan Hills A81005 has been identified to have come from the Moon (2). In this context, it is important to get some information on its age and ^{40}Ar-^{39}Ar analyses were applied to two kinds of samples from Yamato-791197.

For ^{40}Ar-^{39}Ar analyses, clasts were carefully separated by hand-picking to remove any groundmass part. A large clast ($\sim$ 4 mm in diameter) was included in the clast-sample (Y-791197, 96). Such clasts are regarded to be composed of mostly plagioclase together with minor pyroxene and olivine (1). Groundmass part (Y-791197, 97) was also analysed for comparison.

Samples were wrapped in Al-foil and irradiated in the JMTR of Tohoku University receiving total fast neutron fluence of about 5×10^{17} nvt/cm^2. The standard sample MMhb-1 (hornblende, K-Ar age : 519.5 ± 2.5 Ma) (3) was used as the age monitor. Ar gas was extracted at the Isotope Center, University of Tokyo and analysed with a Nier-type mass spectrometer at the Yamagata University with a resolving power of about 600. Nine temperature steps (600 - 1600°C) were taken for each sample. System blanks and the effects of Ca- and K-derived interfering isotopes were corrected to calculate an ^{40}Ar-^{39}Ar age. Details are the same as reported before (4).

Preliminary results have revealed that the clast sample (Y-791197, 96; 0.062 g) show ^{40}Ar-^{39}Ar ages of 3.9 - 4.1 b.y. at higher temperatures (900 - 1600°C). These ^{40}Ar-^{39}Ar ages are similar to those reported for lunar highland samples such as anorthositic breccia (5). However, more than half of ^{39}Ar was released in the lower temperature fractions (600 - 800°C), resulting in young ^{40}Ar-^{39}Ar ages of 1.0 - 2.2. b.y. for these low temperature fractions. Such apparent young ^{40}Ar-^{39}Ar ages may be at least partly affected by the secondary contamination for K. The matrix sample (Y-791197, 97; 0.095 g) has contained very large amount of Ar of solar wind composition. The $^{40}Ar/^{36}Ar$ ratio has decreased to about 2.6 at higher temperatures (1000 - 1600°C) and most Ar gas was degassed at the highest temperature. Total amount of ^{40}Ar becomes in the order of 10^{-4} cm^{3}STP/g. Hence it was difficult to get meaningful ^{40}Ar-^{39}Ar ages for this sample.

On the basis of these results, it can be inferred that the meteorite Yamato-791197 has surely come from the Moon and the clasts were probably derived from the lunar highland.

References

(1) Yanai, K. and Kojima, H., Abstracts for the Ninth Symposium on Antarctic Meteorites, 42 (1984).
(2) e.g.) Bogard, D.D., Geophys. Res. Lett., 10, 773 (1983).
(3) Alexander, E.C. Jr., Mickelson, G.M. and Lanphere, M.A., U.S. Geol. Surv. Open-File Rep., 78-701, 6 (1978).
(4) Kaneoka, I., Mem. Natl. Inst. Polar Res., Spec. Issue 20, 250 (1981).
(5) Turner, G., Phys. Chem. of the Earth, 10, 145 (1977).

AGE OF ANTARCTIC METEORITES AND ICE

Nishiizumi, K. and Elmore, D.*
Dept. of Chemistry, B-017, Univ. of California, San Diego, La Jolla, CA 92093
*Nuclear Structure Lab., Univ. of Rochester, Rochester, NY 14627

Cosmic ray produced nuclides in Antarctic meteorites provide us with information such as exposure history, terrestrial age, size in space, pairing, influx rate of meteorites and so on. Here, we summarize a few topics from our studies of cosmogenic nuclides ^{36}Cl ($t_{1/2}$ = 3.0×10^5 yrs), ^{26}Al (7.05×10^5 yrs), ^{10}Be (1.6×10^6 yrs) and ^{53}Mn (3.7×10^6 yrs) in Antarctic meteorites and ice.

Terrestrial age: The Allan Hills meteorites clearly show longer terrestrial age than other Antarctic meteorites. The terrestrial ages of Allan Hills meteorites are widely distributed between 1×10^4 and 7×10^5 yrs. On the other hand, many Yamato meteorites have terrestrial ages less than 1×10^5 yrs. Figure 1 illustrates this difference. Note that meteorites found at other Victoria Land sites (such as Meteorite Hills) seem to resemble Yamato rather than Allan Hills objects. The figure also indicates that there is no clear correlation between the terrestrial age of Allan Hills meteorites and their weathering features. These features are important for understanding the accumulation mechanism of Antarctic meteorites and ice movement at the different sites. Of the approximately 5000 Yamato meteorites, Yamato 74372 is the only one not found on the surface of the ice but rather buried in the ice at a depth of a few cm. Our preliminary terrestrial age of Yamato 74372 is $(1.7\pm0.7)\times10^5$ yrs.

Pairing: Combined cosmogenic nuclide and nuclear track data allow us to estimate the size and shielding depth of the specimen in the preatmospheric body. This study ruled out many proposed pairings of Antarctic meteorites (e.g. many of Allan Hills L-6 chondrite sets) and confirmed some sets (e.g. Allan Hills L-3 chondrites) (1). The Derrick Peak iron meteorites originated in a common meteoroid. ^{53}Mn activities for these meteorites range over two orders of magnitude, from 170 to 2 dpm/kg Fe for DRPA78006 and DRPA78008 respectively. The preatmospheric diameter of the Derrick Peak meteoroid was more than 3.5 meters.

Age of Ice: We have demonstrated a new dating method for ice based on $^{10}Be/^{36}Cl$ (2). We measured this ratio in several Yamato and Allan Hills ice samples. However, no clear ages for either area were found yet. The measurement of ice cores is required.

Lunar Meteorites: We have measured ^{36}Cl in Yamato 791197 (12.3 dpm/kg) and ALHA81005 (8.8 dpm/kg) and ^{53}Mn in ALHA81005 (174 ± 18 dpm/kg Fe). ^{53}Mn and ^{36}Cl results in ALHA81005 were compared to our measured cosmogenic nuclide data in the Apollo 15 drill core (3) along with published ^{26}Al and ^{10}Be data (4). ALHA81005 was irradiated by cosmic rays at a depth of 110-160 g/cm^2 in the moon for at least 15 million years before being ejected. The terrestrial age of the meteorite is $(1.8\pm0.7)\times10^5$ yrs. On the other hand, the high ^{36}Cl in Yamato 791197 along with higher ^{10}Be (5) indicates either that the meteorite was ejected from a very shallow depth on the moon, less than 100 g/cm^2, or that the meteorite was exposed to cosmic rays in space longer than ALHA81005 (or some combination). The terrestrial age of Yamato 791197 is less than 1×10^5 yrs. Measurements of ^{53}Mn and ^{26}Al in Yamato 791197 are in progress.

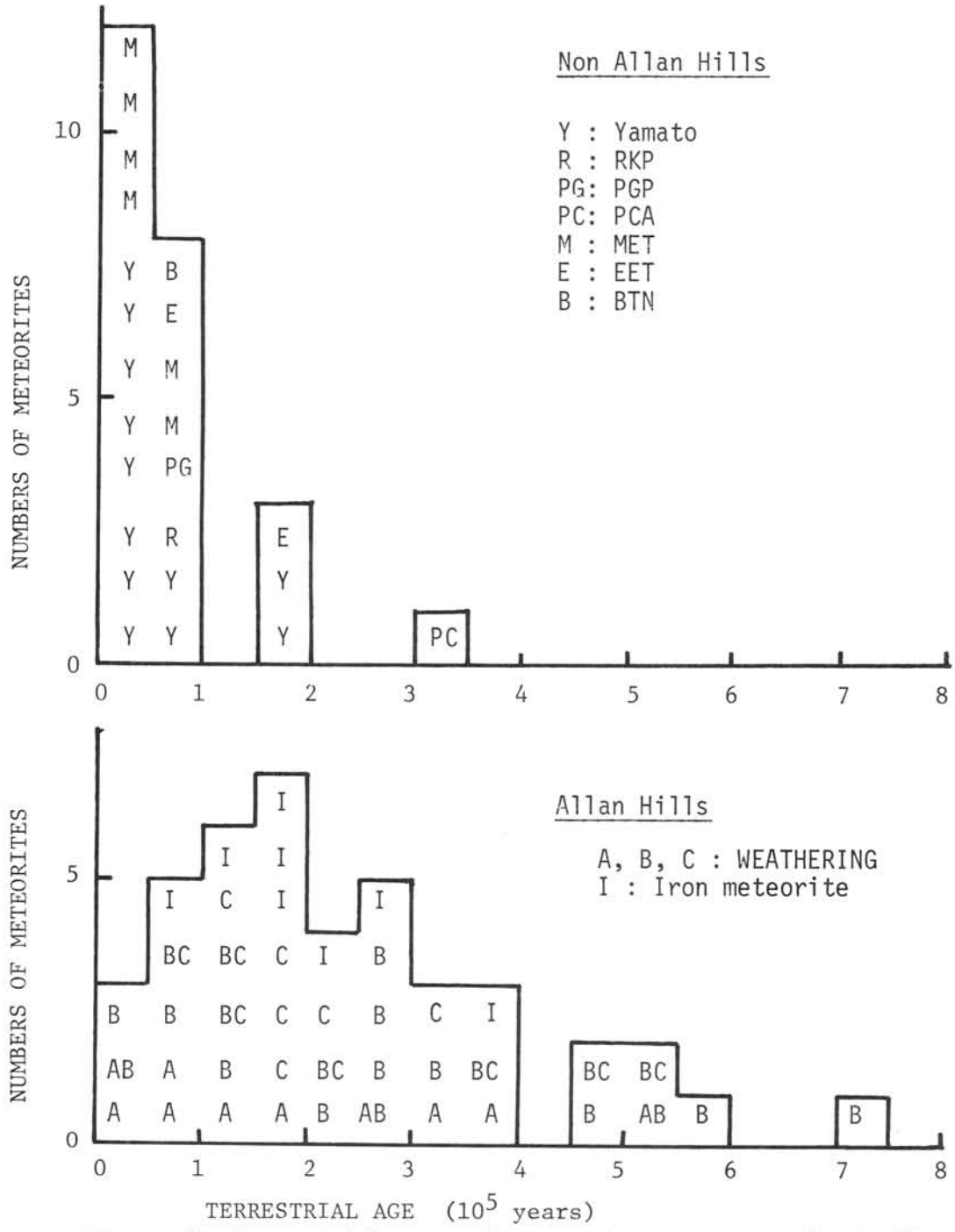

Figure 1. Terrestrial ages of Antarctic meteorites (incl.(6)and(7))

References:
(1) Goswami J. N. and Nishiizumi K. (1983) Earth Planet. Sci. Lett., 64, 1-8.
(2) Nishiizumi K. *et al* (1983) Earth Planet. Sci. Lett., 62, 407-417.
(3) Nishiizumi K. *et al* (1984) Earth Planet. Sci. Lett., 70, 157-163 & 164-168.
(4) Tuniz C., *et al* (1983) Geophys. Res. Lett., 10, 804-806.
(5) Nishiizumi K., Klein J., Middleton R. and Arnold J. R. (1985) unpublished.
(6) Schultz L. and Freundel M. (1984) (abstract) 47th Met. Soc. Mtg. (NM).
(7) Jull A. J. T. *et al* (1984) J. Geophys. Res., (preprint).

A SEARCH FOR NUCLEAR PARTICLE TRACKS IN LUNAR METEORITE YAMATO - 791197

Ghislaine Crozaz; Earth and Planetary Sciences Department and McDonnell Center for the Space Sciences, Washington University, St. Louis, Missouri 63130, USA.

A number of characteristic effects, including radionuclide and nuclear track production and thermoluminescence, are associated with the bombardment of lunar materials and meteorites by energetic solar and galactic cosmic ray particles (see, for example, [1]). These effects can be particularly useful in constraining the thermal and irradiation histories of extraterrestrial materials and, in favorable circumstances, can be used to study the record left by past solar activity.

In the present work, a search for nuclear particle tracks was performed. Grains with nuclear particle track densities of at least 10^8 t.cm^{-2}, if found, would be indicative of irradiation by solar flare particles in the upper few millimeters of the lunar surface prior to breccia formation. Such grains are commonly observed in lunar breccias and account for the majority of the lunar soils. On the other hand, nuclear particle track densities lower than 10^8 t.cm^{-2} are diagnostic of irradiation at deeper depth. The production of these tracks, however, because of the rapid attenuation of very heavy galactic cosmic ray particles with depth, is restricted to the upper few tens of centimeters of the lunar or meteoritic material.

About 100 feldspar grains (250 μm) of sample 791197,89 were mounted in epoxy, polished and etched in boiling 6N NaOH. Essentially all the feldspar grains were so shocked and so highly fractured that they disaggregated even when etched for only a few minutes. A few small crystal areas survived prolonged etching but were devoid of tracks. Olivine grains, present in much lesser abundance in our allocation (~10mg) than feldspars, maintained their integrity during etching and were also devoid of tracks.

These observations are identical with those in lunar meteorite ALHA 81005 [2] and, as in the case of that other lunar meteorite, fail to provide strong constraints on the irradiation history of these objects. However the lack of observable tracks is consistent with a short transit time between Moon and Earth [3] and also implies that the meteorite probably never resided within the outer few centimeters of its parent body. Unfortunately, because the material available for analysis was both shocked and scarce, it was not possible to examine large crystal areas and establish whether the upper limit for the track density is less than 10^6 tracks - cm^{-2} or not.

REFERENCES

[1] Walker R. (1980) Proc. Conf. Ancient Sun, 11-28.
[2] Sutton S. R. and Crozaz G. (1983) Geophys. Res. Lett. 10, 809-812.
[3] Sutton S. R. (1985), this conference.

THERMOLUMINESCENCE OF ANTARCTIC METEORITE YAMATO-791197 AND COMPARISON WITH ALHA-81005 AND LUNAR FINES

S. R. Sutton
McDonnell Center for the Space Sciences and Dept. of Physics,
Washington University, St. Louis, MO 63130, USA

Introduction

Thermoluminescence (TL) measurements on the lunar meteorite ALHA-81005 constrained its thermal and irradiation history and suggested a maximum Earth transit time of 2,500 years [1]. Reported here are the results of analogous measurements on Antarctic meteorite Yamato-791197. In general, the TL properties (glow curve shape, TL stability) of these two anorthositic breccias are quite similar. A major difference, however, is the significantly greater natural TL exhibited by Yamato-791197 suggesting that this meteorite experienced less shielding on the parent body just prior to ejection than did ALHA-81005. The artificial TL glow curve shapes (i.e., those produced after laboratory irradiation) of these two meteorites match well with those exhibited by Apollo 16 fines.

Thermoluminescence Glow Curve Shapes

TL measurements were performed on ~1 mg aliquots of a fragment also studied by INAA and electron microprobe [2]. A heating rate of 2 °C s^{-1} was used and laboratory irradiations were obtained using a ^{90}Sr beta particle source. In general, the natural glow curve provides information on the thermal and irradiation history of a sample while the artificial glow curve shape depends primarily on the type and abundance of TL phosphors. Natural and artificial TL glow curve shapes ("as received" and laboratory irradiated, respectively) are remarkably similar for the two meteorites showing a natural peak near 350°C and lower temperature artificial peak near 150°C (Figures 1 and 2).

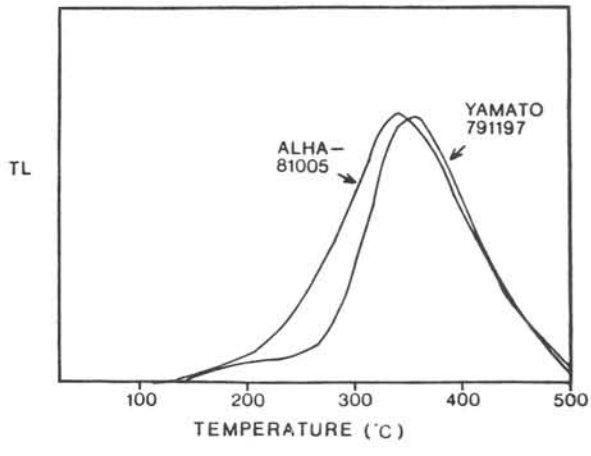

Figure 1: Natural TL glow curves for Yamato-791197 and ALHA-81005 (peak height normalized).

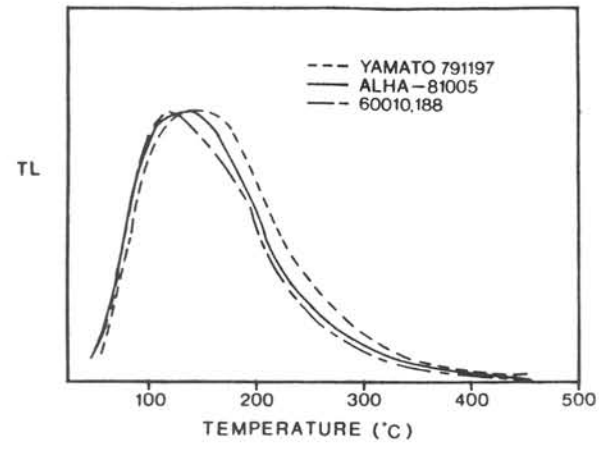

Figure 2: Artificial glow curves (50 krads) for Yamato-791197, ALHA-81005 and Apollo 16 lunar core sample 60010,188 (30 cm depth). (peak height normalized)

The glow curve temperature of the natural TL peak (Figure 1) is undoubtedly determined by the degree of low temperature TL loss by thermal decay. (The natural TL glow curve can be reproduced by preheating the sample to about 300°C after laboratory irradiation.) The similar natural peak positions for Yamato-791197 and ALHA-81005 demonstrate that the two meteorites have experienced roughly the same thermal history. The similarity in artificial glow curve shape indicates the two meteorites have TL phosphors (presumably plagioclase in these samples) with analogous electron trapping and luminescence centers. Lunar fines returned by the Apollo missions show a great diversity of artificial glow curve shapes (Figure 3), the majority exhibiting substantial TL emission at all glow temperatures. Even individual lunar soil grains within a given fines sample vary tremendously (see e.g. [3]). Glow curves for Apollo 16 (a highlands site) fines possess only a low temperature TL peak and match those of Yamato-791197 and ALHA-81005 remarkably well (Figure 2).

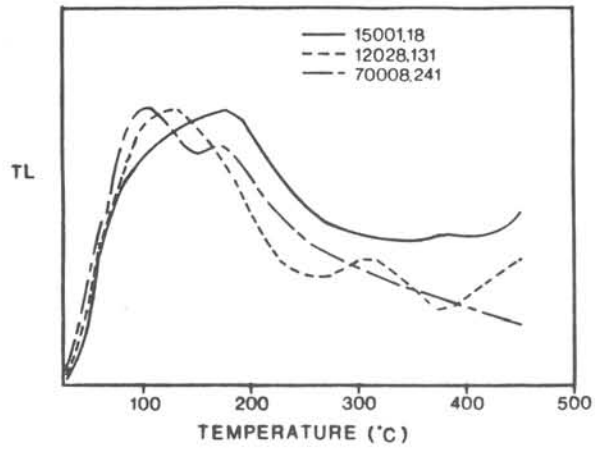

Figure 3: Artificial glow curves for three lunar core samples from Apollo 12 (12028,131; 36 cm), 15 (15001,18; 2.4 m) and 17 (70008,241; 36 cm)(peak height normalized).

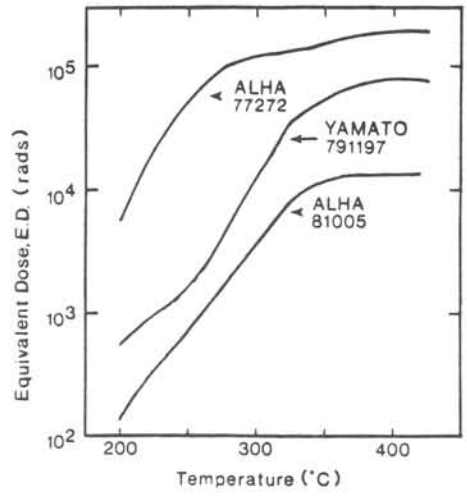

Figure 4: Equivalent dose, ED, curves for Yamato-791197, ALHA-81005 and Antarctic chondrite ALHA-77272 (terrestrial age = 0.54 Ma [4])

Equivalent Dose Curves

Equivalent dose (ED) curves (Figure 4), plots of the laboratory radiation dose required to reproduce the natural TL, are similar in shape for Yamato 791197 and ALHA-81005 showing reduced low temperature ED due to thermal decay and a high temperature plateau. By comparison with the ED curves of Antarctic chondrites with long radiometrically-determined terrestrial ages, filled electron traps responsible for TL emission above about 275 °C are thermally stable at Antarctic storage temperatures. The fact that Yamato 791197's ED at 300 °C is only 10^4 rads, much lower than the high temperature plateau (equilibrium) level, suggests that, like ALHA-81005, this meteorite experienced thermal loss of low temperature TL prior to its arrival on Earth. This heating could have been caused by shock heating during ejection, solar heating in a near sun orbit and/or atmospheric entry heating. Although none of these possibilities can be ruled out from the TL data

alone, shock heating is considered the most probable cause of the observed thermal decay. (No fusion crust was associated with this aliquot and near sun orbits are rare [5].) If this interpretation is correct, the fact that the natural TL (ED) has not reaccumulated to the equilibrium level, represented by the plateau ED, constrains the maximum length of time the meteorite was exposed to space radiation after lunar ejection. At the estimated minimum galactic radiation dose-rate of 10 rads yr^{-1} [1] and the observed anomalous fading rate (15% loss in 10 days, see below), the objects space exposure must have been less than 2,000 years. This result is analogous to the 2,500 year upper limit obtained for ALHA-81005 suggesting the two meteorites experienced similarly short Earth transit times.

Parent Body Shielding

Although the ED curve shapes are similar, Yamato-791197 plots at significantly higher dose than ALHA-81005 (Figure 4). The difference in high temperature plateau levels (a factor of 5) is particularly interesting because this level represents a pre-ejection thermal equilibrium between TL induced by lunar irradiation and TL lost by thermal decay (due to the Moon's internal heat). Equilibrium differences due to anomalous fading [6] are negligible since fading measurements show the rate of this decay to be essentially equivalent in the two meteorites. (At 400°C glow curve temperature, Yamato-791197 artificial TL shows 15 ± 7% loss after 10 days storage at room temperature compared to 25 ± 6% for ALHA-81005. Assuming this anomalous TL loss obeys a power law time dependence [1], this phenomenon could account for at most a factor of 2 difference in equilibrium level.) The greater high temperature equilibrium ED level exhibited by Yamato-791197 therefore demonstrates that this meteorite resided at a cooler, more heavily irradiated depth than ALHA-81005, i.e. nearer to the lunar surface. Since the equilibrium time of the natural TL associated with the ED plateau is of the order of 10^4 years [Hoyt, et al., 1972], an ED of ~10^4 rads corresponds to a dose-rate of the order of 1 rad yr^{-1}, or about an order of magnitude lower than the surface dose-rate [7]. Shielding of the order of meters is required to attenuate galactic protons to this degree [8]. A depth difference between the two bodies of the same scale is required to obtain the necessary dose-rate difference.

Summary and Conclusions

Yamato-791197 and ALHA-81005 exhibit similar natural and artificial glow curve shapes. Artificial glow curves match well with those of highland fines from the Apollo 16 site but are distinct from those of other Apollo fines. Analogous thermal histories are indicated for the two meteorites by the close agreement in natural TL peak positions. A comparison of ED curves shows that both objects experienced similarly short Earth transit times. These similarities strongly suggest, but do not prove, that the two meteorites derive from a single lunar impact. The pre-ejection equilibrium level is consistent with a parent body shielding depth of the order of meters for both objects but the greater ED of Yamato-791197 indicates that it resided nearest to the surface with a depth difference of the same scale.

References: [1] Sutton, S. R. and G. C. Crozaz (1983) GRL 10, 809-812. [2] Lindstrom, et al., this issue. [3] Hoyt, H. P., Jr., et al. (1972) Geochim. et Cosmochim. Acta supplement 3, 2997-3007. [4] Nishiizumi, K. et al. (1981) EPSL 52, 31-38. [5] Melcher, C. L. (1981) EPSL 52, 39-54. [6] Wintle, A. G. (1977) Jour. Lum. 15, 385-393. [7] Hoyt, H. P., Jr., et al. (1973) Geochim. et Cosmochim. Acta supplement 4, 2489-2502. [8] Reedy, R. C. and J. R. Arnold (1972) JGR 77, 537-555.

NOBLE GASES IN YAMATO-791197: EVIDENCE FOR LUNAR ORIGIN.

Nobuo Takaoka, Dept.of Earth Sciences
Yamagata University.

Yamato-791197 is an anorthositic breccia which is very similar to lunar rocks in the mineral chemistry and in the texture(Yanai and Kojima,1984). Identification of a lunar meteorite is of great importance in the following respects. It demonstrates existence of an ejection mechanism which could propel lunar surface material toward the earth, suggesting a possibility of Mars-origin meteorite. Y-791197 might be a new type of lunar material.

Small chips of whole rock(10.14mg) and clast(10.52mg) were heated at 1750 °C. Concentrations and isotopic compositions of noble gases were determined by mass spectrometry. Part of result is given in Table 1. The gas released from the whole rock was essentially a pure trapped component, while the gas from the clast was a mixture of the trapped and the spallogenic components.

The whole rock contains large amounts of solar-type gases, originated by implantation of solar wind. Fig.1 shows comparison of noble gas abundance between the Y-791197 whole rock, lunar highlands soil 65501(Bogard and Nyquist,1973) and matrix of ALH-81005(Bogard and Johnson,1983) which is the first lunar metaorite. There is good agreement between them. An agreement with the lunar highlands soil is excellent except for ^{4}He.

The isotopic compositions of solar gases in Y-791197 is also identical to lunar regolith. The $^{40}Ar/^{36}Ar$ ratio of 2.56 is very similar to the ratio(2.77) for lunar highlands soil 65501(Bogard and Nyquist,1973). There are no data on K contents in the present samples. However, if the K contents are similar to those reported for ALH-81005(Laul et al.,1983; Boynton and Hill,1983), ^{40}Ar determined in the clast would be produced by the in-situ decay of ^{40}K in 4.0 b.y. If ^{36}Ar in the clast is due to solar Ar found in the whole rock, excessive $^{40}Ar(1 \times 10^{-6}cc/g)$ would be produced in 1.1 b.y. from the ^{40}K decay. On the other hand, the whole rock contains 60 times ^{40}Ar produced by the ^{40}K decay in 4.5 b.y., large excess of ^{40}Ar, as many lunar regolith materials do.

The isotopic compositions of Xe are shown in Fig.2 in comparison to solar Xe and Xe in the ALH-81005 lunar meteorite(Bogard and Johnson,1983). Y-791197 is identical to lunar highlands soil and ALH-81005 in this point. Spallogenic Xe is relatively enriched in the clast. The isotopic ratio of spallogenic Xe is: 0.55/=1/1.53/ 3.24/0.89/4.48/0.53/0.03/=0. This is also in good agreemwnt with that in lunar soils(Basford et al.,1973) except for ^{129}Xe.

The concentrations of spallation ^{21}Ne are (70 $\pm$ 11) x 10^{-8} cc/g for the whole rock, approximately twice the value for ALH-81005 (Bogard and Johnson,1983), and 13 x 10^{-8} cc/g for the clast. Spallogenic ^{126}Xe is 29 x 10^{-12}cc/g for the whole rock and 12 x 10^{-12} cc/g for the clast. Large difference in the concentrations of spallogenic nuclides between two parts suggests that the matrix part of Y-791197 was probably irradiated near the lunar surface for a long time, whereas the clast had been buried in a deep place untill it was dug out by impact metamorphism. Estimation of an exposure age is difficult because there are no data on the chemical composition and on shielding depth.

The large concentrations of solar wind gases, the relative elemental abundances and the isotopic compositions of noble gases in Y-791197 are all compatible with an origin from lunar highlands regolith.

References

Basford,J.R. et al.(1973), Proc.4th Lun.Conf.,vol.2, 1915.

Bogard,D.D and Nyquist,L.E.(1973),ibid , vol.2, 1975.

Bogard,D.D. and Johnson,P.(1983),Geophys.Res.Lett.,10,801.

Boynton,W.V. and Hill,D.H.(1983), ibid, 10, 837.

Laul,J.C. et al.(1983), ibid, 10, 825.

Yanai,K. and Kojima,H.(1984), Abstract 9th Symp.Antarct.Meteor.

Table 1. Isotopic abundances(cc/g) of noble gases from whole rock and clast of Y-791197.

Isotope	Whole rock	Clast
^{3}He(10^{-8})	201.	2.22
^{4}He(10^{-5})	450.	2.45
^{3}He/^{4}He(10^{-4})	4.46$\pm$0.02	9.16$\pm$0.23

Table 1 (continued)

Isotope	Whole rock	Clast
$^{20}Ne(10^{-6})$	947.	5.78
$^{21}Ne(10^{-6})$	3.10	0.142
$^{22}Ne(10^{-6})$	76.4	0.611
$^{20}Ne/^{22}Ne$	12.39±0.04	9.46±0.04
$^{21}Ne/^{22}Ne$	0.0406±0.0002	0.233±0.002
$^{36}Ar(10^{-6})$	348.	3.22
$^{38}Ar(10^{-6})$	65.4	0.914
$^{40}Ar(10^{-6})$	889.	9.34
$^{38}Ar/^{36}Ar$	0.188±0.001	0.284±0.002
$^{40}Ar/^{36}Ar$	2.555±0.017	2.90±0.03
$^{84}Kr(10^{-9})$	173.	2.23
$^{132}Xe(10^{-10})$	245.	3.19

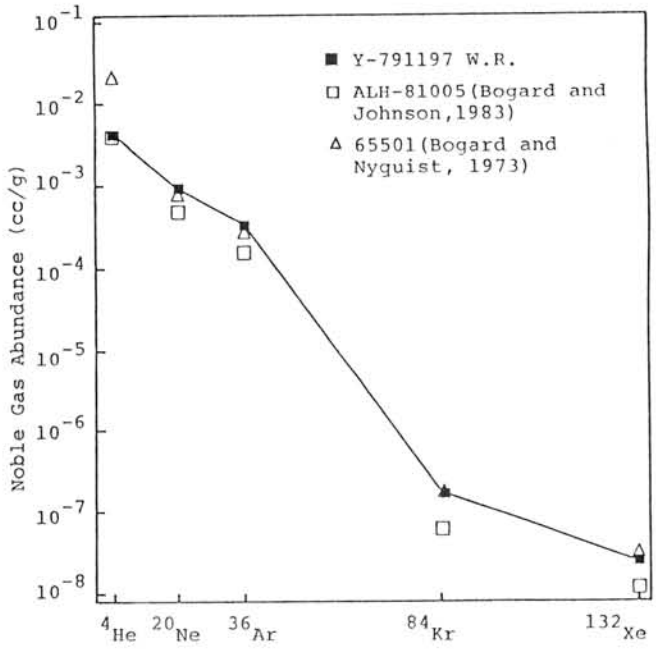

Fig.1, Noble gas abundance for Y-791197 whole rock.

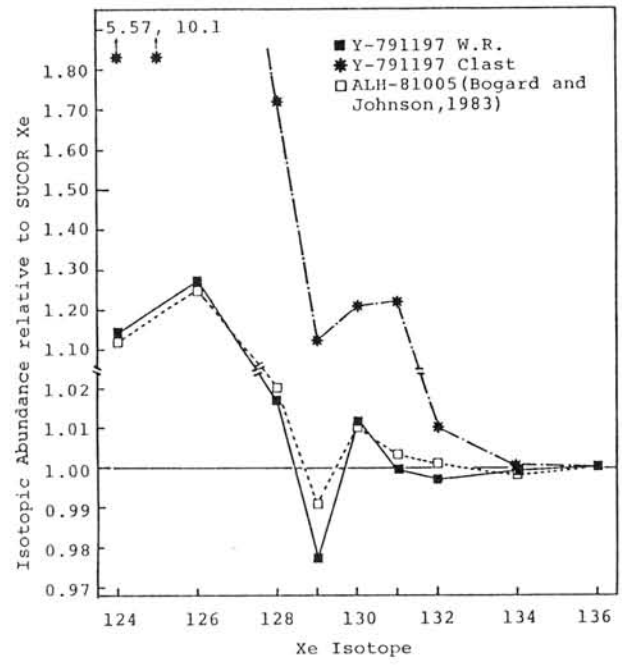

Fig.2, Xe isotopic abundance relative to SUCOR-Xe.

Magnetic Properties of Yamato 791197 Meteorite in Comparison with Those of Apollo 15418 Lunar Breccia

Takesi Nagata and Minoru Funaki

National Institute of Polar Research

As pointed out by Yanai and Kojima (1984), Yamato 791197 is an anorthositic breccia, the bulk chemical composition of which is similar to that of lunar highland anorthositic breccias and igneous rocks, particularly Apollo 15418, and is considerably different from that of the ordinary eucrites. In particular, ratios FeO/MnO in both Yamato 791197 and ALHA 81005 are very close to the characteristic value (75 ± 5) of the ratio in all kinds of lunar materials. It has been suggested on the basis of these data and others that Yamato 791197 (ALHA 81005 as well) may be a fragment of the lunar highland anorthositic breccia.

As the magnetic properties of both lunar materials and achondrites have been reasonably well examined to date, the characteristic magnetic properties of Yamato 791197 are compared with those of lunar materials and achondrites.

1. Ferromagnetic Composition

A unique magnetic characteristic of the lunar materials is the co-existence of apparently pure metallic iron with kamacite of more than 5% in Ni content, whereas no such a co-existence has ever been observed in meteorites (Nagata 1980). As illustrated in Fig. 1, the thermomagnetic analysis shows that the ferromagnetic component of Yamato 791197 consists of (i) apparently pure iron (25%), (ii) kamacite of 5-12%Ni (54%) and (iii) taenite of 32-39%Ni (21%), while that of Apollo 15418 comprises (i) apparently pure iron (20%), (ii) kamacite of 5-8%Ni (71%) and (iii) taenite of 32-35%Ni (9%).

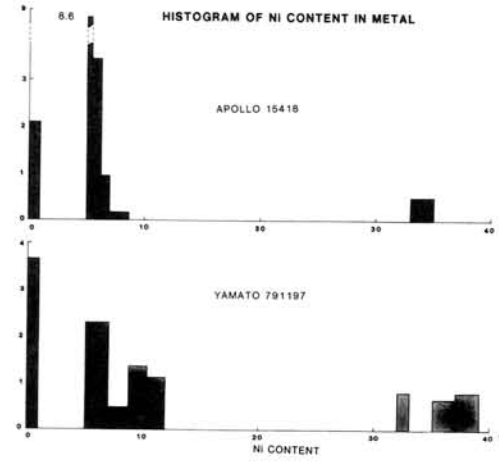

Fig. 1

The apparently pure metallic iron phase in the lunar materials has been identified either to (a) the pure metallic iron which was produced by a subsolidus reduction of fayalite and other Fe-bearing silicate minerals by severe impacts (e.g. El Goresy et al 1973), or to (b) schreibersite which was exsolved from a Fe-Ni-P system caused by a severe impact metamorphism (e.g. McKay et al, 1973).

Since a co-existence of the apparently pure metallic iron phase is very common in lunar surface materials (including Apollo 15418) but it is not observed in meteorites, it seems very likely that the ferromagnetic composition of Yamato 791197 is nearly same as that of lunar highland anorthositic breccias, represented by Apollo 15418.

2. Paramagnetic Composition

The paramagnetism of natural rocks is mostly subjected to the contents of Fe^{2+}, Fe^{3+} and Mn^{2+}. Fig. 2 shows the paramagnetic sus-

ceptibility (χ_ρ) at 295°K of Yamato 791197 in comparison with two histograms of the χ_ρ (295°K) values of a group of Apollo lunar materials and the other group of Antarctic achondrites. The fully black parts of the lunar rock histogram indicates the χ_ρ (295°K) values of lunar anorthositic igneous rocks, breccias and fines. The Antarctic achondrite group covers eucrites, diogenites, howardites and ureilites. It will be obvious that the paramagnetic characteristics of Yamato 791197 belong to those of the lunar surface anorthositic materials, but not to those of the ordinary achondrites.

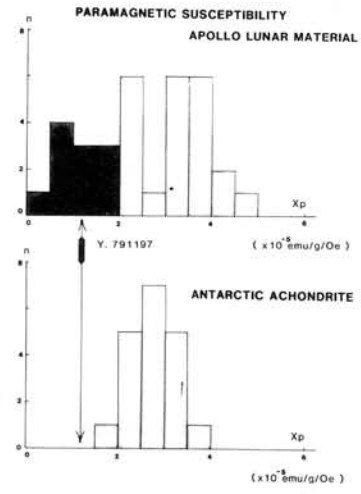

Fig. 2

3. Other Magnetic Properties

The magnetic coercivity dependent on temperature and the natural remanent magnetization characteristics of Yamato 791197 are examined in comparison with those of Apollo lunar materials and Antarctic achondrites. Although no positively strong evidence can be pointed out, there is no problem in these magnetic properties for identifying Yamato 791197 to a fragment of the lunar anorthositic breccia.

References

El Goresy A., Ramdohr P. and Medenbach O., (1973). Proc. 4th Lunar Planet. Sci., 732-750.

Mc-Kay G.A., Kridelbough S.J. and Weill D.F. (1973). Proc. 4th Lunar Planet. Sci., 811-818.

Nagata T., (1980). Proc. 5th Symp. Antarc. Meteor., 243-257.

Yanai K. and Kojima H., (1984). 9th Symp. Antarc. Meteor., (Abstract), 17.

LUNAR METEORITES YAMATO 791197 AND ALHA 81005: THE SAME YET DIFFERENT.

Marilyn M. Lindstrom, David J. Lindstrom, Randy L. Korotev, and Larry A. Haskin
Department of Earth and Planetary Sciences, Washington University, St. Louis, Missouri 63130.

Antarctic meteorite Yamato 791197 is a breccia from the lunar highlands. This was inferred from the preliminary examination [1] and confirmed by our compositional and petrographic analyses. It is similar, but not identical, to other previously analyzed lunar samples and thus is an important contribution to lunar science, and our understanding of the Moon.

We separated our sample of the meteorite (791197,89) into 5 subsamples. We attempted to separate clasts from the breccia, but the clasts were small and the matrix coherent, so we were only able to obtain subsamples enriched in the largest clast lithologies. These still contain at least 50% matrix and smaller clasts. Subsample Y-1 is rich in a green clast; Y-2 is rich in a light gray melt rock; Y-3 is chips of the bulk breccia; and Y-4 is fine residue from the chipping process. The remaining 20 mg were used for fission track and thermoluminescence studies [2]. The other four subsamples were analyzed by instrumental neutron activation analysis for twenty-five major and trace elements. The results are given in Table 1 and REE are plotted normalized to chondrites [3] in Figure 1.

Yamato 791197 is definitely a lunar breccia. Its low Na and high Cr concentrations distinguish it from terrestrial rocks and its low Fe and high Ca concentrations distinguish it from meteorites. Concentrations of the siderophile elements Co, Ni, Ir, and Au are typical of polymict lunar samples. The composition is very similar to that of meteorite ALHA81005 [4], Apollo 16 anorthositic gabbro 67215 [5], and estimates of the average lunar highlands [6]. As in A-81005, incompatible element concentrations in Y-791197 are lower than those of average highlands and most Apollo polymict breccias, presumably due to an absence of KREEP [4]. By analogy to other lunar samples, we estimate the concentrations for the major elements not determined here to be 44-48% SiO_2, <0.6% TiO_2, 24-28% Al_2O_3, and 4-9% MgO.

Following INAA studies, the three large subsamples were made into polished mounts for study on our JEOL 733 electron microprobe. Backscatter electron imaging and energy dispersive X-ray analysis provided textural and semi-quantitative compositional information on clasts and matrix. Quantitative analyses were done on 19 clasts selected to represent the range of clast types. Y-791197 is a glassy matrix breccia with numerous small mineral, glass, and lithic clasts of widely varying compositions. In areas where the matrix is crystalline, clast boundaries are unclear and matrix grades into clasts. Most of the identifiable lithic clasts are ferroan highland rocks (Mg' = molar % Mg/(Mg+Fe) = 45-65. The analyzed lithic clasts include: 1) Two granular to cataclastic ferroan anorthosites with more than 85% plagioclase (An 95-98) and varying proportions of olivine (Mg'=55), pigeonite (Mg'=61), clinopyroxene (Mg'=59-67) and Fe, Ti, Cr opaque oxides. 2) One subophitic-granular ferroan anorthositic gabbro consisting of ~70% plagioclase (An 95), ~30% clinopyroxene (Mg'=46) and minor opaques. 3) Plagioclase vitrophyres (green clasts in Y-1) consisting of approximately equal amounts of plagioclase (An 97.5) and highland glass (Al_2O_3 ~20%, Mg'=62). 4) Four fine-grained feldspathic melt rocks (the gray melts in Y-2) with Al_2O_3 ~ 26.5% and Mg'=55. 5) One melt rock and one glass clast with noritic composition (Al_2O_3 ~16%, Mg' 60). 6) One granulitic, magnesian gabbroic anorthosite consisting of plagioclase (An 97), olivine (Mg'=80), orthopyroxene (Mg'=82) and clinopyroxene (Mg'=86). 7) Two VLT (very low

titanium) mare basalts, one subophitic-granular and one quench textured. The subophitic basalt consists of plagioclase (An 90-93) and clinopyroxene (Mg' 47) with minor ilmenite. The other is a quenched melt consisting of glass and abundant clinopyroxene with minor interstitial plagioclase (An 89) and ilmenite. The bulk composition of the clast has 13% Al_2O_3, 19.4% FeO, 7.7% MgO, and 1.9% TiO_2, and Mg'=41. 8) A mare basalt fragment consisting of a 0.3 mm grain of exsolved clinopyroxene (host pigeonite Mg'=38, bulk Mg'=44), adjacent to a complex assemblage of a 0.1 mm grain of pyroxferroite, a 0.04 mm grain of troilite, and an area of hedenbergite peppered with small grains of troilite. Identifiable monomineralic clasts include granular plagioclase (An 95.7), Mg,Al(Fe) spinel, olivine (Mg'=51), clinopyroxene (Mg'=45-57), and exsolved clinopyroxenes similar to the large clast above. Most of these mineral clasts are derived from the ferroan highlands rocks, but several large, exsolved pyroxenes from mare basalts are found. Fragments of magnesian (Mg'>70) minerals were not identified.

Most of these clast types have been observed in other lunar samples. Ferroan anorthosites and granulitic magnesian gabbroic anorthosites are common in the highlands. Ferroan anorthositic gabbros are rare, but have been observed at North Ray Crater, Apollo 16. Monomict granulitic breccia 67215 is the best example. VLT mare basalts are found at the Apollo 17 and Luna 24 sites. Melt rock and glass clasts are regional, representing an average of local components. While each of these components has been observed in returned lunar samples, they were not all found together at any Apollo or Luna site. However, all four of the primary components were observed in A-81005, but the proportions of clasts types in the two lunar meteorites are very different. A-81005 is dominated by magnesian granulitic breccias, with ferroan anorthosites secondary and both ferroan gabbros and mare basalts rare. Our sample of Y-791197 is dominated by ferroan anorthosites and gabbro, with VLT mare basalt more abundant than magnesian granulite. In addition, the secondary clast types, melt rocks and glasses, are distinct in the two meteorites. Those in A-81005 are magnesian (Mg'~80), while those in Y-791197 are ferroan (Mg'~60) gabbroic anorthosites. These major differences in clast proportions are reflected in the small differences in composition between the two meteorites. Relative to A-81005, Y-791197 is 1.5 times richer in Sc, 1.12 times richer in FeO, and 1.4-1.7 times richer in REE and other incompatible elements. The relative concentrations of the light REE are slightly depleted with respect to A-81005 (Figure 1). Y-791197 is presumably poorer in MgO, based on the ferroan nature of its clasts. These differences may be accounted for by the observed increase in ferroan highlands and mare basalt components, but a tiny (<0.8%) addition of KREEP component cannot be eliminated.

The differences in clast proportions and compositions are significant because the ferroan and magnesian highland rocks have very different origins. As most clast types occur in both breccias, both could have come from the same region of the Moon and been ejected in the same impact. At least this amount of heterogeneity has been observed among lunar samples from specific lunar regions. Each of the Apollo-Luna sites has a distinct suite of rock types which occur in various proportions in the breccias from that site, but the clast suite at each site differs from that at other sites. For example, Apollos 15 and 16, the clast suite includes both ferroan anorthosites and magnesian rocks, but the Apollo 15 suite is relatively KREEP-rich and the Apollo 16 suite relatively KREEP-poor. A better example is the amount of variation in clast proportions in breccias from a single impact, North Ray Crater, Apollo 16 [5,7]. Clasts include ferroan anorthosites, anorthositic gabbros and melt rocks, magnesian

granulites and KREEPy melts, and alkali gabbronorites. Each breccia is dominated by a different set of components, yet most breccias contain minor amounts of the other components. Thus it is possible for breccias from the same impact to have very different proportions of clast types. We thus conclude that it is probable that ALHA81005 and Yamato 791197 were ejected from the Moon by the same impact. At least, they come from regions of the Moon with very similar source lithologies. Since their compositions are close to that expected for typical highlands [6], we cannot rule out origins from different regions. No property we observed must be regarded as unique to a single source.

Table 1. Element concentrations in 4 samples of the Yamato 791197 meteorite and comparison to ALHA81005 [4], Apollo 16 sample 67215, and estimate of lunar crustal average composition [6]. Values in ug/g, except oxides in cg/g (total element as oxide) and Ir and Au in ng/g.

	green clast rich	gray melt rich	black breccia	res-idue	unc. +/- 1 s.d.	mass wt'd. mean Yamato 791197	mass wt'd. mean ALHA 81005*	Apollo 16 67215	Lunar crust average
SiO2	n.a.	n.a.	n.a.	n.a.	---	n.a.	46.5[8]	n.a.	45.
TiO2	n.a.	n.a.	n.a.	n.a.	---	n.a.	0.23	0.38	0.56
Al2O3	n.a.	n.a.	n.a.	n.a.	---	n.a.	25.1	25.8	24.6
FeO	5.98	6.06	6.27	5.99	0.06	6.09	5.46	7.1	6.6
MgO	n.a.	n.a.	n.a.	n.a.	---	n.a.	8.8	6.0	6.8
CaO	15.0	15.1	14.9	14.8	0.3	15.0	14.9	15.5	15.8
Na2O	0.324	0.334	0.331	0.331	0.003	0.329	0.321	0.30	0.45
K2O	0.025	0.027	0.023	0.023	0.014	0.025	<0.04	0.011	0.075
Sc	12.87	13.78	14.02	12.82	0.13	13.43	8.81	15.2	10.
Cr	940.	933.	938.	906.	9.	935.	900.	860	680
Co	21.6	17.1	19.4	19.2	0.2	19.7	22.5	13.5	15.
Ni	214	152	185	193	8-13	189	243	40.	100
Br	0.15	0.27	0.18	0.46	0.03	0.21	0.33	n.a.	n.a.
Sr	148.	152.	149.	141.	9-16	149.	141.	130.	120
Zr	47.	47.	42.	40.	13-24	45+/-15	19+/-12	n.a.	63
Ba	30.	32.	36.	38.	3-5	33.	24.	18.	66
La	2.24	2.95	2.55	2.59	0.03	2.53	1.86	1.19	5.3
Ce	5.7	7.4	6.6	6.7	0.3	6.45	4.54	3.2	12
Nd	3.6	4.7	4.3	3.6	1.2	4.1	2.6	2.4	7.4
Sm	1.11	1.44	1.25	1.24	0.02	1.24	0.866	0.72	2.0
Eu	0.750	0.791	0.770	0.762	0.012	0.766	0.702	0.73	1.0
Tb	0.26	0.33	0.29	0.30	0.02	0.29	0.19	0.20	0.41
Yb	0.97	1.17	1.08	1.03	0.02	1.05	0.69	0.77	1.4
Lu	0.143	0.174	0.159	0.155	0.003	0.156	0.106	0.125	0.21
Hf	0.85	1.03	0.93	0.93	0.03	0.92	0.63	0.78	1.4
Ta	0.103	0.128	0.107	0.108	0.009	0.110	0.079	0.09	n.a.
Ir	9.7	4.5	6.6	4.0	0.5	7.1	7.6	1.0	n.a.
Au	1.8	1.4	3.4	4.2	0.4	2.4	n.a.	n.a.	n.a.
Th	0.31	0.36	0.33	0.29	0.02	0.33	0.198	0.12	0.9
U	0.10	0.13	0.12	0.13	0.02	0.12	0.09	n.a.	0.24
mass (mg)	36.35	21.62	30.34	8.22		96.53	77.71		

n.a. = not analyzed or reported
* From [4], with FeO and REE data normalized to standard values used in this work.

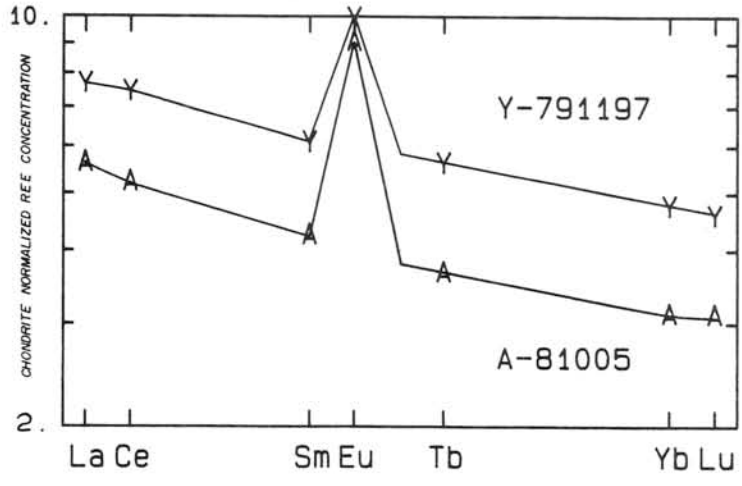

ACKNOWLEDGEMENTS: We are grateful to Professor Nagata and Dr. Yanai of the National Institute of Polar Research, Tokyo, for the opportunity to study fragments of the Yamato 791197 meteorite. This work was funded in part by NASA under grant NAG 9-56.

REFERENCES [1] Yanai K. and Kojima H. (1984) Ninth Symp. on Antarctic Meteorites, 42-43, National Inst. of Polar Res., Tokyo. [2] Crozaz G. and Sutton S., this volume. [3] Nakamura N. (1974) Geochim. Cosmochim. Acta 38, 757-775. [4] Korotev R.L., Lindstrom M.M., Lindstrom D.J., and Haskin L.A. (1983) Geophys. Res. Lett. 10, 829-832. [5] Lindstrom M.M. and Salpas P.A. (1983) Proc. Lunar Planet. Sci. Conf. 13, J. Geophys. Res. 88, suppl. A671-A683. [6] Taylor S.R. (1982) Planetary Science: A Lunar Perspective, (Table 5.5), 480 p., Lunar and Planetary Institute, Houston. [7] Lindstrom M.M. (1984) Proc. Lunar Planet. Sci. Conf. 15, J. Geophys. Res. 89, suppl. C50-C62. [8] Palme H., Spettel B., Weckwerth G., and Wanke H. (1983) Geophys. Res. Let. 10, 817-820.

LUNAR METEORITE ALLAN HILLS A81005: A REVIEW

Keil, K.
Dept. of Geology, Institute of Meteoritics, Univ. of New Mexico, Albuquerque, N.M. 87131, USA.

Meteorite ALHA81005 was found by J. Schutt on Jan. 18, 1982, the last day of field work for that season by the US search party, on the middle western ice field, Allan Hills, Antarctica (Marvin, 1983a,b). During preliminary investigations, Score (1982) described the 31.4 g rock as an unusual looking sample with light clasts up to 8 mm in size, embedded in a black matrix. Mason (1982) classified it as an anorthositic breccia and noted its similarity to lunar highland rocks. Samples of mostly matrix with small clasts were then allocated to 22 investigator teams who reported unambigous evidence that the rock is of lunar highland origin (Lunar Planet. Sci. XIV, 1983; Geophys. Res. Lett. 10, 1983). Additional allocations were later made to a consortium led by K. Keil with the main aim to characterize and possibly date clasts (the latter was not possible, due to small clast sizes) (e.g., Goodrich et al., 1984a,b,c, 1985, in press).

ALHA81005 is a polymict, anorthositic regolith breccia and consists of a matrix of swirly, brown glass and very fine-grained mineral fragments, into which are embedded a variety of lithic clasts (~30 vol.%, Simon et al., 1983a,b; Bischoff and Stoffler, 1984). These include granulitic and impact melt polymict breccias (Korotev et al., 1983a; Kurat and Brandstatter, 1983a,b; Ryder and Ostertag, 1983a,b; Treiman and Drake, 1983a; Warren et al., 1983a,b), an impact melt clast with Mg-suite mineral compositions (derived from a Mg-suite norite?) (Treiman and Drake, 1983a), granoblastic ferroan gabbroic norite (Goodrich et al., 1984c), VLT basalt (Treiman and Drake, 1983a,b), ferroan anorthosites (Drake, 1983; Treiman and Drake, 1983a; Warren et al., 1983a,b; Goodrich et al., 1984c), and probably pristine olivine-pyroxene-troilite assemblage (Warren et al., 1983a,b), ferroan mafic clasts (Treiman and Drake, 1983a; Warren et al., 1983a,b), hyperferroan anorthosites (Ryder and Ostertag, 1983a; Treiman and Drake, 1983a; Goodrich et al., 1984c), and an apatite-rich (~3 vol.%) ferroan anorthositic troctolite (Goodrich et al., in press). The latter two have not been found in Apollo and Luna samples. FMR measurements are consistent with a lunar regolith origin of the matrix (Morris, 1983). INAA-RNAA of matrix and clasts confirm the highland origin of the rock and indicate low incompatible element (KREEP) contents (Boynton and Hill, 1983a,b; Goodrich et al., 1984c; Kallemeyn, 1983; Kallemeyn and Warren, 1983; Korotev et al., 1983a,b; Palme et al., 1983a,b; Verkouteren et al., 1983a,b). Hyperferroan anorthosite clasts are a significant component of the rock, and extreme iron enrichment and high REE abundances indicate that these formed late in the evolution of the magma from which the ferroan anorthosite suite originated (Goodrich et al., 1984 b,c). The apatite-rich ferroan anorthositic troctolite probably formed by magma mixing of a P_2O_5-rich (2.5-3%), quartz-normative, basaltic magma that had crystallized pyroxene, plagioclase and phosphates, with an olivine-saturated magma of lower P_2O_5 content (Goodrich et al., 1984a, in press). Electron and ion microprobe measurements of REE in whitlockite and apatite suggest, however, that crystallization history of the source rock before apatite formation was more complex, or that the original liquid from which it crystallized was unusual and had undergone a complex evolution (Goodrich et al., 1985). Oxygen and silicon isotopic

compositions of an anorthositic clast and adjacent finer-grained breccia are identical to those of lunar highland rocks (Mayeda and Clayton, 1983; Mayeda et al., 1983). The rock contains solar wind-implanted gases in absolute and relative concentrations similar to lunar regolith samples but not to other meteorites (Bogard and Johnson, 1983a,b). Furthermore, a large excess 40Ar component is identical to that in lunar fines implanted from the lunar atmosphere, and large concentrations of cosmogenic 21Ne, 82Kr and 126Xe indicate a total cosmic ray exposure age of $\geq$200 Myrs, nearly all of which took place on the moon. Measurements of 10Be and 26Al imply that the time in space for this rock was much shorter than that of most asteroidal meteorites (Evans and Reeves, 1983; Tuniz et al., 1983a,b), in agreement with Monte Carlo calculations which show that about 70% of objects ejected from the moon and captured by the earth traveled in space $<$ 2 Myrs (Wetherill, 1968). No nuclear particle tracks were found in lithic fragments, indicating that clasts never resided at the very surface of the parent body (Sutton and Crozaz, 1983a,b). If the unusually low natural thermoluminescence is due to thermal decay as a result of parent body impact, then the space exposure time must have been less than 2,500 yrs. (Sutton and Crozaz, 1983a,b). Laboratory and remote sensing data, including X-ray, γ -ray and near - infrared reflectance measurements suggest that the source region of ALHA81005 was the near-side limb or the lunar farside (Pieters, 1983; Pieters et al., 1983). This conclusion is supported by trace element studies (the lack of KREEP; e.g. Palme et al., 1983a,b; Kallemeyn and Warren, 1983) and petrologic studies, which support an origin away from heretofore sampled regions of the moon (e.g., Warren et al., 1983a,b,c). The very young crater Giordano Bruno has been suggested as a possible source (Ostertag and Ryder, 1983; Ryder and Ostertag, 1983a). Experimental and computer modeling data show that rocks can be ejected by impact from the moon and would survive impact acceleration (Gault, 1983; Melosh, 1983; Nyquist, 1983; O'Keefe and Ahrens, 1983). The recent discovery of two additional lunar meteorites, Yamato 791197 and 82192 (Yanai and Kojima, 1984; Yanai et al., 1984) opens up a host of important questions, most notably whether the three lunar meteorites represent three, or fewer, separate impact events on the moon. These questions must be addressed by detailed comparative studies of the three rocks.

References:

Bischoff, A. and Stoffler, D., LPS XV, 62-63, 1984. Bogard, D.D. and Johnson, P., GRL 10, 801-803, 1983a; LPS XIV, Spec. Sess., 1-2, 1983b. Boynton, W.V. and Hill, D.H., GRL 10, 837-840, 1983a; LPS XIV, Spec. Sess., 12-13, 1983b. Drake, M.J., LPS XIV, 164, 1983. Evans, J.C. and Reeves, J.H., LPS XIV, Spec. Sess., 6-7, 1983. Gault, D.E., LPS XIV, Spec. Sess., 8-9, 1983. Goodrich, C.A., Taylor, G.J. and Keil, K., LPS XV, 314-315, 1984a; Proc. 15th LPSC, part 2, JGR, Suppl. (in press). Goodrich, C.A., Taylor, G.J., Keil, K., Boynton, W.V. and Hill, D.H., LPS XV, 316-317, 1984b; Proc. 15th LPSC, part 1, JGR, Suppl., 89, C87-C94, 1984c. Goodrich, C.A., Taylor, G.J., Keil, K., Reed, S.J.B., Boynton, W.V. and Hill, D.H., LPS XVI, 1985. Kallemeyn, G.W., LPS XIV, Spec. Sess., 10-11, 1983. Kallemeyn, G.W. and Warren, P.H., GRL 10, 833-836, 1983. Korotev, R.L., Lindstrom, M.M., Lindstrom, D.J. and Haskin, L.A., GRL 10, 829-832, 1983a. Korotev, R.L., Haskin, L.A. and Lindstrom, M.M. LPS XIV, Spec. Sess., 12-13, 1983b. Kurat, G. and Brandstatter, F., GRL 10, 795-798, 1983a; LPS XIV, Spec. Sess., 14-15, 1983b. Laul, J.C., Smith, M.R. and Schmitt, R.A., GRL 10, 825-828, 1983a; LPS XIV, Spec. Sess., 16-17, 1983b. Marvin, U.B., GRL 10, 775-778, 1983a; LPS XIV, Spec.

Sess., 18-19, 1983b. Mason, B., in "Antarctic Meteorite Newsletter" 5, No. 4, Nov. 1982. Mayeda, T.K. and Clayton, R.N., LPS XIV, Spec. Sess., 20, 1983. Mayeda, T.K., Clayton, R.N. and Molini-Velsko, C.A., GRL 10, 799-800, 1983. Melosh, H.J., LPS XIV, Spec. Sess., 21-22, 1983. Morris, R.V., GRL 10, 807-808, 1983. Nyquist, L.E., LPS XIV, 574-575, 1983. O'Keefe, J.D. and Ahrens, T.J., LPS XIV, 578-579, 1983. Ostertag, R. and Ryder, G., LPS XIV, Spec. Sess., 23-24, 1983. Palme, H., Spettel, B., Weckwerth, G. and Wanke, H., GRL 10, 817-820, 1983a; LPS XIV, Spec. Sess., 25-26, 1983b. Pieters, C.H., LPS XIV, Spec. Sess., 27-28, 1983. Pieters, C.M., Hawke, B.R., Gaffey, M. and McFadden, L.A., GRL 10, 813-816, 1983. Ryder, G. and Ostertag, R., GRL 10, 791-794, 1983a; LPS XIV Spec. Sess., 29-30, 1983b. Score, R., in "Antarctic Meteorite Newsletter" 5, No. 4, Nov. 1982. Simon, S.B., Papike, J.J. and Shearer, C.K., GRL 10, 787-790, 1983a; LPS XIV, Spec. Sess., 31-32, 1983b. Sutton, S.R. and Crozaz, G., GRL 10, 809-812; LPS XIV, Spec. Sess., 33-34, 1983b. Treiman, A.H. and Drake, M.J., GRL 10, 783-786, 1983a; LPS XIV, Spec. Sess., 35-36, 1983b. Tuniz, C., Pal, D.K., Moniot, R.K., Savin, W., Kruse, T.H., Herzog, G.F. and Evans, J.C., GRL 10, 804-806, 1983a; LPS XIV, Spec. Sess., 37-38, 1983b. Verkouteren, R.M., Dennison, J.E. and Lipschutz, M.E., GRL 10, 821-824, 1983a; LPS XIV, Spec. Sess., 39-40, 1983b. Warren, P.H., Taylor, G.J. and Keil, K., GRL 10, 779-782, 1983a; LPS XIV, 828-829, 1983b; LPS XIV, Spec. Sess., 41-42, 1983c. Wetherill, G.W., in "Origin and distribution of the elements" (L.H. Ahrens, ed.), Pergamon, 423, 1968. Yanai, K. and Kojima, H., 9th Symp. Antarctic Meteorites, NIPR, 42-43, 1984. Yanai, K., Kojima, H. and Katsushima, T., 47th Meteoritical Soc. Meet., Albuquerque, Q6, 1984.

METEORITIC BRECCIAS

KEIL, K.
Dept. of Geology, Institute of Meteoritics, Univ. of New Mexico, Albuquerque, NM. 87131, USA.

During the past 15 years, comparative planetology has taught us that the surfaces of many planets and moons have been shaped by impacts, resulting in the formation of breccias (clastic rocks composed of angular, broken rock and mineral fragments, embedded into a finer-grained matrix). Modeling and observational data suggest that many asteroids (parent bodies of most meteorites) have also been severely affected by impacts and have developed regoliths, a fact confirmed by the abundance of various breccia types among nearly all meteorite classes (e.g., Keil, 1982, and references therein). Meteoritic breccias have been studied extensively because they shed light on the nature of regolith processes on small parent bodies, (including regolith thickness, age, depths of burial and excavation, nature of lithification processes); on impact and cratering mechanics including disruption of parent bodies and gravitational reassembly of debris; on abundance of crushed, melted and fractionated material; on heat sources that metamorphosed rocks prior to and after breccia agglomeration; on number of asteroidal parent bodies and internal and horizontal stratigraphy; and on comparison of meteoritic and lunar breccias.

Regolith breccias formed by shock-lithification of unconsolidated, fragmental debris that originated by repeated impacts on or near the surfaces of parent bodies. Some, but not all, have characteristic light-dark structures; they contain solar wind-implanted noble gases, solar flare tracks, impact melt and exotic clasts. Fragmental breccias consist of clastic material (rock and mineral fragments, including melt-rock clasts) but are devoid of solar wind-implanted gases. Thus, they did not reside in a regolith for any length of time and probably involve few impacts or possibly formed by disruption of parent bodies and gravitational reassembly of debris. Impact melt breccias have igneous matrices; some are totally igneous, whereas others contain unmelted, clastic material. Still others consist of black, shock-melted veins that cut through unmelted, generally light-colored clastic material. Granulitic breccias are metamorphosed fragmental breccias and consist of rock and mineral fragments with granulitic and granoblastic textures. They must have been buried to considerable depth after brecciation to account for the texture. Primitive breccias are composed almost entirely of primitive components, such as well-preserved chondrules, opaque and recrystallized fine-grained silicate matrix, and rock clasts. Some contain no equilibrated material and may have formed before peak metamorphism, i.e., may be accretionary.

Conclusions: 1. Among meteorites, textural analogs to lunar regolith, fragmental, impact melt and granulitic breccias exist. Primitive breccias (some accretionary) also exist, but not among differentiated meteorites and lunar rocks. 2. Meteoritic breccias formed by repeated impacts in regoliths; single (or a few) major impacts; disruption and reassembly of parent bodies; and possibly accretion. 3. Disruption and gravitational reassembly of H-chondrite and enstatite achondrite parent bodies is a documented process for excavation from, and burial to, great depth. 4. Shock melting of interstital grains mostly $<100\ \mu m$ in size is responsible for lithification of loose regolith into regolith breccias on meteorite parent bodies. 5. Although most materials

in meteoritic breccias are ancient, regolith and breccia formation occurred on meteorite parent bodies throughout the history of the solar system. 6. Except for meteorites of the eucrite-howardite-diogenite parent body clan, polymict breccias are rare, suggesting that many meteorite parent bodies of distinct chemical and mineralogic compositions existed. 7. Gas-rich regolith breccias with homogeneous matrix and clast minerals indicate that large, petrologically uniform areas must exist on parent bodies. Some regoliths may have been largely of local origin, with little admixture of material of different petrologic grade from laterally and/or vertically distant sources. 8. Equilibrated clasts in gas-rich chondritic regolith breccias were equilibrated in different locations prior to breccia formation; breccias were not subsequently heated above 650 K. 9. Host material of types 4-6 ordinary chondrite fragmental breccias (most H) with unequilibrated melt rock clasts was metamorphosed prior to breccia formation, early in the history of the solar system; those with equilibrated melt rock clasts (most L, LL) were metamorphosed after breccia agglomeration. 10. 15% of seemingly unbrecciated types 4-6 ordinary chondrites contain rare olivine and low-Ca pyroxene objects (single grains, chondrules, clasts) with Fe/Fe+Mg ratios quite different from their hosts. This suggests that these chondrites are breccias that formed after peak metamorphism, not that olivines and pyroxenes were never homogenized during metamorphism. Most ordinary chondrites are probably breccias, but their brecciated nature is often difficult to recognize. 11. Cooling rates of Ni,Fe grains in H6 clasts in the Cangas de Onis gas-rich regolith breccia are coherent but vary from clast to clast between 8-80 K/My, indicating that highly metamorphosed material was buried at different depth by the time it cooled through 650K. This, combined with the lack of a correlation between cooling rates and petrologic grade of H chondrites, is inconsistent with the onion shell model but favors the metamorphosed-planetesimal model for its parent body.

Reference:
Keil, K, in "Workshop on lunar breccias and soils and their meteoritic analogs", LPI, Techn. Rep. 82-02, 65-83, 1982.

Wednesday, March 27, 1985

0900 - 1645	Symposium, Auditorium
1645 - 1730	Special lecture Dr. Roy S. Clarke, Jr. (Smithsonian Institution)

Search for the Extra-terrestrial Materials in Deep-sea Sediments

Sachiko Amari[1][2], Minoru Ozima[2]

(1) Division of Science of Materials, The Graduate School of Science and Technology, Kobe University

(2) Geophysical Institute, Faculty of Science, University of Tokyo

It is well established that the $^3He/^4He$ ratio of some deep sea sediments(up to 1×10^{-4}) are higher than that is observed in common terrestrial materials(10^{-5} - 10^{-8}) [1) 2) 3)], and the high $^3He/^4He$ ratios are now generally believed to be caused by fallout of cosmic dust. In order to identify the extra-terrestrial materials which have high $^3He/^4He$ ratio, we made magnetic separation of some deep sea sediments. The magnetic separates are then subjected to He isotopic analysis and to thermomagnetic analysis.

A deep sea sediment sampled by a piston corer from the Pacific Ocean(26° 00.8'N, 150° 00.0'E) was separated into magnetic(M) and non-magnetic(NM) fractions by a hand magnet. Then magnetic fraction(M) was further separated into three fractions(M1, M2, M3) according to the magnetic intensity(M1 > M2 > M3). He isotopic ratio and He content were measured for each fraction. The highest $^3He/^4He$ ratio (2×10^{-4}) as well as the highest He content (^3He : 4×10^{-9} cm^3STP/g) were observed for M1. We conclude that the extra-terrestrial materials are concentrated in the most magnetic fraction. Stepwise heating(520,690,770,860,950,1040,1140,1700°C) was applied for

M1, the $^{3}He/^{4}He$ ratios are almost constant (2×10^{-4}) for all the temperature fractions. It is surprising to find that a considerable fraction(10 %) of He was extracted even at 950 C. From the stepwise heating, we estimated the activation energy of the He diffusion which is about 16 Kcal/mol.

Thermomagnetic analysis of M1 gives a Curie temperature of about 540°C, suggesting that M1 is titanomagnetite. Considering the very high He content($\leq 10^{-1} cm^{3} STP/g$) in cosmic dust[4], extra-terrestrial materials in M1 could be less than 1 % ,and more than 99 % of M1 should be terrestrial origin. Titanomagnetite with high Curie temperature(>500°C) is the major ferromagnetic minerals in deep sea sediments. Extra-terrestrial material could be magnetic component oter than the titanomagnetite which we do not know at present. Further work should be needed to identify the ferromagnetic component which is responsible for high $^{3}He/^{4}He$ ratio.

References:

1) Merrihue C., Ann.N.Y.Acad.Sci. 119,351 (1964)

2) Krylov A.Ya et al., Geocem.Int. 10,202 (1973)

3) Ozima M. et al., Nature 311,448 (1984)

4) Rajan R.S. et al., Nature 267,133 (1984)

POSITIVE CERIUM ANOMALY OF LUNAR 14310 AND ALH-765: EXAMINATION BY $^{138}Ce/^{142}Ce$

Tanaka, T.*, Shimizu, H.**, Shibata, K.* and Masuda, A.**

*Geological Survey of Japan, Higashi 1-1-3, Yatabe, Ibaraki 305 Japan
**Laboratory for REE Microanalysis, Dept. of Chemistry, Fac. of Science, The University of Tokyo, Hongo, Tokyo 113 Japan

Positive cerium anomaly of some lunar samples was reported in 1972 [1]. However, REE research groups other than ours did not pay much attention to the Ce anomaly, probably due to the fact that the anomaly is fairly small (several to ten percent) and highly reliable La, Ce and Nd abundances are required to identify the anomaly. Recently, we succeeded in employing the $^{138}La \xrightarrow{\beta-} {}^{138}Ce$ isotope decay as a tool for isotope geochemistry [2]. For example, positive Ce anomaly on Antarctic achondrite[3] was defined as a terrestrial alteration effect [4][5][6].

Here, $^{138}Ce/^{142}Ce$ as well as $^{143}Nd/^{144}Nd$, $^{87}Sr/^{86}Sr$ and REE abundances are determined for the lunar sample 14310 which was examined previously and found to have 13 % of positive Ce anomaly [1]. The results and our previous results on ALH-765 are discussed together. A sliced 5.08 gr. chip(14310,578) supplied by the curatorial office was lightly crushed in a tungsten-carbide mortar to pass through a #100(149 μm) sieve. A part of crushed sample was used as a "whole rock" split and another part was resieved to provide three size fractions, # 100-200(149-74 μm), # 200-400 (74-37 μm) and smaller than # 400 (37 μm). Finer fraction than 37 μm was put into a small beaker containing acetone and stirred in the medium. The ultra-fine and powdery materials hard to settle were also separated (approximately less than 20 μm). In advance of the magnetic separations, highly magnetic materials were taken out and also analysed. Two plagioclase dominant and two pyroxene dominant fractions were separated from two larger grain size fractions by using an isodynamic separator (Fig. 1).

Fig.1

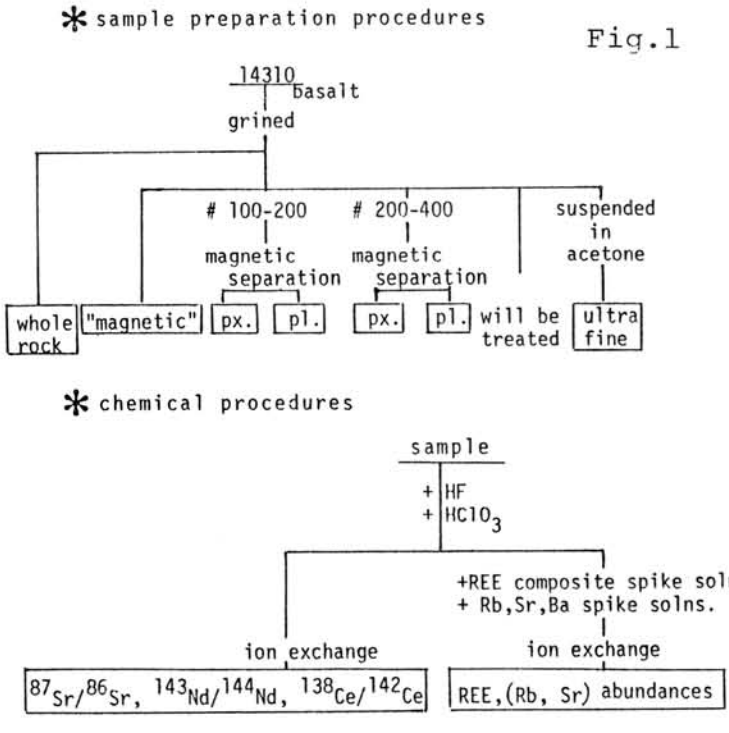

The experimental procedures used are almost identical to those of Tanaka and Masuda [2]. To get a good intensities for Ce isotopes (2-3 volt output of $^{142}Ce^{16}O^+$ for more than 24 hours), small improvements are done, but the $^{138}Ce/^{142}Ce$ value for Johnson Matthey reagent is not altered (0.0228553 ± 13, a typical single measurement after modification). $^{138}Ce/^{142}Ce$, $^{143}Nd/^{144}Nd$ and $^{87}Sr/^{86}Sr$ ratios were measured and were normalized against $^{136}Ce/^{142}Ce = 0.01720$, $^{146}Nd/^{144}Nd = 0.7219$ and $^{86}Sr/^{88}Sr = 0.1192$, respectively.

In the following discussions, $\lambda_{\beta}{}^{138}La = 2.58 \times 10^{-12} yr^{-1}$, $\lambda_{EC}{}^{138}La = 4.59 \times 10^{-12} yr^{-1}$, $\lambda_{\alpha}{}^{147}Sm = 6.54 \times 10^{-12} yr^{-1}$ and $\lambda_{\beta}{}^{87}Rb = 1.42 \times 10^{-11} yr^{-1}$ are used.

Leedey-normalized REE patterns are shown in Fig. 2. The REE pattern of whole rock sample currently analysed is quite identical with our former result [1], except a little difference in its absolute REE concentration. Although the spike solution used currently was prepared independently after the previous analysis, agreement between two patterns is very good. Positive Ce anomaly is also reconfirmed, but 8.2% anomaly of the whole rock is smaller than our previous analysis (13 %). It has also been pointed out [1] that the extent of Ce anomaly is variable from site to site. Also the extent of positive Ce anomaly is different among minerals as shown in Table 1.

Rb-Sr, Sm-Nd and La-Ce isochron plots are shown in Figs. 3, 4 and 5, respectively. Former two ages are in good agreement with each other, though Sm-Nd age includes a large uncertainty. The 3.8 Ga age obtained here also agrees with Rb-Sr [7][8], K-Ar [9] and U-Th-Pb [8] ages which were obtained by other laboratories. $^{143}Nd/^{144}Nd$ initial ratio of the 14310 is identical with that of a different KREEP basalt 15386 [10]. $^{138}La/^{138}Ce$ variation of the separated mineral fractions is not large enough to give a good La-Ce isochron age (Fig. 5).

Table 1

Sample	$^{138}Ce/^{142}Ce \pm 2\sigma_m$		Ce-anomaly (%)*
whole rock	0.0228484	30	8.2
pyroxene 1	0.0228485	16	8.1
pyroxene 2	0.0228482	12	9.0
plagio. 1	0.0228498	13	4.5
plagio. 2	0.0228502	16	5.4
ultra-fine	0.0228494	14	7.8
"magnetic"	—		9.7

* relative to "regular" values estimated from rectilinear lines fitting La, Nd and Sm.

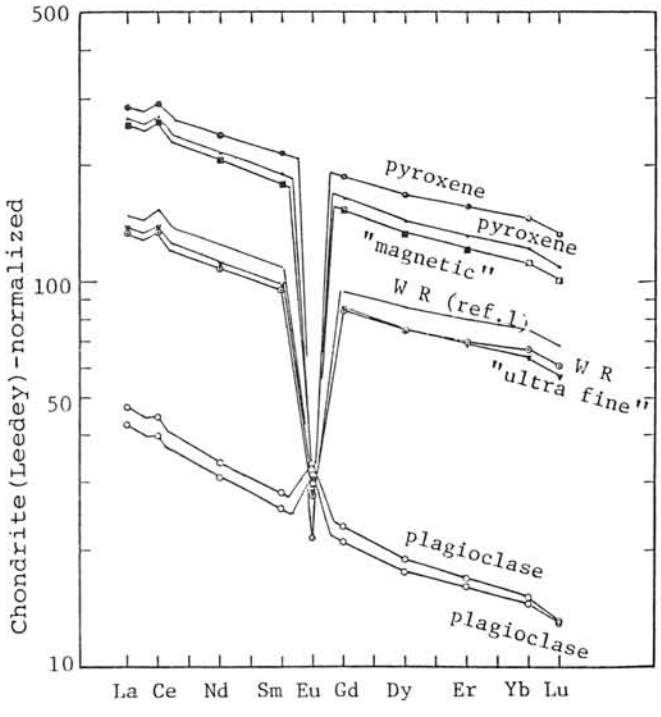

Fig. 2

Chondrite(Leedey) -normalized rare earth pattern of 14310 and separated minerals.

Assuming that the 14310 was derived from "chondritic" parent material and that the Ce there lied on a rectilinear line fitting La, Nd and Sm on the REE pattern (i.e. Ce-normal pattern, $^{138}La/^{142}Ce = 0.00340$) since 3.8 Ga ago, then present $^{138}Ce/^{142}Ce$ values of the 14310 is calculated to be 0.022856 (see Fig. 6). But all of the $^{138}Ce/^{142}Ce$ values obtained (Table 1) are significantly smaller than the 0.022856. This means that the actual La/Ce ratio has been smaller than the value of Ce-normal pattern during fairly long time. Calculated $^{138}Ce/^{142}Ce$ growth curve using the measured La/Ce ratio is shown in Fig. 6. The curve does not meet with chondritic grouth curve. This leads us to a conclusion that the positive Ce anomaly of the 14310 was brought into being at a period predating 3.8 Ga ago.

As shown in Table 1, the extent of positive Ce anomaly of 14310 is different among the constituent minerals. Pyroxene has a greater Ce anomaly than plagioclase. The Ce anomaly can not be explained by our current knowledge on REE fractionation during *usual* magmatism.

Two alternatives may be conceivable on the Ce anomaly. One is to invoke an exotic microcomponent which might have bombarded the lunar surface rocks and have been incorporated preferentially into pyroxene. Another is an indigeneous alteration effect due to the chemical activity of H_2O in any state. It is shown that some Antarctic meteorites suffered from a certain

Fig. 3

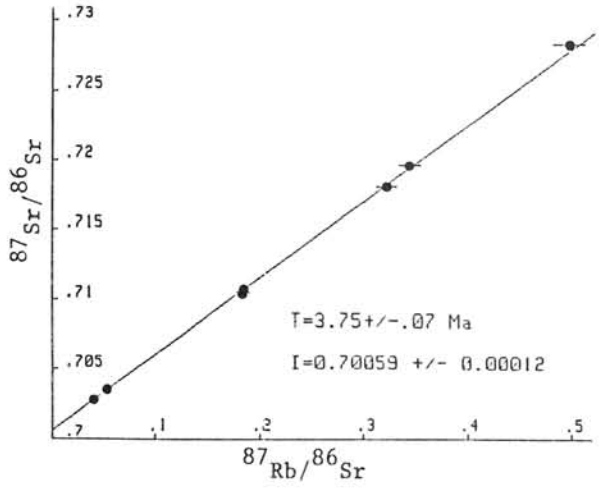

Rb-Sr (Fig. 3)
Sm-Nd (Fig. 4)
La-Ce (Fig. 5)
isochron plots of 14310

Fig. 4

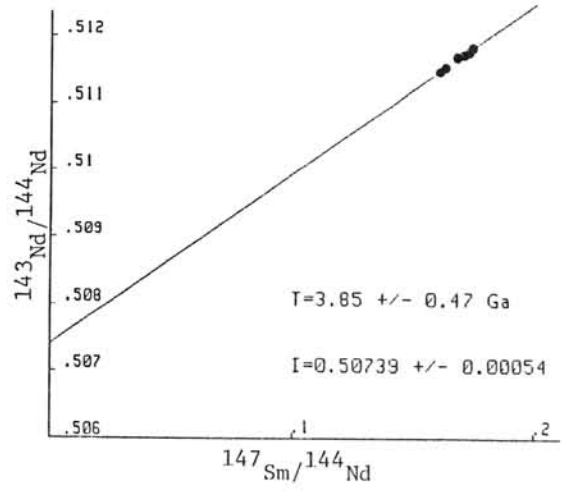

Fig. 5

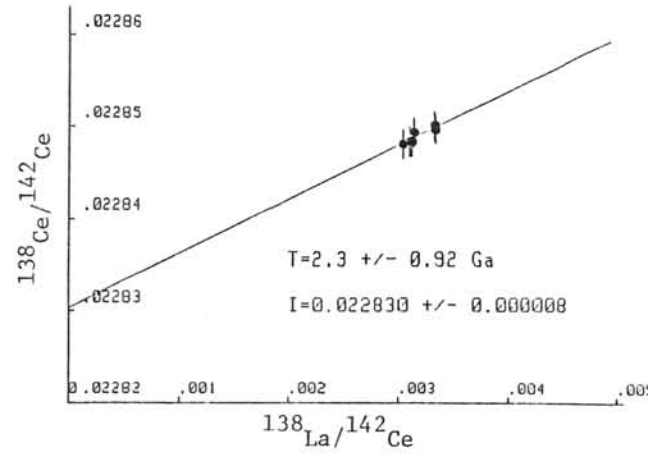

alteration in ice which yields large positive Ce anomaly especially for pyroxene and for outer part of Antarctic meteorite body [4][5]. From the analogy with the alteration on the Antarctic meteorite, many lunar rocks with Ce anomaly are considered to have been subjected to some oxic (hydrothermal / aquaous / ice) alteration in the earlier stage of the lunar history, than 3.8 Ga ago. Then, H_2O escaped quickly from the moon and hydrated minerals were completely modified to unhydrous, reduced minerals. Mare basalt with curved REE pattern which formed at a rather later dried stage has no Ce anomaly [11]. It is worth pointing out that some ice is expected to remain even today in the bottom of the craters near the lunar poles [12].

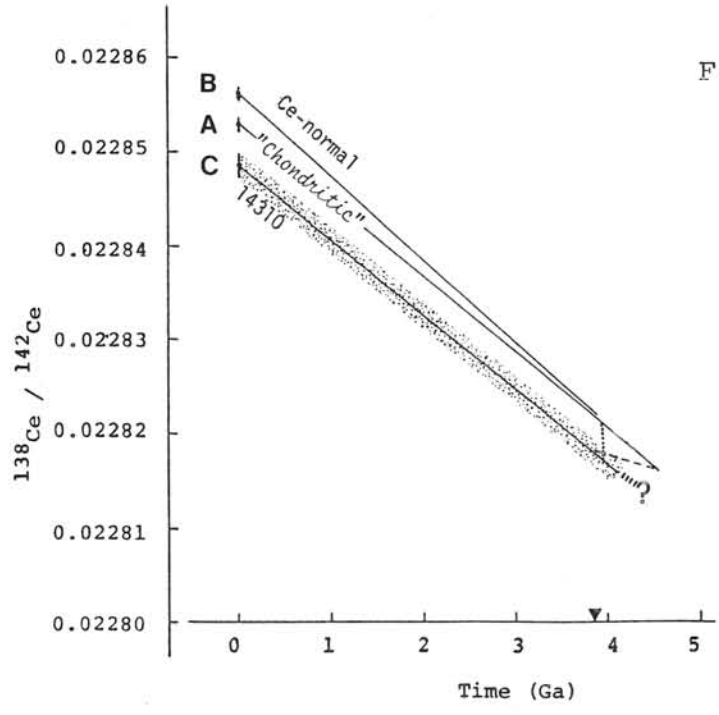

Fig. 6

A: growth curve of "chondritic" material

B: growth curve of "Ce-normal" 14310 which derived from chondritic parent material at 3.8 Ga ago

C: growth curve of 14310 calculated using measured (Ce-anomalous) La/Ce ratio.

'''' ---- .... conceivable growth curves before 3.8 Ga ago

References

[1] Masuda, A., Nakamura, N., Kurasawa, H. and Tanaka, T. (1972) Proc. 3rd. Lunar Sci. Conf. 2, p. 1307.

[2] Tanaka, T. and Masuda, A. (1982) Nature 300, p. 515.

[3] Nakamura, N., Masuda, A., Coffrant, D. and Tatsumoto, M. (1979)Meteoritics 14, p. 492.

[4] Tanaka, T. Shibata, K. and Masuda, A. (1983) Abst. 8th Symp. Antarctic Meteorites p. 71.

[5] Shimizu, H., Masuda, A. and Tanaka, T. (1983) Proc. 8th Symp. Antarctic Meteorites, p. 341.

[6] Shimizu, H., Tanaka, T. and Masuda, A. (1984) Nature 307, p. 251.

[7] Papanastassiou, D.A. and Wasserburg, G.J. (1971) EPSL 12, p. 36.

[8] Tatsumoto, M., Hedge, C.E., Doe, B.R. and Unruh, D.M. (1972) Proc. 3rd. Lunar Sci. Conf. 2, p.1531.

[9] Turner, G. Huneke, J.C., Podosec, F.A. and Wasserburg, G.J. (1971) EPSL 12, p. 19.

[10]Carlson, R.W. and Lugmair, G.W. (1979) EPSL 45, p. 123.

[11]Nakamura, N. (1974) Geochem. J. 8, p. 67.

[12]Watson, K., Murray, B.C. and Brown, H. (1961) JGR 66, p. 3033.

MAGNESIUM ISOTOPE ABUNDANCE IN ALH-77304 AND ALH-77003

Okano, Jun*, Ueda, Chiaki** and Nishimura, Hiroshi*
*Institute of Geological Sciences, college of General Education Osaka University
**Department of Physics, Faculty of Science, Osaka University

Isotopic ratios of $^{24}Mg/^{25}Mg$ and $^{26}Mg/^{25}Mg$ have been measured for Mg-rich portions of ALH-77304(LL3) and ALH-77003 (C3) with an ion microprobe mass spectrometer. The magnesium isotope ratios for the metearites were compared with those for a laboratory standard of terrestrial olivine(FO).

The results for ALH-77304 and for ALH-77003 are shown in Fig. 1 and Fig. 2, respectively. The data for FO in each run were taken as the origins of the figures. The typical error of $\delta(24/25)^*$ and $\delta(26/25)^*$, $2\sigma_m$, for each meteorite data was 2 ‰. As for ALH-77304, among the thirty seven measured portions, thirty three showed positive $\delta(24/25)$ compared with the data for FO. The positive data points were distributed up to 11 ‰ and the mean value for all the data was about 5 ‰. The data poins for ALH-77003 also showed a tendency to distribute in the positive $\delta(24/25)$ area. The maximum δ value was 14 ‰, and the mean for all the δ values was about 3 ‰. From these results, it would be concluded that the most measured portions of ALH-77304 contained the excess of ^{24}Mg and that many measured portions of ALH-77003 also contained the excess of ^{24}Mg. Together with the previouly reported results [1-3] for Y-74191(L3) and ALH-77278

---

* $$\delta(m/25) = \left[\frac{(^{m}Mg/^{25}Mg)sample}{(^{m}Mg/^{25}Mg)lab.std.} - 1 \right] \times 1000 \quad (m=24,26)$$

(LL3) and Allende (C3), the excess of ^{24}Mg found for ALH-77304 (LL3) and ALH-77003(C3), would be an evidence to support the hypothesis that the early solar nebula was isotopiclly heterogeneous due to the injection of materials which contained now-extinct ^{26}Al and were rich in ^{16}O and ^{24}Mg.

Both Fig. 1 and Fig. 2 show the tendency that the data points fall in the positive areas of $\delta(26/25)$. The mean value are 1.5 ‰ for ALH-77304 and 3 ‰ for ALH-77003. Futher study for various meteorites will be necessary to decide whether these results are ascribable to an actual existence of ^{26}Mg excess.

In order to examine the interference of molecular and multiply-charged ions with magnesium isotope ions and to investigate correlations between the δ values and the elemental composition, mass spectra for all the analyzed portions of the meteorites were taken from mass 12 to 60. Figure 3 shows the correlation between $\delta(24/25)$ and $^{28}Si^+/^{24}Mg^+$ for ALH-77003. It can be seen that there is a weak correlation between them. The correlation shows that the materials with the excess of ^{24}Mg are preferentially contained in the portions with a low Si/Mg ratio. This result is consistent with those for Y-74191 and ALH-77278. However, no correlation between $\delta(24/25)$ and $^{28}Si^+/^{24}Mg^+$ was found for ALH-77304. The correlation may be changed by the extent of thermal metamorphism suffured through the history.

References

1) H. Nishimura and J. Okano, Mem. Natl Inst. Polar Res., Spec. Issue, 20, 229 (1981)

2) H. Nishimura and J. Okano, Mem. Natl Inst. Polar Res., Spec. Issue, 25, 171 (1982)

3) H. Nishimura and J. Okano, Mem. Natl Inst. Polar Res., Spec. Issue, 30, 332 (1983)

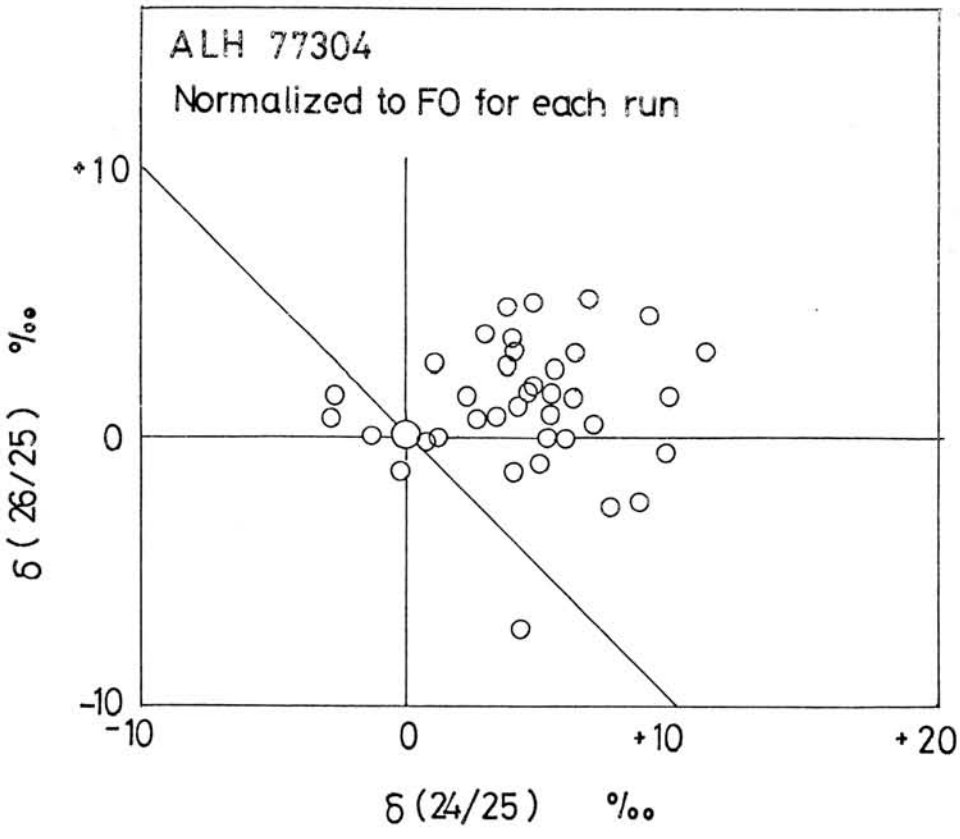

Fig.1
Three isotope plot of magnesium for ALH-77304. (LL3)

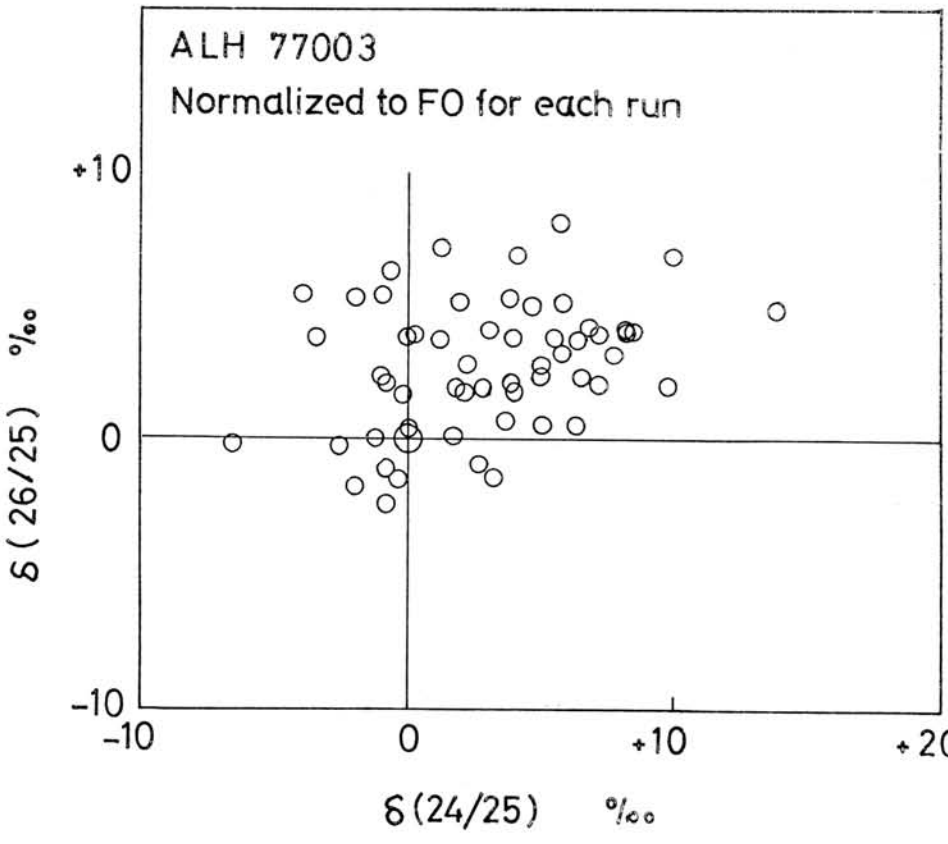

Fig.2
Three isotope plot of magnesium for ALH-77003 (C3)

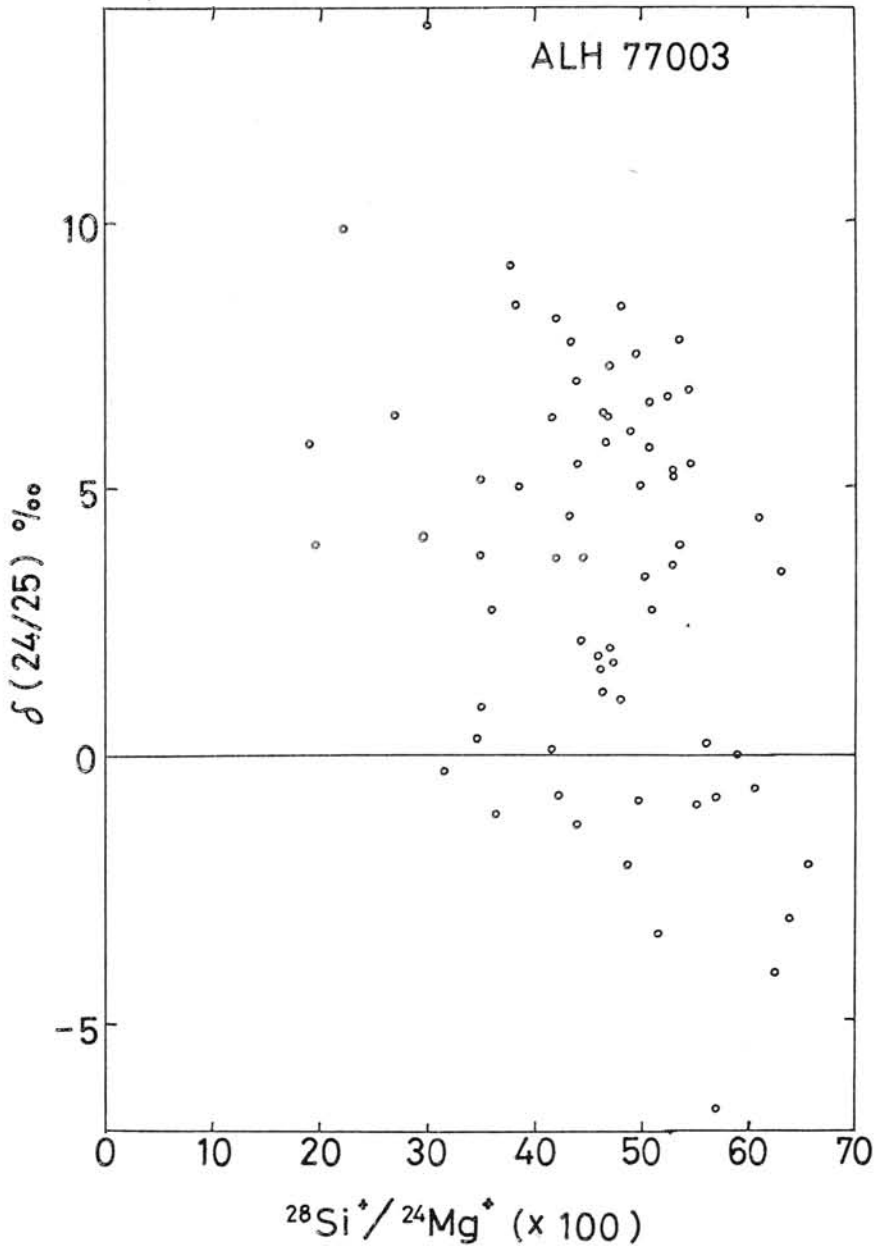

Fig.3 Correlation between $\delta(24/25)$ and $^{28}Si^{+}/^{24}Mg^{+}$ for all the analyzed portions in ALH77003.

59—1

REE Abundances in Several Diogenites

Kazuya Takahashi, Hiroshi Shimizu and Akimasa Masuda
Department of Chemistry, The University of Tokyo

The diogenites have been known to have the wide REE (rare-earth elements) variation in absolute concentration and in mutual abundance ratio, in spite of their narrow range for major element composition. We determined REE abundances precisely for several diogenitic samples (two matrix samples and two coarse-grained Opx-clasts in Johnstown, whole rock of Roda, and the clast composed of orthopyroxene in the Kapoeta howardite) by mass spectrometric isotope dilution method.

Fig. 1 shows the REE patterns of four Johnstown samples and Fig. 2 shows those of the other diogenites and the clast in Kapoeta. From Figs.1 and 2, one can classify the observed REE patterns roughly into two groups.

A group (a), to which two Opx-clasts in Johnstown and Opx-clasts in Kapoeta belong, shows the REE pattern with a large negative Eu anomaly and depletion in the light REE, particularly characterized by the concave curvature for the light REE span (La-Nd). These curves have the minimum position between Ce and Nd. We consider that these features are common to the diogenites which are presumably of cumulate origin, and that the shape of these patterns reflects orthopyroxene partition coefficients.

In view of the REE abundance level and the features for the light the REE, the samples other than mentioned above (group (a)), all showing relatively flat pattern with smaller Eu anomaly than that of the above group, would be subdivided into two groups, the group (b) involving matrix-1 of Johnstown, Roda and Y-75032 and the group (c) involving matrix-2, Y-74010 and ALH-77256. The latter group (c) shows slightly curved pattern for the light REE (La-Sm).

Fig.3 is a plot of the normalized value ratios of Lu to Gd versus those of Sm to Nd. The former ratio represents the slope of the pattern for the heavy REE and the latter that for the lighter REE. As shown in Fig. 3, the points of each group fall on its characteristic line in order of REE abundance; The order of integers 1-3 corresponds to that of absolute abundances. These observations suggest that various systems of differentiation might have formed the diogenite assembly, or that one diogenite group might bring into being other diogenite group(s). As one of possibilities, it is possible to consider as follows: The group (c) belongs to a series of the primarily differentiated material within the parent body, and from this group the group (a) was derived as a solid phase by fractional crystalization, then the group (b) as a residual liquid phase. Fig. 4 is an example of the calculation based on this assumption; the initial material had the REE pattern which was like that of ALH-77256 (group (c)), and the surface equilibrium held good during the fractional crystalization. And the partition coefficiets are assumed to be the value as represented by the ratio of the matrix-1 to the Opx-clast in Johnstown. Though the calculated patterns for the solid

phase fit those of group (a) well, the patterns for the liquid phase are different from those of group (b) for the light REE. In order to examine this hypothesis thoroughly, practical and precise orthopyroxene partition coefficients, which is applicable to this system, will be required. Further, there remain some questions, such as the relationship between the diogenitic initial material and eucrite or howardite. For the present, we presume as follows: Most of the diogenites were derived by two or more stages of differenciations. Perhaps the "primary" diogenites had some genetic relationship with the eucrites (or howardites), and the secondary diogeites were formed by the following stage, controlled by the different partition coefficients from those of the first stage. However we think that the propriety of the dividing between the group (b) and the group(c) is still disputable. It is hoped that further studies will help us decipher still more or less ambiguous aspects concerning the genetic relations among diogenitic materials.

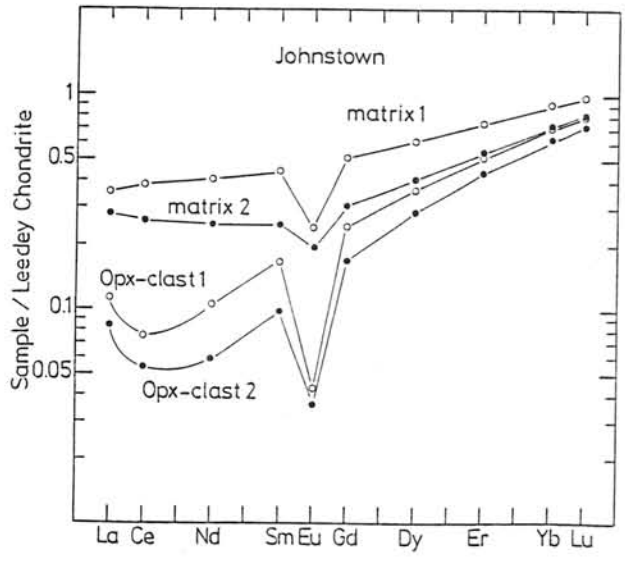

Fig. 1 REE patterns of four Johnstown samples

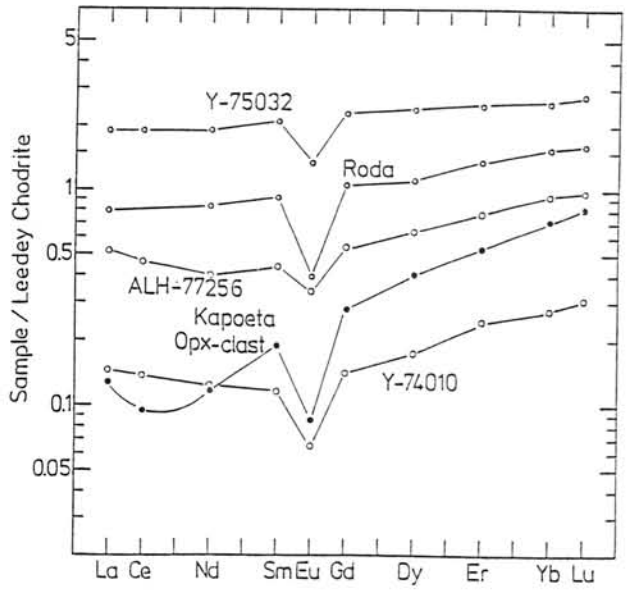

Fig. 2 REE patterns of some diogenites and a clast in Kapoeta
Data on Y-75032 and ALH-77256 are from Shimizu et al., (1981) and data on Y-74010 from Masuda et al., (1979)

Fig. 3 A plot of the normalized value ratios of Lu to Gd versus those of Sm to Nd

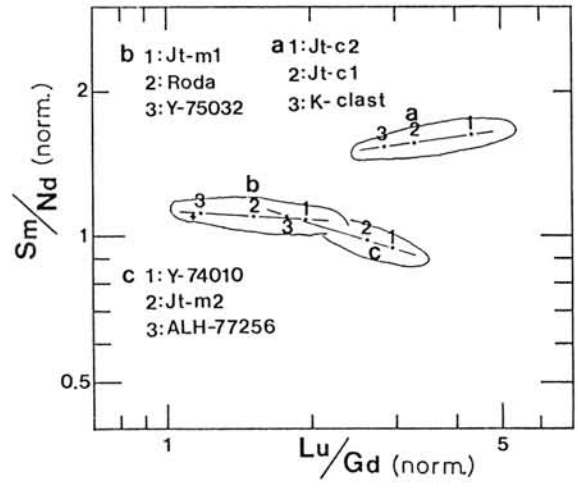

Fig. 4 Calculated REE patterns for diogenites

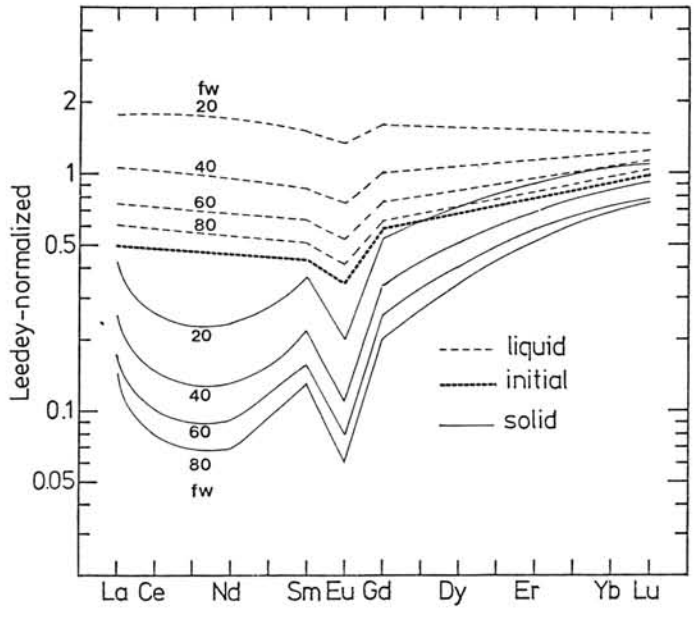

References:

Masuda, A., Tanaka, T., Shimizu, H., Wakisaka T. and Nakamura, N. (1979): Rare-earth geochemistry of Antarctic diogenites. Mem. Natl Inst. Polar Res., Spec. Issue, 15, 177-188

Shimizu, H. and Masuda, A. (1981): REE, Ba, Sr and Rb abundances in some unique Antarctic achondrites. Mem. Natl Inst. Polar Res., Spec. Issue, 20, 211-220

REE patterns of eucrites and their genetic implications

Hiroshi Shimizu and Akimasa Masuda

Deptartment of Chemistry, Faculty of Science, The Univ. of Tokyo

Eucrite is one of the most common achondrites and several models on the origin and evolution of eucrite have been proposed. Two conflicting models of fractional crystallization and partial melting persist on the eucrite evolution (Basaltic Volcanism Study Project, 1981). Rare earth element (REE) patterns of eucrites have been interpreted from both standpoints of fractional crystallization and partial melting, individually. In this study, we will report highly precise abundance data of REE, Ba and Sr in eucrites and will discuss the evolution of eucrite on the basis of the precise REE abundance data and strict examination of REE pattern. At the same time, we will add new abundance data of REE, Ba and Sr in chondrites to reexamine the chondritic normalization value for REE.

Eucrite samples used in this study are the Juvinas, Pasamonte, Cachari, Stannern and Antarctic eucrites. The Antacrtic eucrites analyzed are Y-74450,63,D+G; Y-75015,20,E+F; Y-75011,73; Y-790007,61,F; Y-75011,84,D-1 and Y-790007,61,E-4. The last two samples are eucrite clasts in polymict eucrites. The other samples of the Antarctic eucrite are matrix in polymict eucrite. Mineralogical and Nd-Sr-isotopical studies on some of the same Antarctic eucrites have been partly published already (Takeda et al., 1983a and b; Wooden et al., 1983). Chondrite samples used in this study are Leedey(L6), Holbrook(L6), Khohar(L3) and Jilin(H4). REE, Ba and Sr abundances in the eucrites and chondrites have been measured by the mass-spectrometric stable isotope dilution method. The precisions of analyses are believed to be below 0.5% in most cases.

Some sets of REE abundance suites in chondrite have been used for normalization of REE abundances in geo- and cosmochemical samples. We have employed the REE abundances in the Leedey chondrite reported by Masuda et al. (1973). In the present study, however, we adopt the newly determined REE abundances of the Leedey chondrite. (We designate these new REE abundance data for the Leedey chondrite as the "Leedey-84".)

Fig. 1 shows the REE-Ba-Sr patterns of eucrites normalized by the "Leedey-84" REE-Ba-Sr abundances. All patterns show relatively flat REE patterns having Eu anomalies. In the patterns, middle REE (except of Eu) have slightly larger normalized values than those of lighter and heavier REE. All of the Antarctic eucrites have higher REE abundances and the REE abundances in them are similar to those in the Stannern eucrite. REE abundances in two eucrite clast samples are higher than those in the Stannern and matrix samples of the Antarctic eucrites. It has been pointed out that the Antarctic eucrites show the positive Ce anomaly (Nakamura and Masuda, 1980; Shimizu and Masuda, 1982) and that these Ce anomalies were caused by terrestrial weathering (Shimizu et al., 1983 and 1984). Among the Antarctic eucrites studied in this work, only one matrix

sample of Y-790007,61,F possesses the negative Ce anomaly and REE patterns of the other samples exhibit no Ce anomaly. Fig. 2 shows the REE-Ba-Sr patterns of the Stannern and Antarctic eucrites,which are normalized by the REE-Ba-Sr abundances in the Juvinas eucrite. All of the observed points of REE except for Eu lie on a linear inclined line in each pattern. With the exception of the REE pattern of the Y-790007,61,F, the other REE patterns run parallel in Fig. 2. Further, in this diagram, the inclination of linear lines becomes steeper in eucrites with higher REE abundances, excepting Y-790007,61,F.

The results shown in Fig.2 suggest that the eucrites with higher REE abundances such as the Stannern and Antarctic eucrites were produced as residual liquid in fractional crystallization process in common from an initial melt having the composition of the main group of eucrites (e.g., the Juvinas eucrite).

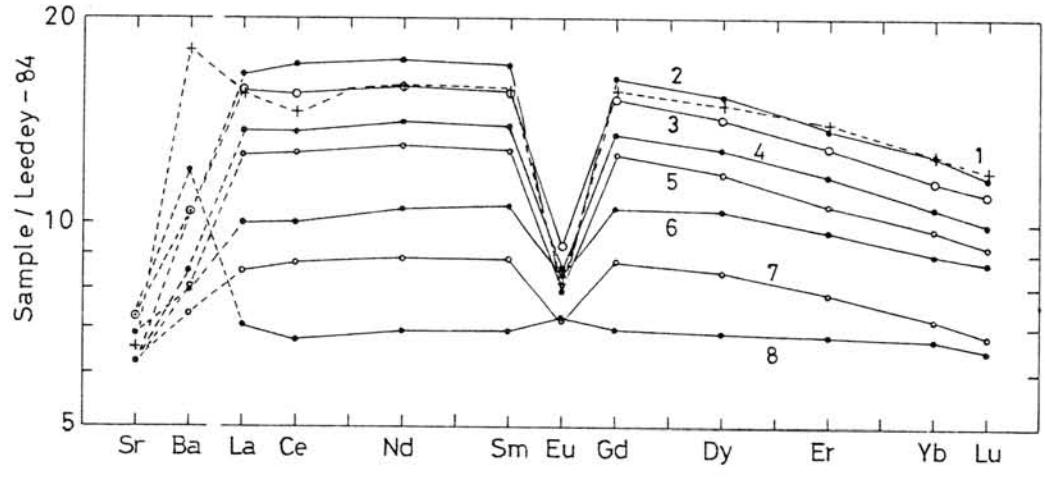

Fig. 1. REE-Ba-Sr patterns of eucrites normalized by "Leedey-84".

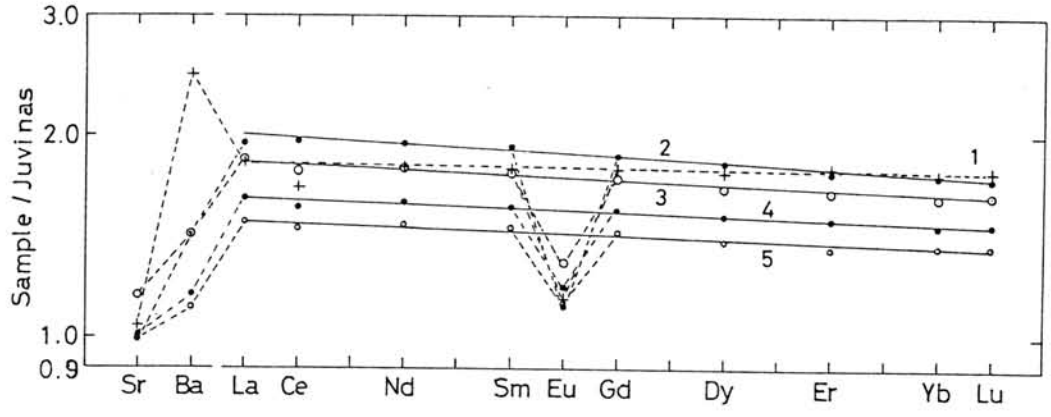

Fig. 2. REE-Ba-Sr patterns of the Stannern and Antarctic eucrites normalized by the Juvinas eucrite.

[1:Y-790007,61,F(matrix), 2:Y-75011,84,D-1(clast), 3:Stannern, 4:Y-75011,73(matrix), 5:Y-74450,63,D+G(matrix), 6:Pasamonte, 7:Juvinas, 8:Cachari]

[References]
Basaltic Volcanism Study Project (1981) Basaltic volcanism on the terrestrial planets. Pergamon.
Masuda, A., Nakamura, N. and Tanaka, T. (1973) Geochim. Cosmochim. Acta 37, 239.
Nakamura, N. and Masuda, A. (1980) Mem. Natl Polar Res. Spec. Issue 17, 159.
Shimizu, H. and Masuda, A. (1982) Mem. Natl Polar Res. Spec. Issue 25, 145.
Shimizu, H., Masuda, A. and Tanaka, T. (1983) Mem. Natl Polar Res. Spec. Issue 30, 341.
Shimizu, H., Tanaka, T. and Masuda, A. (1984) Nature 307, 251.
Takeda, H., Mori, H., Delaney, J. S., Prinz, M., Harlow, G. E. and Ishii, T.(1983a) Mem. Natl Polar Res. Spec. Issue 30, 181.
Takeda, H., Wooden, J.L., Mori, H., Delaney, J.S., Prinz, M. and Nyquist, L. E. (1983b) Proc. Lunar Planet. Sci. Conf. 14th, Pt. 1, B245 (J. Geophys. Res., 88, Suppl.).
Wooden,J.L., Takeda,H., Nyquist,L.E., Wiesmann,H. and Bansal,B. (1983) Mem. Natl Inst. Polar Res. Spec. Issue 30, 315.

DISTRIBUTION OF RARE EARTH ELEMENTS AND URANIUM IN ORDINARY CHONDRITES INCLUDING ANTARCTIC METEORITES

Ebihara, M.

Department of Chemistry, Faculty of General Studies, Gunma Univ. 4-2 Aramaki, Maebashi, Gunma 371

Rare earth elements (REE) and uranium were studied for their distribution in various component phases of ordinary chondrites, Kesen(H4), Richardton(H5), Bruderheim(L6), St.Severin (LL6), and some Antarctic meteorites. Selective dissolution method was applied for phase separation. REE were analyzed by neutron activation method and uranium was determined by neutron-induced fission track method.

Fig.1 and Fig.2 show dissolution patterns of Sm and Ca in EDTA(ethylenediaminetetraacetic acid) and hydrochloric acid treatments for Yamato-74191(L3) and ALH-78084(H3), respectively. Excellent parallelism can be observed in dissolution patterns of these two elements, suggesting that REE are also present in the Ca-phosphate for type 3 ordinary chondrites but the fractions of REE attributable to Ca-phosphate seem to be somewhat lower compared with those of type 4 to 6 ordinary chondrites. In type 3 ordinary chondrites, some 30-50% of the total Sm were recovered in HCl-residual fractions, which consist of pyroxene and/or plagioclase for the most part. Present results suggest that REE (and possibly U) were largely redistributed during a metamorphic sequence of petrologic types between 3 and 4.

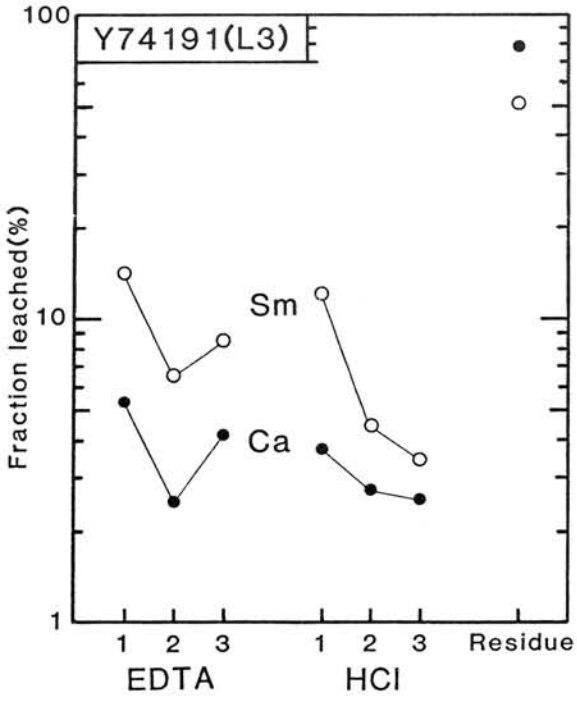

Fig.1

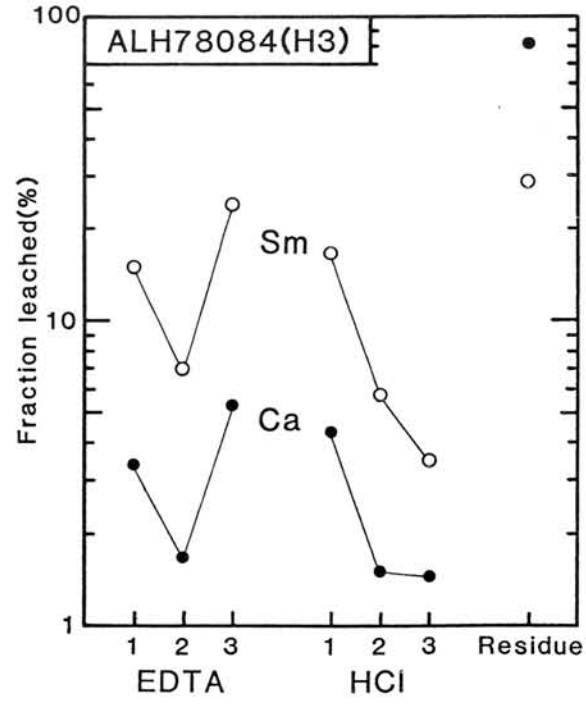

Fig.2

Precise Determination of REE Abundances in Individual Chondrules from Allende (CV3) and Hedjaz (L3) Chondrites

Keiji MISAWA and Noboru NAKAMURA

Department of Earth Sciences, Faculty of Science, Kobe University, Nada-ku, Kobe 657, Japan

We have established a direct-loading, isotope dilution method which allows precise analyses of REE in ≥20μg size of chondritic material.

In this study, abundances of REE, K, Rb, Sr, Ba, Mg, Ca and Fe in ten chondrules and two inclusions separated from the Allende (CV3) and the Hedjaz (L3) chondrites were determined by the method, together with major-chemical and petrological examinations for some of these samples using an electron microprobe analyzer.

Results show that REE patterns of chondrules, normalized to the average of ordinary chondrites, are generally flat but more or less fractionated from sample to sample, and some of them have Eu, Ce and Yb anomalies (Fig.1). It is pointed out that REE abundances vary at least a factor of ten among chondrules, and in some cases much more. The chondrules with higher REE abundances show, generally, negative Eu anomalies but those with lower REE exhibit the positive ones. However, the degree of the anomalies is not necessarily related to the common REE abundances. Nd is positively correlated with Ca and the Nd/Ca ratio is generally similar or greater than that of Cl for four Allende chondrules (Fig.2). This correlation suggests that these chondrules are mixture of a Nd,Ca-rich, refractory precursor and a chondritic component. Specifically, a barred olivine chondrule (A-1) with more fractionated REE (Fig.1) needs at least two components; one with highly fractionated REE (such as an ultra-refractory condensate) and the other with chondritic REE.

During analyses of Hedjaz chondrules, we found an unusual REE component in an inclusion (H-1) which shows highly fractionated (Group II) REE pattern (Fig.3). The inclusion consists of mainly coarse-grained (>100μm) "euhedral" olivine (Fa22) and clinopyroxene together with some interstitial plagioclase (An90), and the petrographical texture is variable from portion to portion. This is the first occurrence of Group II REE object in L-group chondrites. Additional analyses of the different parts of the inclusion failed to confirm such a highly fractionated REE pattern (Fig.3). Thus, it is suggested that a micro-component which carries Group II REE exists hetedogeneously within or in the margin of the inclusion, and that the inclusion was formed by sub-solidus sintering of the precursor materials.

Fig.1. REE patterns of chondrules and inclusion from Allende and Hedjaz.

Fig.2. Nd vs. Ca plots for chondrules and inclusions.

Fig.3. REE patterns for the different fragments from Hedjaz inclusion H-1. Shaded area exhibits range for the specimens H-1-2, -3, -4, -5.

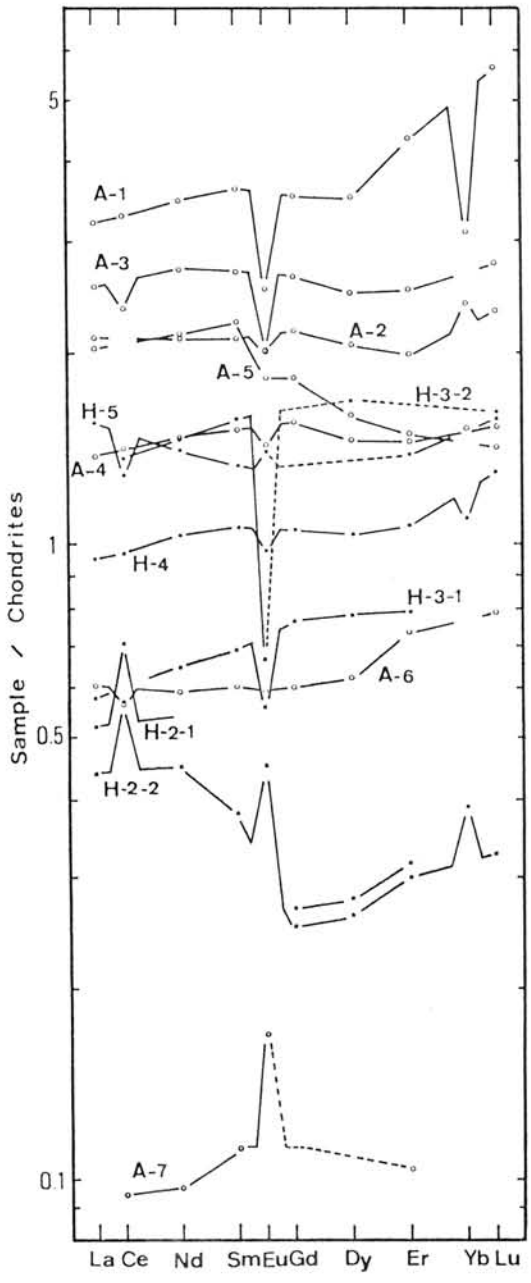

Fig.1.

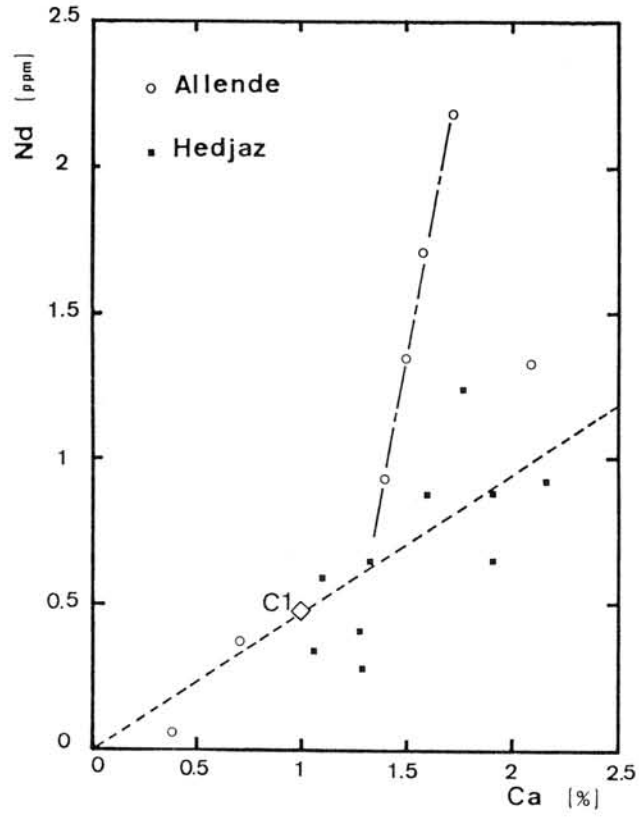

Fig.2.

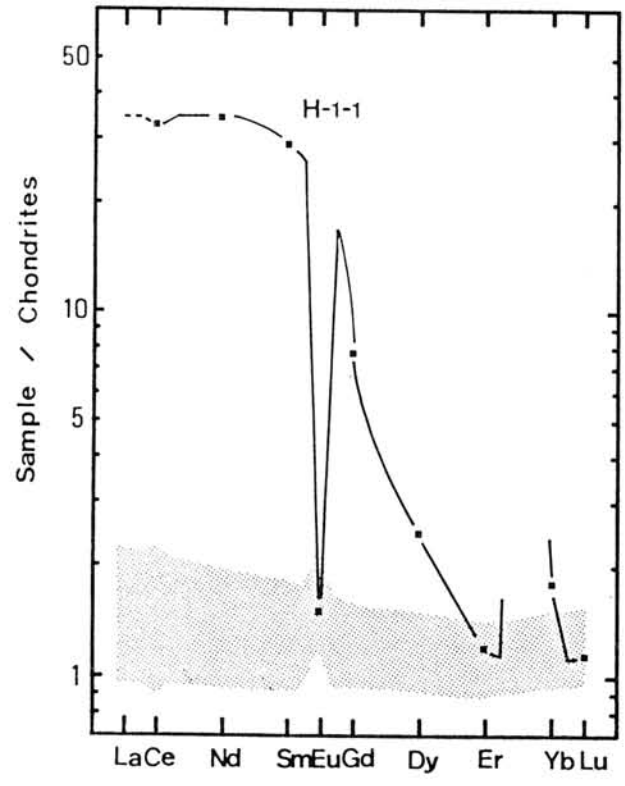

Fig.3.

NOBLE GASES IN THE KIRIN (JILIN) CHONDRITE

Matsuda, J.[1], Nagao, K.[2], Yamada, Y.[1] and Chang, S.[3]

1) Kobe University, Kobe 657, Japan.
2) Okayama University of Science, Okayama 700, Japan.
3) Peking University, Beijing, China.

The Kirin chondrite is the largest known stony meteorite, which fell on Mar. 8, 1976, in the district of Kirin, China (1). The intensive studies of cosmogenic nuclides in the Kirin meteorite have well established a two-stage irradiation model i.e. 2π-irradiation (8×10^6 y) and 4π-irradiation (0.4×10^6 y) (2). However, $^3He/^{21}Ne$ was low in all samples, and it was not clear whether this is due to a heavy shielding effect or a partial preferential loss of ^3He (2, 3). The young K-Ar ages (2.5-4.0 b.y.) and ^{40}Ar-^{39}Ar studies (4, 5) clearly suggest the outgassing of radiogenic ^{40}Ar from the sample.

Noble gases (He~Xe) in the Kirin chondrite were determined by stepwise heating for the purpose of studying thermal history of the meteorite. We made an experiment for 10 temperature franctions from 700°C to 1800°C. Almost all noble gases were degassed below 1600°C fraction. The light noble gases of ^4He and ^{20}Ne show significant enrichment at 900°C fraction (Fig.1). The heavy noble gases of ^{36}Ar, ^{84}Kr and ^{132}Xe were mainly released at 1300°C fraction although they show small peaks at 900°C fraction. The neon isotope data fall near the cosmogenic corner (Ne-S) for all tempepature fraction (Fig.2), which suggests that ^{20}Ne is of cosmogenic origin. The ^4He correlates with ^{40}Ar of which released pattern had high 900°C peak. Therefore, 900°C peaks of light noble gases seem to reflect cosmogenic and radiogenic components rather than the primordial one. The Xe isotopes are also enriched in cosmogenic component for all temperature fractions, and the whole pattern is well understood by mixture of cosmogenic and AVCC Xe (Fig.3). Excess ^{129}Xe from extinct ^{129}I was obtained in all temperature fractions.

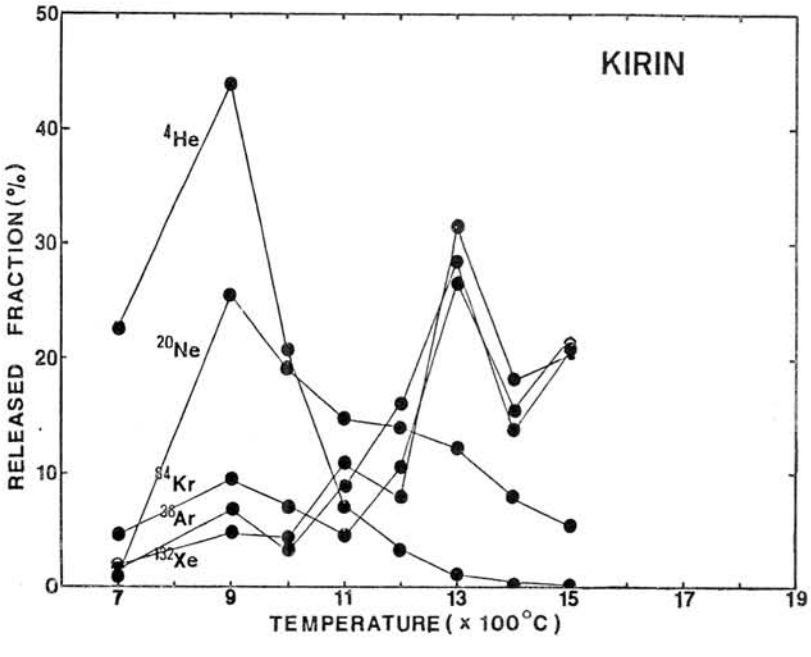

FIG. 1

References

1) Joint Investigation Group of the Kirin Meteorite Shower, 1977. Sci. Sinica 20, 502.
2) Honda, M., Nisiizumi, K., Imamura, M., Takaoka, N., Nitoh, O., Horie, K, and Komura, K., 1982. Earth Planet. Sci. Lett. 57, 101.
3) Weber, H. W., Braun, O. and Begemann, F., 1979. Meteoritics 14, 558.
4) Heusser, G., Kirsten, T. and Ries, D., 1979. Meteoritics 14, 412.
5) Wang, S., McDougall, I., Tetley, N. and Harrison, T. M., 1980. Earth Planet. Sci. Lett. 49, 117.

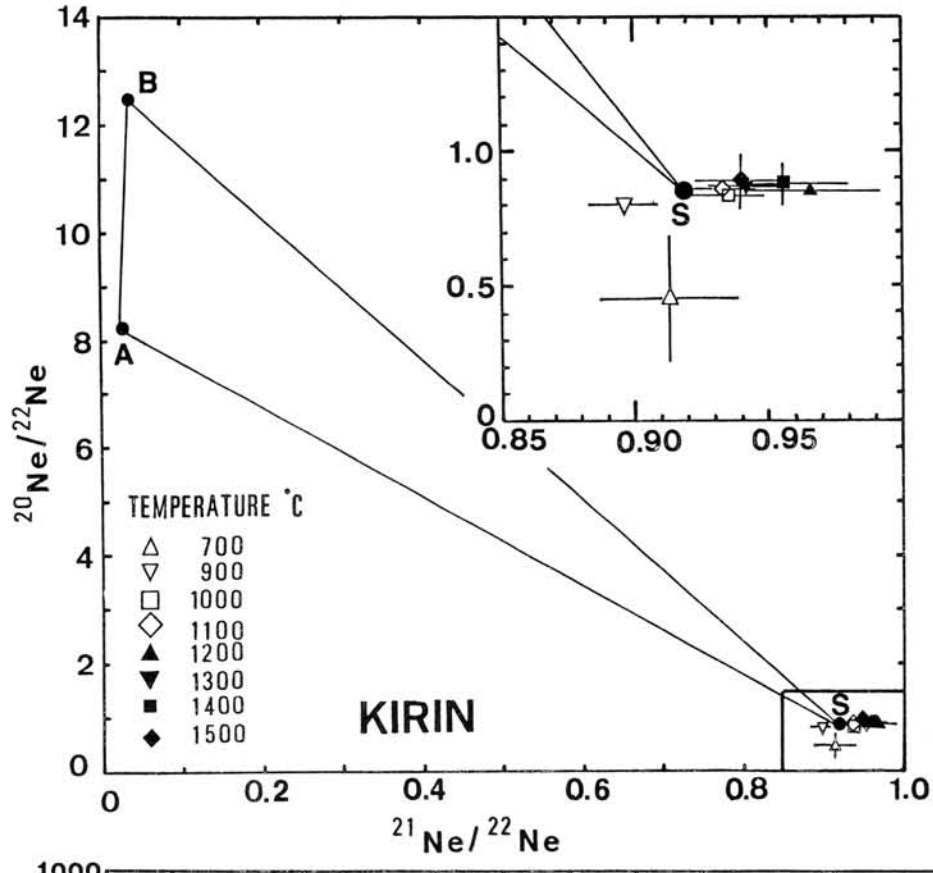
B
A
S
S
KIRIN
TEMPERATURE °C
700
900
1000
1100
1200
1300
1400
1500
$^{20}Ne/^{22}Ne$
$^{21}Ne/^{22}Ne$

FIG. 2

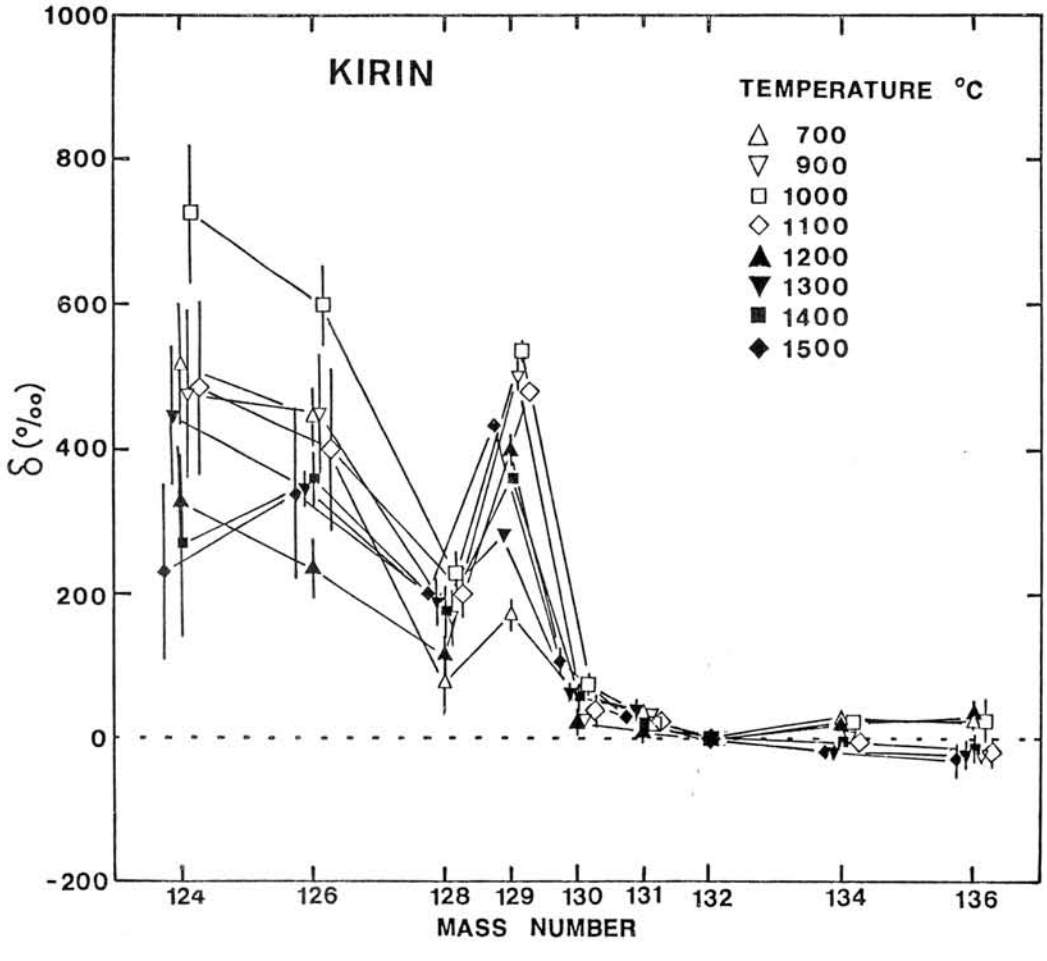
KIRIN
TEMPERATURE °C
700
900
1000
1100
1200
1300
1400
1500
δ (‰)
MASS NUMBER

FIG. 3

PRIMORDIAL RARE GASES IN CARBONACEOUS CHONDRITES

Nagao, K.*, Matsuda, J.** and Inoue, K.*
* Okayama University of Science, ** Kobe University

A new component of Kr and Xe enriched in 84Kr and 132Xe was found in high extraction temperature fractions of Belgica-7904 C2 chondrite(Nagao et al., in press). The component may be produced in the Ne- and C-shells of a supernova where the neutron density is low and the photodisintegration-dominated nucleosynthesis occurs(Heymann and Dziczkaniec, 1980).

Because of this interesting results, we intended to investigate this meteorite more precisely. As a preliminary experiment, a small pieces of Belgica-7904 were separated to two fractions according to the grain size with a pore filter of 8μm in diameter after decomposing the samples with freeze-thaw disaggregation method. The fractions of coarse grains(>8μm) and fine grains(<8μm) were analyzed for rare gas isotopic compositions with stepwise heating extraction. Sample weights were 37.9 and 6.61mg for coarse grains and fine ones, respectively.

Rare gas elemental compositions and concentrations for the coarse grains are similar to those for the bulk sample, whereas the concentrations for fine grains are higher than those for the bulk by a factor of 2 or 3. Ne-E was found only in the coarse grains and was enriched by a factor of about 2. Because of a small amount of fine grains, analysis of Ne isotopic ratios was difficult. Ne-E was not found in the fine grains. 20Ne seems to be enriched in this sample. 40Ar/36Ar ratios in the fine grains are lower than those in the coarse ones. 132Xe enrichments were also found in the high extraction temperature fractions for both samples. The enrichments in 132Xe support the previous results for the bulk sample of Belgica-7904. 84Kr enrichment could not be identified because of the relatively large experimental errors arising from a small amount of Kr. CCF-Xe was also found in 900°C fraction.

Other carbonaceous chondrites Yamato-74662(C2) and Yamato-791198(C2) were also analyzed for rare gas compositions. He and Ne concentrations in Y-791198 are much higher than those in Y-74662. However, Ne isotopic ratios for both meteorites are very similar. The ratios for 1000 and 1100°C fractions are $^{20}Ne/^{22}Ne=4$ and $^{21}Ne/^{22}Ne=0.3\sim0.4$. The ratios are plotted below the mixing line between Ne-A and Ne-S in three isotope plot, and indicate the presence of Ne-E component in both the samples. Xe isotopic ratios did not show the 132Xe enrichment. The ratios for the temperature fractions higher than 900°C are as same as those for AVCC-Xe. In 900°C fraction, a small contribution of CCF-Xe was found for both meteorites.

References: Nagao et al., Memoirs Natl Inst. Polar Res. , in press; Heymann and Dziczkaniec,Proc.Lunar Planet. Sci.Conf., 11th, 1179-1213.

65—1

NOBLE GAS STUDIES OF ANTARCTIC METEORITES

Nobuo Takaoka and Shuichi Sekii

Dept. of Earth Sciences
Yamagata University

Concentrations and isotopic compositions of noble gases were determined for fifteen antarctic meteorites. Table 1 shows the meteorites used in this work and part of results. While Y-74662 (C2), Y-75029(H3) and ureilite carbon contain trapped He, spallation He is dominant in the other meteorites. Two ureilites and three unequilibrated chondrites contain trapped Ne. Although ALH-77299(H3) contains trapped heavy gases, light gases are lost from it. The $^{22}Ne/^{21}Ne$ ratios of spallation Ne in equilibrated chondrites and eucrites range from 1.122 to 1.188. Cosmic-ray irradiation ages calculated from spallogenic ^{21}Ne are listed in Table 1, and compared to those for non-antarctic meteorites in Fig.1. Both of ureilites were heated stepwise and gases released at each temperature step were analysed. From three-isotope plots of Ne (Fig.2), spallogenic $^{22}Ne/^{21}Ne$ ratios were estimated to be 1.271 for Y-74123 and 1.130 for ALH-77257. The large $(^{22}Ne/^{21}Ne)_{sp}$ ratio suggests that the Y-74123 ureilite was irradiated by cosmic-rays in a small meteoroid or near the surface of meteoroid.

Gas retention ages calculated from radiogenic ^{4}He and ^{40}Ar are listed in Table 1. Potassium contents were assumed to be 830 ppm for H-, 860 ppm for L-, 830 ppm for LL-chondrites(Goles,1971). In most cases, ^{4}He ages are younger than ^{40}Ar ages, suggesting diffusive loss of He.

Y-75029(H3) contains large concentrations of solar-type trapped gases. This chondrite is a gas-rich meteorite. Since Y-75028 (H3) is a gas-rich meteorite(Takaoka, et al.,1981), these H3 chodrites are probably fragments of the same fall.

Carbon separate from ALH-77257 ureilite was analysed by step-heating to give $^{20}Ne/^{22}Ne=10.52 \pm 0.14$ and $^{21}Ne/^{22}Ne=0.0298 \pm 0.0017$ for trapped Ne. While the $^{20}Ne/^{22}Ne$ ratio is identical to that of Ne-C, solar flare Ne directly implanted in meteorites(Black,1972), the $^{21}Ne/^{22}Ne$ ratio is significantly lower than that of Ne-C. As shown in Fig.2 in expanded scale, the $^{21}Ne/^{22}Ne$ ratio

for Ne-C is 0.042 ± 0.003(Black,1972). Difference between ureilite Ne and Ne-C is beyond errors, and suggests that Ne-C is a mixture of dominant part of a spallation-Ne-free component and a minor portion of spallogenic Ne. A fact that this ureilite Ne falls on a trend line through the end members of Ne identified in meteorites and in the terrestrial atmosphere strongly suggests that it should be one of the end members of meteorite Ne. The ureilite trapped Ne is probably the spallation-Ne-free component in Ne-C, or an independent component. $^{40}Ar/^{36}Ar$ for trapped Ar in ALH-77257 is $(1.9 \pm 0.2) \times 10^{-3}$.

Eucrites contain considerable amounts of spallogenic gases. Their cosmic-ray irradiation ages are very long(Table 1). Radioactive isotope ^{81}Kr was found in Y-74450. ^{81}Kr is produced by spallation reactions along with other Kr isotopes. For a long irradiation age, ^{81}Kr is in radiation equilibrium between production and disintegration. After fall on the earth, concentration of ^{81}Kr decreases with a half-life of 2.1×10^5 years because of no cosmic-ray irradiation. Thus the spallogenic $^{81}Kr/^{83}Kr$ ratio depends on a terrestrial age of meteorite. The spallogenic $^{81}Kr/^{83}Kr$ ratio is 0.0020 ± 0.0004 for Y-74450. With this value and the ^{81}Kr production rate estimated from spallogenic ^{80}Kr and ^{82}Kr, we have (14 ± 3) $\times 10^4$ y. for the terrestrial age of Y-74450.

References,

Black,D.C.(1972), Geochim. Cosmochim. Acta, 36, 347.

Goles,G.G.(1971), Handbook Elem.Abund.Met.,ed.B.Mason.

Takaoka,N.et al.(1981),Mem.Natl Inst.Polar Res.Spec.Issue 20,264

Table 1, Noble gas concentrations and gas retention and cosmic-ray irradiation ages.

Meteorite(Class)	^4He	^{20}Ne	^{36}Ar	^{84}Kr	^{132}Xe	T_4	T_{40}	T_{21}
	10^{-8} cc/g			10^{-10} cc/g		b.y.		m.y.
Y-74662(C2)	5360	23.8	74.4	105	121	--	--	--
ALH-77299(H3)	1460	9.53	26.9	21.8	17.4	3.8	4.2	28.
Y-75029(H3)	75900	1330	88.6	10.2	5.4	--	--	--
Y-74355(L4)	1340	12.3	3.40	0.90	1.16	2.7	4.0	30.
ALH-77272(L6)	281	1.67	0.548	1.98	1.02	0.67	2.0	4.0

Table 1 (continued)

Meteorite (Class)	^{4}He	^{20}Ne	^{36}Ar	^{84}Kr	^{132}Xe	T_4	T_{40}	T_{21}
	10^{-8} cc/g			10^{-10} cc/g		b.y.		m.y.
Y-74174 (L6)	207	1.68	0.556	0.42	1.00	0.43	1.3	4.3
Y-74372 (L6)	439	5.19	0.782	0.45	0.49	0.87	3.1	13.
ALH-77278 (LL3)	3600	40.2	18.6	21.3	11.0	--	4.0	20.
Y-74442 (LL4)	1600	2.85	1.60	2.03	2.06	3.7	3.4	6.6
Y-74450 (Eu)	5590	15.8	7.47	0.72	0.65	--	--	63.
Y-75011 (Eu)	7840	13.2	7.50	0.84	0.37	--	--	52.
ALH-77256 (Di)	2070	9.21	0.59	--	--	--	--	21.
ALH-77257 (Ur)	312	10.6	1320	566	981	--	--	5.8
Carbon	11300	199	41500	--	22500	--	--	--
Y-74123 (Ur)	122	6.84	349	272	121	--	--	4.9

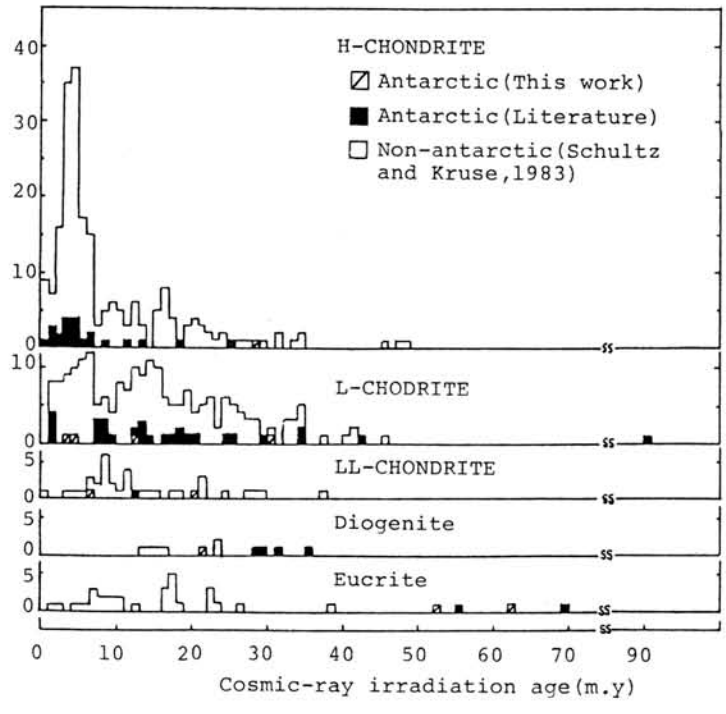

Fig.1, Comparison of Cosmic-ray irradiation age between antarctic and non-antarctic meteorites.

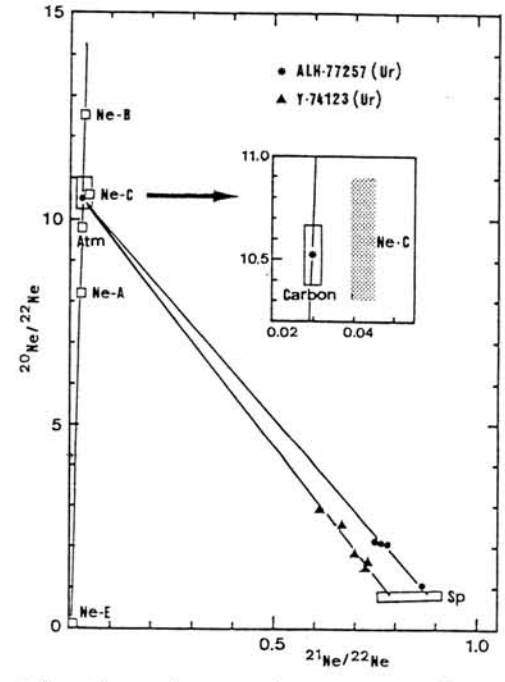

Fig.2, Three-isotope plot for ureilite Ne

Additional evidence of Rb-Sr systematics and REE abundances for 1.2 b.y. impact-melting event on LL-chondrite parent body

Osamu OKANO[1] and Noboru NAKAMURA[1),2)]

1) Department of Science of Material Differentiation, Graduate School of Science and Technology, Kobe University, Nada, Kobe 657, Japan
2) Department of Earth Sciences, Faculty of Science, Kobe University, Nada, Kobe 657, Japan

Recently, we obtained the youngest Rb-Sr internal isochron age of 1.2 b.y. (Fig. 1), together with the somewhat fractionated REE pattern, for one of Yamato-79 unusual LL-chondrites, Y-790964 (Nakamura and Okano, 1984; Okano et al., 1984). In order to examine further details of Rb-Sr isotopic and chemical characteristics of the meteorites, additional analyses were carried out for other whole rocks and mineral separates from the chondrite as well as other Antarctic LL-chondrites.

Compared with well-defined Rb-Sr isochrons of usual chondrites, Rb-Sr data for these impact-melted LL-chondrites show relatively larger deviations in the Rb-Sr evolution diagram. It is considered that this was not due to terrestrial weathering but essentially to the effects of the impact event(s). This explanation could be supported by the additional whole rock data (Fig. 2) as follows; whole rock data points deviate not only from the 1.2 b.y. isochron but also from the 4.55 b.y. line, and an average data point of all the whole rock samples of the impact-melted LL-chondrites is on the 4.55 b.y. line and has a Rb/Sr ratio similar to those of usual LL-chondrites. Therefore, it is suggested that Rb-Sr systems of all the Yamato-79 unusual LL-chondrites had been basically undisturbed from 4.5 b.y. to 1.2 b.y. but were more or less perturbed by the 1.2 b.y. event. In addition. it is pointed out that the meteorites contain a small amount of relic chondrules and olivine in a glassy and recrystallized matrix, and chemical composition of the brown glass is quite variable (Sato et al., 1982; Nakamura and Okano, 1984). In view of the Rb-Sr isotopic, chemical and petrologic characteristics, our best explanation of the results is that intensive impact-melting and assimilation processes were prevailing for the whole meteorites and then the Rb-Sr system was perturbed significantly by the event(s), resulting in establishment of local Sr isotopic equilibrium (possibly within mm-size area).

While the K-Ar dating of meteorites shows variable ages through 4.6 b.y. ago to recent, the meaning of younger ages (particularly $\sim$1 b.y.-age) have not been well-examined so far by other methods such as Rb-Sr or Sm-Nd method, except for a few cases such as St. Mesmin chondrite or SNC meteorites. In this connection, the 1.2 b.y. Rb-Sr age obtained here would be the clearest and youngest one among those of many young perturbed meteorites, and thus considered to be important to understand evolutionary history of meteorites. It is interesting that the 1.2 b.y.-age for the Y-790964 is close to the K-Ar age of 1.4 b.y. for an H-clast of St. Mesmin LL-chondrite (Schultz and Signer, 1977) and to the 1.3 b.y.-age of SNC meteorites, and also that significant number of the K-Ar ages of $\sim$1 b.y. have been known so far. Hence, it appears that the 1.2 b.y.-age obtained for the Y-790964 LL-chondrite is a non-trivial marker of evolution of meteorites. It is not clear, however, whether this is a real effect of thermal event on meteorite parent planet or due to sampling bias. If the former case, one should seriously consider the impact-related processes as major thermal one on meteorite parent planets at as recent as <1.4 b.y.

References

Nakamura, N. and Okano, O. (1984) (Submitted to Nature)
Okano, O., Misawa, K., Nakamura, N., Honma, H. and Goto, H. (1984) Mem. Natl Inst. Polar Res., Spec. Issue (in press).
Sato, G., Takeda, H., Yanai, K. and Kojima, H. (1982) Papers presented to the 7th symposium on Antarctic Meteorites (Abstract), 9-10.
Schultz, L. and Signer, P. (1977) Earth Planet. Sci. Lett., 36, 363-371.

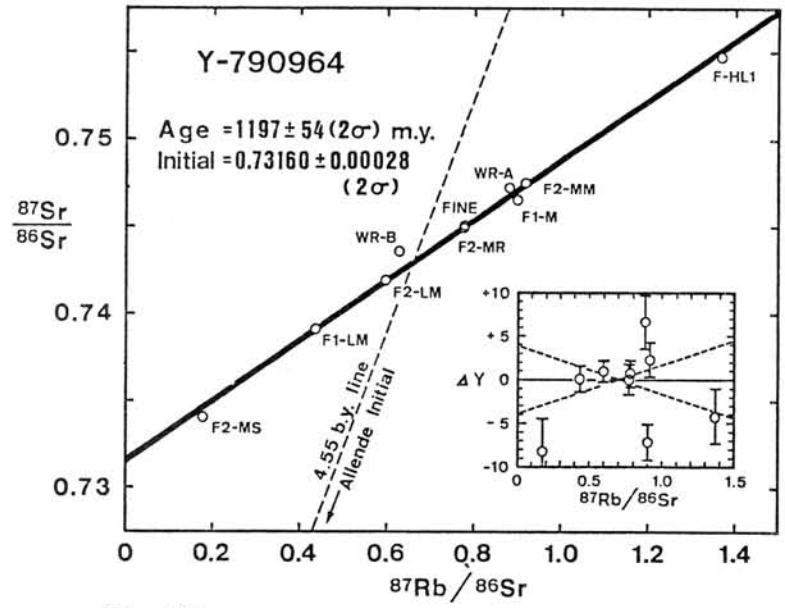

Fig. 1. ^{87}Rb-^{87}Sr evolution diagram of the Yamato-790964. (Nakamura and Okano, 1984)

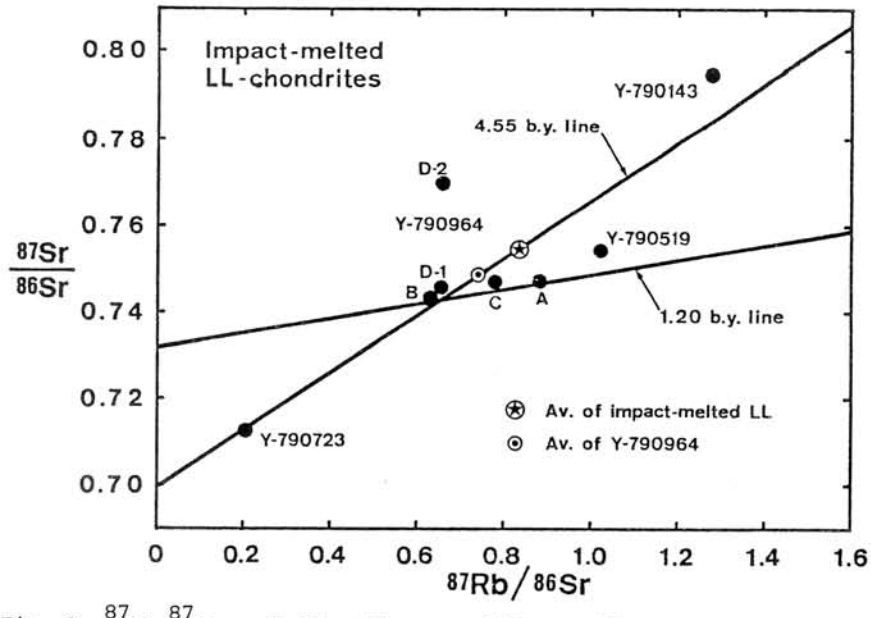

Fig. 2. ^{87}Rb-^{87}Sr evolution diagram of Yamato-79 unusual LL-chondrites.

Rb-Sr AND Sm-Nd INTERNAL ISOCHRON AGES OF A SUBOPHITIC BASALT CLAST FROM THE Y75011 EUCRITE.

L.E. Nyquist (SN4/NASA Johnson Space Center, Houston, TX 77058), B.M. Bansal, C.-Y. Shih, H. Wiesmann (Lockheed-EMSCO, 2400 NASA Rd. 1, Houston, TX 77058), J.L. Wooden (MS937/U.S. Geological Survey, 345 Middlefield Rd., Menlo Park, CA 94065), and H. Takeda (Mineralogical Inst., Faculty of Science, Univ. of Tokyo, Hongo, Tokyo 113, Japan).

We report Rb-Sr and Sm-Nd isotopic analyses of Y75011 performed as part of a consortium study of the Yamato polymict eucrites. Some preliminary results have been reported earlier (1). Rb-Sr results are also being reported elsewhere (2).

Polymict eucrite Y75011 contains several coarse-grained, mesostasis-rich, subophitic basalt clasts. Clast Y75011,84 consists of pyroxene, plagioclase, olivine, silica, ilmenite, troilite, and other minor phases (3). The silica and opaque minerals occur in a dark mesostasis. This clast may represent the least altered basalt type ever recovered from eucritic lavas, although Takeda et al. (3) have noted that mineral phases show evidence of mild shock deformation with peak shock pressures of 10-20 GPa and a short duration reheating to a maximum temperature of 1100° C. Thus, analysis of Y75011,84 offered an excellent opportunity to obtain an internal Rb-Sr isochron on an eucritic lava. The pristinity of Y75011,84 and $^{39}Ar/^{40}Ar$ ages of ~ 4.0 b.y. for similar polymict eucrites (4,5), possibly from the same fall (3), also suggested the possibility that this clast might be younger than more heavily metamorphosed ordinary eucrites.

Shimizu and Masuda (6) have reported REE data for Y75011,84 which show that it is among the most differentiated eucrites. Chondrite-normalized REE abundances are similar to but slightly higher than those of the Stannern eucrite. Takeda et al. (7) have reported major element compositions for Y74159 and Y74450, two polymict eucrites which are similar to Y75011. These two meteorites have comparatively high TiO_2 contents of ~ 1% , also similar to the Stannern value (8). Values of Mg/(Mg+Fe) are ~ 0.44 so that these polymict eucrites are slightly displaced from the main "Stannern trend" on a plot of TiO_2 vs. Mg/(Mg+Fe) (8). The Rb concentration in clast Y75011,84 is only ~ 0.21 ppm and is about four-fold lower than that in Stannern (8). (The Rb value of 0.246 ppm reported earlier for Y75011,84B (1) is incorrect due to an arithmetical error. The actual result for that analysis was 0.204 ppm.) Thus, although Y75011,84 bears compositional similarities to Stannern, it is likely that it represents a distinct magma type from the surface of the eucrite parent body.

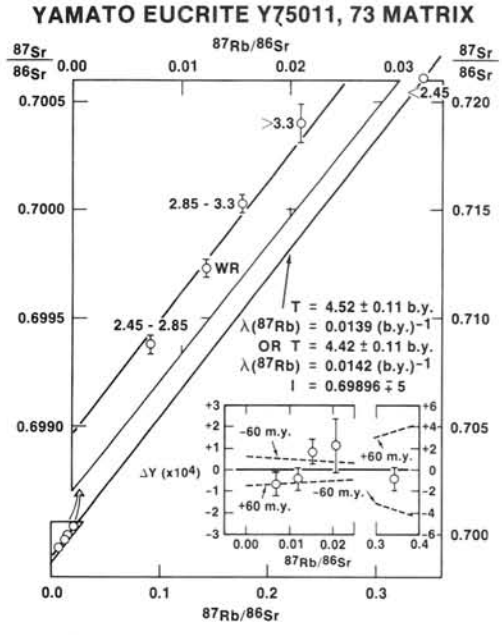

Figure 1.

Two similar experiments were performed on the clast (,84) and matrix (,73) of Y75011. The matrix was analysed first to establish the adequacy of mineral separation techniques. After crushing, a portion of the 100-325 mesh fraction was taken for mineral separation. Fractions with densities <2.45, 2.45-2.85, 2.85-3.3, and > 3.3 g/cm3 were prepared. Results of Rb-Sr analyses of these fractions and a whole rock sample are shown in Fig. 1.

The < 2.45 g/cm3 fraction contained a phase, probably silica from the mesostasis, with the highest Rb/Sr ratio so far reported for eucrites, four-fold higher than Rb/Sr of the "glass" phase of Juvinas (9). Data for the whole rock and density fractions determine an isochron corresponding to an age of 4.52 b.y. for $\lambda(^{87}Rb)$ = 0.0139 (b.y.)$^{-1}$ or 4.42 b.y. for $\lambda(^{87}Rb)$ = 0.0142 (b.y.)$^{-1}$. The corresponding initial $^{87}Sr/^{86}Sr$ = 0.69896±5 and is within analytical uncertainty of BABI = 0.69898±6 (10). (Analyses of the NBS-987 Sr standard during this investigation yielded an average value of 0.71021±2.) The 2-sigma error estimate given by the York (11) program for the age is ± 0.11 b.y. when the data are weighted inversely as the square of the individual error estimates. For an approximately constant percentage error in Rb/Sr, this procedure assigns a weighting factor to the $^{87}Rb/^{86}Sr$ ratio of the < 2.45 g/cm3 fraction which is < 1% of the weight assigned to the other data. Consequently, the age uncertainty calculated by the program is considerably greater than is obtained by a direct calculation which considers the uncertainty in the initial ratio and the analytical uncertainties of the <2.45 g/cm3 fraction, which controls the slope of the isochron. The directly calculated uncertainty is dominated by the ± 1.4% error in the Rb/Sr ratio of this fraction and is ~ 60 m.y. Deviations of isochrons differing from the best fit isochron by ± 60 m.y. are shown in the inset in Figure 1. It should also be noted that application of the York (11) program with equal weight assigned to all the data yields a 2-sigma error limit of only ± 0.03 b.y. It appears that because of the unusual bimodality of the data and the presence of only one high Rb/Sr

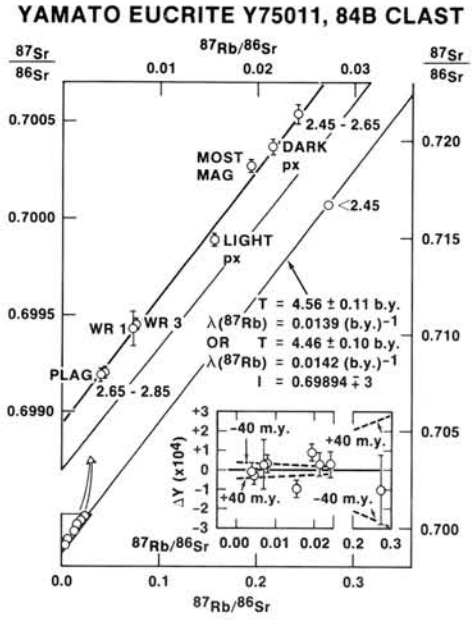

Figure 2.

datum the 2-sigma error limits from the York (11) program with "inverse square" weighting are unrealistically high. Thus, we prefer the directly calculated error limit of ± 60 m.y.

The clast Y75011,84 was analysed in a similar manner to the matrix. Rb-Sr results are shown in Fig. 2. As for the matrix sample, the fraction with density < 2.45 g/cm^3 had the highest Rb/Sr ratio. A fraction of density 2.65-2.85 g/cm^3 was estimated to be ~95% plagioclase. Another fraction of density 2.45-2.65 g/cm^3 apparently contained a significant portion of the high Rb/Sr phase in addition to plagioclase. The > 3.3 g/cm^3 fraction was magnetically subdivided into three phases called "light px", "dark px" and "most magnetic". Low Sr concentrations of 10, 8, and 17 ppm, respectively, show that any plagioclase contamination of these separates was minor. Comparison to pyroxene compositions (3) and consideration of the magnetic susceptibilities suggests that the "light px" was enriched in low-Fe, low-Ca pigeonite cores, the "most magnetic" separate was enriched in high-Fe, high-Ca rims plus ilmenite, and that the "dark px" was an intermediate pyroxene composition. A least squares fit to all the clast data yields an age of 4.56 b.y. for $\lambda(^{87}Rb)=0.0139$ (b.y.)$^{-1}$ or 4.46 b.y. for $\lambda(^{87}Rb)=0.0142$ (b.y.)$^{-1}$. The calculated uncertainty is ±0.11 b.y. when the data are weighted inversely as the square of individual error estimates and ±0.02 b.y. when all data are weighted equally. As for the matrix data we prefer an error estimate based on the estimated uncertainty of the < 2.45 g/cm^3 datum, or ±0.9 % (±40 m.y.) in this case. Deviations of isochrons differing by ± 40 m.y. from the best fit isochron are shown in the inset in Figure 2. The calculated initial $^{87}Sr/^{86}Sr$ is 0.69894±3 for inverse square weighting and 0.69895±3 for equal weighting. Initial $^{87}Sr/^{86}Sr$ for clast and matrix are thus identical within error limits as well as being in satisfactory agreement with the BABI value (10).

The clast data show less scatter about the best fit isochron than do the matrix data suggesting that the latter may have been slightly disturbed during brecciation. All the clast data except that for the "light px" and "most magnetic" fractions lie on the isochron well within error limits (Figure 2 inset). The aberrancy of these two data points might be due to the presence of Fe-rich olivine veinlets filling fractures in the pyroxenes as described by Takeda et al. (3). These authors suggest that the veinlets could have been produced either by decomposition of Fe-rich rim pyroxene or by remelting of mesostasis to form an Fe-rich immiscible liquid during a short reheating event at high temperature. The complementary nature of the data for the "most magnetic" and "light px" fractions and the tentative identification of these fractions with pyroxene rims and cores, respectively, suggests a net transfer of Rb from trace element rich rims to trace element poor cores at a time after 4.5 b.y. ago. The most plausible time of this redistribution is 4.0 b.y. ago, assuming that Y75011 was subjected to the same event as recorded in the $^{39}Ar/^{40}Ar$ ages of similar polymict eucrites. Omitting the "most magnetic" and "light px" fractions from the linear regression of the data does not change the calculated age or initial $^{87}Sr/^{86}Sr$ ratio, but decreases the error limits to ±0.05 b.y. and ±0.00002, respectively, for inverse square weighting of the data. We conclude that the probable error on the Rb-Sr age obtained here for Y75011,84 is ~ 1%.

Sm-Nd data for both clast and matrix are shown in Figure 3. Data reported earlier for the whole rock samples of Y75011,73 and Y75011,84 (1) have been adjusted downward by 0.000080, based on analyses of the CIT n(Sm/Nd)β Nd standard, to be comparable to analyses from the Caltech laboratory and to recent analyses from the JSC laboratory. Data for the mineral separates required no adjustment. The York (11) regression of all the clast data yields an age of 4.54 ± 0.21 b.y. and initial $^{143}Nd/^{144}Nd$ = 0.50591 ± 28 (2-sigma error limits). However, as shown by the inset, the "most magnetic" fraction is slightly aberrant in the Sm-Nd system as well as in the Rb-Sr system. If this datum is omitted from the regression, the calculated age becomes 4.52 ± 0.16 b.y. and the calculated initial $^{143}Nd/^{144}Nd$ = 0.50593±22. A regression of all data from both clast and matrix yields a calculated age of 4.59 ± 0.17 b.y. and initial $^{143}Nd/^{144}Nd$ = 0.50583 ± 28. These results are clearly in agreement with the more precise Rb-Sr age.

For an assumed age of 4.56 b.y. the calculated initial $^{143}Nd/^{144}Nd$ = 0.505877±25 for the clast data is in good agreement with the Chondritic Uniform Reservoir (CHUR) value of 0.505893 (12,27). Nakamura et al. (21) have reported a Sm-Nd age of 4.52 ± 0.09 b.y for Antarctic polymict eucrite ALH-765 and an initial $^{143}Nd/^{144}Nd$ value which is higher than the CHUR value by ~ 1 epsilon-unit (10^{-4}) at 4.55 b.y. ago. However, these authors also report a value for BCR-1 which is higher by 0.7±0.5 epsilon units than the value given by Wasserburg et al. (26). This result, combined with our data for Y75011,84, makes it seem unlikely that a real difference exists between the chondritic

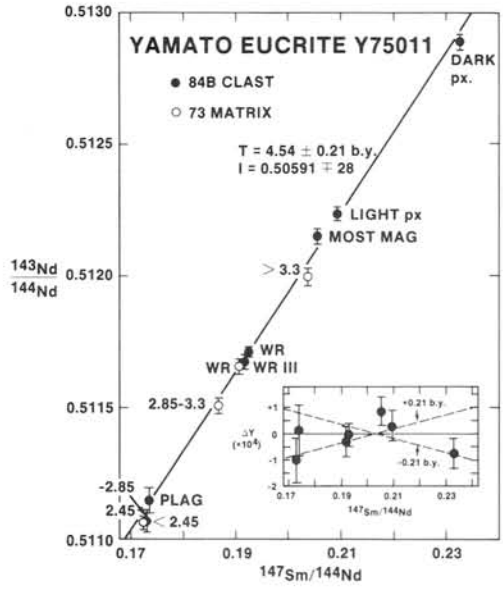

Figure 3.

initial $^{143}Nd/^{144}Nd$ ratio and that of the parent body of the Antarctic polymict eucrites.

The concordancy of the Rb-Sr ages of the matrix and clast strongly suggests that the Rb-Sr systematics of the < 2.45 g/cm^3 fractions have not been seriously disturbed since ~ 4.5 b.y. ago. Any effect due to brecciation would be expected to be more severe for the matrix than for the clast and cannot be resolved at the 1-2% level. Furthermore, the isochrons obtained are not simple mixing lines since a plot of Rb vs. Sr clearly shows the presence of at least three components. Thus, the Rb-Sr age of pristine clast Y75011,84 can be considered as the crystallization age of this basalt. This age is greater than the internal Rb-Sr isochron ages of several ordinary eucrites studied by Birck and Allegre (13) and nearly identical with the Rb-Sr age of 4.57±0.13. b.y. for $\lambda(^{87}Rb)$=0.0139 (b.y.)$^{-1}$ which they obtained for combined whole rocks and minerals of Juvinas and Ibitira. The age is also within error limits of the 4.60±0.02 b.y. ($\lambda(^{87}Rb)$=0.0139 (b.y.)$^{-1}$) whole rock age of chondrites (14). Using $\lambda(^{87}Rb)$ = 0.01402 (b.y.)$^{-1}$ as suggested by Minster et al. (14) from comparison of Rb-Sr and U-Th-Pb ages of chondrites gives an age of 4.52±0.05 b.y. for Y75011,84 in agreement with the $^{207}Pb/^{206}Pb$ age of 4.54±0.02 b.y. cited in (15) as the crystallization age of eucrites. However, reported Sm-Nd ages provide some evidence of age variation among eucrites. Lugmair et al. (28) reported an age of 4.41±0.02 b.y. for the cumulate eucrite Serra de Mage' and Jacobsen and Wasserburg (27) reported a Sm-Nd age of 4.46±0.03 b.y. for the cumulate eucrite Moama. However, Hamet et al. (18) had previously reported an age of 4.51±0.05 b.y. (recalculated according to (20)) for Moama and Nakamura et al. (19) have reported an age of 4.53±0.04 b.y. (also recalculated according to (20)) for the cumulate eucrite Moore County. The average Sm-Nd age of the non-cumulate eucrites Juvinas (main group), Pasamonte (Nuevo Laredo group) and ALH-765 (Stannern group) is 4.53±0.04 b.y. (Ref. (16), (21), and (17), recalculated according to (20)). Isotopic systematics of the most highly differentiated ordinary eucrite, Stannern, are disturbed with the Sm-Nd system showing the least disturbance. An apparent age of 4.48±0.07 b.y. has been reported for Stannern, but the plagioclase analysis shows clear evidence of disturbance (29). The possibility that many of the younger internal isochron ages have been partially reset during brecciation must be seriously considered. This is particularly true for those isochrons which are heavily reliant on the analysis of only two mineral phases as is the case of the cumulate eucrites. In the case of Y75011,84 a "young" age of 4.46±0.05 b.y. is also obtained if $\lambda(^{87}Rb)$ = 0.0142 (b.y.)$^{-1}$ is used. However, comparison of the Y75011,84 results to the $^{207}Pb/^{206}Pb$ ages of eucrites and the Sm-Nd ages of non-cumulate eucrites, as well as comparison of the Rb-Sr and U-Th-Pb ages of chondrites (14) and the Rb-Sr and $^{39}Ar/^{40}Ar$ ages of KREEP basalts (22), VHA melt rocks (23), and VHK basalts (24,25) suggests that this value of the decay constant probably biases Rb-Sr ages to lower values than obtained by other dating methods. We thus conclude that the pristine clast Y75011,84 formed at the same time as most ordinary eucrites and within ~ 50 m.y. of the formation of chondrites.

REFERENCES: (1) Wooden J.L. et al. (1983) Mem. NIPR 30, 315. (2) Bansal B.M. et al. (1985) Lunar and Planet. Sci. XVI, submitted. (3) Takeda H. et al. (1983) PLPSC 14, B245. (4) Kaneoka I. et al. (1979) Mem. NIPR 12, 186. (5) Kaneoka I. (1981) Mem. NIPR 20, 250. (6) Shimizu H. and Masuda A. (1984) Geochem. Soc. Japan, Nagoya. (7) Takeda H. et al. (1978) Mem. NIPR 8, 1978. (8) Basaltic Volcanism on the Terrestrial Planets, Chapter 1. (9) Allegre C.J. (1975) Science 187, 436. (10) Papanastassiou D. A. and Wasserburg G.J. (1969) EPSL 5, 361. (11) York D. (1966) Can. J. Phys. 44, 1079. (12) Jacobsen S.B. and Wasserburg G.J. (1980) EPSL 50, 139. (13) Birck J.L. and Allegre C.J. (1978) EPSL 39, 37. (14) Minster J.-F. et al. (1982) Nature 300, 414. (15) Basaltic Volcanism on the Terrestrial Planets, Chapter 7. (16) Lugmair G.W. (1974) Meteoritics 9, 369. (17) Unruh D. et al. (1977) EPSL 37, 1. (18) Hamet J. et al., PLPSC 9, 1115. (19) Nakamura N. et al.(1977) Lunar Sci. VIII, 712. (20) Nakamura N. et al. (1982) GCA 46, 1555. (21) Nakamura et al. (1983) Mem. NIPR 30, 323. (22) Shih C.-Y. (1985) GCA, in press. (23) Reimold W.U. et al. PLPSC 15, in press. (24) Shih C.-Y. et al. (1984) Lunar and Planet. Sci. XV, 774. (25) Bogard D.D. et al. (1985), Lunar and Planet. Sci. XVI, submitted. (26) Wasserburg G.J. et al. (1981) GCA 45, 2311. (27) Jacobsen S.B. and Wasserburg G.J. (1984) EPSL 67, 137. (28) Lugmair G.W. et al. (1977) Meteoritics 12, 300. (29) Lugmair G.W. and Scheinen N.B. (1975) Meteoritics 10, 447.

TERRESTRIAL AGES OF FOUR YAMATO ACHONDRITES

Schultz, L.

Max-Planck-Institut für Chemie, D-65 Mainz (W-Germany)

The terrestrial age of meteorites can be obtained from the measurement of cosmic-ray-produced radioactive nuclides with suitable half-lifes. Antarctic meteorites yield terrestrial ages up to $7 \cdot 10^5$ years (Nishiizumi, 1984). For ages less than about $5 \cdot 10^4$ ys ^{14}C and for older ages of metal-containing meteorites ^{36}Cl were used successfully (Fireman, 1983; Nishiizumi et al., 1983).

^{81}Kr with a half-life of about $2 \cdot 10^5$ ys is another cosmogenic nuclide which can be applied to determine terrestrial ages of Antarctic meteorites. However, the concentration of this isotope in chondrites is very low (about 10^{-14} ccSTP/g). It is also difficult to obtain the cosmogenic Kr component due to the presence of trapped gases and neutron effects on bromine. Therefore, the determination of terrestrial ages using ^{81}Kr is restricted to achondrites with higher concentrations of target elements for the production of cosmogenic krypton.

Freundel et al. (1983) and Schultz and Freundel (1984) have reported ^{81}Kr-terrestrial ages of Antarctic eucrites. The terrestrial age is calculated from the apparent ^{81}Kr-Kr-exposure age and the "true" exposure age deduced from cosmogenic ^{38}Ar. The production rate of this isotope as a function of the chemical composition of the sample was determined from measurements on four eucrite falls.

For 4 Yamato achondrites concentration and isotopic composition of Ar, Kr and Xe were determined mass spectrometrically. Exposure ages as well as terrestrial ages are given in Tab. 1. Included are also data of 3 Yamato eucrites given by Freundel et al. (1983). These ages are recalculated using production rates of ^{38}Ar calculated with the now known chemical composition of the samples.

The polymict eucrites Y74450 and Y790007 have identical exposure and terrestrial ages. This is strong evidence that both eucrites belong to the same fall. Thus, Y790007 seems to be not an individual fall as provisionally suggested by Delaney et al. (1983). The 3 polymict eucrites Y790122, Y790260 and Y790266 have similar exposure and terrestrial ages. They are paired but do not belong to the Y74450 eucrite family.

The terrestrial age of the diogenite Y75032 is in agreement with previous ^{14}C determinations of Y74013 (Fireman, 1983; Jull et al. 1984). The terrestrial age of the howardite Y790727 is with about 225 000 years so far the longest age observed for Yamato meteorites. At the moment the terrestrial age of only 10 Yamato meteorites are known but it seems that these meteorites have on an average younger terrestrial ages than Victoria Land finds.

References:
Delany, J.S., Takeda, H., and Prinz M. (1983) Mem. Nat. Inst. Polar Res., Special Issue 30, 206.
Fireman, E.L. (1983) Mem. Nat. Inst. Polar Res. Special Issue 30, 246.
Freundel M., Crabb J., and Schultz L. (1983) Meteoritics 18,299.
Nishiizumi,K., Arnold J.R., Elmore D., Ma X., Newman D.m and Grove H.E. (1983) Earth Planet. Sci. Lett. 62, 407.
Nishiizumi K. (1984) In"Field and Laboratory Investigations of Meteorites from Victoria Land, Antarctica"(ed. U.B. Marvin and B. Mason). Smithsonian Institution Press, p. 105.
Schultz L., and Freundel M. (1984) Meteoritics 19 (in press).
Jull, A.J.T., Zabel T.H., Donahue D.J., and Fireman E.L.(1984) Lunar Planet. Sci. XV, 421.

Tab. 1: Exposure age and terrestrial age of Yamato achondrites

Meteorite	Class	Exposure age (in 10^6 years)	Terr. age (in 10^3 ys.)
Y74450	p. Euc	73.3 ± 6.4	-34 ± 44
Y790007	p. Euc	73.5 ± 7.2	-31 ± 34
Y75032	Dio	17.2 ± 1.6	22 ± 56
Y790727	How	12.7 ± 1.2	225 ± 58
Y790122 *	p. Euc	24.4 ± 1.8	111 ± 31
Y790260 *	p. Euc	21.6 ± 1.7	140 ± 32
Y790266 *	p. Euc	22.0 ± 2.0	150 ± 33

*: Recalculated values from Freundel et al. (1983)

69－1

Gas permeability of some Antarctic chondrites

N. Sugiura, T. Matsui and D.W. Strangway
University of Toronto, University of Tokyo

Gas permeability of chondrites is an important physical parameter which might have determined redistribution of volatile elements in meteorite parent bodies during the period of thermal metamorphism.

We have measured the gas permeability of 11 Antarctic chondrites. Together with the previous results on 15 chondrites (Sugiura et al. 1984; Matsui et al. 1985), the permeability data on H and L chondrites show well-defined trends.

Fig. 1 shows the relationship between confining pressure dependence of gas permeability (ordinate) vs. driving (gas) pressure dependence of gas permeability (abscissa). The confining pressure dependence is considered to be a good indicator of the dependence of the permeability on cracks. The driving pressure dependence is an indication of the size of the channels through which the gas permeates. Threfore, the positive correlation in Fig. 1 suggests that the size of cracks is larger than that of genuine (spherical) pores.

In Fig. 2 the permeability (at 8 bar) is plotted against porosity (porosity data from Yomosida and Matsui, 1983). The permeability increases with increasing porosity at lower porosities. At porosities more than 8% the permeability is almost constant, independent of the porosity. H chondrites seem to follow the trend of all chondrites, although their permeability is more variable than that of L chondrites.

As far as the L chondrites are concerned, the least porous and least permeable 5 chondrites are heavily shocked (type d and e of Dodd and Jarosewich, 1979), and the shock events are fairly recent ones. Therefore, the typical gas permeability of L chondrite parent body in the early solar system is considered to be 10E-3 Darcy.

References

N. Sugiura, N.S. Brar, T. Matsui and D.W. Strangway Proc. 14th Lunar Planet. Sci. Conf. (1984) 641-644.
T. Matsui, N. Sugiura and N.S. Brar, submitted to G.R.L.
R.T. Dodd and E. Jarosewich, Earth Planet Sci. Lett. 44 (1979), 335-340.
K. Yomogida and T. Matsui, J. Geophys. Res. 88 (1983) 9513-9533.

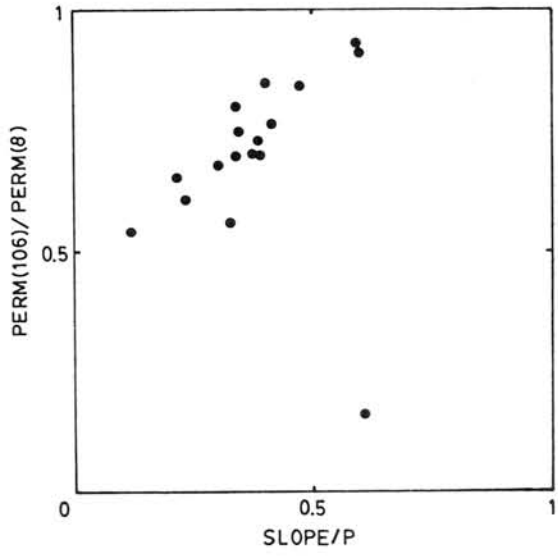
PERM(106)/PERM(8)
1
0.5
0
0.5
1
SLOPE/P

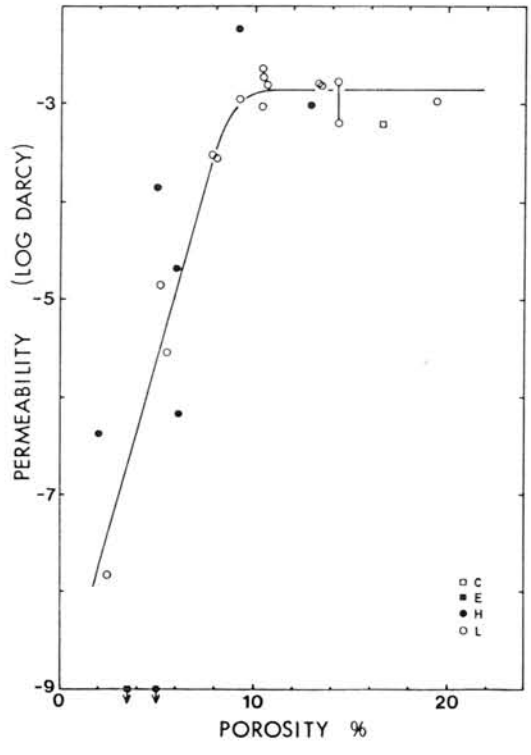
PERMEABILITY (LOG DARCY)
-3
-5
-7
-9
0
10
20
POROSITY %
C
E
H
L

COSMOGENIC Al-26 IN YAMATO METEORITES AND THEIR TERRESTRIAL AGES

Komura, K., Tan, K. L. and Sakanoue, M.
Low Level Radioactivity Laboratory, Kanazawa University, Wake, Tatsunokuchi, Ishikawa 923-12

Cosmogenic Al-26 in 12 Yamato meteorites (9 chondrites, 2 eucrites and 1 diogenite) was measured by means of non-destructive γ-spectrometry. In order to obtain the detection efficiencies for the γ-rays, mockup sources having almost the same shape and density as those of the meteorite samples were fabricated from mixture of plasticine (containing natural U, Th and K) and metallic nickel powder for each specimen and measured under the same counting geometry.

Results are summarized in Table 1 together with the K content, Cs-137 and Mn-53 activities (1). The Al-26 activities of chondrites range from 40 to 56 dpm/kg, while those of the eucrites and diogenite show rather high value of 72-75dpm/kg due to the high abundance of SiO_2 as the target material which produces Al-26. As shown in Table 1, K contents of L- and H-type chondrites are well confined in the range between 0.07 % and 0.08 %, but those of the eucrites and diogenite, particularly the latter, are much lower than those of the chondrites. Artificial fallout nuclide Cs-137 derived from nuclear testings was observed for all of the specimens. This may be used as an indicator to know the level surface contamination of the meteorite by terrestrial substances.

Among these meteorites, Y-75109, -75111, -75112 and -75113 are considered to be fragments of the same meteorite. K contents in these specimens agree well within the limit of counting error, while rather large differences were observed for their Al-26 activities (41-55 dpm/kg). These difference may be explained by considering that the specimen with low Al-26 activity was located near the surface portion of the preatmospheric body of rather small meteorite. Measurements of other cosmogenic nuclides such as Mn-53, Cl-36, Ne-22, etc. are

required to solve this problem.

Cosmic-ray exposure and terrestrial ages of Yamato meteorites have been estimated from the data of the nuclide pair of cosmogenic Al-26 and Mn-53. Fig. 1 shows a simple method to estimate both the exposure and terrestrial ages by drawing Al-26 — Mn-53 correlation for the Antarctic meteorites measured in our laboratory since 1979. The Mn-53 activities were taken from the data compiled by M. Honda (1). Here, Al-26 and Mn-53 activities are plotted against their saturation activities.

Al-26 : 60 dpm/kg for L, LL type chondrites

: 57 dpm/kg for H type chondrites

: 72 dpm/kg for diogenites and eucrites

Mn-53 : 430 dpm/kg-Fe+1/3Ni

The exposure and terrestrial ages of each meteorite can easily be read off from the figure. As can be seen in Fig. 1, there are some cases in which the Al-26 and/or the Mn-53 acvitities are higher than their saturation activities assumed here. This is caused by the use of improperly low saturation activity. The inverse, namely higher saturation activity, should, however, be considered evern for the case apparently reasonable plot.

The ages obtained by the simple method shown here are, of course, not very accurate but are useful to estimate approximate values of exposure and terrestrial ages of the Antarctic meteorites.

(1) Honda, M., private communication (1981).

Table 1. Cosmogenic nuclides, natural K and fallout Cs-137 in Yamato Meteorites.

Meteorite	Type	Weight (g)	Al-26 (dpm/kg)	K (%)	Cs-137* (cpm)	Mn-53** (dpm/kg-Fe+1/3Ni)
Y-74647	H5	100.82	52±4	0.071±.011	0.252±.007	329±17
Y-74650	L6	160.50	51±4	0.074±.009	1.131±.022	380±17
Y-74663	LL6	99.96	40±4	0.077±.013	0.147±.007	255±11
Y-75011	Euc	62.88	72±6	0.043±.001	0.583±.014	
Y-75015	Euc	77.17	75±6	0.051±.002	0.578±.011	460±21
Y-75028	L3	112.66	50±4	0.076±.008	0.266±.006	237±10
Y-75032	Dio	104.86	73±4	0.012±.002	0.977±.019	
Y-75097	L6	247.15	56±3	0.075±.012	0.327±.011	425±18
Y-75109	L6	428.40	55±2	0.075±.019	0.607±.012	
Y-75111	L6	103.00	41±3	0.073±.006	0.260±.006	
Y-75112	L6	114.47	48±5	0.081±.009	0.333±.009	
Y-75113	L6	153.29	45±3	0.072±.007	0.531±.012	

* Contamination by fallout Cs-137 is limitted only to surface portion.
** Compiled date by M. Honda (1981).

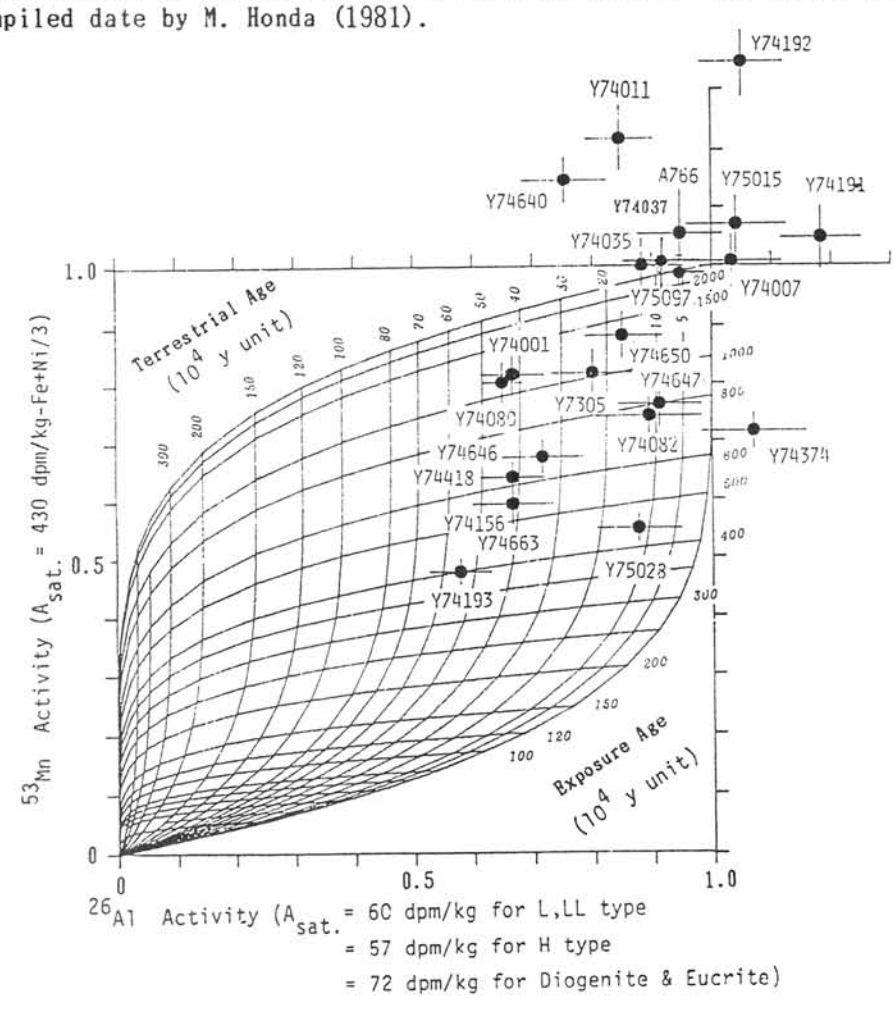

Fig. 1 Estimation of exposure and terrestrial ages of Antarctic meteorites.

CARBON-14 TERRESTRIAL AGES OF ANTARCTIC METEORITES

Matsuda,E, and Kigoshi,K.

Department of Chemistry, Gakushuin University, Mejiro, Toshima-ku Tokyo 171

The three Yamato meteorites, Y-74013,Y-74097 and Y-74136 which are all diogenites, were found at sites apart from one to two kilometers each other on the bare ice sheet in Antarctica. However, they are considered to be a single meteorite because of their unique textures. The terrestrial ages of these meteorites may provide an evidence for a single meteorite.

This paper presents the results of the determination of the terrestrial ages of these three meteorites. The carbon was recovered as carbon dioxide at 600°C and 1200°C in a vaccuum system. The carbon recovered at 600°C contained terrestrial carbon resulting from weathering, and the cosmic-ray-produced carbon-14 was released at 1200°C. The carbon dioxide obtained at 1200°C was converted to acetylene, and its beta-activity was measured in a proportional counter having a sensitive volume of 53.0 ml.

The terrestrial ages were obtained by comparing the carbon-14 activities with those of recent falls,Allende and Bruderheim. The results were given in Table 1.

Table 1. Carbon and carbon-14 contents and terrestrial ages of meteorites.

Meteorite (Wgt)	Recovered carbon at 1200°C (mg)	^{14}C (dpm/kg)	$^{14}C/C$ (dpm/g carbon)	Terrestrial age (years)
Y-74013 (16.9 g)	0.54	7.1 ± 1.0	222 ± 31	16,000 ± 1000
Y-74097 (15.8 g)	0.67	5.3 ± 1.1	120 ± 30	19,000 ± 2000
Y-74136 (14.9 g)	0.81			
Allende (18.5 g)	____	49.1 ± 1.8	_____	Modern
Bruderheim (16.7 g)	_____	52.9 ± 2.3	_____	Modern

72

Terrestrial age of an antarctic meteorite by thermoluminescence technique.

S.Miono, H.Kujirai, M.Yoshida, K.Ninagawa‡ N.Takaoka**

Osaka City University, Okayama University of Science‡
Yamagata University**

We have continued the experiment to establish the method and technique for the purpose of determinning the terrestrial age of meteorite by thermoluminescence of fusion crust. We will discuss the problem encountered on routine work.

STUDY OF TERRESTRIAL AGE OF ANTARCTIC METEORITES BY THERMOLUMINESCENCE TECHNIQUE

Ninagawa,K.*, Takaoka,N.**, Yamashita,Y.***, Wada,T.***, and Yamamoto,I*
* Okayama University of Science, Okayama JAPAN 700.
** Yamagata University, Yamagata, 990.
***Okayama University, Okayama, 700.

The thermoluminescence (TL) technique used for dating the terrestrial ages of the meteorites (SEARS and DURRANI,1980; MELCHER, 1981) was based on the TL fading of interior samples. The depth dependence of the TL for Antarctic meteorites with fusion crust was measured (NINAGAWA, et. al. 1983). In this time, we have measured emission spectra and spatial distribution of TL of Antarctic meteorite [MET-78028(L6)] by using TV-camera system.

TV-camera system.

The system is shown in Fig. 1. TL data is recorded by video cassette tapes. TL data are able to be analysed repeatedley via video image processor. For the case of taking emission spectra of TL, we have exchanged a spectroscope with a camera lens and a filter.

Emission spectra of TL.

Emission spectra of TL of MET-78028(L6) is showen is Fig. 2. This sample is powdered meteorite (MET-78028) irradiated with X rays ($\sim 10^5$ R). The meteorite TL has a wide spectral band with a maximum at about 450 nm. So in the TL measurement of MET-78028 we have used the band pass filter, Corning 4-96 (blue-green).

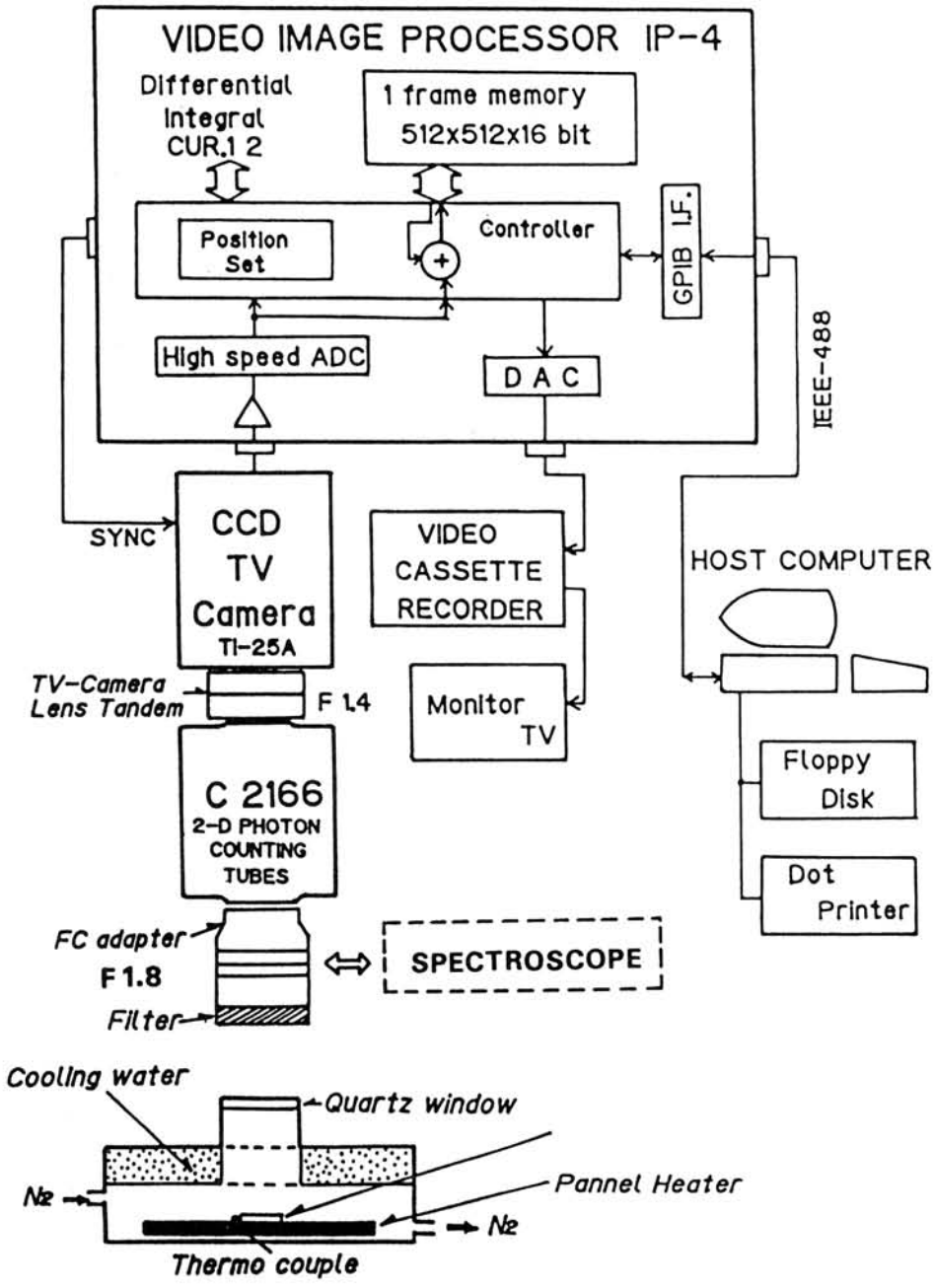

Fig. 1. Block diagram of the measuring and analysing system for the TL of Antarctic meteorites. For the TL emission spectrum, a spectroscope (NC-10N) is used by exchanging with a camera lens and a filter.

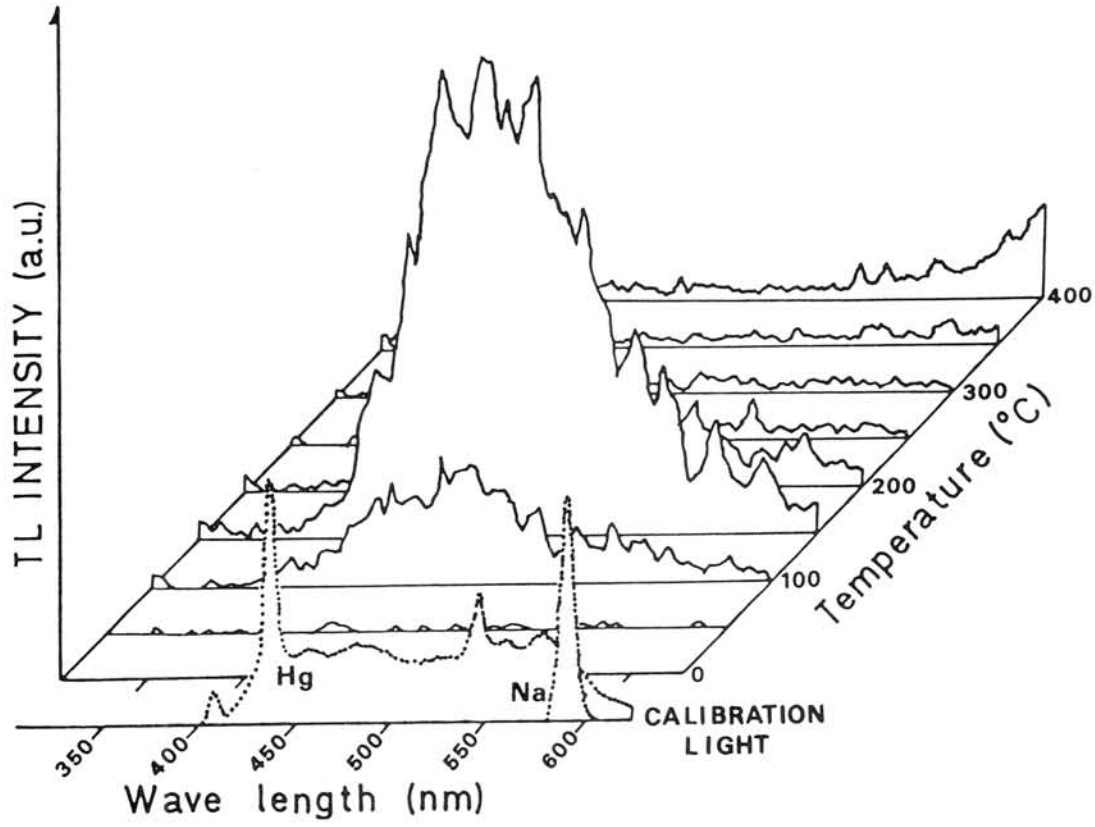

Fig. 2. Emission spectra of TL of MET-78028 at each temperature. For calibration light, a Na-lamp and a fluorescent lamp are used.

Spatial distribution of TL

In this time, as Antarctic meteorite, MET-78028(6L) is used. Samples are slices of this meteorite shown in Fig. 3.

One slice in pairs was artificially exposed to ^{60}Co 1 KR γ rays. By using TV-camera system shown in Fig. 1, a pair of slices and interior of this

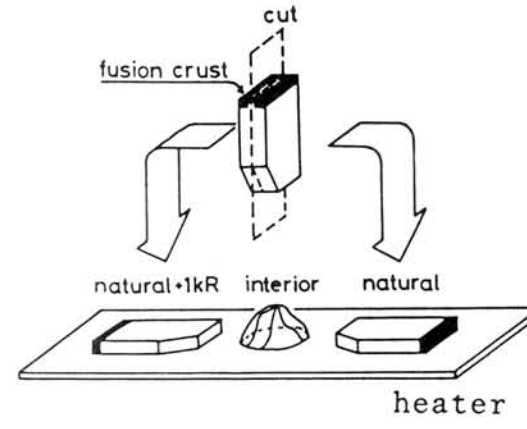

Fig. 3. Cutting and setting.

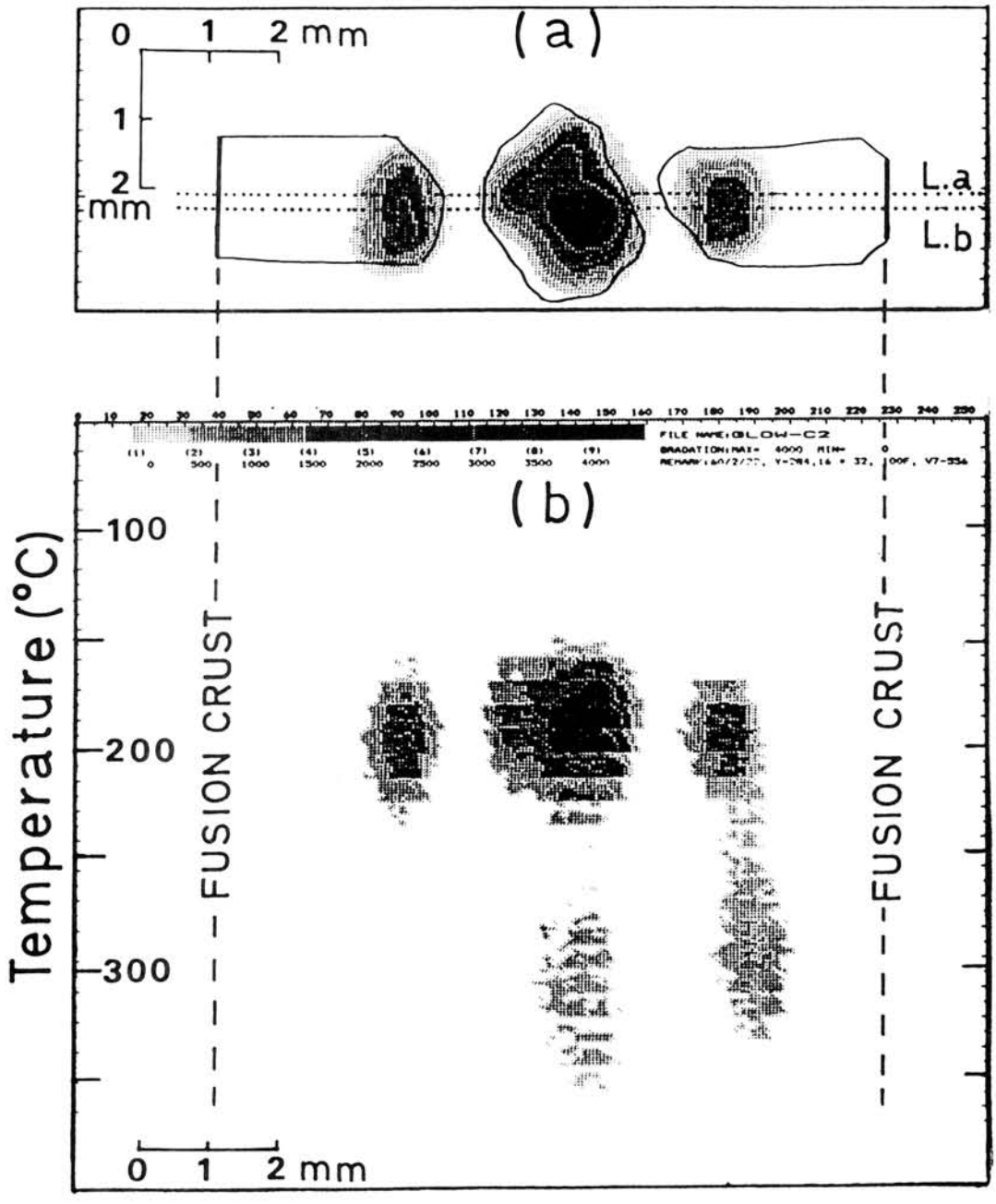

Fig. 4. a) TL-spatial distribution of slices in pair and interior, (b) Time variation (corresponding to temperature) of TL for the area from line L.a. to line L.b.

meteorite were heated (rising rate: 2.3 °C/sec) and TL spatial distributions of these sample were recorded in video cassette tape for about 160 sec (∿5300 frames).

TL data are able to be read out from video tape via video image processor. Two examples of read out are shown in Fig. 4a, b. The Fig. 4a is TL spatial distribution of samples.

The TL yield of both slices was not measured at near fusion crust. The Fig. 4b is shown the TL variation of heating temperature at the area from line L.a to line L.b. The TL at higher temperature was measured at the fusion crust side comparing with the TL at lower temperature.

Spatial distribution of TL sensityvity.

After natural TL read-out, samples corresponding to Fig. 4a were irradiated with X rays (∿10^5 R). These irradiated samples were also heated and TL spatial distributions of tnese samples were read out, (shown in Fig. 5). The Fig. 5 shows spatial distributions of TL sensitivity of these samples. Slices in pairs of MET-78028 have low TL sensitivity near fusion crust.

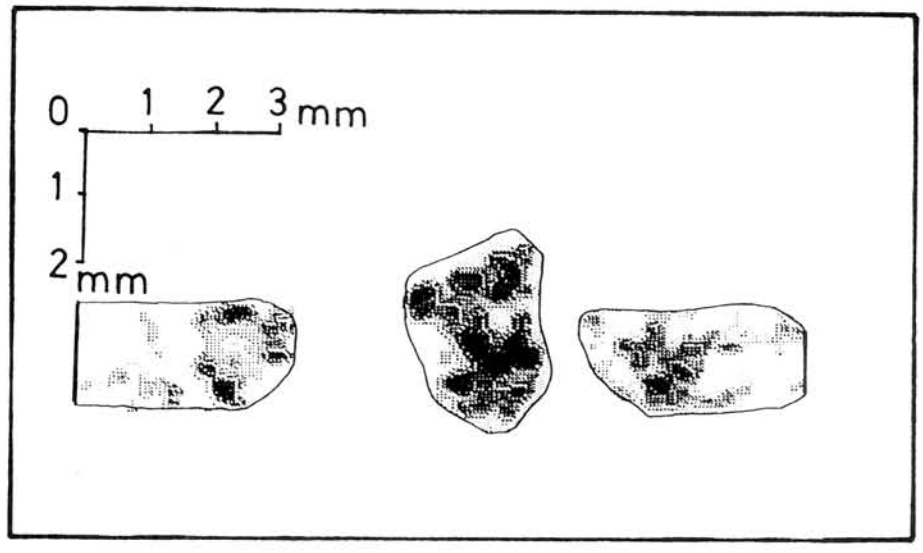

Fig. 5. Spatial distribution of TL sensitivity.

74—1

TRACE ELEMENT INVESTIGATIONS ON A SIKHOTE-ALIN IIB IRON METEORITE SAMPLE

H. H. Weinke, W. Kiesl, F. Kluger, and C. Koeberl

Institute of Geochemistry, University of Vienna
P.O. Box 73, A-1094 Vienna, Austria

Sikhote-Alin is well known as the largest mass seen to fall in historical times (Feb. 12, 1947). It is a member of group IIB (coarsest octahedrite). The sample which was at our disposal had a weight of about 125 g, containing large troilit nodules, graphite, and schreibersite. Sikhote-Alin metal contains large and irregularly kamacite, the bandwidth of which has been determined from various etched sections to be 9±5 mm. The borders of the kamacite are very often surrounded with about 1 mm wide schreibersite lamellae. Widmannstätten bands are rare, but Neumann bands with 1-10 µm width are abundant. Also taenit and plessite are also rather rare, in accordance with the low nickel content of this meteorite. Schreibersite has been found at the phase boundary of the troilite nodules (with graphite) and at the borders of the kamacite.

Studies of the samples at our disposal have been made using various techniques. Major element variations have been investigated using an electron microprobe (fully automated ARL-SEMQ electron microprobe). The phases investigated with the microprobe were kamacite, schreibersite, troilite, graphite, and chromite. The latter is abundant as accessory mineral in the form of very small inclusions in the troilite, and has the approximate composition 12.4% Fe, 48.7% Cr, and 7.16% Mg. Olivine, which has been described adjoining the troilite and the chromite, was not found in our sample.

For activation analysis, the troilite and the metal phase were seperated carefully. About 300-500 mg have been irradiated for four days at a neutron flux of about $1.7 \cdot 10^{13}$ n $cm^{-2}s^{-1}$, and processed after three days cooling, following a radiochemical analysis scheme decribed in principle by Kiesl et al. (1967). The results are given in the table on the next page. Only results from radiochemical neutron activation analysis is given here, data analysis of rapid instrumental neutron activation analysis (RINAA, see Koeberl and Grass, 1983), INAA, and other neutron activation methods on different phases (phosphide, troilite, etc.) is in progress.

In addition, trace element determinations in some phases using an ion microprobe have been made. The instrument used was a Cameca IMS-300 ion microprobe. Spectra have been taken with mass resolution 5000 between mass numbers 23 and 76. The following elements have been determined: Na, Mg, Al, Si, P, K, Ca, Sc, Ti, V, Cr, Mn, Fe, Co, Ni, Cu, Zn, and Ga.
The dispersed chemical abundances within the IIAB group point to a chemical rather inhomogeneous parent body, with the

possibility of fractional crystallisation in the core.

References: Kiesl, W., Seitner, H., Kluger, F., and Hecht, F. (1967) Monathefte Chemie 98, 972.

Koeberl, C., and Grass, F., (1983) Meteoritics 18, 325.

Table: Selected trace elements in troilite and metal phases in the Sikhote-Alin meteorite, determined by radiochemical neutron activation analysis

	metal	troilite
Zn	0.3 ppm	0.41 ppm
As	8.4 ppm	1.2 ppb
Se	4 ppb	99.6 ppm
Mo	9.5 ppm	3.3 ppm
Ru	4.4 ppm	10 ppb
Re	2.2 ppb	0.4 ppb
Os	19 ppb	5 ppb
Ir	27 ppb	0.7 ppb
Au	0.85 ppm	1.2 ppb

75—1

SCANDIUM AND SILVER IN IRON METEORITES.

M.Honda, H.Nagai, T.Kume and K.Maeda

Department of Chemistry, College of Humanities and Sciences, Nihon University,Setagaya-ku,Tokyo,156.

In the previous meeting of this symposium, we presented some preliminary work on the determinations of cosmogenic scandium-45 in several specimens of iron meteorites[1]. We will discuss this topic again with our recent results.

In irons, because of their high purity, the stable cosmogenic nuclides of Cr,V,Ti,Ca and K are detectable except for their most abundant isotopes. The contents of these products areusually in the range of 1-10 ppb. Intrinsic co-existing elements in the irons are called siderophile elements. On the other hand, the lithophile elements mentioned above, including scandium, are essentially seen as foreign impurities. In fact, the presence of typical lithophile elements has recently been studied extensively. In the results, their reported contents have been reduced substantially and in many cases no reliable figures for their lower limits have been established yet. The contents of natural K,Ca,Pb, and U, and more recently of Ag, have been found to be extremely low, even as low as 10^{-12} g/g.

As described above, the level of cosmogenic Sc-45 is usually 1-3 ppb. but sometimes the content is much lower. Scandium is monoisotopic, and some substantial blank corrections must be made for natural scandium,if there is any, and this will cause an ambiguity in the determinations of cosmogenic components. To minimize the cosmic ray irradiation effects, some samples have been selected from extremely large objects,and the lowest level of cosmogenic Sc-45 was expected to be less than 0.01 in respect to ordinary levels. Such a level can be estimated from the contents of other stable products such as He-3, when available, or else indirectly from the data of Mn-53.

In this study, the neutron activation method has been applied extensively. For levels of 1 ppb or less, 0.1-1 g size

samples have been irradiated with neutron doses of 10^{17}-10^{19} n/cm^2. For the samples which contain higher scandium the Triga II reactor, at the Atomic Energy Research Institute, Rikkyo Univ. have been used, and for the low-level samples (Toluca and DRP78008) the irradiation was carried by the JRR4 and JRR2 at the Japan Atomic Energy Research Institute, Tokai. Sample preparation is important in this work. The cleaning of terrestrial contaminations from the sample surfaces was carried out using nitric acid and aqua regia. The surface etchings were performed before and after the irradiation; and after the etchings, the metal phases were dissolved in dil. nitric acid in the presences of Sc and Ag carriers of ca.5mg each. In some cases, unattacked inclusions were left behind and they should be separated by filtration. The radio-chemical separations of Sc-46 and Ag-110m from Fe+Ni and from other activities such as Co-60, Ir-192, and Mn-54 were performed as described in our previous paper[1]. The removal of radioactive impurities was satisfactorily made afterone or two runs of a cation exchange processes. The yields were usually 60-80%, determined by weighing Sc_2O_3 and AgCl, before counting and also by reactivation for Sc after countings.

(I). Scandium:

The results are shown in Table 1. Our older data are also listed with higher uncertainties. In this work, our keen interest was to find out the representative value of the natural scandium content already existing in alloys of Fe+Ni before influenced by cosmic rays. As far as we have found in this study that level seems to be 10^{-11} g/g in general.

The neutron activation method we employed may have been interferred from several sources. One of them is a side reaction caused by co-existing titanium. The reaction Ti-46(n,p)Sc-46, with the Q value of -1.6 Mev, will interfere, especially in the Triga II reactor which has a low Cd ratio, lower than 10. The problem is to look at the contents of natural titanium in the samples and the yield of this reaction due to high energy neutron components. According to the irradiation experiments, Sc-46

production through the (n,p) in Ti should be equivalent to about 10^{-5} timesthe same quantity of Sc; that is, one ppm Ti causes an additional production of Sc-46 at the level of 0.01 ppb (Nitoh,1980)[2]. On the other hand, the contents of Ti in irons are rather obscure. In the Grant and Aroos meteorites, Imamura et al(1986) reported that 0.1-1 ppm Ti were found by dilution mass-spectrometry. They may be the upper limits in these irons because of a possible laboratory contamination of the Ti in the chemical processes. Data from other literatures are not reliable, especially as older analyses reported higher than 10, or even up to 100 ppm Ti in other meteorites. Titanium in inclusions, however, can be higher because of the charcophile nature of this element under extreme reducing conditions. In any case, the influence seems to be low, but not negligible in some cases, by irradiation in the RSR of the Triga reactor. If necessary, Ti contents may be measured directly by detecting Sc-47 activities produced via Ti-47(n,p), which should give us a signal at about a 200 times higher sensitivity just after the shorter irradiation[2].

The effects of inclusions, such as sulfides and phosphides, may also result in a high Sc blank from the sample. These inclusions in the sample may be examined through observation during the dissolution step with nitric acid.

(II). Silver:

Some preliminary studies have been extended for Ag along with Sc. As described in the reports by Wasserburg's group[4], the contents of silver are really low after an extensive removal of the surface materials by etchings. Before the Sc chemistry, AgCl was precipitated with the carrier from the nitric acid solution of the meteorites. Ag can be purified by a cation echange, applying the NH_4R form column for the ammoniacal solution of Ag^+ and followed by the elution of $Ag(NH_3)_2^+$ using 2N NH_4NO_3. The gamma rays of Ag-110m were detected.

According to the present work, the contents of silver

Table 1. Scandium found in Iron Meteorites.

Sample	ID	Sample size	Scandium found	Cosmogenic Sc-45 estim. from others	Other cosmogenic nuclides (liter.)	
					Mn-53	He-3
		g	ppb	ppb	dpm/kgFe	10^{-8} cc/g
DRP78008		0.10	0.027±0.002	<0.01	2.7±0.2	
Odessa	H91-2	0.75	0.05 ±0.05	<0.1	20 ±3	2--290
	H91-3	1.9	0.06 ±0.04	<0.1	190 ±25	
Toluca	128-388	1.9	0.083±0.005	0.0	4	
Gibeon		1.02	0.135±0.012	0.0	low	
Braunau		1.45	0.13 ±0.13	0.03	512 ±20	3.3
Canyon Diablo	34-5031	2.5	0.20 ±0.01	0.03-1	165 ±40	10-280
Xiquipilco (syn.Toluca)	128-400	1.21	0.34 ±0.32	0.0		
Nativitas	112-30	0.64	0.34 ±0.20			
Y790517		0.55	0.39 ±0.22			
Y790724		0.54	0.20 ±0.16			
PGP77006		0.61	1.10 ±0.03		569 ±23	
Treysa	center	0.88	1.8 ±0.2	1.8	322 ±13	580
Trenton	AII-22-2	1.03	1.92 ±0.42	1.5	499 ±28	414
Grant	K-100	0.91	1.54 ±0.04	1.6	320 ±40	490

Literature: Data compilation by Schultz and Kruse(1983) and by Nishiizumi(1982).

do not match with the behaviors of Sc. At least, however, the Ag content may indicate the extent of cleanings for other impurities, including Sc (Table 2). In the case of the Gibeon meteorite, the apparent content has been found to be about 0.2 ppb, but the contribution due to Pd-108(n,γ)Pd-109→Ag-109(n,γ)Ag-110m was predominant and the net natural Ag-109 can be estimated after the subtraction of this effect.

Table 2. Comparison of Ag and Sc found in Irons.

Sample	Etching treatment	size g	Ag found ppb	Sc found ppb
Gibeon	before	1.0	1.2±0.3	0.14±0.01
	after first	0.5	≤0.02	
	after second	0.4	≤0.02	
Toluca	after first	0.8	16	0.08±0.005
	after second			
	aliq. 1	0.3	14	0.11±0.006
	2	0.7	7	0.08±0.005
Grant	before	0.9	1.8±1.7	1.54±0.04

Reference:

1). M.Honda et al, abstract, 9th Symposium on Antarctic Meteorites,Mar.21-24(1984)p.102; Proc. of Inst. of Natural Sciences,Nihon Univ.,No.20,11-20(1985).

2). O.Nitoh, private communications (1980).

3). M.Imamura et al, Massspectroscopy,16,291(1968); M.Shima et al,"Meteorite Research" ed.P.M.Millman,p.335(1968).

4). T.Kaiser and G.J.Wasserburg, Geochim. et Cosmochim. Acta, 47,43 (1983).

Magnetic properties of Clear Taenite in Toluca iron meteorite

Minoru Funaki NIPR
Takesi Nagata
J. Danon CBPF

1. Introduction

Toluca is a polycrystalline, coarse octahedrite iron meteorite with clearly defined Widmanstatten pattern by nacked eyes. It is consisted of kamacite wilth Newmann bands, taenite, plessite, cloudy taenite and clear taenite. These minerals are included commonly in L and LL chondrites. The magnetic properties of kamacite and taenite in the meteorites are measured from achondrite, E and H class chondrites. However, it is difficult usally to measure the individual property of the plessite, the cloudy taenite and the clear taenite. The magnetic properties of the L and the LL chondritse are interpreted as the superpositions of those minerals.

2. Specimens of clear taenite

The clear taenite lamellae are obtained from the Toruca iron meteorite performing of chemimal dissolution into 2.5 N hydrochloric acid during 20 days. Since the clear taenite rims are formed around the cloudy taenite and plessite lamellae, two clear taenite specimens are obtained from one lamella. The surface of these specimens have metallic brightness on the kamacite side and dark on the cloudy taenite side. The thickness of these specimens are usually less than 10 microns and the maximum length is 5 mm.

Table 1. magnetic properties of tetrataenite in toluca iron meteorite.

Sample	heating	Is emu/g	Ir emu/g	Hc Oe	Hrc Oe
1	before	(143.5)	28.0	450	729
	after	141.8	5.0	12	30
2	before	(152.5)	70.8	695	877
	after	163.5	19.0	22	30
3	before	(133.5)	27.0	445	704
	after	130.4	15.5	18	23

Is = Saturation magnetization. Ir = Saturation remanent magnetization. Hc = Coercive force, Hrc = Remanent coercive force.

(e

3. Results

The natural remanent magnetizations (NRM) of the clear taenite specimens, 0.1-0.5 mg in weitht, range from E-1 to E-2 emu/g intensity. They are fairly stable against AF demagnetization up to 1000 Oe: the median demagnetization field (MDF) exceeds 500 Oe. The stabilities against thermal demagnetization, as shown in Fig. 1, are also stable up to 500 C, but the intensities decrease steeply from 550 to 600 C and have almost no significant magnetization at 600 C. Although the specimens acquired the anhysteresis remanent magnetization (ARM), they are not saturated up to 1200 Oe. The ARM after heated specimens at 650 C are saturated to 150 Oe. The thermomagnetic curves obtained at 10 kOe are irreversible: its magnetizations decrease steeply from 500 to 600 C in the heating curves but increase gradually from 650 C to room temperature in the cooling curves. The results of magnetic hysteresis analyses show that the coercive force (Hc) and remanent coercive force (Hrc) change to small by heating at 650 C.

From these viewpoints, the clear taenite in Toluca iron meteorite is tetrataenite as mentioned Clarke (1980). The coercivity is almost twice compared with that of Y-74160 (Nagata and Funaki, 1982). Since the NRM is very strong and stable, the existing of the tetrataenite in meteorites is important even though its amount is small.

References:

Clarke, R.S. (1980): American Mineralogy, 65, 624-630.
Nagata, T. and Funaki, M. (1982): Mem. Natl. Inst. Polar Res., Spec. Issue, 25, 222-250.

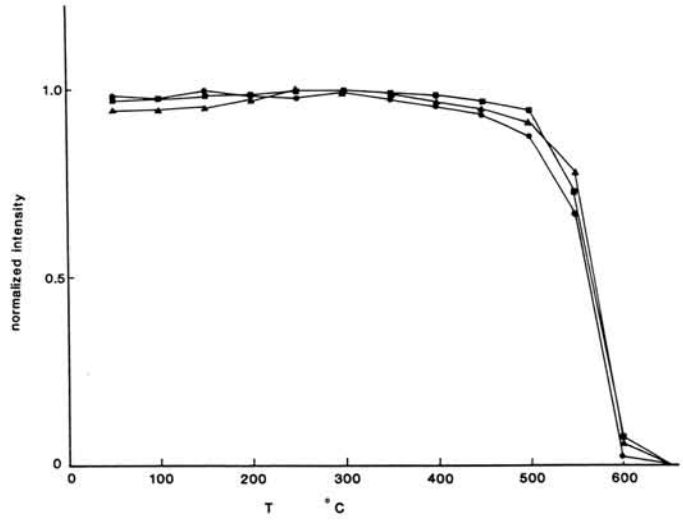

Magnetic Properties of Tetrataenite-rich Stony Meteorites (II)

Takesi Nagata and Minoru Funaki (NIPR), J.R. Dunn (University of California), J.A. Danon (Centro Brasileiro de Pesquisas Fisicas, Brazil)

Magnetic properties of tetrataenite-rich meteorites appear to be important for the paleomagnetic studies of the primordial solar system, because of the uniquely large magnetic coercivity of tetrataenite. The magnetic properties of tetrataenite-rich stony meteorites such as Yamato-74160 (LL7), ALH-77260 (L3) and ALH-77219 (mesosiderite) have been examined along the research direction (Nagata and Funaki 1982,1983).

The extremely stable NRM characteristics of the St. Séverein (LL6) had been noted before the super-lattice structure of tetrataenite crystal in it metallic component was found by Danon et al. (1979). Combined with the Mössbauer spectral studies, magnetic analyses of the St. Séverin, and the Appley Bridge (LL6) and Tuxtuac (LL5) also, are newly carried out.

1. Composition and structure of metallic component.

Results of Mőssbauer analysis show that the composition of metals of St. Séverin is given by Tetrataenite: Taenite: Kamacite = 0.51:0.095:0.395, where the ordinary taenite phase exhibites the paramagnetic characteristics at room temperature.

2. Magnetic coercivity.

The coercive force (H_C), the remanence coercive force (H_{RC}), and ratio of the saturated remanent magnetization (I_R) to the saturation magnetization (I_S), i.e. (I_R/I_S) of the St. Séverin at 295 K before and after heating up to 800 °C in 10^{-5} Torr atmosphere are summarized with those of other tetrataenite-rich stonv meteorites in Table 1.

Table 1.

Magnetic properties	St. Séverin (LL6) matrix	clast	metal	Y-74160 (LL7)	ALH-77260 (L3)	ALH-77219 (Mesosiderite)
H_C (Oe)	590	340	860	255	85	46
H_C (after heating)	35	38	4	8	120	16
H_{RC} (Oe)	1950	1310	2140	460	1150	520
H_{RC} (after heating)	210	300	47	240	400	140
I_R/I_S	0.193	0.125	0.176	0.101	0.031	0.015
I_R/I_S (after heating)	0.017	0.024	0.0016	0.0033	0.068	0.011
Θ_c (°C)	560	565	560	560	570	560

As shown in Table 1, the initial values of H_C, H_{RC} and I_R/I_S of the St. Severin are uniquely large, but they are much reduced by the heat treatment, owing to a transformation from tetrataenite to the ordinary taenite of a wide range of Ni content. Θ_c in the table is Curie point of the taenite phase.

3. Thermomagnetic characteristics.

An example of the thermomagnetic curve of the St. Séverin is shown in Fig. 1. In the initial heating thermomagnetic curve, Curie point (Θ_c) of tetrataenite phase is 560 °C, which corresponds to taenite of 54% Ni. In addition, kamacite of 5% Ni ($\Theta^*_{\alpha\to\gamma}$=770 °C, $\Theta^*_{\gamma\to\alpha}$=665 C) is present. The tetrataenite super-lattice structure is almost completely destroyed by heating to 800 °C, and a wide range of Ni-content (30-50% Ni) of cubic taenite replaces the original tetrataenite in the cooling thermomagnetic curve and in further repeated thermomagnetic cycle curves. This change would be caused by a homogenization of tetrataenite phase of 50-56% Ni and cubic taenite phase of 25-30% Ni (paramagnetic) by the heat treatment.

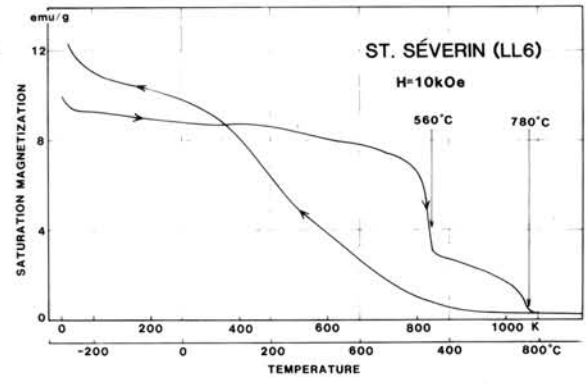

Fig. 1

4. Natural remanent magnetization (NRM).

NRM of the St. Séverin is extremely stable against the AF-demagnetization, as shown in Fig. 2. However, the stable NRM can be thermally demagnetized almost completely between 530°C and 580°C. It is expected therefore that NRM of the tetrataenite component of stony meteorites can well represent the paleomagnetic field in the primodial solar system when the meteorites were formed. The thermal stability of tetrataenite phase and the paleointensity of a magnetic field in the primodial solar system deduced from NRM of the 4 tetrataenite-rich stony meteorites will be critically discussed.

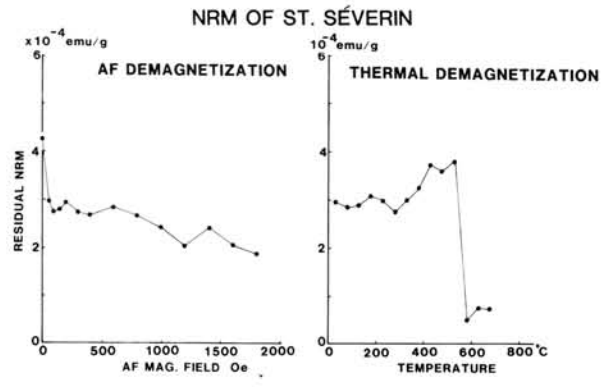

Fig. 2

References.

Danon J., Scorzelli R.B., Souza Azevedo I. and Christophe Michel-Leoy M., (1979). Nature 277. 283-284.

Nagata T. and Funaki M., (1982). Proc. 7th Symp. Antar. Meteor. 222-250

Nagata T. and Funaki M., (1983). Antar. Rec., 79. 1-10.

IRON-NICKEL PARTIAL ORDERING IN TETRATAENITE BY SYNCHROTRON RADIATION

T. Tagai[1], H. Takeda[1], M. Tokonami[1] and J. Danon[2]
[1] Mineralogical Institute, University of Tokyo, Tokyo 113, Japan
[2] Centro Brasileiro, de Pre quisas Fiscas, Rio de Janeiro, Brazil

Tetrataenite (Clarke and Scott, 1980) is the low temperature form of taenite which is one of the FeNi minerals commonly found in meteorite. It is characterized by the ordered Fe/Ni distributions. The ordering of Fe/Ni is assumed to require extremely slow cooling of 1 - 100 degrees per million years for the temperature interval of 700 - 350°C (cf. Albertsen, 1981). The determination of the ordering can be carried out by Mössbauer spectroscopy or measurement of magnetic anisotropy. But is is not so easy to determine the ordering by those methods if Fe/Ni is partially ordered. The partial ordering of Fe/Ni can more easily be determined by X-ray diffraction with applying anomalous scattering of Fe and Ni atoms. The X-ray from synchrotron radiation is ideal for this purpose because of its strong intensity and the tunability over the wide range of wave length. When we use the normal MoKα-radiation λ=0.70169 A), the scattering factors of Fe and Ni atoms are 11.47 and 12.91 ($\sin\theta/\lambda$=0.5) respectively and these atoms can not be differentiated. If the X-ray of λ=1.746 A is used, the scattering factors of Fe and Ni are 5.17 and 10.17 ($\sin\theta/\lambda$=0.5), respectively (imaginary parts are not considered).

A single crystal of tetrataenite of about 70 μm in diameter has been separated from the Saint Severin meteorite (LL6). The ordering of Fe/Ni was studied using the X-ray of λ=1.746 A from synchrotron radiation, Photon Factory, Labor. of High Energy Phys., Tsukuba, Japan. The intensities were measured on the 4-circle diffractometer. All the possible superstructure reflections were observed and no systematic extinction of the reflections was found. The intensity distribution of the reflections from the present crystal show clear tendensy of tetragonal symmetry. Assuming the space group symmetry of P4mm, the Fe/Ni ordering was refined by the least squares program. The results of refinement shows that the Fe/Ni atoms in the tetrataenite form Sait Severin meteorite are partially ordered of about 80%.

The partial ordering found by this study suggests that some iron meteorites may show different degrees of the ordering depending on their thermal history because the degree of ordering be the indicator of the cooling rate experienced by an iron meteorite.

Albertsen, J.F. (1981). Physica Scripta 23, 301-306.
Clarke Jr., R.S. and Scott, E.R.D. (1980). Am. Min. 65, 624-630.

79—1

MAGNETIC FRACTIONATION IN THE EARLY SOLAR SYSTEM

D.W. Strangway and N. Sugiura
Department of Geology, University of Toronto

Over the past few years there have been a number of studies of the remanent magnetization carried by meteorites. These have almost invariably show that there is a magnetic field recorded by various samples. These have been recorded by a number of authors including Brecher and Arrhenius (1974), Banerjee and Hargreaves (1972), Butler (1972), Stacey et al. (1961), Sugiura et al (1979), Strangway and Sugiura (1983), Funaki et al, (1981), Nagata and Funaki (1983). Sonnett (1978) reviews data measured by Russian investigators. The picture that emerges from these studies is one of strong magnetic fields, typically .1-5 oersted that were present when the samples became magnetized, whether they are carbonaceous chondrites, ordinary chondrites or enstalite chondrites.

Our studies have shown that chondrules contain a stable component of magnetization which remains randomly oriented (Sugiura and Strangway, 1983, Sugiura and Strangway, in press) in spite of accretion and other subsequent heating events. This high temperature component in chondrules suggests the presence of early fields subsequently unmodified. The matrix also appears to carry a component which in Allende is quite uniform in direction over much of the meteorite and was acquired at 320°C or less. It is not clear whether this records a heating event in the presence of a magnetic field (e.g. accretion or later metamorphism) or whether it records a chemical event (e.g. sulfidization) in the presence of a field (Wasilewski and Saralker, 1981). In either case, the matrix also appears to record fields present in the early solar system.

Models for the accretion of the solar system include those of Alfven (1954) and Alfven and Arrhenius (1970a, b) which used the presence of strong magnetic fields to cause strong element fractionation depending upon the presence of ionized gases in the solar nebula. The resulting chemistry would be determined by the ionization potential. Dodd (1981) reviews various models and points out that the chemistry of the solar system is not consistent with a model based on ionization potentials. Current models of solar system chemistry involve accretion from a high temperature gas cloud in which there are no charged particles (Dodd, 1981). These models have been remarkably successful at explaining the chemistry of meteorites and planets. Larimer and Ander (1970) however indicate that there remains a difficulty in explaining a major fractionation between silicates and metals. They review the evidence from a chemical point of view and suggest that this fractionation took place between 1050°K and 680°K. Dodd states that "at present magnetic fractionation is the only strong candidate in a very narrow field."

The view builds on the model proposed by Harris and Tozer (1967) where they suggest that single domain particles could stick together by magnetostatic action and thereby cause the initial clumping of fine iron particles. Banerjee (1967) reminds us that single domain particles of iron are restricted to the range from approx. 150°A to aproximately 3300°A. Below this size range, no remanence is present to cause the clumping and above this multidomains sharply reduce the magnetic moment.

In this paper, we propose a separate mechanism for the fractionation. Magnetic particles can be separated in the presence of magnetic fields and magnetic field gradients as a result of conventional magnetostatic effects

based on the susceptibility. The meteorite magnetism shows that there were significant fields present and we suggest that as the particles grew, the more magnetic or iron-rich ones were separated by the action of these fields after the temperatures had fallen to the Curie point.

There has been much speculation on the source of such a field. Levy and Sonnett (1978) consider that the cause was either a strong solar dipole spread into the solar wind, associated with the early sun and a T-Tauri stage or with a hydromagnetic dynamo associated with the solar nebula itself. Ip (1984) suggests a further possiblity which depends upon enhancement of a field associated with an intense solar wind of charged particles interacting with the solar nebula.

The presence of a widespread magnetic field together with the presence of iron-rich particles (150°A or perhaps less due to superparamagnetion could lead to metal-silicate fractionation once the dust particle temperature is below the Curie point of iron (approx. 1050°C).

References

Brecher, A. and Arrhenius G., 1974, J. Geophys. Res., 79, 2081; Banerjee, S. and Hargraves, R., 1972, E.P.S.L., 17, 1170; Butler, R., 1972, E.P.S.L., 17, 120; Stacey, F., Lovering, J., and Parry, L., 1961, J. Geophys. Res., 66, 1523; Sugiura, N., Lanoix, M. and Strangway, D., 1979, Phys. Earth Planet Int., 20, 342; Strangway, D. and Sugiura, N., 1983, Adv. Space Res., 2, 47; Strangway, D., 1980, Precambrian Res., 10, 167; Lanoix, M., Strangway, D. and Pearce, G., 1978, Geophys. Res. Letters, 5, 73; Funaki, M. Nagata, T. and Momose, K., 1981, Proc. Sixth Syp. Antarctic Meteorites, 300; Nagata, T. and Funaki, M., 1983, Proc. Eight Symp. Antarctic Meteorites, 403; Levy, E. and Sonnett, C., 1978 in Protostars and Planet, U. of Arizona Press; Sonnett, C., 1978, Geophys. Res. Letters, 5, 151; Sugiura, N. and Strangway, D., 1983, E.P.S.L., 62, 169; Sugiura, N. and Strangway, D., J. Geophys. Res., in press; Wasilewski, P. and Saralker, C., 1981, Proc. 12th L. Pl. Sc. Conf., 1217; Alfven, H., On the origin of the solar system, Oxford Press; Alfven, H. and Arrhenius, G., 1970a, Astrophys. Space Sci., 8, 338; Alfven, H. and Arrhenius, G., 1970b, Astrophys and Space Sci.,9, 3; Dodd, R., Meteorites Cambridge; Larimer, J. and Anders, E., 1970, Geochim. Cosmochim Acta, 34, 367; Harris, P. and Tozer, D., 1967, Nature, 215, 1449; Banerjee, S., 1967, Nature, 216, 781; Ip, W., 1984, Nature, 312, 625.

MAGNETIC PROPERTIES OF THE SANTA CATHARINA Ni RICH ATAXITE

J. Danon*, M.Funaki**, T.Nagata**

*Centro Brasileiro de Pesquisas Físicas, Rio de Janeiro,Brazil
** National Institute of Polar Research, Tokyo, Japan.

Since the characterization of the ordered taenite (tetrataenite) in meteorites, the Santa Catharina Ni-rich ataxite (32.6 wt%) has been object of several studies by Mossbauer spec - troscopy, X-ray diffraction, electron microscopy and microprobe measurements. However only one investigation was reported more than twenty years ago on its magnetic properties. These results have been discussed in connection with a proposed magnetic classi fication of the iron meteorites (1).

Elemental distribution and compound analysis of a Santa Catharina sample from the Museu Nacional of Rio de Janeiro, Brazil has been investigated with a Computer Aided Micro-Analyser JCMA-733. The Ni/Fe ratio ranges from 0,85 to 1.1 in about 40% of the scanned area. This in agreement with the presence of about 50% of ordered taenite in this meteorite(2).

Table I lists the magnetic hysteresis characteristics of Santa Catharina.

Magnetic	Initial		After heating	
Parameter	25°C	-269°C	25°C	-269°C
I_s (emu/g)	59	70	93	142,5
I_R (emu/g)	42.5	51	0.225	0.35
H_C (Oe)	2.800	3.950	9.5	14
H_{RC} (Oe)	4.060	5.200	335	253
χ_p (emu/g/Oe)	1.5×10^{-3}	1.2×10^{-3}	8×10^{-4}	5.0×10^{-4}

The remarkable results are the very large decrease in H_C and I_R after heating up to 940°C. This is a consequence of the transformation of the magnetically coercitive tetrataenite to the magnetically soft ordinary taenite.

The thermomagnetic curve of Santa Catharina shows the same typical shape of other tetrataenite rich meteorits being flat up to 500°C and droping the cooling curve is convex and re- sembles the thermomagnetic curve for ordinary ferromagnetic mate-

rials.

Possible causes for the observed flatness of the thermomagnetic curve of tetrataenite have been discussed. In a recent prived communication to one of us (J.D.) Professor L.Néel suggested that the real Curie point of the tetrataenite should be much higher than that of the disordered 50.50 Fe-Ni taenite, possibly between 900-1.000°C. However, due to disordering during heating this cannot be observed directly, but it would strongly contribute to the flatness of the thermomagnetic curve.

In conclusion, the magnetic properties of the Santa Catharina ataxite are similar to those observed in tetrataenite rich meteorites like Yamato-74160 (LL7), ALH-77260(L3) and St. Severin (LL6).

(1) Nagata T. - Proc.7th Symposium on Antartic Meteoritis, 216-221, NIPR (1982).

(2) Danon J., Scorzelli, R., Souza Azevedo, I., Curvello, W. Albertsen, J.F. and Knudsen, J.M. Nature, 277, 283-284 (1979).

(3) Nagata T. and Funaki M., Proc.7th Symposium on Antartic Meteoritis, 222-250, NIPR (1982).

81

Antarctic Iron Meteorites: A review(tentative)

Roy S. Clarke, Jr.

Division of Meteorites, Smithsonian Institution, Washington D. C. 20560

FRACTAL DIMENSIONS OF FRACTURE SURFACES OF ROCK FRAGMENTS

Akio FUJIMURA, Muneyoshi FURUMOTO, Yasuhiko TAKAGI,
and Hitoshi MIZUTANI
Dept. Earth Sciences, Nagoya University, Nagoya 464, Japan

The textural features of meteoritic materials is expected to carry the significant information on the physical environment which the materials have experienced in the early stage of planetary evolution. Among the textural features, the geometrical irregularity of inclusions such as broken chondrules and lithic fragments in meteorites reflects the conditions of the fracturing and subsequent mechanical abrasion processes during collision and cratering in space and/or on the parent bodies. The study of the irregularity may help to understand the mechaniocal conditions of the accretion of planetary bodies. It is, however, often difficult to represent the irregularity quantitatively (Fujii et al., 1982). In this study, we investigated the fractal geometry (Mandelbrot, 1982) of the surfaces of rock fragments prepared experimentally.

The fractal geometry of surface is characterized by a number D, called fractal dimension. The fractal dimension is a mathematical extension of the ordinary Euclidean dimension. It ranges from 2 to 3: when the surface is flat, D=2. As the surface becomes more irregular, it increases from 2 to 3. Similarly, the fractal dimension D' of a curve is given by a number of $1 \leq D' < 2$.

The fractal dimension D of a surface can be estimated by the island analysis (Mandelbrot et al., 1984). When the rough surface with the fractal dimension D is sectioned by a plane parallel to

the average trend of the surface, "islands" which are surrounded by the intersecting curves appear. The "coastlines" are of fractal dimension D'=D-1. The theory of fractals suggests the relations as follows.

$$D' = 1 - \log L / \log r \qquad (1)$$

and

$$A^{1/2} \propto L^{1/D'} \qquad (2)$$

where L is the perimeter of the island, r is the opening of the dividers used to measure the perimeter, and A is the area of the island. Equation (1) is identified for every island, on the other hand, eq.(2) is applied to the whole data of area-perimeter relation. Thus two independent methods using eq.(1) or eq.(2) are available for determination of the fractal dimension D'.

We prepared the fragments of basalt (Chausu-yama, Aichi prefecture; Takagi et al., 1984) and dunite (Horoman, Hokkaido) fractured by either high speed impacts or uniaxial loading experiments. Each fragment was thinly coated by silver with a vacuum evaporation technique and moulded in epoxy resin. Then the specimen was polished down until the islands of the bare basalt or dunite appeared. The islands were photographed through a reflection microscope and the coastlines on the photos were digitized by an X-Y reader.

Figure 1 shows the area-perimeter relations (eq.(2)) for the fragments of the impact fracture experiments. The linear relationship among the data covering a wide range of sizes demonstrates that the fractured surfaces of both basalt and dunite are fractals. The solid lines shown in the figures

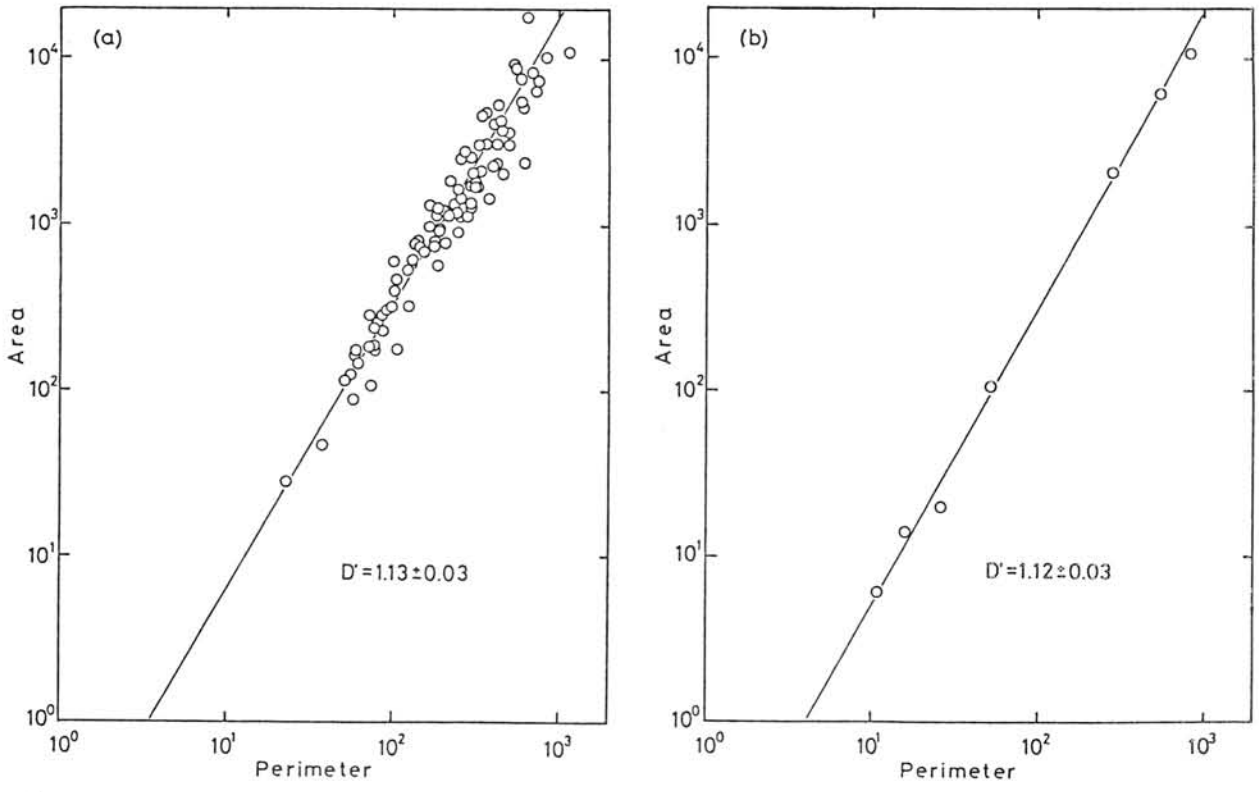

Fig.1 Area-perimeter relationship for islands on the surfaces of impact-fractured a) basalt and b) dunite.

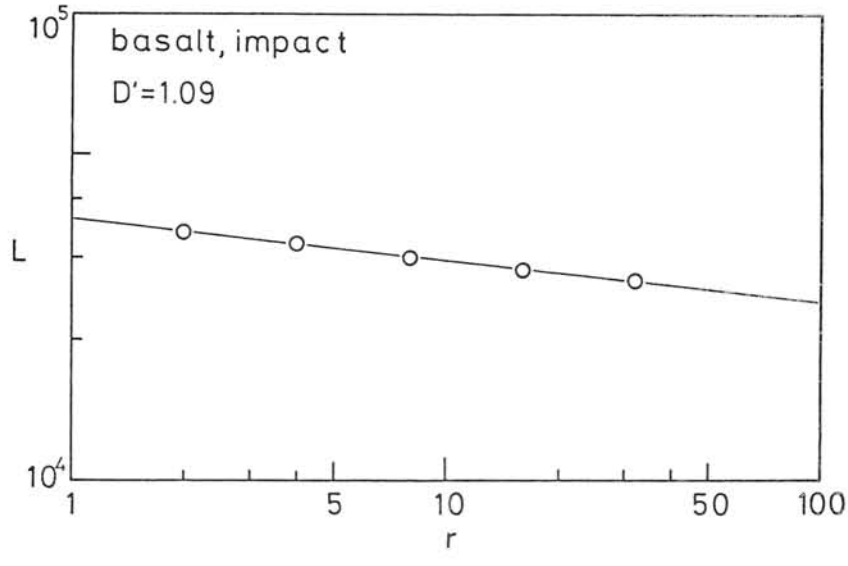

Fig.2 The linear relation between log(L; perimeter) and log(r; scale of divider). The measured surface (No.8A32) is produced by an impact experiment (impact velocity; v=0.6 km/s, projectile (Al) mass; m=10 g and target mass; M=1050 g) for basalt.

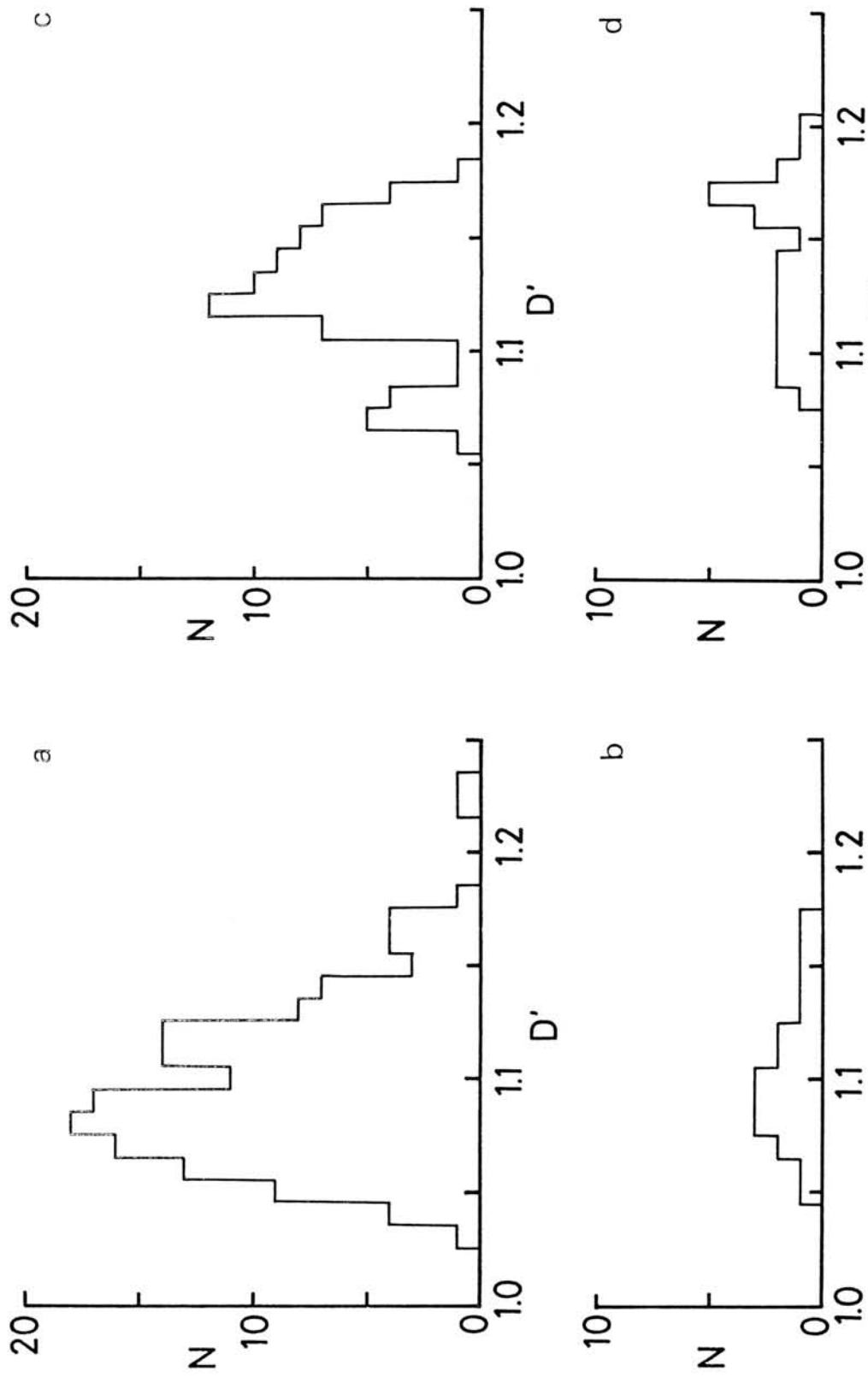

Fig.3 Histogram of fractal dimensions D'. Left; fragments of a) basalt and b) dunite by impact experiments (v=0.3-0.8 km/s, m=5-10 g and M=30-1000 g for basalt, and v=0.3 km/s, m=7 g and M=80 g for dunite). Right; fragments of c) basalt and d) dunite by uniaxial loading experiments (strain rate; $\log(\dot{\varepsilon})=-4\sim-5$ (/s) for basalt and $\log(\dot{\varepsilon})=-4$ (/s) for dunite).

represent the relationship for D'=1.13 and 1.12. This indicates that the surface irregularity of impact-fractured basalt resembles that of impact-fractured dunite. It is a striking fact that these two materials with different mechanical properties have a similar value of D'.

In order to investigate the surface geometry in detail, we determine the fractal dimension D' of each island by using eq.(1) (Fig.2). The histograms of the fractal dimensions are shown in Fig.3. The most frequently observed values are 1.08 and 1.09 for the impact-fractured surfaces of basalt and dunite, respectively. In the case of the fragments produced by static loading, the most frequently observed values are 1.12 for basalt and 1.17 for dunite. The fractal dimension of the surface produced by impact is certainly lower than that by static loading, though the number of data for dunite is small. The different physical properties of basalt and dunite may lead to the different fractal dimension D' in the case of static loading. The difference of the distributions of the fractal dimensions may be diagnostic in distinguishing the fracturing processes of the lithic fragments in meteorites.

REFERENCES

Fujii,N., M.Miyamoto, Y.Kobayashi and K.Ito, Mem. Natl. Inst. Polar Res., Spec. Issue 25, 319-330, 1982.

Mandelbrot, B.B., The Fractal geometry of Nature, Freeman, San Francisco, 1982.

Mandelbrot, B.B., D. Passoja, and A. Paullay, Nature, 308, 721-722, 1984.

Takagi,Y., H.Mizutani and S.Kawakami, Icarus, 59, 462-477, 1984.

PETROLOGY OF Y-791493, LODRANITE

Hiroko Nagahara and Kazuhito Ozawa, Geol. Inst., Univ. Tokyo, Hongo, Tokyo 113, Japan

Y-791493 is classified as a lodranite [1], but is different from Lodran in the presence of plagioclase (pl; An17-20) and abundance of clinopyroxene (cpx) (Fig. 1). It is coarse-grained (up to 1.0 mm) showing similar appearance to terrestrial lherzolite under optical microscope, except for the presence of Fe-Ni metal (metal; 6.0-6.8 wt% Ni, 0.15wt% P) and troilite. It consists of euhedral to subhedral olivine (ol), orthopyroxene (opx), and interstitial, anhedral cpx, metal, troilite, pl, and whitlockite. Spinel (sp) occurs as a large (~0.5mm) subhedral grain, small (<30μm) rounded inclusions in olivine, or medium-grained (>30μm) euhedral grain along metal-silicate or troilite-silicate grain boundaries.

Structure and Petrofabric Two plagioclase-rich bands are recognized (Fig. 1), suggesting the existence of layered structure. Large olivine grains tend to lie parallel to these bands. The olivine fabric is characterized by a strong Y concentration normal to the thin section plane, indicating strong lineation probably parallel to the plagioclase rich layers. The X and Z directions display no strong concentration, but there is a remarkable concentration of these axes along a faint girdle perpendicular to the Y maximum. The fabric pattern for olivine clearly indicates that the layering does exist in Y-791493.

Cooling history Ol is homogeneous inside the grains (Fo87-88) and generally has Mg enrichment toward margin; however, some olivine grains show no zoning detectable by EPMA. Strong enrichment (Fo90) toward sp was observed (Fig. 2). The enrichiment toward sp results from the diffusion-controlled Mg-Fe exchange between ol and sp during cooling at subsolidus temperatures [2]. Mg/(Mg+Fe) ratio at the core of spinel decreases remarkably with decrease in grain size of spinel. Cooling rate was estimated on the basis of this grain size dependence of core Mg/(Mg+Fe) of sp by the same procedure applied to the terrestrial peridotites [2]. The estimated cooling rate is 10^3 °C/my in the temperature range of 800-600° C (Fig. 3). Opx is homogeneous for Mg-Fe (En87-89) with Ca depletion from core to margin (Wo3 to 1.3; Fig. 4). Cpx occurs as lamellae in opx as well as anhedral isolated grains. Cpx is heterogeneous (Wo41-45) within a grain, but does not show any systematic zoning. Application of the two-pyroxene thermometer revised by Lindsley [3] gives 1100°C for the core and 800°C for the rim of opx. In thin sections studied, neither taenite nor schreibersite is present, making it unable to evaluate metallographic cooling rate. However, petrographic similarity to Lodran suggests the approximate cooling rate of 10^3°/m.y. at about 500°C[4, 5]. These geospeedometries suggest continuous cooling for Y-791493 from about 1100°C to, at least 500°C without any thermal interruption, such as reheating or sudden cooling.

Oxygen fugacity Although zoning in the rim of ol toward sp was formed during cooling, that without neighboring sp should have caused by another process: probably by reduction. Reverse zoning is also reported for Lodran [6] and ureilites [7]; in the latter case, graphite is actually present and it is evident that graphite was a reducing agent. On the contrary, in Y-791493 and Lodran, graphite is not found. Heating of coexisting ol, opx, and metal under the closed system without other buffering materials may explain the reverse zoning. However, as Y-791493 cooled continuously from high to low temperatures, reverse zoning could not be formed by thermal reheating. Therefore, reduction by certain agent such as graphite is necessary. Oxygen

fugacity of Y-791493 before the reduction and cooling took place (>1100°C) was a little lower than that of H chondrites, because Fo content at the core of olivine is about 87.5, which is higher than that of type-6 H chondrites (Fo~82) [8].

Formation of Y-791493 Texture and structure suggest that Y-791493 is an "orthocumulate"; ol and opx are "cumulus" minerals, and metal, troilite, pl, cpx, and whitlockite crystallized from interstitial melt. The petrofabric analysis of ol also supports this interpretation. As euhedral ol has sp inclusions, sp crystallized at first followed by ol. Rounded ol is often enclosed within opx, suggesting that opx crystallized next to ol. Opx is rarely enclosed in ol, thus ol and opx once crystallized simultaneously. Cpx is almost anhedral, which shows that cpx crystallized after ol and opx. During crystallization of ol, opx and cpx, two melts were possibly present, silicate melt and Fe-Ni-S melt. This is suggested by the fact that minute blebs (<5 μm) of metal, troilite, or both often accompanying sp or whitlockite show planar arrangement inside ol, opx and cpx. In olivine grains, these planes are commonly parallel to the (021) plane. These blebs are probably trapped Fe-Ni-S melt containing sp and silicate melt. Rarely, minute blebs rim euhedral olivine grains or rounded olivine inclusions in opx. Similar feature is reported for pallasites and ureilites, and the blebs are considered to be trapped liquid [9, 10]. Although Y-791493 shows remarkable resemblance to terrestrial orthocumulates in texture, structure, and petrofabric, it has a peculiarity. Considerable amounts of silicate melt, ol, opx, and Fe-Ni-S melt coexisted to the final stage of crystallization regardless of their significant density difference. This indicates that extensive separation of silicate and metal melts did not take place. Therefore, Y-791493 is not a typical cumulate, but is a residue crystallized from partially molten primitive materials of a parent body without extensive seggregation and separation of silicate melts. Fe content of Y-791493 is slightly greater than that of average H chondrite but is remarkably greater than that of L or LL chondrites. Total iron of Y-791493 is similar to H chondrite but is greater than L or LL chondrites. These facts suggest that the original materials were probably H chondrite, because extensive enrichment in Fe (metal) is possible only by marked separation of silicate melt. This interpretation is also supported by comparison of chemical composition of silicate portions of Y-791493 and average H chondrite; the silicate portions of Y-791493 is slightly depleted in SiO_2, CaO, Na_2O, and K_2O as compared to that of H chondrites (Table 1). Metal-sulfide liquid could be trapped in ol-px mesh as experimentally shown by Takahashi, though in that case light silicate melt should have been lost upwards [11]. Effective seggregationof silicate melt might have been prevented because of the small gravity and pressure in small parental body.

References [1] K. Yanai, and H. Kojima (1982) Meteoritics, 17, 300. [2] K. Ozawa (1984) G.C.A., 48, 2597-2611. [3] D. H. Lindsley (1983) Ame. Min., 68, 477-493. [4] M. Prinz et al. (1978) Lunar Planet. Sci., IX, 919-921. [5] C. Narayan and J. I. Goldstein (1985) G.C.A., 49, 397-410. [6] R. W. Bild and J. T. Wasson (1976) Mineral. Mag., 40, 721-735. [7] J. L. Berkley et al. (1976) G.C.A., 40, 1429-1437. [8] R. J. Wliliams (1971) G.C.A., 35, 407-411. [9] J. L. Berkley et al. (1980) G.C.A., 44, 1579-1597. [10] P. R. Buseck (1977) G.C.A., 41, 711-740. [11] E. Takahashi (1983) Mem. Natl. Inst. Polar Res. Spec. Issue No. 30, 168-180. [12] H. Haramura et al. (1983) Mem. Natl. Inst. Polar Res. Spec. Issue 30, 109-121.

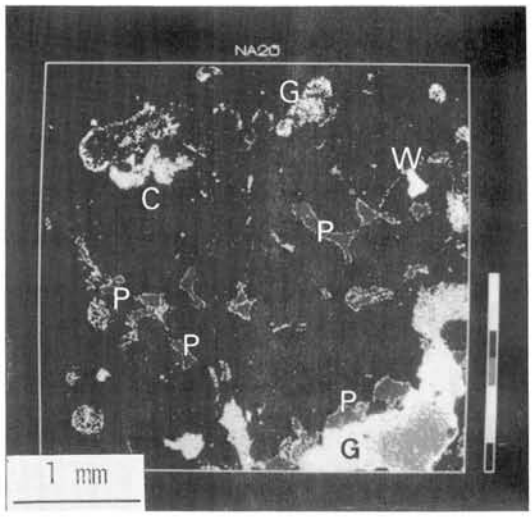

Fig. 1 Na distribution in Y-791493. Distribution of plagioclase (P) defines bandded structure. White area in the lower right corner is glass mount (G). Whitlockite (W) and clinopyroxene (C) are present.

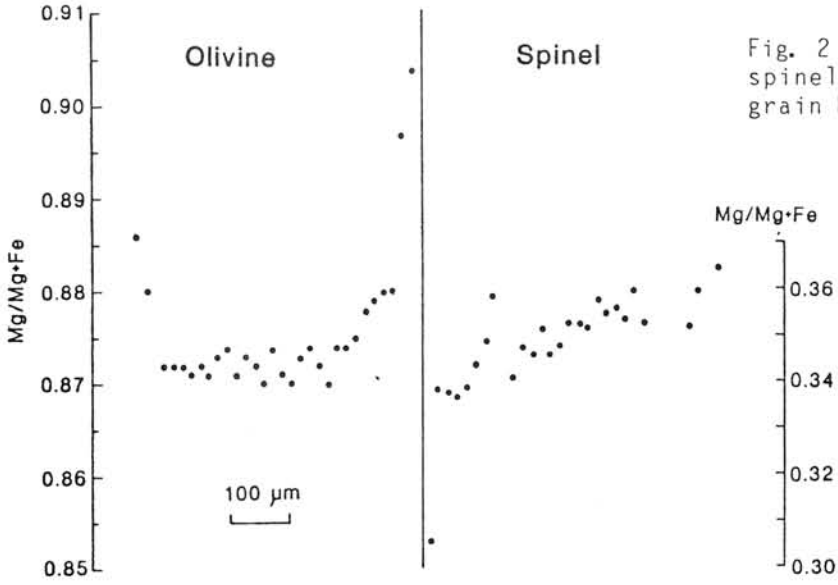

Fig. 2 Mg/(Mg+Fe) variation in spinel and olivine at their grain boundary.

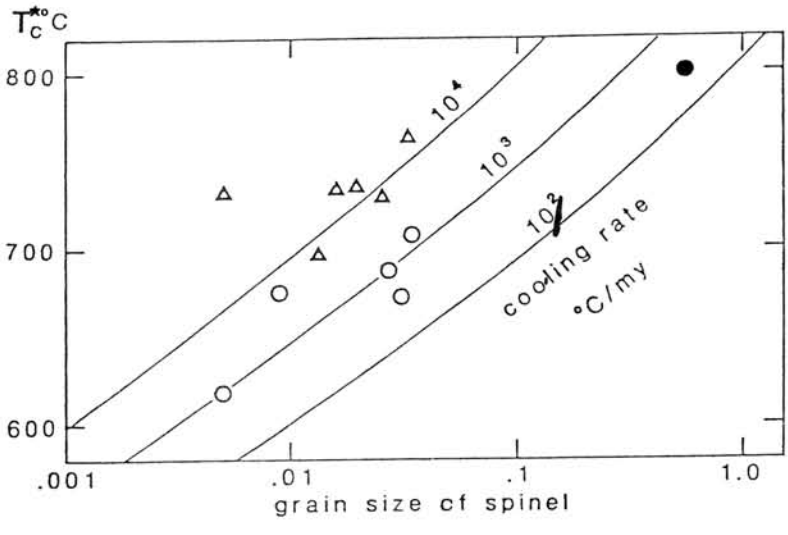

Fig. 3 Relation between grain size of spinel and temperature calculated by paring core of olivine and spinel (T_c^*). Open triangle; spinel present at the markedly zoned margin of olivine. (These data were not used for geospeedometry.) Open circle; spinel present at the homogeneous core of olivine or at the moderately zoned rim of olivine. Closed circle; large spinel grain. Diffusion data used to calculate the constant cooling rate curves are: Q_{ol} =3.45 (eV), Q_{Sp}=3.6, $D_{\phi,ol}$ =3.0 (cm^2/sec), $D_{\phi,Sp}$=5.0. These values are for spinel with Cr/(Cr+Al)~0.80. The constant cooling rate curves for Y-791493 (Cr/(Cr+Al)=0.82-0.91) may slightly shift to high T_c^*.

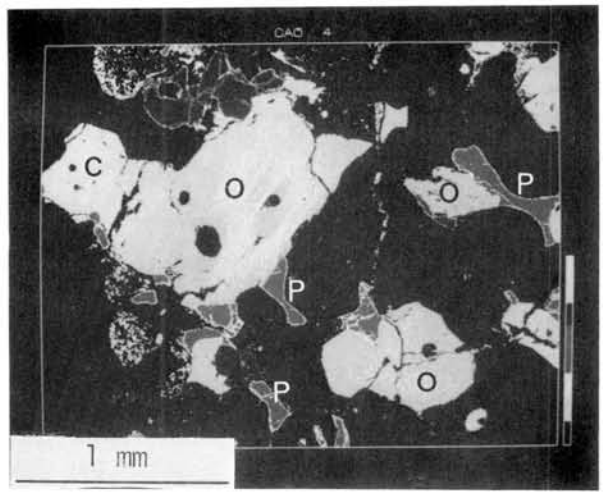

Fig. 4 Ca distribution in Y-791493; bright area; orthopyroxene (O) with abundant clinopyroxene lamellae at the core, dark gray in the upper left; clinopyroxene(C), gray; plagioclase(P).

Table 1.

	1	2	3
SiO2	34.9	45.9	46.5
TiO2	0.05	0.06	0.13
Al2O3	0.90	1.18	2.61
FeO	6.12	9.44	15.3
Fe2O3	6.02		
MnO	0.42	0.55	0.36
MgO	29.5	38.8	30.9
CaO	1.54	2.02	2.29
Na2O	0.21	0.28	0.95
K2O	0.02	0.02	0.10
P2O5	0.49	0.64	0.30
Cr2O3	0.81	1.07	0.60
H2O(-)	1.1		
H2O(+)	0.04		
Fe	14.3		
Ni	1.13		
Co	0.07		
FeS	2.1		
Total	99.7		

1. Bulk chemical composition of Y-791493.
   Analyst: H. Haramura
2. Silicate portion recalculated to 100%.
3. Silicate portion of average H chondrite from antarctic. Recalculated to 100%.
   After [12]

* Fig. 1 and Fig. 4 were taken at JEOL by JCMA-733. We are greatful to the people of the EPMA Application Laboratory of Electron Optics Technical and Engineering Division of JEOL for their CMA analyses.

84—1

TRACE ELEMENT ANALYSES IN CAPE YORK IIIAB IRON AND TROILITE

H.H. Weinke, W. Kiesl, F. Kluger, and C. Koeberl

Institute of Geochemistry, University of Vienna
P.O. Box 73, A-1094 Vienna, Austria

The IIIAB iron meteorite Cape York is the second largest iron meteorite recovered to date. In addition, it is the largest meteorite in the IIIAB group. It is divided into several large masses, according to the spots of recovery. A sample from one of these masses-Agpalilik- has been used in this study. Details of petrographical and metallurgical descriptions of the differences between the samples from the diverse masses can be found in Buchwald (1975).
In general, it has been observed that the Cape York meteorite is not very homogeneous. Some elements (like Re, Ir, Au) are rather constant within one mass, but show considerable differences between the individual masses (Esbensen et al., 1982). Other elements are variable already within one mass.

Our investigations have concentrated on the trace element content of troilite and iron phases. In addition, microprobe analyses (using a fully automated five spectrometer ARL-SEMQ electron microprobe) have been performed. Different layers of the sample (especially the rim between sulphide and metal) were inspected optically and by electron microscopy. The variation of minerals in the sulphide rim is extreme, and already present in the microstructure. One side of the sulphide nodule contains chromite, copper, and Ni-rich metal, and the other part is rich in phosphates. Different phosphate phases have been found, like also reported by Kracher et al. (1977). The chromite crystals seem to be almost pure $FeCr_2O_4$, with Mn, V, and Zn in accessory amounts. In addition to earlier work, a Ni-rich taenite, containing 58.77% Ni and 0.37% Co,has been found. The Ni-rich grain is surrounded almost completely by troilite, and has itself an inclusion of kamacite (containing 6.96% Ni). The Ni-rich taenite has a concentration gradient of about 60% Ni at the inner part to about 55% Ni on the outer side adjoining the metal phase.

For the determination of the trace elements mainly neutron activation analysis has been used. Methods used were instrumental neutron activation analysis (taking advantage of a fast pneumatic transfer system, installed directly at the nuclear reactor), and radiochemical procedures. For the INAA work also phosphide grains have been isolated by magnetic and chemical seperation, in addition to troilite and metal phases. The usage of a fast transfer system allows the determination of some rather short lived isotopes. Rh may be a good example, with 42 seconds half life (Rh-104). The usages for analyses of meteorite phases with very fast transportation systems (RINAA), enabling incorporation of millisecond isotopes, have

been discussed shortly by Koeberl and Grass (1983) and will be used for further iron meteorite analyses.

The method used for the radiochemical seperation following the neutron irradiation follows in principle the method decribed by Kiesl et al. (1967). The results are given in the table below, together with the results from other methods. The enrichment ratios of some of the elements (including volatile, chalcophile, and siderophile elements) between the metal phase and the troilite may yield some interesting conclusions on the formation of the meteorite in the final phases of the magmatic processes in the parent body.

Further investigations have been made using an ion microprobe (Cameca IMS-300). Trace element distributions in kamacite, plessite, troilite, and chromite have been measured with the ion microprobe. The following elements have been determined, but are not included in the table below: Na, Mg, Al, Si, P, K, Ca, Sc, Ti, V, Cr, Mn, Fe, Co, Ni, Cu, Zn, and Ga.

References: Buchwald, V. (1975) Handbook of Iron Meteorites, Univ.of California Press, 1418pp.
Esbensen,K.H., Buchwald,V.E., Malvin,D.J., and Wasson,J.T. (1982) Geochim.Cosmochim.Acta 46,1913
Kiesl,W., Seitner,H., Kluger,F., and Hecht,F.(1967) Monatsh. Chemie 98, 972.
Koeberl, C., and Grass,F. (1983) Meteoritics 18,325
Kracher,A., Kurat,G., and Buchwald,V.E. (1977) Geochem. Journ. 11, 207.

Table: Trace element content in Cape York, by INAA, RNAA, and thermochemical methods (C, N, and S)

	metal	sulphide	phosphide
C	83 ppm	n.d.	n.d.
N	40 ppm	n.d.	n.d.
S	15.3 ppm	n.d.	n.d.
Ti	<17 ppm	24 ppm	<14 ppm
V	0.06 ppm	3.7 ppm	9.9 ppm
Mn	n.d.	200 ppm	n.d.
Co	4800 ppm	5.2 ppm	1090 ppm
Ni	7.71 %	n.d.	32.6 %
Cu	189 ppm	110 ppm	390 ppm
Zn	1.50 ppm	8.7 ppm	n.d.
Ga	14.5 ppm	<1.5 ppm	12 ppm
As	6.1 ppm	1.9 ppb	n.d.
Se	5.5 ppb	90.4 ppm	n.d.
Mo	7.2 ppm	5.6 ppm	n.d.
Ru	4.5 ppm	16 ppb	n.d.
Rh	1.65 ppm	<0.2 ppm	2.0 ppm
Re	0.40 ppm	<0.4 ppb	n.d.
Os	3.8 ppm	<5 ppb	n.d.
Ir	4.60 ppm	3 ppb	n.d.
Au	1.4 ppm	1.4 ppb	n.d.

SULFIDATION OF FE-NI METALS IN ALH-764 (LL3) CHONDRITE: AN ESTIMATION OF MINIMUM OF COOLING TIME SCALE IN THE PRIMORDIAL SOLAR NEBULA.

Satoshi MATSUNAMI:
Geological Institute, University of Tokyo, Tokyo 113.

The kinetics of sulfidation of iron has been shown by various authors to be parabolic at PS_2 in the range of 10^{-11} - 1 atm for the range 400-800°C (e.g., 1,2). Moreover, they have concluded that the growth of FeS scale on Fe occurred by an outward diffusion of Fe ions via cation vacancies in the FeS lattice. The parabolic rate constant of sulfidation mainly varies as a function of T and PS_2. Consequently, the textural and compositional variations of Fe-Ni metal-iron sulfide aggregates observed in highly unequilibrated ordinary chondrites, which would have been formed by sulfidation reaction, should be related to the cooling history below about 700°K in the solar nebula, the PS_2-T path, and the kinetics of sulfidation of Fe-Ni metal grains. Furthermore, it seems probable that the parabolic rate constant of sulfidation is also significantly affected by the chemical composition of Fe-Ni metals, especially by the Ni content (4). Although sulfidation behaviour of Fe-Ni metals is not so known, especially at low PS_2 and temperature conditions, the author presents a simple model for the growth of iron sulfide layer on Fe-Ni metal grain during the cooling of the solar nebula to estimate minimum of the cooling time scale of the primordial solar nebula below 700°K. Assuming parabolic rate law of sulfidation behaviour of pure Fe, according to Fryt et al. (2), for those of Ni-poor Fe-Ni alloys (Ni $\lesssim$ about 6 wt%) and $T=T_0 \exp(-t/\tau_{cool})$, where τ_{cool} is cooling time scale, for the cooling history of the nebula below 700°K, then maximum thickness of iron sulfide on Fe-Ni metal grains at a given τ cool, Xmax, is approximately given as follows (2,3),

$$Xmax = \left(\int_0^t 2\,\tilde{D}\,\Delta\delta\,dt\right)^{1/2} \cong (2\Delta\delta \cdot \tilde{D}(0) \cdot RT_0\,\tau\,cool/Ea)\ ,$$

$$\therefore\ \tau cool = Xmax^2 \cdot Ea/(2\Delta\delta\,\tilde{D}(0) \cdot RT_0) \quad -----(1),$$

where $\Delta\delta$ represents the change in non-stoichiometry of iron sulfide ($Fe_{1-\delta}S$) when equilibrated at the outer and inner interfaces with sulfur and iron, respectively, R: general gas constant, T_0: temperature of the beginning of sulfidation (at t=0), $\tilde{D}(0)$: chemical diffusion coefficient (2) at t=0, i.e., $T=T_0$ (, where $\tilde{D}=\tilde{D}_0 \exp(-Ea/RT)$; $\tilde{D}_0=6.7\times10^{-2}$ cm^2/sec and Ea=20.9 kcal/mole).

Application of Eq. (1) to sulfidation of Fe-Ni metals in ALH-764 chondrite.--- Next, the minimum of τ cool is estimated. Maximum thickness of iron sulfide on individual metal-sulfide aggregates in ALH-764 is ranging from about 10μm to 120μm, which is obtained by the observation of polished thin section under microscope. EPMA analyses of Ni-free iron sulfide of

metal-sulfide aggregates in ALH-764 show that the metal/sulfur atomic ratio (Fe/S) of these iron sulfides is ranging from 0.965 to 1.000, with an average of about 0.980 (4), suggesting the presence of non-stoichiometry in iron sulfides of ALH-764 chondrite, (however, further examinations by means of XRD are needed to draw more definite conclusion). Therefore, one may adopt 120 μm, 0.02 and 700°K for Xmax, $\Delta\delta$ and T_o in Eq.(1), respectively, then minimum estimate of τ cool is obtained as follows,

$$\tau \text{ cool} = 31.3 \text{ days } (\text{Xmax}/120\mu\text{m})^2 \cdot (\Delta\delta/0.02)^{-1} \quad \text{---- (2).}$$

From Eq.(2), it is suggested that most of Fe-Ni metals in ALH-764 chondrite might have cooled below 700°K for more than about one month in the primordial solar nebula to form thick iron sulfide layers.

References:

(1) Strafford, K.N. and Manifold, R. (1969): Corrosion Sci., 9, 489-507.
(2) Fryt, E.M. et al. (1979): Jour. Electrochem. Soc., 126, 683-688.
(3) Kingery, W.D. et al. (1976): Introduction to Ceramics. 2nd edition, John Wiley & Sons, New York.
(4) Matsunami, S. (1985): unpublished data.

ZHAODONG,ZAOYANG AND NINGQIANG CHONDRITES---THE RECENTLY FALLEN METEORITES

WANG DAODE, LIN WENZHU AND CHEN YONGHEN
Institute of Geochemistry, Academia Sinica, Guiyang, Guizhou Province, The People's Republic of China

The Zhaodong Chondrite fell at 45°49'--46°03' N latitude, 125°55'--125°58' E longitude within the territory of Zhaodong county, Heilongjiang Province on October 25, 1984 at 1505 hours Beijing time. After a bright fireball and detonation, 4 pieces were recovered from this area. The largest fragment (No.I) was weighed about 25 kg. No.II, No.III and No.IV were 14.5, 1.6 and 0.8 kg, respectively. The total weight was estimated to be about 42 kg. A fireball was observed travelling from SW to NE. These fragments were almost completely covered by a black fusion crust generally about 0.5–1 mm thick. This meteorite belongs to an olivine-hypersthene chondrite(L5) and consists largely of olivine and orthopyroxene. Most silicate grains show intensively distinct undulatory extinction and fractured feather, and kink bands are also observed in some orthopyroxene grains. Chondrules are moderately abundant but poorly defined, tending to merge with the granular groundmass.

On October 18, 1984, at 1815 hours Beijing time and at 32°18' N, 112°45' E a stone meteorite fell in Taiping village of Zaoyang county, Hubei Province. A fireball was observed travelling from SW to NE. The approximate flight path was NE 29°. The noise of the impact was said to be heard within a range of 30 square kilometers. A single mass as large as 31x29x14 cm weighing 14.15 kg was recovered.It was almost completely covered with fusion crust. Chondrules are fairly abundant and are set in granular groundmass which consists largely of olivine and pyroxene, with minor nickel-iron and troilite. On the basis of its chemical composition and petrographic investigation the meteorite is classified as an H5 chondrite.

On June 25, 1983 at 1900 hours Beijing time and at 32° N,106° E, a stone meteorite fell in Ningqiang county, Shaanxi Province. This meteorite was completely covered by a brownish-black fusion crust generally about 0.1–0.3 mm thick; the interior is pale gray, granular, with traces of chondritic structure. The meteorite contains olivine, enstatite, augite, kamacite, taenite, troilite, magnetite, apatite, calcite, dolomite, plagioclase and chromite. The bulk chemical composition of the meteorite is shown as follows: SiO_2 32.12, CaO 2.20, MgO 23.71, FeO 22.12, Al_2O_3 5.63, K_2O0.038, Na_2O 0.25, P_2O_5 0.25, MnO 0.18, TiO_2 0.14, Cr_2O_3 0.49, CO_2 1.39, FeS 5.92, C 1.32, Fe^o 1.57, and Ni 1.38. The meteorite is classified as a first carbonaceous chondrite fallen in China.

Reference: Wang, S.C. et al., Preliminary study of Ningqiang chondrite Abstracts submitted to the Second Conference of the Chinese Society of Space Science(Session on Space Chemistry and Space Geology), 1984, Guangzhou.

Mineralogical and Petrological Investigation of Shuangyang Chondretes

Chang Shuyuan and Meng Yanxi
Department of Geology, Peking University, Beijing, China

Shuangyang meteorites shower fell in the range of Shuangyang county of Jilin Province of China in 1971. Five integrated meteorites and two fragments were collected, of which the total weight was 6.8 kg.

According to the mineralogical and petrological investigation, Shuangyang meteorites are olivine-bronzite chondrites of type H-5. The major transparent and opaque minerals, olivine, pyroxene, troilite, kamacite, taenite,etc., have been studied by the means of electron microprobe analysis, optic test and X-ray diffraction. The olivine and bronzite are relatively stable in chemical composition with Fa being 16-18.5 and Fs 13-15 in average. According to electron microprobe anaysis, there are at least two kinds of glass different in chemical composition. The feldspars are observed in different occurrence with the scanning electron microscopy.

The high resolution electron microscopy study of bronzite have been carried out and preliminary results have been obtained, which is considered a direct evidence supporting the metamorphism pattern of ordinary chondrites. Many writers have observed that most of the low-Ca pyroxene in type 3 chondrites and much in type 4 chondrites are monoclinic, while that in type 5 and type 6 is chiefly orthorhombic. We have found out the complete history of the Ca-poor pyroxenes in Shuangyang chondrites included: protobronzite to clinobronzite to orthobronzite. The relationship between type 3,4 and type 5 seems to be revealed. Calculation indicated that the metamorphic temperature of Shuangyang chondrite is $870^{0}C \pm 43^{0}C$.

88—1

STUDY OF CHEMICAL COMPOSITION OF 35 IRON METEORITES AND ITS APPLICATION TO TAXONOMY

Wang Daode*, D.J.Malvin** and J.T.Wasson**

*Institute of Geochemistry, Academia Sinica, Guiyang, The People's Republic of China

**Institute of Geophysics and Planetary Physics, University of California, Los Angeles, Ca.90024,USA

Based on structural observations and the concentrations of Cr, Co, Ni, Cu, Ga, Ge, As, Sb, W, Re, Ir and Au determined by neutron-activation analysis we have classified 14 Chinese iron meteorites, 11 Antarctic iron meteorites and 10 other iron meteorites(Table 1). Of the Chinese irons, four fall into IVA group, four IIIA, two IIICD, one IIIE, one IA, one IVA-an and one ungrouped[1]. Chinese Xingjiang iron meteorite previously classified as IIIAB has been reclassified as IIIE because of its lower Ga/Ni and Ge/Ni ratios and its wider, swollen kamacite bands and the ubiquitous presence of haxonite, $(Fe,Ni)_{23}C$[2]. The band width of kamacite in the Xingjiang iron is 1.2-1.3 mm, but for IIIB iron, it is 1 mm. However, the Ni content in the kamacite is similar, indicating the property of swollen or augmentation of the kamacite band. Both haxonite and graphite can be observed in the plessite of the Xingjiang iron meteorite and the concentrations of Ga and Ge are similar to IIIE. IIICD Dongling appears not to be a new meteorite, but to be paired with Nantan. In addition, Guanghua, Huangling and Yingde iron meteorites of IVA group are quite similar in chemical composition and structure. The first two are found in Hubei Province and the Yingde iron is found in the south of Guangdong Province. Therefore, the Guanghua and Huangling irons are tentatively considered as paired meteorites.

Of the Antarctic meteorites, 6 belong to the normal members of IAB group; two IIAB, one IVA, one pallasite-anomalous and one ungrouped. IAB group has the characteristics of low Ni and high Ge. Allan Hills(ALH) A 77283 obviously belong to this group for it contains diamond of impact origin, which is also the case of Canyon Diablo, a typical IAB iron. The chemical composition and structural features of the two irons are also similar. Purgatory Peak A 77006 iron(IA) has a Ge concentration 12%, lower than that of ALH A 77283, indicating that it is another fall. ALH A 78100 iron(IIA) is a hexahedrite with a relatively large amount of schreibersite inclusions. Reckling Peak A 79015 is a mesosiderite rich in metal. The concentrations of Ni, Ga and Ge are a little higher than those of mesosiderite while the concentration of Ir is 5-10 times lower than that of previously studied mesosiderites. Therefore, the ALH A 79015 was classified as mesosiderite-anomalous meteorite. ALH A 77255 is an ataxite. Its structural features are similar to those of Nordheim iron. Spindle-shaped kamacite is dispersed in the groundmass of fine plessite. Whereas, the chemical compositions of the two irons are not completely the same. So, ALH A 77255 is designated as ungrouped meteorite. Derrick Peak A 78009 is a normal coarsest octahedrite of IIB group. Four Antarctic iron meteorites IAB Allan Hills A 77250, A 77263, A 77289 and A 77290 are classified as paired meteorites

based on the similarity in structure and the concentration of Cr, Co, Ni, Cu, Ga, Ge, As, Sb, W, Re, Ir and Au between these irons.

The remaining ten irons from the United States and other countries belong to IIAB, IIE, IIIAB, IIIE, IVA, IIICD-anomalous groups separately with two ungrouped ones.

In the study of chemical composition of 35 iron meteorites and other iron meteorites we have found that Cu shared certain properties with Ga and Ge that make them excellent taxonomic parameter. Because K_{Cu} in solid and liquid phases is near unity [3] Cu varies over a small range within most magmatic groups and, because of its moderate volatility, obvious variations are observed between groups.

References

[1] Wang Daode et al., Geochemistry, 2(1983), 34-44.

[2] Scott,E.R.D. and Wasson,J.T., Geochim Cosmochim Acta, 40(1976), 103-115.

[3] Willis,J. and Goldstem, J.I., Proc. Lunar, Planet Sci. Conf. 13th A435-445.

Table 1. Chemical composition and classification of 35 iron meteorites

Name	Group	Band-width (mm)	Struc-tural class	Ni (mg/g)	Ga (μg/g)	Ge (μg/g)	Ir (μg/g)
Chinese iron meteorites							
Dongling	IIICD	1.5	Og	72	83	-	1.6
Guixi	IIIA	1-1.5	Om	83	21	39.7	2.4
Guanghua	IVA	0.30	Of	78	1.9	0.091	2.9
Huangling	IVA	-	-	78	1.9	0.18	2.8
Hebei	IIIA	1.1	Om	75	20	36.9	5.3
Jianshi	IIIA	1.0	Om	84	21	44.5	0.4
Leshan	un-grouped	0.5	Om	96	20	68.9	4.1
Liangcheng	IIIA	1.3	Om	82	21	45.7	0.5
Longchang	IVA-an	-	-	86	2.1	0.4	4.0
Ningbo	IVA	0.21-0.36	Of	82±3	2.3	0.134	2.0
Nantan	IIICD	1.5-2.0	Og	68	77	293	1.7
Xingjiang	IIIE	1.2-1.3	Om	96±3	16.9	31.3	0.2
Yingde	IVA	0.3	Of	77	1.8	0.11	2.9
Yongning	IA	3	Ogg	62	98	480	3.7
Antarctic iron meteorites							
ALH A77250,4	IAB		Og	69	93	410	2.5
ALH A77263,5	IAB		Og	67	98		2.5
ALH A77289,5	IAB		Og	69	92		2.5
ALH A77255,6	un-grouped		D	124	0.083	0.058	10
ALH A77283,5	IA	1.8	Og	75	77.2	320	2.0
ALH A78100,2	IIA		H	55	61	181	27
ALH A78252,5	IVA	0.4	Of	93	2.5	0.138	0.4
Purgatory Peak A77006,4	IA	1.8	Og	74	77.2	284	2.1
Derrick Peak A78009	IIB	5	Ogg	65.4	55.1	135	0.010
Reckling Peak A79015,11			anom	100	12.9	42.9	0.51
ALH A77290,3	IAB		Og	69	92	-	2.5
Others							
Ballinger(b)	IVA		anom	110	2.1	0.14	0.18
Floydada	IIIB	0.9	Om	91	21	41.5	0.013
Glen Rose	un-grouped	0.1	Off	94	0.74	0.305	3.9
Glen Rose(b)	IIAB		anom	56	62		9.7
Paloduro	IIIE	1.6	Og	91	19.7	37.7	0.090
Techado	IIE	0.6	Om	88.8	23	70.2	4.8
Tonganoxie	IIIA	1.1	Om	75.4	19.9	38	3.8
Quarat al Hanish	IIICD-an	0.4	Of	128.5	17.2	29.7	0.86
Sombrerete	un-grouped		anom	98	19.1	11.3	0.08
Siratik	IIA		anom	55.5	59	188	11

CHEMISTRY OF LIGHT AND DARK LAYERS IN MUONG-NONG TYPE INDOCHINITES

C. Koeberl

Institute of Geochemistry, University of Vienna
P.O. Box 73, A-1094 Vienna, Austria

Muong Nong type tektites are a subclass of the tektites from the Australasian strewn field. In contrast to the normal (so-called splash-form tektites) they show some important deviations from the characteristics of these tektites. They are known to be enriched in volatile elements, contain large and often not spherical bubbles, are of blocky and chunky appearance, have many inclusions (like chromite, cristobalite, rutile, zircon, and corundum), and show a layered structure. The chemistry of the Muong-Nong type indochinites has been decribed previously in a series of papers by the author and collaborators (see e.g. Koeberl et al. 1984a,b,c,d,e,f).

One of the most interesting characteristics of the Muong Nong type indochinites are the dark and bright layers, which are very abundant in the microstructure of the tektites, e.g. when viewed in a microscope (using thin sections). We have investigated the chemistry of these layers, first using microprobe studies (a fully automated, five spectrometer ARL-SEMQ electron microprobe) of polished sections across the boundaries of the layers. Although similar investigations have been reported by Yagi et al. (1982), they have failed to discover any chemical variability. We have found, in clear contrast to Yagi et al. (1982), a remarkable variation in chemistry between the light and the dark layers. Table 1 on the next page shows the average chemical composition of two light and dark layers from our sample MN8302. In this table only the elements showing a deviation (i.e. showing a difference between the layers) have been included. So we can see clearly that of the mayor elements only Si is depleted in the light layers, a results which may be surprisingly. If one assumes an effect associated with dilution (meaning that a lighter colour is the results of the dilution of darker material), then this would not be the expected results. In contrast, Fe, Al, Ti, and Mg are depleted in the darker layers. All other major elements do not show any remarkable behaviour.

In addition, we have investigated the abundances of trace elements in individual layers using neutron activation analysis. A careful seperation between the layers (resulting in 3-20 mg samples) has been made. The trace elements show a trend which is very similar to that of our microprobe analyses. Many elements are depleted in the darker layers, including Co, Cr, Sc, Th, U, and the REE. In Table 2 on the next page we give an example of the chemical differences in trace elements between two layers in our sample MN8319. More results are given in Koeberl (1985) and Koeberl et al., in preparation.

References: Koeberl, C., Kluger, F., Kiesl, W., and Weinke, H.H. (1984a) Lunar Planet. Sci. 15, 445.
Koeberl, C., Berner, R., and Kluger, F., (1984b) Lunar Planet. Sci. 15, 441.
Koeberl, C., Kluger, F., Berner, R., and Kiesl, W. (1984c) Lunar Planet. Sci. 15, 443.
Koeberl, C., Kluger, F., and Kiesl, W. (1984d) Meteoritics 19 in press
Koeberl, C., Kluger, F., and Kiesl, W. (1984e) Proc. of the 15th Lunar and Planet. Sci. Conf. Pt. 1, J. Geophys. Res. 89, C351-C357.
Koeberl, C. (1985) Lunar Planet. Sci. 16 in press
Yagi, K., Kuroda, Y., and Koshimizu, S. (1982) Proc. of the 7th Symp. on Antarctic Meteorites, Nat. Inst. of Polar Res., p. 162.

Table 1 Average chemical composition of dark and light layers in sample MN8302. Only elements showing a difference are given. Electron microprobe analyses. Wt.%.

	FeO	SiO_2	MgO	Al_2O_3	TiO_2
light l.	4.38	76.3	1.68	12.26	0.75
dark l.	3.33	81.3	1.23	9.28	0.55

Table 2 Trace element distribution in dark and light layer from sample MN8319, neutron activation data, in ppm.

	dark layer	light layer
Sc	7.72	10.0
Cr	61	70
Mn	640	670
Co	10.9	14.5
As	1.4	7.2
Rb	160	140
Zr	700	n.d.
Cs	4.4	5.2
Ba	340	n.d.
La	26.6	30.9
Ce	68	78
Nd	34	75
Sm	4.70	5.90
Eu	0.76	0.65
Tb	0.9	1.9
Dy	3.1	7.4
Yb	2.4	3.4
Lu	0.42	0.51
Hf	7.8	10.5
Ta	1.9	n.d.
Th	12.5	17
U	2.4	4.7

GEOPHYSICAL CHARACTERISTICS OF THE LAKE LAPPAJÄRVI METEORITE IMPACT SITE, WESTERN FINLAND

L.J. Pesonen and S. Elo
Geophysics Department
Geological Survey of Finland
SF-02150, Espoo 15, Finland

Interpretation of the Landsat satellite immagery, geophysical and topographic maps and geological data suggests that there are several recognized meteorite impact sites in the Fennoscandian (Baltic) Shield. The strongest evidence in support for a meteorite impact comes from Lake Dellen, Siljan Ringen and Lake Mien (Sweden) from Lake Kaalijärvi and Lake Jänisjärvi (USSR)and Lake Lappajärvi (Finland). The radiometric age determinations of the impact rocks range from recent (Lake Kaalijärvi) to 700 Ma (Lake Jänisjärvi).

Regional geophysical studies of Bouguer gravity , aeromagnetic and topographic maps and paleomagnetic investigation of rocks of the Lake Lappajärvi area (western Finland) on the Proterozoic Svecokarelian terrain of the Fennoscandian Shield strongly support the concept earlier reached by mineralogical, petrological and geochemical studies, that the Lake Lappajärvi depression represents geologically "young" (ie. less than 200 Ma) impact site caused by a hypervelocity meteorite body.

91—1

K-RICH PHASE IN NIHO-3(MIYANO) H3 AND ANTARCTIC CHONDRITES

Miúra, Yasunori
Department of Mineralogical Sciences and Geology, Faculty of Science, Yamaguchi University, Yoshida, Yamaguchi, 753.

The Niho-3(Miyano) meteorite of 19.18 grams fell in Miyano, Yamaguchi-shi, Yamaguchi-ken Japan (34 12'N, 131 34'E) on August 8, 1897. The meteorite is considered to be the same fragment with the Niho-1 and -2 (H3) chondrites discovered at a distance 6.2 km north-east away. The ellipsoidal dark-gray meteorite was originally 3x2x1.5cm (density 3.59 gr/cm^3). Electron microprobe analyses of 165,600 analyzed points by the JCMA-733 yield the bulk composition of the meteorite as follows in weight percent: SiO_2 35.57, Al_2O_3 2.54, Cr_2O_3 0.59, FeO 22.04, MnO 0.39, MgO 21.23, CaO 2.31, Na_2O 0.95, K_2O 0.08, NiO 0.23 and BaO 0.04. Modal mineral contents (in volume percent) are orthopyroxene 32, clinopyroxene 24, olivine 24, plagioclase(-like) 8, metal phases 9.0 and K-rich phase 1.0. The meteorite contains numerous glassy and crystalline chondrule (up to 2.2x1.2 mm in size). Various sizes of orthopyroxenes of inhomogeneous composition (En_{83-87} $Fs_{10-16}Wo_{0-5}$) show microporphyric chondrules. The large pyroxene chondrule (2.2x1.2mm) consists of orthopyroxene ($En_{85}Fs_{14}$) at the rim and clinopyroxene (Wo_{46} En_{46}) in the core. Olivine occurs in the microporphyric chondrules and has inhomogeneous composition ($Fo_{82-99}Fa_{1-18}$). The metal phases consist of kamacite(86 vol.%), plessite(11 vol.%) and taenite(3 vol.%). The fine-grained plagioclase(-like) grains consist of glassy (maskelynite, $An_{17-19}Or_{2-3}$; Fe/(Fe+Mg)=0.1-0.2) and crystalline phases (An_{18} Or_{2-3}; Fe/(Fe+Mg)=0.9-1.0). K-rich phase is irregularly distributed in the matrix and chondrule, and shows composition of $Or_{33}An_{40}$ with enriched Mg (i.e., Fe/(Fe+Mg)=0.2; Fig. 1)[1].

Frequency distribution of iron contents of olivine and orthopyroxene, and textural characteristics suggest that the Niho-3 meteorite belongs to the H-group and petrologic type 3 of Dodd(1981) classification [2]. It is confirmed that the Niho-3 meteorite is the same type and group with the Niho-1 (H3) reported by Shima et al. (1984)[3].

The Niho meteorites might be differentiated fragments within the IID-E parent body at the primordial stage by the following reasons: (1) The K-rich phase of alkali-feldspar has been discoveréd in type IIE iron meteorite and Naklites (but not in chondrites) so far. (2) Oxygen-isotope data for the group IIE silicate inclusions suggest that they are related to H-group chondrites[4]. (3) The Niho-2 chondrite shows gas-rich of ^4He and trapped Ne, and age of 4.51 b.y.(by ^{40}Ar dating)[3]. (4) The values of Fe/(Fe+Mg) in the Niho-3 are almost the same in orthopyroxenes(0.15), olivine (0.15), maskelynite grains (0.15), and K-rich phase(0.20)[1]. The detailed study will show whether the Kuga iron meteorite might be the different fragments from the Niho parent body or not.

The K-rich phase was also found recently in Antarctic meteorites; that is, Y-74646,93(LL5-6), Y-74647,95-3(H5-6), ALH-768, 65-2(H6), and ALH-77214,93-1(L3?) (cf. Fig. 2). The EPMA data show that the most K-rich content of the K-rich phases is found in the Y-74647,95-3 (K_2O=11.04 wt.%), and that the most Fe-rich content of the K-rich phases is observed in the ALH-77214,93-1 (FeO=8.52 wt.%), whereas the most Mg-rich content of the K-rich phase is still in the Niho-3(Miyano) H3 chondrite (MgO=11.01 wt.%). The result in this study suggests that (1) K-rich phase (with much Mg-content and $An_{40\pm}$) exists in the primordial stage of chondrite formation, and that (2) the type 3 chondrite contains more Mg-rich than those of types 4-6, and vice versa.

The author thanks to Dr. K. Yanai, Messrs. H. Kojima and G. Azuma of the National Institute of Polar Research of Japan for their help in preparing the polished thin sections of Antarctic chondrites. The sample of Niho-3(Miyano) chondrite is supplied from Yamaguchi Prefectural Museum.

REFERENCES:

[1] Miúra, Y. and Shibuya, G. (1985): Lunar and Planetary Science XVI. Houston, Lunar Planetary Institute (in press).
[2] Dodd, R.T. (1981) In Meteorites, p.24. Cambridge University Press.
[3] Shima, M., Okada, A., Takaoka, N. and Murayama, S. (1984) The Niho chondrite and the Higashi-Kohen chondrite (abstract in Japanese). 1984 Annual Geochem. Soc. Japan (Nagoya, Oct. 18-20), p.94.
[4] Clayton, R.N. and Mayeda, T.K. (1978) Earth Planet. Sci. Lett., 40, p.168-178.

Fig. 1. The value of Fe/(Fe+Mg) and An(mol%) in the K-rich phase, maskelynite and crystalline plagioclase of the Niho-3 (Miyano) H3 chondrite.

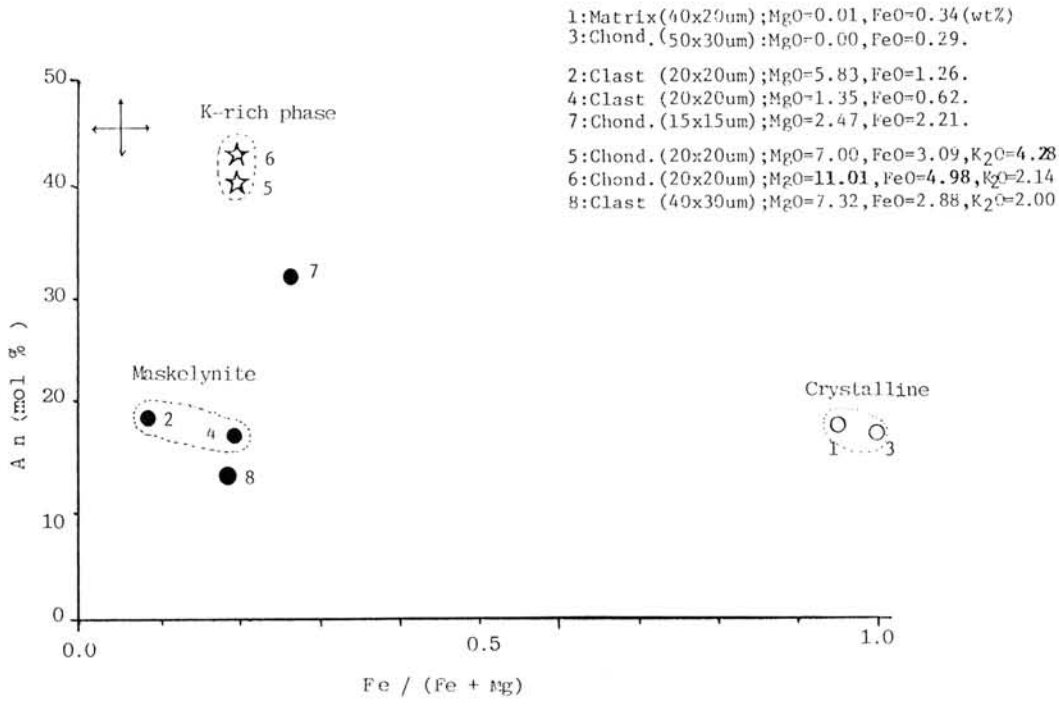

Fig. 2. The Fe/(Fe+Mg) and Or(mol%) diagram of the K-rich phases in the Niho 3(Miyano) H3, Y-74646,93(LL5 6), Y-74647,95-3(H5-6), ALH-768,65-2(H6), and ALH-77214,93-1(L3?) chondrites.

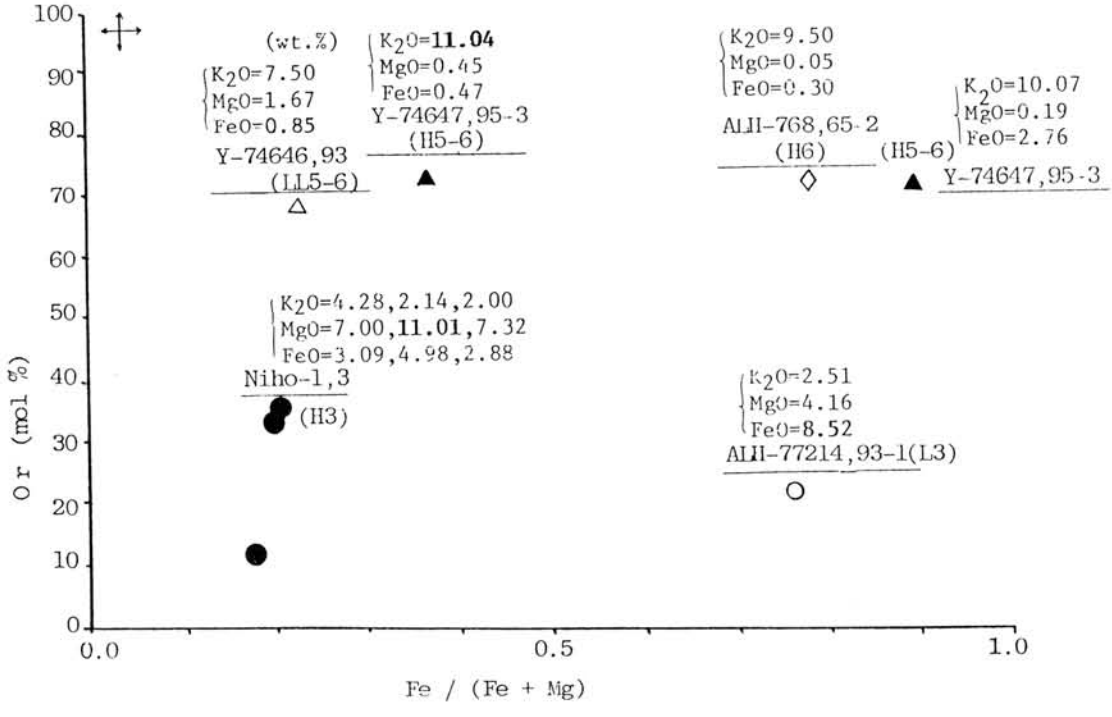

THE ROLE OF TEPHRA LAYERS IN THE METEORITE ICEFIELD AS A TIME MARKER

Fukuoka, T.[1], Arai, F.[2] and Nishio, F.[3]

1 Dept. of Chemistry, Gakushuin University, Toshima, Tokyo 171
2 Dept. of Geology, Gunma University, Maebashi, Gunma 371
3 National Institute of Polar Research, Itabashi, Tokyo 173

From the age of ice in the meteorite icefield, it is not only possible to get the informations of ice dynamics but also to get the age of the meteorite fall indirectly. Unfortunately, we have not succeeded to get the age of ice by direct determination method like ^{14}C so far.

There are many dirt bands in the ice at the Yamato and Allan Hills meteorite icefield. It was confirmed recently that dirt band consist of volcanic ash (tephra) layers. Because it is considered that one tephra layer was introduced by single volcanic event, we can estimate the age of ice from the age of tephra layer. That is, tephra layer will play a possible time marker of ice. Therefore it is possible to know the age of meteorite falls from those of tephra layers indirectly.

In this study, in order to test the role as a time marker of ice, the abundances of more than 20 elements in glass separated from three dirt bands in Yamato region and five in Allan Hills region have been determined by instrumental neutron activation analysis (INAA). The refractive indices of glass samples have been also determined. Sampling sites of tephra layers (dirt band) in the Allan Hills meteorite icefield are shown in Fig.1.

Fig.2 shows the chondritic normalized abundance patterns of lithophile minor and trace elements. The refractive index ranges of glass samples are shown in Table 1. Based on the comparisons of the values of refractive index and chemical abundance between the tephra of Yamato region and those of Allan Hills region, those are distinguished each other easily. Based on the chemical characteristics, we classified into two kinds of tephra from three of Yamato, although we cannot distinguish those one another based on the values of reflactive index. That is, the tephra of the sites K-26 and K-26' are possibly the same. Two kinds of tephra were recognized in No.8 tephra layers of Allan Hills by the both of the chemical characteristics and the reflactive index. We classified into four kinds of tephra from six of five sampling sites of Allan Hills. It is suggested that tephra No.1 and 9, and No.4 and 5 are the same, respectively. Although the

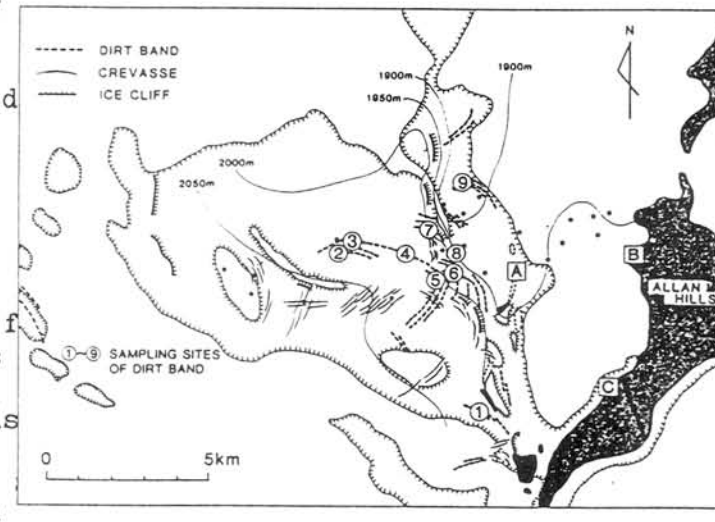

Fig.1. Sampling sites of tephra layers (dirt band) in the Allan Hills meteorite icefield.

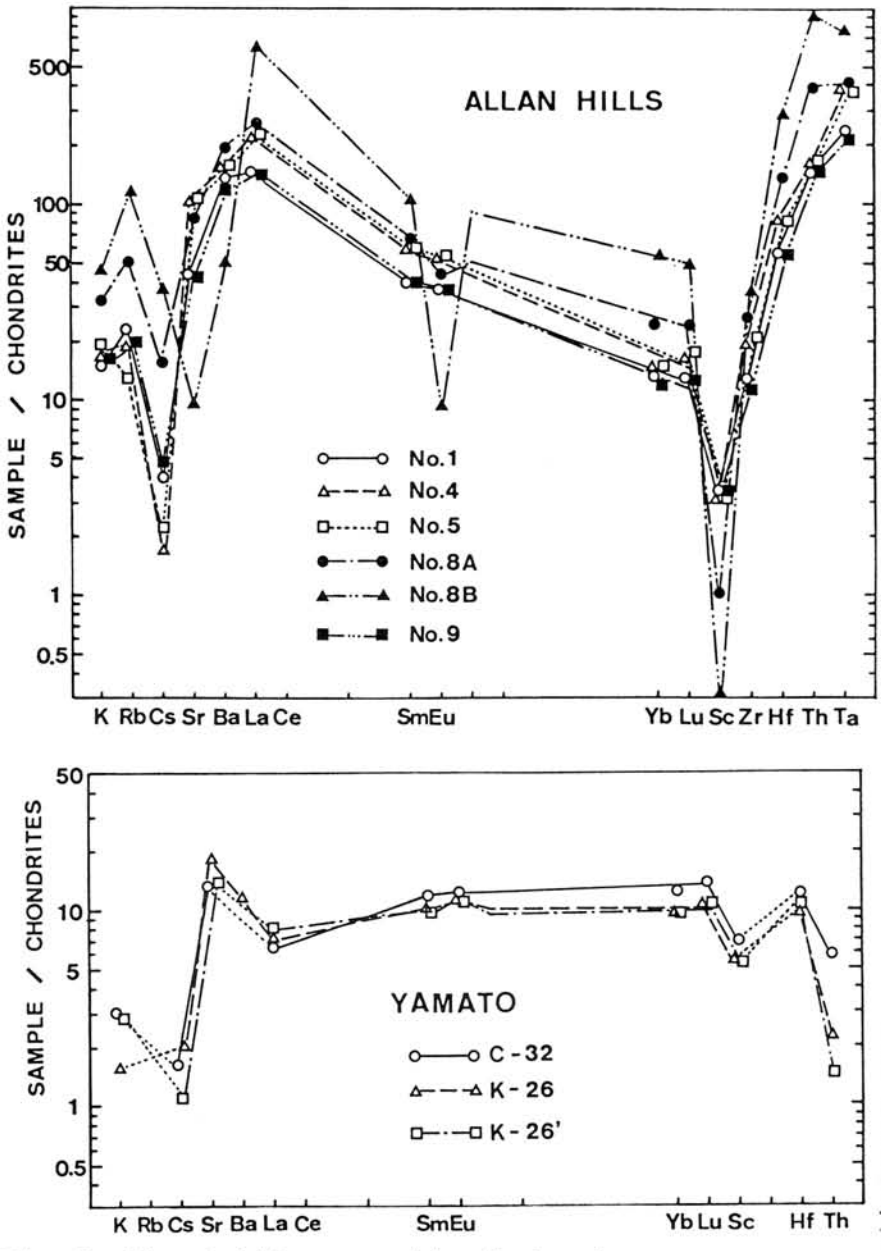

Fig.2. Chondritic normalized abundance patterns of minor and trace elements in glass separated from tephra layers in the ice at the Yamato and Allan Hills meteorite icefields.

sampling site No.1 is about 7 km away from the site No.9 (Fig.1), the age of ice of both sites is possibly the same. This is not only important to understanding the ice dynamics of the Allan Hills meteorite ice-field, but also to understand the difference between the field occurrence of meteorite collection and the distribution of meteorite fall.

In this study it is suggested that the meteorites collected from the distant site are derive from the same meteorite fall.

Table 1. Refractive index range of glass separated from tephra layers in the ice at the Yamato and Allan Hills meteorite icefield.

Sample	Refractive Index
Yamato	
C-32	1.564 - 1.571
K-26	1.566 - 1.571
K-26'	1.566 - 1.573
Allan Hills	
No.1	1.607 - 1.615
No.4	1.616 - 1.624
No.5	1.614 - 1.624
No.8A	1.544 - 1.553
No.8B	1.516 - 1.522
No.9	1.607 - 1.615

YAMATO 791197- MAJOR MINERALOGICAL CONSTITUENTS AND ITS RELATION TO REMOTELY SENSED REGIONS OF THE MOON FROM REFLECTANCE SPECTROSCOPY

L.A. McFadden[1], C.M. Pieters[2], R. L. Huguenin[3], T.V.V. King[4], M.J. Gaffey[5], B. R. Hawke[4]

[1]University of Maryland, College Park, MD, [2]Brown University, Providence, RI, [3]University of Massachussetts, Amherst, MA, [4]University of Hawaii, Honolulu, HI, [5]RPI, Troy, NY

Reflectance spectra of Y791197 indicate that its major mineralogical components are characteristic of the lunar highlands. Absorption bands due to low and high calcium, iron-rich pyroxene and high calcium plagioclase are present. The reflectance of chips and meteorite powder increases with increasing wavelength a spectral feature generally associated with lunar agglutinates. A spectrum of fusion crust shows an absorption band centered at ~ 1.08 μm which is almost twice as deep as the pyroxene bands in the crystalline material.

Experimental Procedures - Bidirectional reflectance was measured with the RELAB spectrometer at Brown University (1). It was operated at $i = 0^{o}$ $e = 30^{o}$ through the wavelength range of 0.4 - 2.6 μm at 0.010 μm intervals. The beam size was 6 mm enabling measurements of almost the whole cm^2 piece of Y791197,72. A second specimen consisting of mm-sized chips (Y791197,90) was measured, dry-crushed with mortar and pestle, passed through a 250 μm sieve and remeasured. The mean particle size was probably less than 100 μm. Microscopic examination showed that the particles were lumped together and coated with fine powder.

Interpretation - Visual examination of the whole rock and powder spectra of Y791197 shows absorption features due to Fe^{2+} in pyroxene at 1 and 2 μm and plagioclase at 1.3 μm. There is no olivine signature in these spectra. However there could be as much as 30% olivine present in Y791197,72 which would not be evident in the whole rock spectrum. The spectrum of the fusion crust (Figure 1) shows a strong broad absorption due to Fe^{2+} in glass. This band is stronger than the absorption due to the brecciated clasts in the unmelted meteorite. Spectra of Y791197,90 (chips and powder) have strong 1 and 2 μm pyroxene bands and a prominent plagioclase band at 1.3 μm (Figure 2). The position and strength of the plagioclase band indicates an Fe^{2+}-rich anorthite (2). Only lunar samples and basaltic achondrite meteorites show such a prominent plagioclase band, however the steeply increasing reflectance with wavelength is a decidedly lunar reflectance feature generally attributed to agglutinates (3). We are confident in excluding olivine as a constituent from this sample based on the position of the 1-μm band, it is at too short a wavelength for olivine and its symmetry is distorted only by the 1.3 μm plagioclase band and not by multiple bands due to olivine.

A second level of analysis in addition to visual examination was applied to these spectra. A multiple high order derivation analysis (4) was used to determine absorption band positions (Table I). This technique defined absorption bands that indicate the presence of both a low (Ca/Ca+Mg+Fe ~ 10-15%) and high calcium (Ca/Ca+Mg+Fe ~ 45%), iron-rich pyroxene. The corrected calibration (5) of Adams (6) was used to constrain pyroxene chemistry. In addition weak absorption bands in the visible were located at wavelengths

consistent with those seen in other lunar pyroxenes (7). Some bands might be attributed to olivine (8) but the full complement of Fe^{2+} spin forbidden olivine bands are not present. All expected pyroxene spin-forbidden bands are present. There are some bands that remain unidentified.

Conclusion - If there is any difference between Y791197 and ALHA 81005 (9) that can be determined from reflectance spectroscopy, it is in the spectrally apparent absence of olivine. However, because the spectrometer optics have been upgraded since measuring ALHA 81005, we cannot tell whether creating a composite spectrum by averaging spectra from 2 mm-sized areas as was done for ALHA 81005, introduces an olivine signature that is not representative of the whole rock sample or if there is less modal olivine in the piece of Y791197 compared to ALHA 81005. Knowing the inhomogeneous nature of breccias and metoerite samples, the absence of olivine is not sufficient evidence to conclude that these two meteorites are from different regions of the moon. In fact the mineralogy determined from reflectance spectroscopy is entirely consistent with the composition of highland craters with possibly some maria components mixed in (10,11).

(1) Pieters, C.M., J. Geophys. Res. 88, 9534-9544 (1983).
(2) Adams, J.B. and Goullaud, L.H. Proc. 9th Lunar and Planet. Sci. Conf. 2901-2909 (1978).
(3) Adams, J.B. and McCord, T.B. Proc. 4th Lunar Sci. Conf. 163-177 (1973).
(4) Huguenin, R.L. and Jones J., in prep. (1985).
(5) Gaffey, M.J., Icarus 60, 83, (1984).
(6) Adams, J.B, J. Geophys. Res. 79, 4329, (1974).
(7) Hazen, R.M. et al. Proc. 9th Lunar Planet. Sci. Conf., 2919-2934 (1978).
(8) Hazen, R.M. et al. Proc. 8th Lunar Planet. Sci. Conf., 1081-1090 (1977).
(9) Pieters, C.M. et al. Geophys. Res. Lett. 10, 813-816 (1983).
(10) Pieters, C.M., in prep. (1985).
(11) McCord, T.B. and Adams, J.B., The Moon, 7, 453-474 (1973).

Table I

λ (μm)	Mineral	λ(μm)
2.295 ± .066	diopside	1.052 ± .030
2.112 ± .061	pigeonite	0.947 ± .028
1.949 ± .056	pigeonite	
1.300 ± .037	plagioclase	
0.838 ± .008	undesignated	0.682 ± .018
0.628 ± .008	olivine?	
0.586 ± .009	undesignated	
0.554 ± .004	clinopyroxene	0.437 ± .010
0.506 ± .005	clinopyroxene (olivine?)	0.460 ± .010

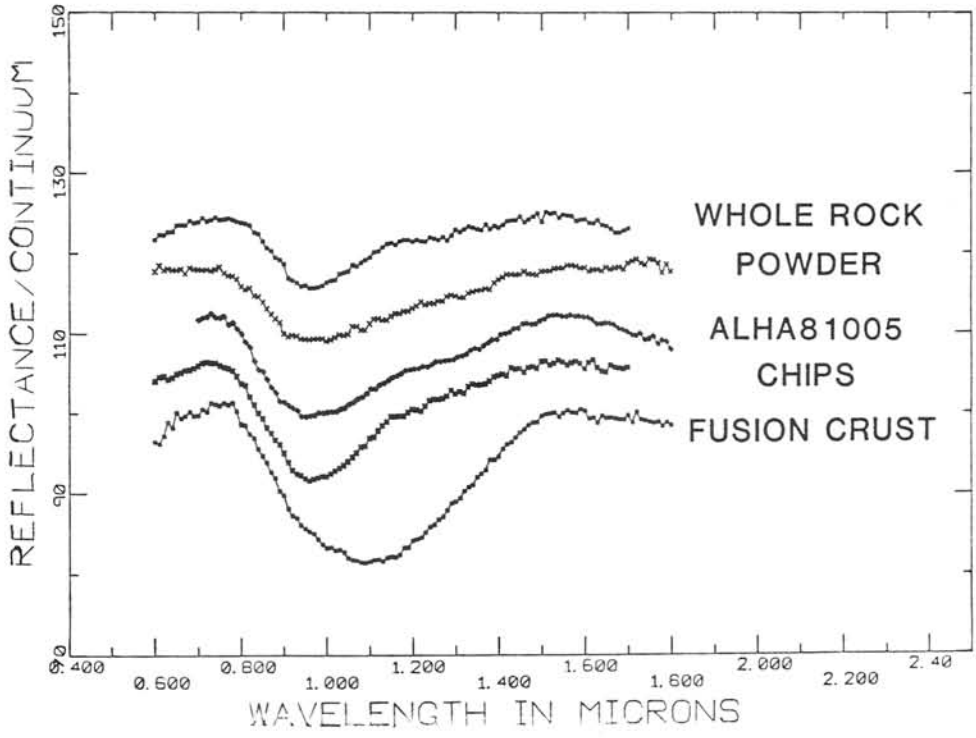

Figure 1- Continuum removed spectra of components of Y791197 and composite spectrum of ALHA 81005 (9).

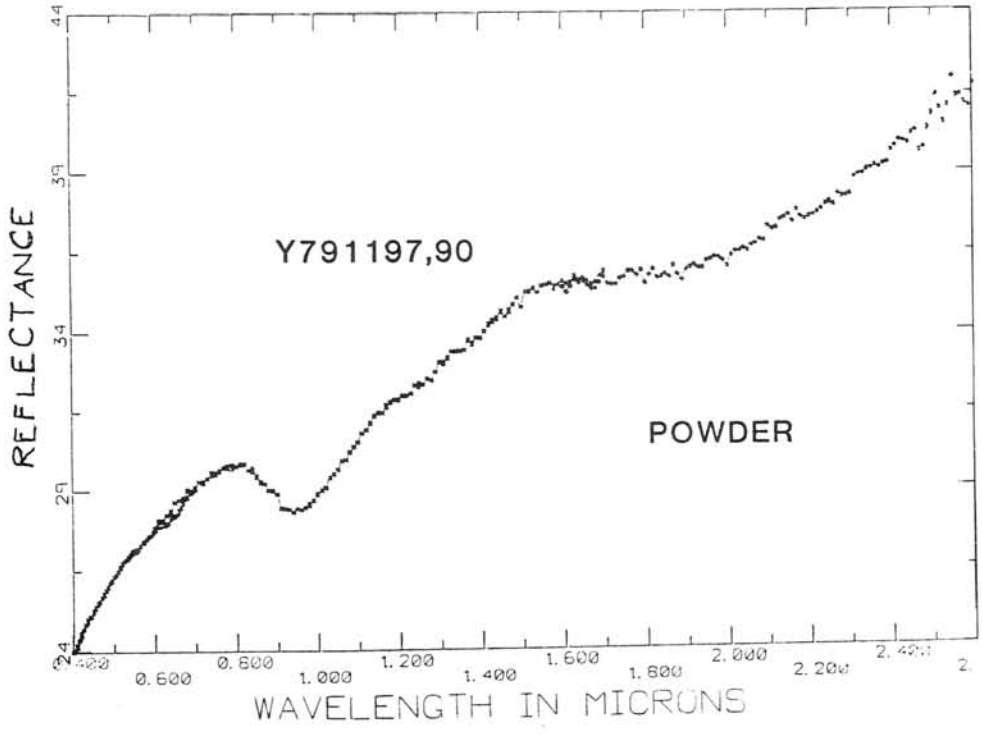

Figure 2- Bidirectional reflectance of Y791197,90 powder.

94—1

OLIVINE IN BELGICA 7904 AND OTHER CHONDRITES; EVIDENCE FOR RELIC OLIVINE WITH UNIQUE CHEMICAL AND TEXTURAL FEATURES.

Steele, Ian M., Skirius, C.M., Smith, J.V.
Department of the Geophysical Sciences, The University of Chicago, Chicago, Illinois 60637, U.S.A.

Belgica 7904 is a C2 meteorite collected by the Japanese Antarctic Research Expedition of 1979. A polished thin section was examined with an optical microscope, a cathodoluminescence microscope, and with an electron microprobe. Using catholuminescence, olivine with more than ~98% Mg_2SiO_4 shows bright blue luminescence grading to red and then to dark as the Mg_2SiO_4 component decreases. This technique provides useful textural and qualitative chemical data on a mm scale (1). The electron probe technique was optimized to provide accurate data at the 100 ppm level for minor elements in olivine including Na, Al, P, Ca, Ti Cr, Mn, Fe and Ni. In addition to Belgica 7904, other C2, C3 and unequilibrated ordinary chondrites (UOC) have been examined using similar techniques as part of a comprehensive study of olivine in primitive meteorites.

Polished thin section B7904, 92-3 of ~19 mm^2 has eight 0.5-1 mm sized clasts composed of polygranular olivine and interstitial glass. These in addition to smaller polygranular clasts and single mineral grains occur in an opaque to brown phyllosilicate matrix. The 8 clasts in Belgica 7904 can be divided into 2 groups and all olivine can be divided into three types depending on luminescence color. Six of the eight clasts are composed of equigranular subhedral to rounded olivine in a matrix of greenish-brown cryptocrystalline matrix. Each of these 6 clasts is surrounded by an opaque matrix rim. The olivine of these six clasts shows red luminescence and ranges from Fo_{99-98}. The 2 clasts of the second group show blocky to euhedral Fe-rich olivine (Fo_{83-41}), which lacks luminescence and shows no opaque matrix rim. Within one clast of each group rare blue luminescing grains are present.

The different luminescing olivine types have been described in other carbonaceous chondrites (2) including Murchison (C2) and Allende (C3V) and have since been observed in other C2, C3 and UOC by us. Features common to the blue luminescing olivines from these meteorites as well as Belgica 7904 include: (1) near-absence of inclusions of glass or crystals within the blue areas; (2) sharp luminescence boundaries between blue and red areas; (3) blue areas form cores

with red rims; (4) some blue areas have euhedral to subhedral boundaries often with embayments; (5) the levels of Al_2O_3, TiO_2 and CaO are uniquely high and intercorrelated with Al_2O_3 ranging to 0.45 wt.%, TiO_2 to 800 ppmw, and with detectable vanadium; (6) the sharp luminescence boundaries correspond to a distinct change in minor element concentrations.

Some typical analyses for B-7904 are given in Table 1, and minor element variation diagrams are illustrated in Fig. 1 for B-7904, Murchison and Allende. For B-7904 the blue luminescing points are indicated, but not for Murchison and Allende. From this diagram it is apparent that some chemical trends are similar for C2 meteorites (e.g. MnO vs. Cr_2O_3) and distinct from the trend for Allende. In contrast, other element pairs such as Cr_2O_3 vs. CaO and TiO_2 vs. CaO show differences between the two C2 meteorites. Using minor element trends for olivine such as those in Fig. 1, we have shown that relic olivine grains in deep sea particles have similar chemical features to olivines in some C2 meteorites, especially Belgica 7904 (3).

The distinct textural features as revealed by cathodoluminescence, and the enriched refractory elements in olivine indicate (1), a rapid change in crystallization conditions and (2) an unusual crystallization environment for the blue olivine. We suggest that the blue olivine represents relic olivine around which red luminescing olivine crystallized either as separate grains to form aggregates or in crystallographic continuity. The unique chemistry of the blue olivine reflects a refractory enriched source reservoir and the lack of inclusions in conjunction with euhedral to subhedral morphology suggest free growth possibly from a gas. The above observations extend the range of meteorite types in which relic grains are reccognized (4,5) and show that there is apparently more than one type of olivine which occurs as relic grains.

We acknowledge NIPR for sample loan,≥ and NASA NAG9-47 for support.

References:

(1) Hutcheon, I.D., Steele, I.M., Smith, J.V. and Clayton, R.N. (1978) *Proc. Lunar Sci Conf.* 9th, 1345-1358.
(2) Steele,I.M., Smith J.V. and Skirius C. (1985) *Nature*, **313**, 294-297.
(3) Steele,I.M., Smith J.V. and Brownlee D. (1985) *Nature*, **313**, 297-299.
(4) Nagahara H. (1981) *Nature*, **292**, 135-136.
(5) Rambaldi E.R. (1981) *Nature*, **293**, 558-561.

Table 1. Analyses of olivine luminescent types in Belgica 7904.

	1	2	3	4	5	6	7
SiO_2	43.1	42.5	42.3	42.0	41.9	34.7	41.7
TiO_2	0.042	0.050	0.058	0.057	0.073	0.002	0.104
Al_2O_3	0.165	0.138	0.237	0.236	0.214	0.048	0.549
Cr_2O_3	0.304	0.275	0.442	0.163	0.225	0.589	0.075
FeO	0.705	0.964	0.961	0.824	0.841	46.3	0.313
MnO	0.065	0.037	0.093	0.017	0.029	0.442	0.003
MgO	55.7	55.6	55.3	55.3	55.9	19.3	55.4
NiO	0.020	0.013	0.003	0.012	0.013	0.099	0.006
CaO	0.336	0.435	0.364	0.493	0.478	0.112	0.803
Sum	100.437	100.012	99.758	99.102	99.673	101.592	98.953

Notes: (1,2) red luminescing olivine from two different clasts; (3) red rim with blue core (4); (5) blue luminescing grain in clast with common Fe-rich non-luminescing olivine (6); (7) bright blue luminescing single grain.

Fig. 1. Minor element variation in Belgica 7904, Murchison and Allende.